Smart Gels in Drug formulations

Lamisse Hatem El-Qarra

Doctor of Philosophy

Chemistry

University of York

September 2023

Abstract

Low molecular weight gelators (LMWG) are molecules that form complex fibre-rich networks via non-covalent interactions in the presence of aqueous solvents. Supramolecular hydrogels have shown attractive properties in acting as carriers of drug moieties. This is a result of their high-water content, simple molecular structures, and stimuli responsiveness all of which contribute to the potential use in biomedical applications. The novel Benzyl glutamine hydrogel is the centre of this research. The study begins with the focus on the development of new gelator systems based of the Benzyl glutamine scaffold[1]. By tuning functional groups of the molecule, various derivatives were acquired and knowledge of key components of the structure that control the molecules gelation were determined.

Having been successfully capable of delivering levodopa intranasally[2], we were interested to further examine Benzyl glutamine as a drug delivery system. The hydrogel is used as a platform for the encapsulation and release of drugs with different properties. The study demonstrated the compatibility of the gel with specific molecules and their impact on the integrity of the gel. We observed that the ideal drug cargo profile of the gel are drugs with high-water solubility and low molecular weight.

As a consequence of possessing dynamic non-covalent interactions, LMWGs are generally rheologically weak. To enhance the robustness of Benzyl glutamine, the LMWG was introduced to seaweed polymer extracts, alginate and agarose respectively, forming multicomponent gel beads. We explored the drug delivery application of the novel formulations, our groups LMWG's (DBS-$CONHNH_2$ and DBS-COOH), and their respective hybrid beads with the drugs propranolol and levodopa. The study provided an insight into the different release profiles carried out by each gel system.

A novel approach produced by Fittreman was explored with the Benzyl glutamine gelator to produce self-standing networks. The technique involves an injectable solvent switch methodology, enabling the development of gel filaments and ultimately the formation of 3D printed scaffolds[3]. The investigation discusses the different parameters to consider in developing such constructs and the potential biomedical uses of our LMWG's developed through this technique.

Table of Contents

List of Figures

List of Tables

Acknowledgements

I would firstly like to thank my supervisor, Prof. David Smith, for giving me this opportunity and for his support and guidance throughout the years. My gratitude extends to Dr. Tony Wild for granting me funding for this project.

I would also like to thank the technical staff - Heather Fish, Karl Heaton, and Karen Hodgkinson for their help with NMR, mass spectrometry, and microscopy. I would like to express my gratitude to previous and current research members. I am thankful that I have had the opportunity to work alongside them and for their advice, assistance, and for the many chats we've had. I extend my sincere appreciation to Chayanan Tangsombun for her contribution to the cell growth study in the final chapter. And a special thank you to Carmen Piras for all of the advice and tips she gave me that really pushed me at the end of my PhD.

I am extremely thankful for my family and friends, especially my brother and sister for their constant encouragement and invaluable advice. Most importantly, I would like to dedicate this work to the person who made it all possible, my father Hatem. Words cannot express my appreciation for always believing in me and supporting me throughout my entire life.

Declaration

I hereby declare that this thesis is a presentation of my original work. The work presented is entirely my own, except where otherwise acknowledged. This work has not previously been presented for a degree or other qualification at this University or elsewhere.

Chapter 1 Introduction

1.1 Gels

Gels are colloidal materials in which a solid-like phase comprised of molecular species is suspended in a liquid-like phase. The molecules form hierarchically arranged networks that trap the solvent medium forming a viscous non-flowing material. Typically, the liquid-like phase contributes ca. 99% of the total weight of the gel. Gels are functional materials used in numerous applications such as oil recovery, biomedical and cosmetic applications, food technology, and as delivery systems (pharmaceutical, agricultural, beauty, etc) as a result of their soft nature and properties[4-7]. Properties that are common among this class of materials but do not apply to all gels include elasticity[8], biocompatibility[9], shear thinning behaviour[10], and transparency[11]. These characteristics make them an exciting type of material with the potential to be used in many areas[12-14].

There are several ways to categorize gels as many different factors can determine a gels behaviour. Classification can vary from the type of gelator molecule (peptides, sugars, small organic molecules), the solvent engulfed (organic or aqueous solvents forming organogels and hydrogels respectively), and the type of intermolecular interactions involved within the network (chemical or physical). The gels properties are based on these intermolecular interactions.

Polymer gels are robust gels that are composed of monomers that assemble to give extended polymer chains via either covalent or non-covalent bonds. When the chains interact with each other through the formation of covalent cross-linking it gives rise to form robust, stiff, non-reversible chemical gels. Contact lenses are an example of a gel based on crosslinked polymers which are mouldable and robust. However, a drawback of chemically crosslinked gels can be toxicity associated with the molecules synthesis and any chemical cross-linkers used to form the gel, as well as the absence of stimuli responsiveness due to the permanent nature of the network that is formed. On the other hand, non-covalent interactions between the chains forms gels known as supramolecular or physical gels.

These gels are also often highly robust, because of the large molecular size of the polymeric building blocks, however they can retain a degree of reversibility as a result of the non-covalent interactions holding them together. Examples of polymer physical gels include agar[15], gelatin[16], alginate[17], etc. In general, polymer gels are excellent for handling and shaping as the large polymer molecules strengthen the gel network.

Supramolecular gels can also be further categorised depending on the molecular size of the gelator molecule. Low molecular weight gels are composed from low-molecular-weight building blocks, that are held together via non-covalent interactions. They typically have a molecular weight of less than 3000 daltons. Such physical supramolecular gels are formed via non-covalent interactions such as hydrogen bonding, π-π interactions, electrostatic interactions, and the hydrophobic effect[18, 19].

Supramolecular gels are responsive to their environment and can react to stimuli such as pH, temperature, light, magnetic and electric fields[20]. Sensitivity to stimuli is due to the reversible interactions involved within the network, making them tuneable for desired applications. Nevertheless, the reversible bonds in supramolecular gels mean these gels are less mechanically stable than chemical gels as the dynamic bonds can easily be broken. Supramolecular gels have the potential to disassemble into biocompatible building blocks, and this can lower their toxicity, and also some have special properties such as having self-healing ability. In this Introduction, we will focus on the use of supramolecular gels specifically low molecular weight gelators (LMWG).

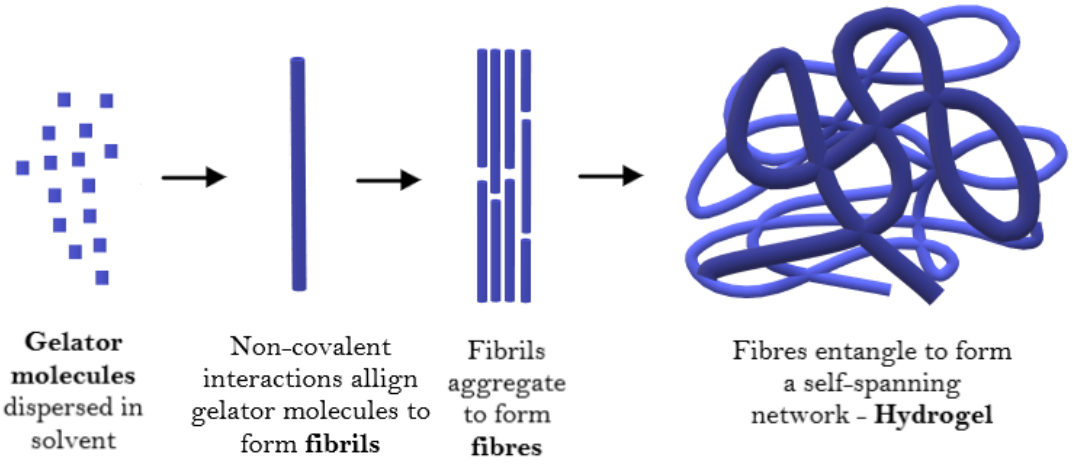

Figure 1. General process for the formation of a supramolecular self-assembled gel.

Gels are formed through self-assembly once exposed to stimuli such as temperature, pH, enzymes, etc. Self-assembly is the spontaneous molecular arrangement of under near thermodynamic equilibrium conditions into structurally well-defined and stable arrangements through non-covalent interactions. The combination of non-covalent interactions come together to form structurally and chemically stable structures[21]. This dynamic assembly begins with the alignment of these small molecules. The molecules are held by non-covalent interactions which form elongated structures called fibrils. The fibrils intertwine and bundle to form larger structures known as fibres. The entanglement of fibres leads to the formation of a complex fibre-rich 3D network as shown in Figure 1.

1.2 Design of LMWG Systems

To design LMWG's, researchers need to understand the role of the molecular building blocks and their accompanying non-covalent interactions. By doing so interesting properties can be acquired. The architecture of a successful gelator molecule typically requires degrees of both hydrophobicity and hydrophilicity in such a way that a balance is maintained to prevent its complete solubility/insolubility in a solvent. Functional groups determine a molecules gelation ability and its respective properties, as each functional group provides different non-covalent interactions that could alter the hydrophilic/hydrophobic balance[22]. Therefore, once a gel ''scaffold'' is determined, researchers can control the properties of the gel by the functionalization of the molecule. Hydrogen bonding is one of the most versatile non-covalent motifs involved in supramolecular hydrogels. Interactions between electron-rich acceptor atoms and electron-poor hydrogen atoms yield strong functional hydrogels despite the water molecules competing with the gelator molecules for hydrogen bonding sites[13]. As for the hydrophobic effect, the thermodynamic driving force is the minimisation of contact between hydrophobic moieties and water, resulting in the aggregation of nonpolar groups with minimal exposure to the surrounding aqueous environment[23]. Van der Waals forces arise as a result of fluctuations in the electron distribution of atoms or molecules which can provide an overall

stability of the hydrogel[24]. Metal–ligand interactions are produced by a metal ion with one or more ligands. However, careful consideration needs to be addressed when choosing the type of metal due to their toxicity, which can potentially limit their biomedical applications. Overall, the non-covalent interactions work synergistically to drive self-assembly and reinforce the 3D network of the gel. This type of molecular interaction engineering is an exciting approach as it can enable researchers to tune gel properties for specific applications.

Another approach of designing a gel system besides chemically changing the structure of the gelator is by producing a multicomponent gel system. These type of systems can be classified into three categories – gelator combined with an additive, a combination of non-gelling components that only self-assemble together, and a combination of individual self-assembling gelators[25]. This method offers greater tunability as there are more than one variable to modify to tune the gels properties. Multicomponent gel systems made by several gelators can be produced by either combining two or more different LMWG's together or a combination of LMWG's with polymer gels. The two or more components can either interact with one another or remain as single independent moieties within the multicomponent network. Forming a system with gels with different traits allows researchers to selectively choose properties within a singular gel system. Overall, the technique eliminates certain weaknesses of individual gels and takes advantage of their unique characteristics, thus producing gels with enhanced properties such as improved mechanical robustness, stability, and stimuli responsiveness that can be utilised in applications.

In the following sections, we will discuss several types of gelator ''building blocks'' capable of forming supramolecular sample-spanning networks and several types of multicomponent gel systems, in order to exemplify some of the general points made above with both recent and classic published work. We will also explore the different applications this class of materials can be used to advance specific fields.

1.2.1 Sugars

Sugars are attractive molecules which have numerous interactive functional groups and rich stereochemistry. The molecules are also derived from abundant natural resources and are biocompatible as they are key building blocks in many biological processes. These water

soluble molecules are generally attached to a hydrophobic moiety to help establish self-assembly and therefore form supramolecular hydrogels[26]. Such structures can be considered as neutral amphiphiles, which assemble primarily as a result of the hydrophobic effect, with the apolar groups shielded on the interior and the polar sugar head groups projecting into the surrounding water.

Gelation of sugar based molecules dates back to work by Fuhrhop in the late 1980's in which hydrogels of *n*-octylgluconamides were investigated[27]. Pushing forward greater advancement throughout the years, with more gelator molecules being discovered and progressing our knowledge of these systems. For example, in the work by Shinkai et al, which describes the discovery of the supergelator consisting of a bolamphiphilic azobenzene with two end sugar groups. It was found that the azobenzene π-π interactions were key for self-assembly along with the hydrogen bonding between hydroxyl groups of the sugar moiety[28]. In another study, the aromatic azobenzene group was also the driving force for the excellent gelation of a tetrameric sugar hydrogel with an azobenzene chromophore as indicated by UV-vis studies and circular dichroism[29]. The study involved the synthesis of several similar analogues of the molecule containing either azobenzene or bis terephthalic amide as the chromophore. Srivastava et al found through characterization techniques that although the new analogues were similar to the original, none succeeded to provide comparable efficient gelation. This study highlights the impact minor structural changes has on self-assembly and the importance of molecular screening to find a gelator[29].

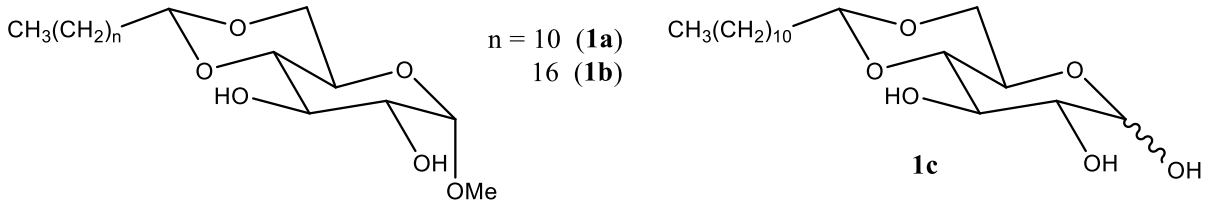

Figure 2. Structures of glucose derivatives 1a–1c[29].

Supramolecular interactions are key contributors in the behaviour and properties of these materials. This can be observed throughout the chapter as researchers discover new gelators with unique properties through slight structural alterations. More recent examples include

the design of a range of glucose derivatives consisting of glucose units and alkyl chains, developed by Watanabe's group[30]. Slight manipulations of the structures led to different properties. For example, gelator 1c (Figure 2) has a hydroxy group instead of a methoxy group, reducing its ability to gel across a range of solvents and only gelling in n-octane. On the other hand, gelators 1a and 1b can gel in a variety of solvents including both organic and protic media. Thermal stability and gelation ability was enhanced with the lengthening of the alkyl chain as van der Waals interactions/hydrophobicity increase. Gelator 1b also exhibited thixotropic behaviour in squalene and ethanol respectively[30].

Sugars are common substrates of enzymes and their exposure to enzymes leads to their breakdown. By adding a sugar moiety to a gelator molecule enzyme instructed self-assembly can be achieved as a method of strategic design forming a "pro-gel". Halila's group introduced an eco-friendly method of producing glycoamphilphile hydrogels. A variety of amphiphilic β-C-glycosylbarbiturates were produced by altering either the carbohydrate (glucose or maltose) and the length of the hydrophobic chain, which led to various self-assembled glyco-nanostructures (ribbons, tapes, vesicles, helices, and fibres). The group also achieved enzyme-Instructed self-assembly of a non-gelating maltose precursor (MalB(OH)-2) into an opaque glucose based gel (GlcB(OH)-2) by Aspergillus niger amyloglucosidase-catalyzed non-reducing D-glucosyl residue hydrolysis (Figure 3). Enzyme triggered gel assembly has considerable potential in biological applications as it provides a way in which gel-phase materials can be made responsive to specific biological processes associated with pathogens or disease pathways[31].

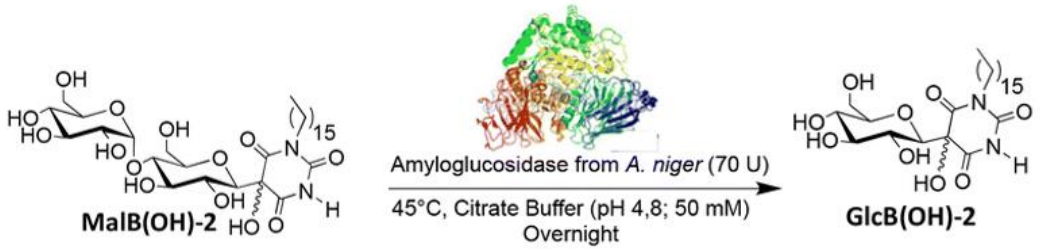

Figure 3. Adapted from Yao, S.[30] A. niger amyloglucosidase-catalyzed glucosyl residue hydrolysis of MalB(OH)-2 into a GlcB(OH)-2 gelator.

Yamanka's group produced a range of LMWG's by coupling the sugar maltose to amphiphilic urea's. Urea functional groups are also privileged in the formation of gels as a result of their ability to form hydrogen bonded tapes, with intermolecular interactions between C=O and N-H groups[32]. Gelation efficiency was found to be controlled by the length of the chain of the alkyl groups on the urea. This was decided based on gelling abilities of the new molecules and characterization techniques (thermal and rheological studies) of the gels. Molecules required to have at least an 8 carbon alkyl chain to form gels, while going up to a 10 carbon alkyl chain produced the most efficient gels. Beyond that length (11 and 12 carbon) led to reduced gelation efficiency, which is a result of a disruption of the hydrophilic/hydrophobic balance. The gel-sol transition could be controlled by the hydrolysis of the α-1,4-glucoside bond of the sugar moiety via the addition of the enzyme α-glucosidase[33]. Hydrolysis of the glucosidic bond at the maltose moiety produces amphipathic urea (Glu−Cn) and glucose, leading to sol formation.

Biswakarma et al. utilized supramolecular sugar-based hydrogels for bio-sensing of cholera toxin (CT). Their design involved the use of pyrene-based amphiphile with C4-alkanoyl spacer and lactose (PyLac) to form a self-assembling network (Figure 4 (a)). By changing the sugar group (lactose or maltose), PyLac exhibited a thixotropic nature, while interestingly the maltose-appended compound (PyMal) did not demonstrate signs of aggregation in the aqueous medium and only produced a viscous solution at high concentrations (10 mM) as shown in Figure 4 (c). It was clear that the hydroxyl groups configuration and 3D orientation of the sugar moiety showed profound influence in controlling the self-assembly, demonstrating how small changes in chemical structure can have significant impacts on the self-assembly event. Indeed, this high degree of tunability is one of the key advantages of working with sugar-based gelators. The terminal galactose residue can bind to the cholera toxin making it useful for CT optical sensing. Spectroscopic fluorescence studies showed a colour change in the presence of the cholera toxin - the solution turned from cyan to blue indicating the presence of CT (Figure 4 (b)). They also found the gel to be sensitive to the cholera toxin as it transitioned from gel to sol upon its exposure[34]. The responsive nature of gels makes them potentially valuable materials in the field of biosensing.

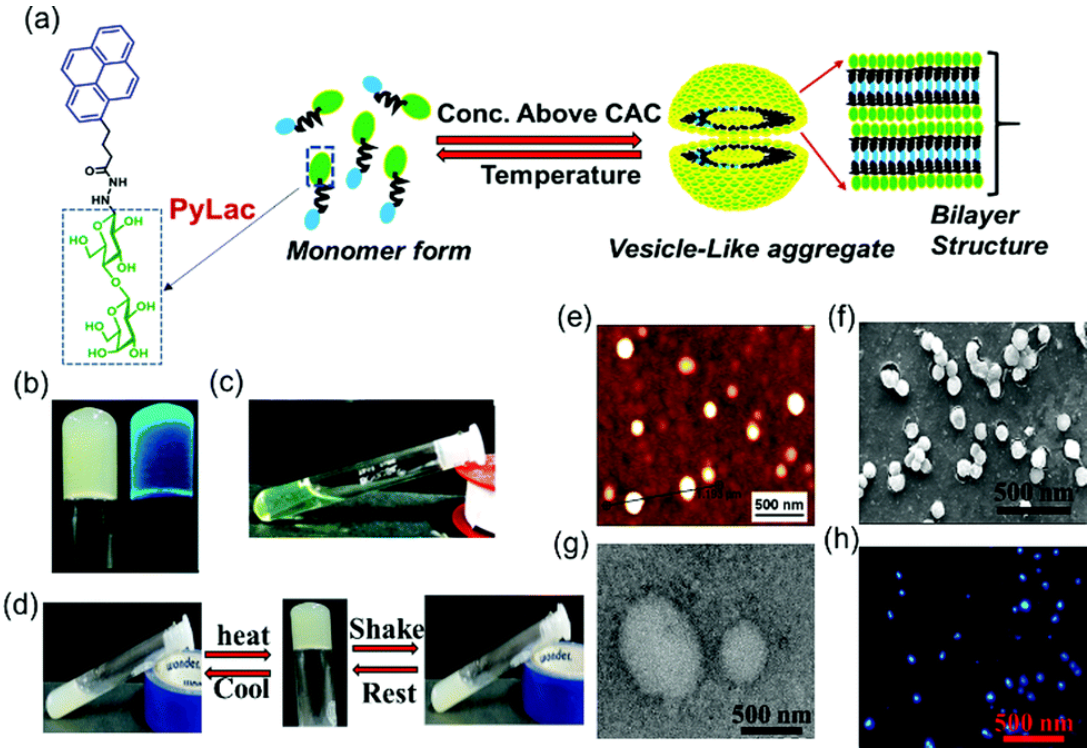

Figure 4. Adapted from Biswakarma, D. [34](a) Illustration of PyLac amphiphiles in water. (b) Picture of PyLac gels (2.5 mM) under daylight and UV lamp (>365 nm). (c) Sol formation at high concentration of 10 mM of PyMal. (d) Gel-to-sol transition in presence of presence of heat/cool and shake/rest. (e) AFM, (f) SEM, (g) TEM images of the solution of PyLac (0.09 mM). (h) Fluorescence microscopy images of the solution of PyLac (0.18 mM).

Dibenzylidene sorbitol (DBS) has been a known sugar gelator for over 100 years, with the earliest report being in 1891 by Meunier[35]. During that period, it has been reported to be used in applications such as in cosmetics, healthcare, and polymer clarification[36]. The molecule has been structurally altered to provide new derivatives of this class of molecule by changing the free alcohols or aromatic wings of the structure. Gelation of DBS occurs due to hydrogen bonding interactions between the sugar units and π–π stacking and solvophobic interactions between the aromatic rings constituting its 'butterfly-like'' wing structure.

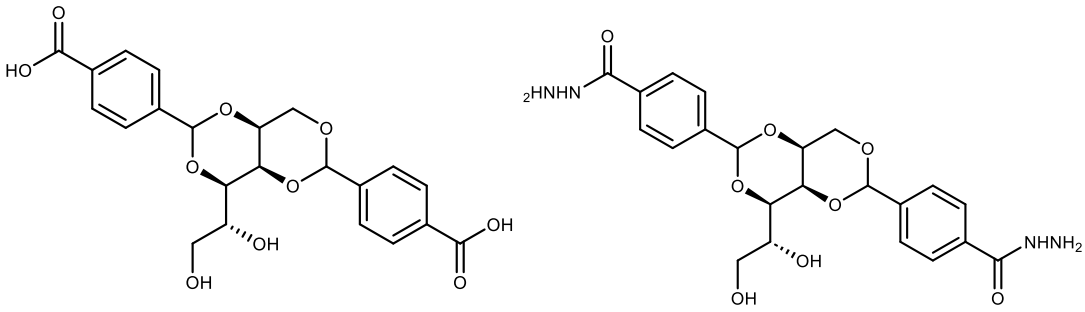

Figure 5. Structures of DBS-COOH (Left) and DBS-CONHNH2 (Right).

In the past several years, our group have performed extensive research on the 1,3:2,4-dibenzylidene-D-sorbitol derivatives DBS-$CONHNH_2$ and DBS-COOH (figure 5) for various biomedical applications[37-39]. DBS-$CONHNH_2$ is a thermally triggered gel that assembles via a heat-cool cycle, while DBS-COOH is a pH-responsive system, that is soluble under basic conditions and assembles into a gel under controlled acidification. The acyl hydrazide groups of DBS-$CONHNH_2$ are capable of interacting with various additive functional groups, a property useful in drug delivery as it can potentially interact with drug molecules[40]. It can also act as a reducing agent to precious metals to form nanoparticles[41]. While the DBS-COOH molecule possesses pH responsiveness, another important property in drug delivery that can be used for controlled drug release[42].

By combining gel systems, our group took advantage of these molecules unique properties and took them a step further in advancing their use in applications. The two LMWG's can be combined to form a hybrid multicomponent gel network in which each component self-assembles by different triggers. Interactions between the two gels in the two-component system resulted in improved mechanical and thermal properties. Piras et al developed multi-component multi-domain gels by achieving spatial control of the DBS-COOH network within a DBS-$CONHNH_2$ gel through a photo-patterning method in which acidification was triggered by the photoirradiation of diphenyliodonoium nitrate[43]. UV-irradiation triggers the release of nitric acid, lowering the pH and promoting DBS-COOH assembly within a pre-formed DBS-$CONHNH_2$ supporting matrix, generating a well-resolved photopatterned multi-domain gel (Figure 6). This strategy permits the control of self-assembly and customizable shaping of the DBS-COOH gel[43].

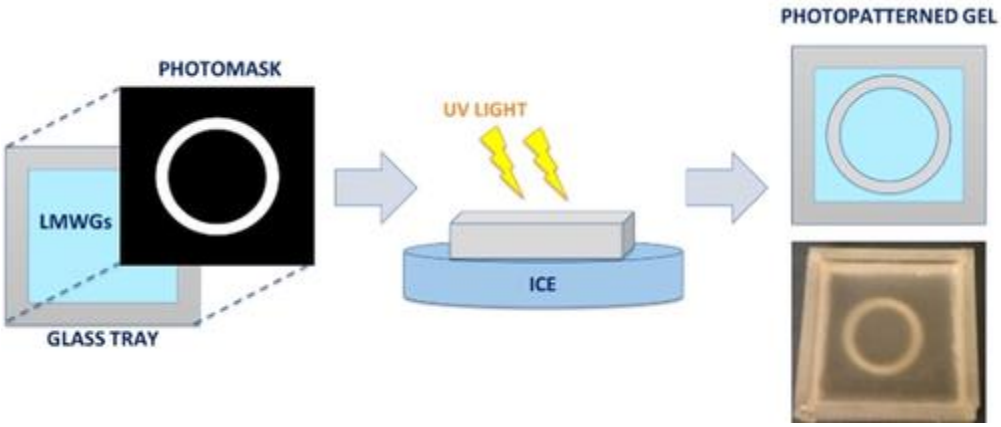

Figure 6. Illustration of hydrogel photo-patterning. Adapted from reference 43[43].

Further work from the Smith group used a proton diffusion method to stimulate assembly of DBS-COOH with either GdL or HCl diffusing from reservoirs cut into the gel. This work demonstrated spatially-resolved transient controlled self-assembly based on the concentration and type of acid, as well as the loading pattern. This approach may be particularly useful in tissue engineering in which the dynamically adapting gel matrix could help direct cell growth in a more dynamic and adaptive manner[44]. By studying the effects of different proton sources (GdL and HCl) on shape patterning efficiency, it was found that kinetics of assembly, shape definition, and gel performance varied. HCl provided a faster self-assembly that generated a more defined shape however TEM and rheological studies suggested inhomogeneous nanofiber formation and poor rheological performance. Conversely, GdL provided a slow assembly of the DBS-COOH with less defined control of the shape, but the patterned material exhibited improved nanofibrillar character and greater rheological robustness.

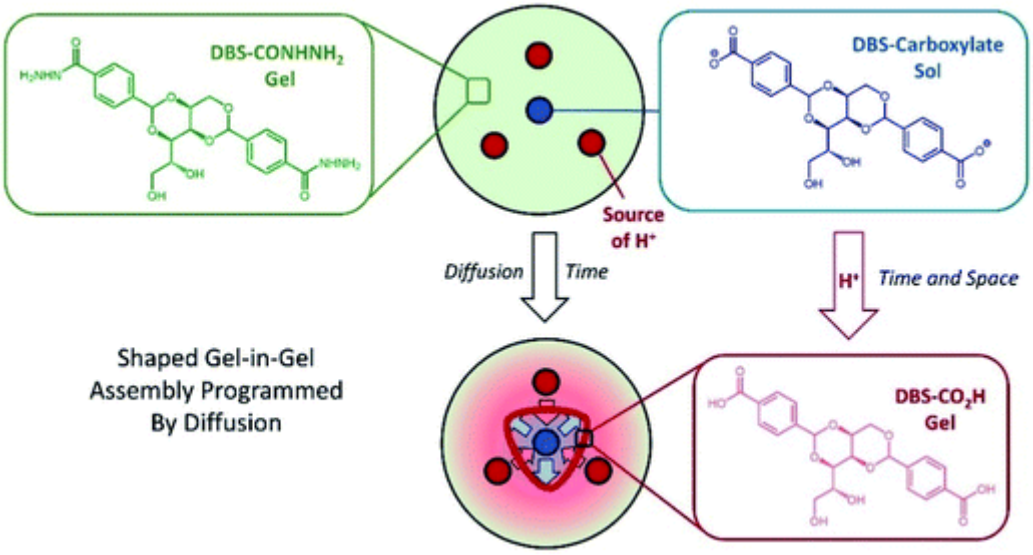

Figure 7. Schematic of diffusion experiment in which DBS-COOH diffuses out from the central reservoir cut into a pre-assembled DBS-CONHNH2 gel. With time the diffusion DBS-COOH undergoes dynamic protonation as it meets an acid diffusing from surrounding reservoir cut into a pre-assembled DBS-$CONHNH_2$ gel. With time the diffusion DBS-COOH undergoes dynamic protonation as it meets an acid diffusing from surrounding reservoir(s). This leads to the self-assembly of the DBS-COOH network. Adapted from reference 43[44].

Another factor that directs patterning is the shape of the central reservoir and the geometry of the external reservoirs in the gel network. To use this approach for tissue engineering a weak acid that's tolerated by cells should be used to facilitate cell growth and proliferation. Our group is currently developing a less invasive approach to trigger diffusion-based self-assembly[45].

And finally, to gain more insight in the role of the chirality of DBS-$CONHNH_2$ gels gelation efficiency a multicomponent gel system containing both L and D enantiomers was investigated. By combining both L and D enantiomers of the gelator, weak gels were self-assembled to form a multicomponent gel with fragmented aggregates and reduced thermal stability and stiffness. This demonstrated that homochiral recognition pathways would be preferred, with the enantiomers disrupting one another's assembly to some extent. Circular dichroism studies indicated a loss of nanoscale chirality on combining enantiomers. Chiral additives (naproxen enantiomers) were loaded into the DBS-$CONHNH_2$ enantiomers and although both gels can load both of the enantiomers of naproxen, they affected the thermal and rheological properties of the gels differently[46].

Overall, sugars comprise interesting frameworks for gelation because of their high degree of tunability and large number of interactive hydrogen bonding functional groups. It is possible to test multiple subtly different sugar units to determine structure-activity relationship effects, and in some cases, as we have seen, sugar groups can interact with specific biological targets such as enzymes. Their biocompatibility gives them potential in applications such as drug delivery or regenerative medicine.

1.2.2 Nucleosides and Nucleotides

Nucleosides and nucleotides are a class of biomolecules composed of a combination of a nucleobase and a five carbon sugar ring (ribose or deoxyribose) linked via a glycosidic bond. Nucleobases are categorised into purines (adenine or guanine) and pyrimidines (cytosine, thymine, or uracil) which both have multiple sites for hydrogen bonding as well as π-stacking of the aromatic structures. The interactions involved between the nucleobases include the famous Watson–Crick base pairing involved in DNA arrangements. The sugars involved also facilitate supramolecular interactions. Phosphorylation of nucleosides leads to the formation of nucleotides which have additional electrostatic interactions due to its anionic phosphate group[47].

To achieve gelation the structures of these molecules require adjustments mostly through increasing their hydrophobicity and the addition of other functional groups to stabilize the network. The exception to this is guanosine due to the three hydrogen bonding moieties on its purine structure that promote self-assembly. The first guanosine based gel was reported in 1910 by Ivan Bang in which highly concentrated 5'-guanosine monophosphate (5'-GMP) gelled in water[48]. In 1962[49], Gellert et al discovered that self-assembly of these gels is based on the G4-quartet building block that is formed as a result of hydrogen bonds formed between guanosine molecules. G4-quartets stack on top of each other and are extended into G-nanowires. Cations such as K+ stabilize G4-quartets (figure 8)[50].

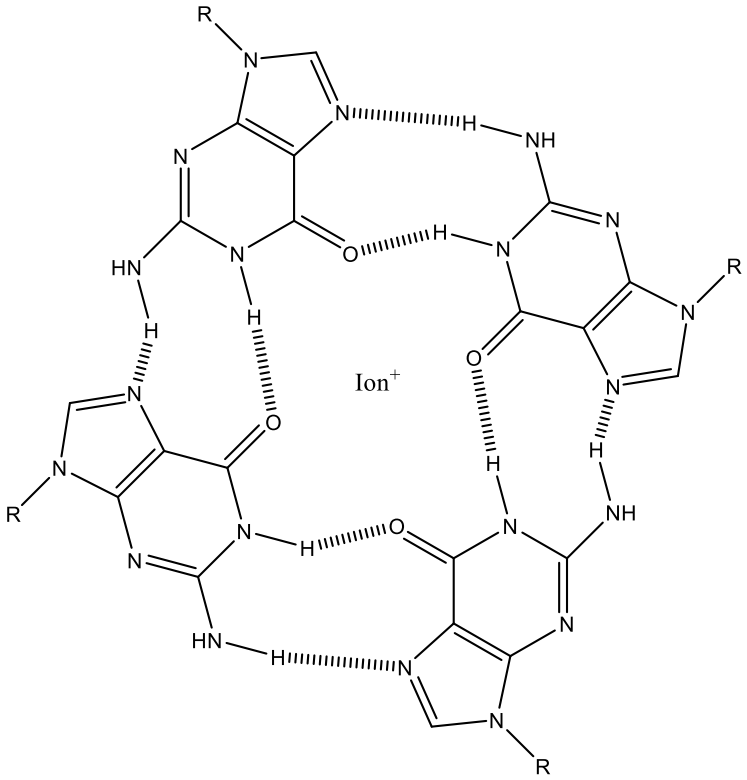

Figure 8. G quartet stabilized by metal ion.

In 2011, Dash et al utilised Ag^+ to mediate the self-assembly of disodium guanosine 5'-monophosphate[51]. Rheological properties were tuned by altering the ratios of both components. TEM images showed the presence of Ag nanoparticles embedded within the fibre network. The gel is capable of binding to protein cytochrome c without disrupting its function. It can also bind to cationic dyes such as methylene blue and Hoechst-33258. Binding with methylene blue promoted stability in the chiral structure, whereas with Hoechst-33258 led to significant disruption of the helically stacked Ag-GMP superstructure[51]. This work presented hydrogels with promise in the biomedical field as they are rheologically tuneable, can be embedded with nanoparticles, and have an ability to bind to relevant biomaterials. The study is an example of how LMWG's properties can be tuned for specific applications by simple changes.

Nucleobase structures contain diols within them, and this has made boronic acids extremely useful additives in this class of gel. Boronic acids form boronate esters with diols, a reversible bond-forming reaction. This can modify the properties of the nucleobase and help trigger gel assembly.

Zhang's group designed a hydrogel consisting of guanosine (G), potassium ion (K^+), aminoglycoside (Ami) and a bifunctional anchor, 2-Formylbenzeneboronic acid (BA)[52]. The guanosine analogues form G-quartets with the alkali metal potassium via hydrogen bonding and coordination interactions, leading to the further assembly into G-quadruplexes and supramolecular hydrogels via π–π stacking. Aminoglycosides are excellent gelators due to their primary amines that react to aldehydes to give Schiff base assembly and numerous hydroxyl groups that contribute the secondary network formation through hydrogen bonding. Self-assembly occurs as BA interacts with cis-diols on the G-quadruplex and amines on aminoglycosides via a dynamic iminoboronate as demonstrated in figure 9. Through structural manipulation it was discovered that the removal of BA, Ami, or G/K^+ from the formulation disrupts self-assembly and prevents gelation, indicating the important roles each component has in self-assembly. As a result of having multiple dynamic interactions in the gel system, it exhibited stimuli responsiveness towards heat, acid, glucose and hydrogen peroxide. The stimuli responsive hydrogel also displayed good antibacterial activity in vitro and in vivo[52].

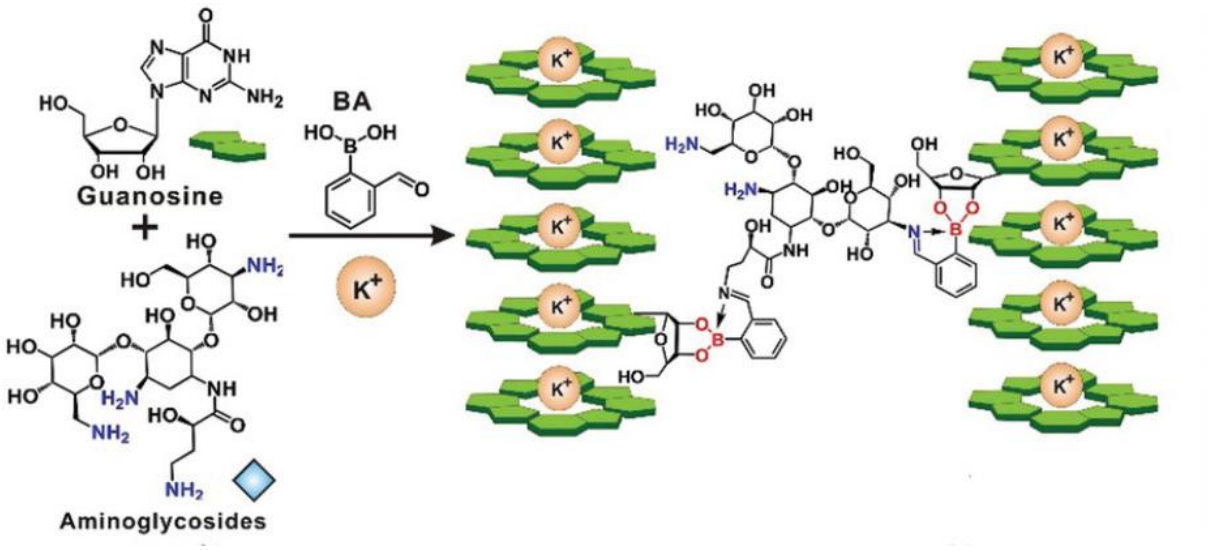

Figure 9. Self-assembly of Aminoglycoside hydrogel assembled from guanosine, K+, aminoglycoside, and a bifunctional anchor BA. The hydrogel is formed by a combination of supramolecular assembly and iminoboronate chemistry. Adapted from reference 55[55].

In another study, a series of gelators based on the nucleoside analogues gemcitabine and lamivudine were synthesized by Skilling et al (Figure 10)[53]. The gemcitabine core contains

hydrogen bond donor and acceptor groups and a pyrimidine base allowing for π- π stacking, while the alkyl groups decrease aqueous solubility and promote the solvophobic forces necessary for gelation under aqueous conditions. Alternating chain lengths provide varying degrees of hydrophobicity. Hydrogels were formed by gemcitabine amide, carbamate, and urea derivatives and the lamivudine amide derivatives. Conversely the ester derivatives gave poor gelators, possibly due to steric hindrance cause by the position of the acyl group. Slight structural changes presented materials of different characteristics. characteristics. Several gels exhibited potent activity toward MIA PaCa-2 and MKN-7 carcinoma cell lines. The gels showed promising applications in localised drug delivery[53].

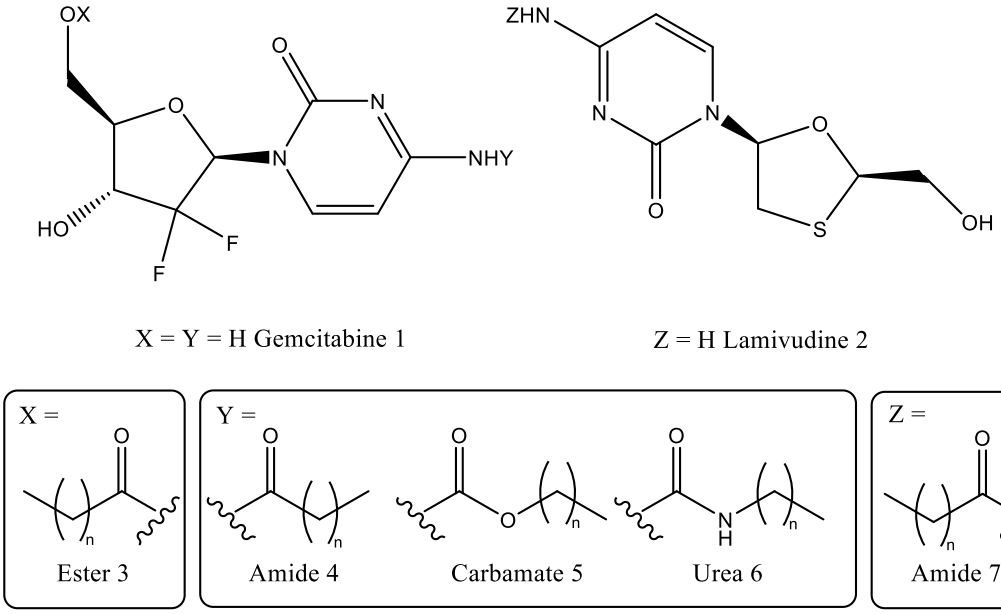

Figure 10. Proposed derivatives of gemcitabine 1 and lamivudine 2[57].

Cytidine based hydrogels were prepared by attaching arylboronic acids to cytidine, that are stabilised by silver acetate. $C^{+}{\cdot}C$ and $C{\cdot}Ag^{+}{\cdot}C$ base pairs collectively take part in the formation of the hydrogel, in which they stack upon one another, together with π–π stacking interactions of aryl rings, forming fibre like aggregations that entrap water to generate hydrogels[54]. Gelation was relatively slow with gels forming after two days. The concentration of Ag^{+} determined gel stability with the most stable gel containing 0.5 equivalents of Ag^{+} with 1 equivalent of cytidine and phenylboronic acid respectively. Reducing/increasing this

concentration of Ag^+ led reduced stability or precipitate. The self healing properties of the gel were confirmed through rheological studies, physical stimuli like mechanical shaking and stirring, and morphological investigation using AFM and TEM techniques. The gel also exhibited antibacterial activity against gram-positive and gram-negative bacterial strains including E. coli, P. aeruginosa, K. pneumoniae, and the multidrug resistant strain M. morganii[54].

In summary, nucleobases make effective gelation systems because they combine flat stackable units with high hydrogen bond potential, while the presence of the 5-membered sugar ring provides further potential for interactions, either through hydrogen bonding, or reaction to form boronate esters. The studies presented demonstrated the need for particular care when altering the structure of the gelator as key functional groups provide a major impact on the properties of the gel system. Furthermore, the biocompatibility of these systems gives them considerable potential for use in biomedical applications.

1.2.3 Amino Acids

Peptides and amino acids are essential biomolecules in living systems. In the case of amino acids and peptides that self-assemble into gels, they very often have amphiphilic structures. These molecules typically aggregate or create micelles in an aqueous environment, with the hydrophilic regions facing the water and the hydrophobic regions hidden inside the aggregate. The aggregates can further unite to form elongated nanofibers that then form hydrogels through supramolecular interactions between them. These LMWGs have attractive properties due to their biocompatibility and biodegradability through enzymatic breakdown. The properties of the hydrogels can also be tuned by varying the type, concentration, and sequence of the peptide or amino acid – indeed, as is well known in biological science, peptide sequence determines function, and can allow these molecules to intervene in very specific ways in biological processes. The variation in properties of altering amino acids can also result from their hydrophobicity, aromatic interactions, chain length, charge, polarity and chirality. Most LMWGs based on short chain peptides (2 or 3 amino acids in length) are modified with a large aromatic group at their N-terminal to help induce self-assembly, with groups such as

9–fluorenylmethyloxycarbonyl (Fmoc), naphthalene, anthracene, carbazole or tert–butoxycarbonyl (BOC), being common. Very often, some of the amino acids also have hydrophobic side chains to help further drive self-assembly.

The Fmoc group has been extensively used to promote the self-assembly of amino acids and peptides[55-63]. The first example of an aromatic Fmoc peptide hydrogelator was reported by Vegners in 1995. The Fmoc-Leu-Asp thermoreversible hydrogel self-assembled upon heat exposure. The gel successfully acted as a delivery platform of antigens and activated an antibody immune response upon injection into rabbits[55]. Later work in 2003 by Xu et al, involved the discovery of Fmoc dipeptide hydrogels which exhibited gel to sol transition as a result of ligand-receptor interactions with vancomycin[64]. Leading to 2007, in which spectrometry studies by Ulijin provided a better understanding of Fmoc diphenylalanines self-assembly. It was found that Fmoc diphenylalanine hydrogels form antiparallel β-sheets which interlock via π–π stacking of the fluorenyl groups and phenyl rings[56]. We will discuss these types of molecules throughout the chapter and how their functionality permits their use in different biomedical applications.

The naphthyl group is also a versatile functional group which once added to a peptide can promote self-assembly through hydrogen bonding and π-π stacking interactions with other aromatic groups. Zu's group introduced a Nap-FFGEY hydrogel that can undergo a reversible gel to sol transition via a kinase/phosphatase switch[65]. In the presence of adenosine triphosphate and kinase, phosphorylation leads to the weakening of the self-assembled network as the phosphate groups repel each other leading to a gel-sol transition. The solution can be converted back into a gel through the addition of phosphatase. In-vivo studies demonstrated the subcutaneous injection of the solution into mice led to a 80% successful conversion self-assembled nanofibers[65].

Tuning key components of these molecules and exploring different methods of preparation has led to the introduction of a library of new peptide hydrogels. Das's group demonstrated that by altering the amino acids in a peptide leads to the development of gels with different gelation abilities[60]. This is a result of the intermolecular interactions formed from the different functional groups. The Fmoc amino acid/peptide functionalized cationic amphiphiles were designed to contain an antibacterial agent pyridinium at the C terminal forming a library of antibacterial hydrogels with activity against both gram positive and gram-negative bacteria.

Through structural changes it was found that π−π interactions and hydrogen bonding played a key role in the self-assembly process.

More recently, Arakawa et al demonstrated that Fmoc-dipeptide hydrogels rheological behaviour and morphologies can be influenced by the position and number of methyl groups placed on the α carbons of the Fmoc-dipeptides by α-methyl-L-phenylalanine[66]. Nilsson's group also presented a study on how structural manipulation can alter morphological properties of gels[67]. Fmoc-Phe derivatives were modified with diaminopropane (DAP) at the carboxylic acid, to significantly improve the water solubility relative to the parent Phe derivatives. Gelation was triggered through the addition of sodium chloride. Fluorination of the benzyl side chain of the Fmoc-Phe-DAP analogues enhanced the gelator's self-assembly potential. Morphological studies on Fmoc-Phe-DAP, Fmoc-3F-Phe-DAP, and Fmoc-F^5-Phe-DAP showed that an increase in the degree of fluorination and hydrophobicity of the gelator, leads to a decrease in the ratio of fibres/tapes to nanotubes. Coassembly of Fmoc-Phe-DAP (1) Fmoc-F^5-Phe-DAP (3) hydrogels of a 1:1 ratio produced intermediate morphological results compared to its intermediate gels. The hydrogels are shear-responsive, and their viscoelastic nature are appropriate for delivery by injection. The diclofenac encapsulated gel systems demonstrated sustained delivery of an anti-inflammatory agent for a period of weeks in-vivo[67].

Structure manipulation is the more obvious type of approach to tune the behaviour of hydrogels however studies have shown that the preparation technique also impacts the stimuli responsive gels. Adams group was interested in understanding the variation of reported rheological properties of this class of LMWG's[57, 63, 68]. In one study, they reported that the final pH of the gel played a crucial role in its mechanical properties. Fmoc diphenylalanine (Fmoc FF) gels produced via a pH change gave weaker gels at physiological pH compared to lower pH. Gelation via a solvent switch in which water is added to a solution of Fmoc FF in DMSO, provided gels with higher G' than the latter method. Addition of buffers to these gels also led to rheological variations suggesting that the final pH is a determining factor in the gels performance[57].

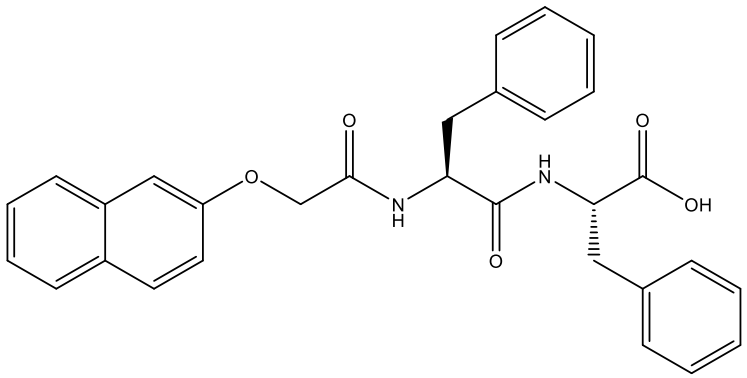

Figure 11. Structure of the LMWG 2NapFF.

In 2017, similar work was presented by the group in which they investigated the effect of using different gelation methods prepared by either gelling in low pH (by addition of either a salt or an acid) or through a solvent switch of a napthyl peptide 2NapFF (figure 11)[69]. The group found that each method formed different fibre arrangements. SEM and confocal microscopy showed pH triggered gels having more uniform distributed fibres with salt triggered gel fibres being less entangled. Whereas solvent switch induced gels had spherulitic domains of fibres. This variation correlates with the rheological studies where in a strain sweep the pH triggered gels were more rigid and broke sharply at low strain while solvent switch induced gels were resistant with G' always being greater than G''. These studies demonstrate how gels can be finely tuned through their method of preparation.

Inspired by this study, Nilsson's group produced a study that focused on the impact of the gelation method on fluorinated Fmoc-Phe derivative hydrogels (Fmoc-3F-Phe and Fmoc-F5-Phe) thixotropic shear behaviour (figure 12)[70]. By comparing two methods of preparation, it was observed that the gel prepared via solvent switch resulted in poorly shear-responsive hydrogels while with the other method (gelation via pH adjustment) resulted in a hydrogel with ideal shear-responsiveness. This may be explained through the mechanism of assembly, as the rate of gel assembly varies with both techniques – it only takes 3 minutes for gelation to occur via solvent switch, but 12-24 hours through a controlled pH change. Fast gelation leads to a cross-linked fibril network that exists in a kinetically trapped state. Precipitation is the more thermodynamically-stable state after the application of shear forces than the kinetic hydrogel. Conversely the slow gelation induces a more stable network hindering precipitate formation. It is worth noting that only TEM images of the gels were compared in the study to

dismiss the role of fibre dependent properties. Nevertheless, the study showed that altering the method of preparation can be a tool to manipulate a gels properties for a desired application[70].

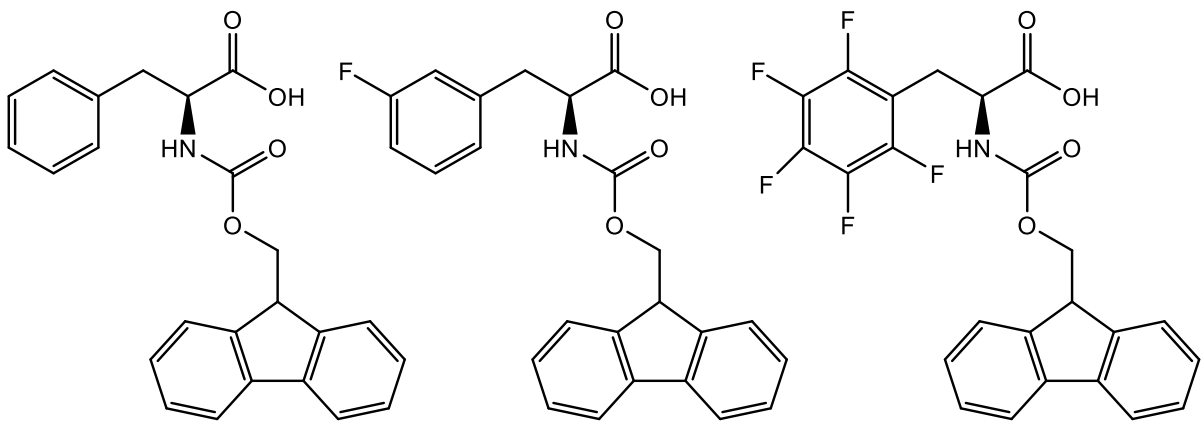

Figure 12. Chemical structures of Fmoc-phenylalanine derivatives[74].

Finally, altering gel behaviour can also be obtained through combining multiple gels with unique properties to form multi-component gel systems. Ujilin's group found that structural manipulation of ultra short peptides led to the formation of gels capable of hosting different cell cultures[71]. This was achieved by altering the amino acid of *n*-protected Fmoc amino acids (Lysine, serine, and glutamic acid) and combining them with Fmoc-diphenylalanine (Fmoc-F_2) respectively to form a co-assembled hydrogels (Fmoc-F_2 and Fmoc-F_2/X where X = Fmoc-lysine (K), Fmoc-serine (S), Fmoc-glutamic acid (D)). Co-assembly did not increase the rheological robustness of Fmoc-F_2 but in fact lowered G'. A live-dead staining assay indicated that all produced gels supported the viability of bovine chondrocytes. Fmoc-F_2/D also supported human dermal fibroblasts. While Fmoc-F_2/S supported all three cells - chondrocytes, 3T3 fibroblasts and Human dermal fibroblasts. The study provides another strategy to discover hydrogels with more suitable surfaces for specific cell types[71].

Bercea's group reported hydrogels co-assembled with two Fmoc amino acids – Fmoc-Trp-OH and Fmoc-Lys-Fmoc-OH. Altering the ratios of gelators in the gel network influences the

stability and rheological properties of the gel. Higher volume ratios of Fmoc-Lys-Fmoc-OH led to more stable gels[72]. The group later introduced an Fmoc-peptide (Fmoc-Lys-Fmoc) to various amino acids (Fmoc-serine or Fmoc-glutamic acid) and a tripeptide (Fmoc-Gly-Gly-Gly) to produce a range of co-assembled hydrogels. Fmoc-Lys-Fmoc functional groups enhance co-assembling because it possesses two fluorenyl groups and an additional –CO-NH group, which can partake in the formation of additional hydrogen bonds, promoting the formation of cross-linking bridges with other amino acids. Co-assembly enhances rheological performance through π-π stacking, multiple hydrogen bonding, and van der Waals interactions. Characterization of co-assembly was assessed by combining different characterization techniques - DLS, FTIR, SEM microscopy, fluorescence, rheology, and thermal analysis[61].

Overall, amino acid/peptide hydrogels are excellent gelators that can offer great tunability. Research has focused on tuning properties via structural manipulation, the method of preparation, as well as forming multicomponent gel systems to enhance gel systems and improve their properties for specific applications.

1.3 Biomedical Applications of Hydrogels

1.3.1 Drug delivery

The versatility of gels allows them to potentially be used to transfer cargoes (drugs, peptides, antibodies) to their target organ sites[73, 74]. The system can act as a barrier to protect the drug from degradation (from enzymes and different pH environments) and therefore improve its handling and applicability. It can also improve the solubility of a drug as well as control drug release kinetics[75, 76]. Hence, when using gel formulation, it is possible to improve drug efficacy and bioavailability. Furthermore, the biocompatible and biodegradable qualities of gels make them an advantageous platform compared to some other delivery vehicle materials. These applications are dependent on the structure of the gelator, which controls stimuli responsiveness, solubility, and non-covalent interactions. Researchers have utilized these characteristics to use LMWGs as drug delivery systems for several areas of therapy.

An example of how LMWG's unique properties can improve drug delivery applications is demonstrated by Cienfuegos's group[77]. One of the major issues for many hydrogel formulations that restricts their clinical use as protein delivery systems is the preservation of a protein's native structure. The crystalline protein form not only improves stability but can exhibit benefits such as ease of handling, higher concentration doses per volume than in their soluble format, and varied dissolution rates. The group created a hydrogel-based method that can enhance the stability of insulin and modify its release profile. Fmoc-AA and agarose were used as platforms for protein crystallization. The hydrogel material is occluded inside the grown crystals which gives rise to composite protein crystals[77]. Both composite insulin crystals displayed greater stability than insulin in solution, with crystals grown in Fmoc-AA hydrogels being stable up to 60°C during a 24 h period. The dissolution rate of Fmoc-AA peptide was slower than the rate of release from the polymer agarose hydrogel. This is due to the non-covalent interactions (hydrogen bonding and π–π interactions) involved between the peptide and protein and indicates how LMWGs can achieve different outcomes to those that might be possible with a more standard polymer gel[78].

There are different modes drugs can be included within gel systems as described in figure 13. The relationship between the drug molecule and the mesh network of the gel directly impacts the drug release profile from the hydrogel. Rapid or burst release of a drug is usually acquired when drug molecules float in between gel fibres with little to no interaction. Release is a result of diffusion with the drug having no effect on the gel system.

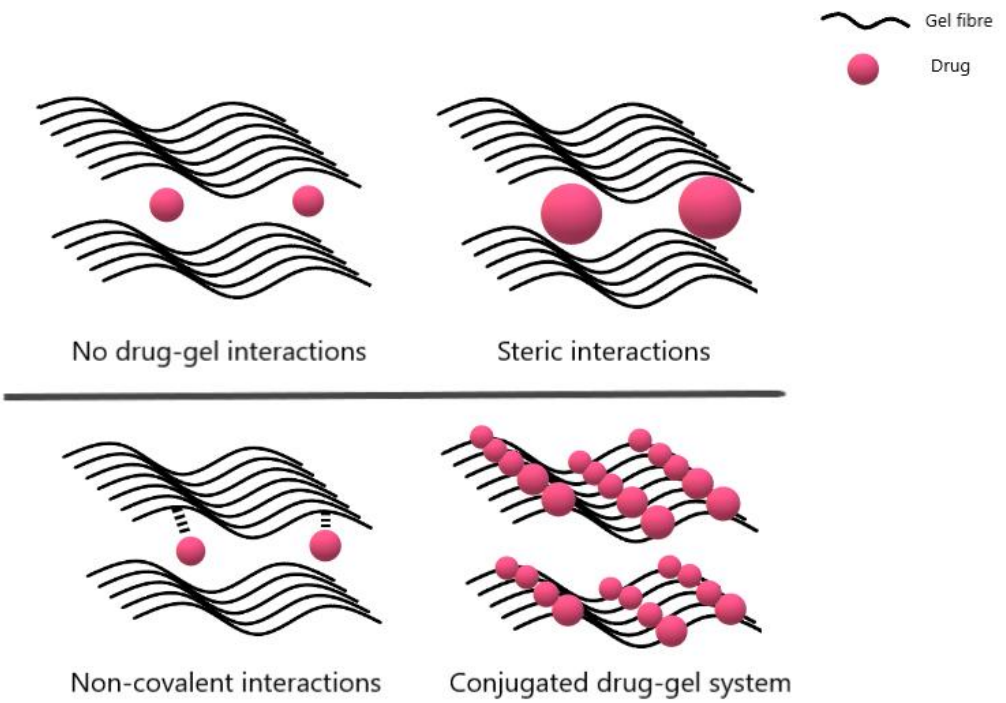

Figure 13. Illustration of the type of interactions involved between gel fibres and drug molecules.

Drug size is also a contributing factor in drug release profiles. Steric interactions between a drug and gel fibres provides more control. This happens when the drug has a similar size to the mesh pores of the gel. The drug is somewhat trapped within the network preventing its rapid release when administered. This was the case in a study conducted by Zhang's group where proteins of various molecular size were encapsulated and released from an acetyl-(Arg-Ala-Asp-Ala)4-CONH2 [Ac-(RADA)4-CONH2] peptide hydrogel[79]. The study demonstrated that the release profile was based on two factors, one of which is the size of the protein with the order of the fastest release rate achieved by the smallest protein – Lysozyme > Soybean trypsin inhibitor > BSA > IgG. The larger the molecule the more difficult it will have leaving the gel system. The second factor was the density of the peptides nanofibers, the more complex the fibre entanglement meant greater difficulty for the proteins to be released. As demonstrated by the group, increasing the concentration of the peptide led to a reduction of protein release[79]. This is a great strategy that could be used to control the drug release rate depending on the application, however it is difficult to determine the size of the pores.

Controlled and sustained release of therapeutic agents is an important tool in therapy. Particularly with chronic illnesses in which drug administration is needed multiple times throughout the day. It reduces the risks of infection, improves compliance, and overall makes treatment much easier for the patient. Sustained release can occur with hydrogels when drugs and gel systems have interactions involved between them such as hydrogen bonding, electrostatic bonding, etc. This involvement hinders and slows down the flow of the drug out of the gel system. The drug remains fixed within the pores as displayed in figure 13.

An example of this is demonstrated by Friggeri et al in which a N,N'-dibenzoyl-l-cystine (DBC) hydrogel was tested to encapsulate and release the drugs 8-aminoquinoline (AQ) and 2-hydroxyquinoline (HQ) respectively[75]. Both drugs displayed interactions within the gel network, the amine group of AQ forms an acid-base interaction with the carboxylic group of the DBC hydrogel, while HQ can form interactions via weaker hydrogen bonding or van der Waals interactions with the network. Drug retention was greater with AQ with the release being slower by 7 folds compared with HQ. The stronger interaction slowed down the release of the drug molecule and provided controlled drug release.

Another type of controlled release can be acquired when the drug is chemically bound to the gel system through covalent interactions. The drug is released by gradual drug cleavage through which the gel degrades as a response to a stimuli (pH, chemical reaction, enzymes, light). This type of system is particularly useful when targeting specific organ sites for treatment.

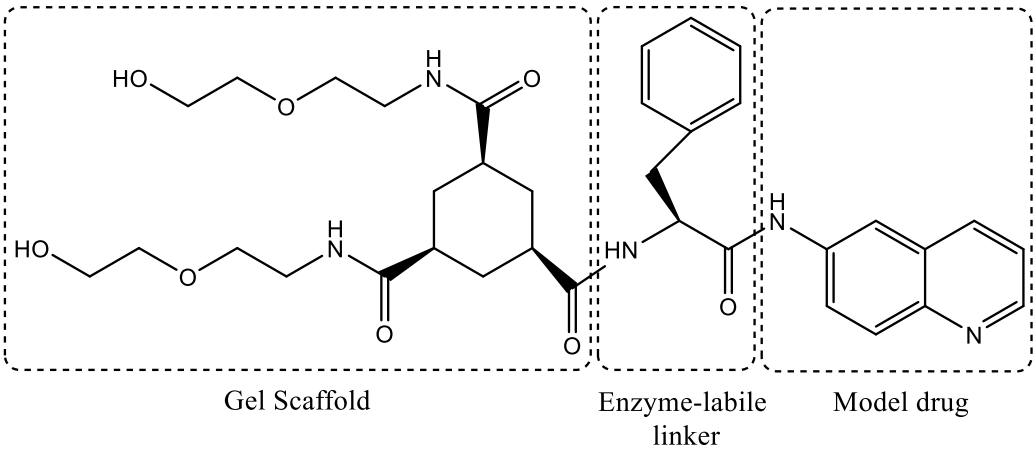

Figure 14. Design of the enzymatically cleavable LMWG capable of releasing 6-aminoquinoline.

Esch's group conjugated the drug aminoquinoline (6-AQ) to a LMWG system[73]. The design involved the coupling of L-phenylalanyl–amidoquinoline (L-Phe–AQ) and two ethylene glycol chains to a cyclohexane trisamide gel scaffold. The enzyme α-chymotrypsin (α-chy) can cleave L-phenylalanyl–amidoquinoline (L-Phe–AQ) to release the drug aminoquinoline (6-AQ). However, by being incorporated into the gel fibres the 6-AQ drug was protected. Gel to sol transition through temperature elevation (25–45°C) led to fibre breakdown and hence molecular exposure to the enzyme led to cleavage increasing the rate of drug release. Although drastic temperature elevation is not a realistic stimulus to occur in the body, the example demonstrates how the gels responsive behaviour could be used to control drug release. This approach of incorporating drugs into gel systems provides protection from biological processes and therefore delivers drugs to the target site where maximum release is achieved.

Localised delivery of therapeutic agents is an excellent approach used to provide a high drug dose to the desired target while dodging systemic side effects and improving patient compliance. Localised drug delivery can be employed to target certain regions in the body such as the skin, eyes, brain, tumour sites, etc. Hydrogels have been explored in this area due their unique properties in which researchers exploit for different areas of treatment.

For example, Pérez-García's group investigated the topical use of a thermoreversible hydrogel for the treatment of rosacea[80]. The hydrogel was formed by a cationic bis-imidazolium based amphiphile. Cationic and neutral drugs (Brimonidine tartrate, betamethasone 17-valerate, and triamcinolone acetonide) were successfully incorporated into the gel system pre-gelation. The researchers were surprised to find the insignificant role of the drugs charge in the systems loading ability as NMR studies indicated a relatively high incorporation of the drugs within the gel network. The gel demonstrated excellent loading abilities of the drugs that comply with standard dosing. SEM images showed how each drug influenced the structure of the gel fibres promoting the idea of drug involvement in the network. Frequency sweep tests of the drug loaded gels gave G'> G'', with triamcinolone loaded gel having insignificant changes to its G' while the remaining drug-loaded gels were softer by 4 folds. All of which are suitable for dermal application. The gel permitted faster drug permeation than commercial products. It also promoted retention of the drug within the skin which is ideal as it can provide a sustained release activity. In-vitro studies which simulate those in the skin-permeation experiments

showed a faster release profile of the drugs compared to commercial products. Furthermore, in-vivo studies on a rosacea rabbit model in which erythema was measured using a skin colorimetric probe demonstrated the efficacy of the gel loaded with brimonidine and triamcinolone respectively. While betamethasone gave insignificant results. The gel system shows promise in its use for the treatment of rosacea and possibly other chronic skin conditions[80].

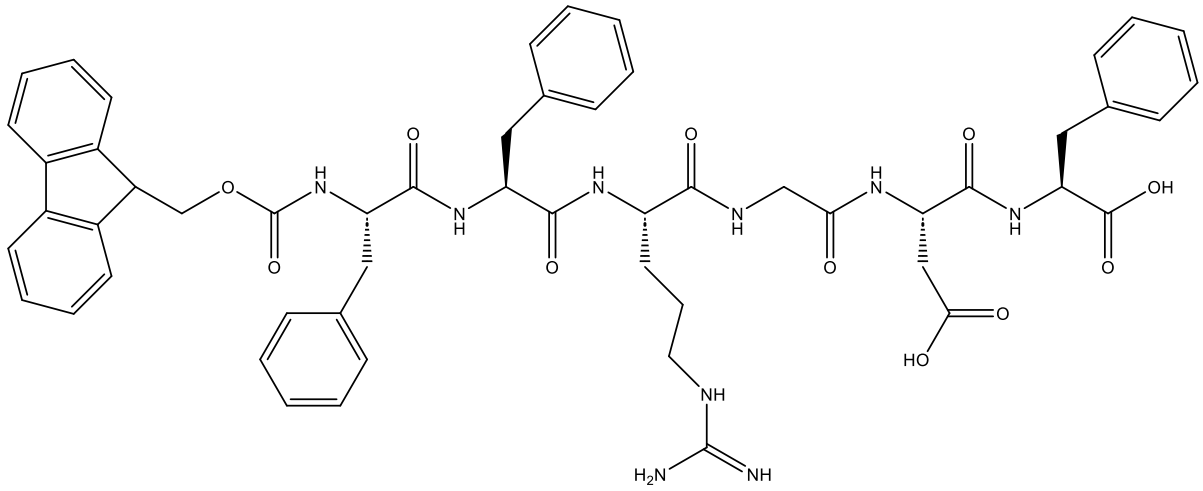

Figure 15. Structure of FMOC-Phe-Phe-Arg-Gly-Asp-Phe.

Hydrogels can also be advantageous in ocular delivery. Despite the success of treatment, ocular drug delivery has its limitations as these formulations undergo rapid drug clearance as a result of biological clearance mechanisms such as blinking and tear flushing. There is also the hurdle of passing through protective physiological barriers (The corneal barrier, blood-retinal barriers, and blood-aqueous humour)[81, 82]. All of which lead to poor bioavailability resulting to the need of frequent dosing and thus increasing potential risk of toxic side effects. Hydrogels viscous, thixotropic, and biocompatible properties can be beneficial in this line of treatment. As the gel could be injected/inserted into the eye and improve residence time of the drug. The viscous nature of the gel can provide targeted delivery and prevent the spreading of the drug to neighbouring tissue. Xu et al. developed a self-assembling hydrogel composed of a peptide backbone containing an Arg-Gly-Asp (RGD) sequence and a Fmoc tail[83] as shown in figure 15. The biocompatible gel was designed to be used as an ocular implant for the sustained release of the drug 5-flouracil (5-FU). 5-Fu injections are frequently administered in the eye via subconjunctival injection post-surgery to prevent scleral flap

fibrosis. The injections are uncomfortable and expose surrounding ocular tissue to the drug, leading to conjunctival and corneal epithelium toxicity. In-vivo studies conducted on rabbits eyes demonstrated the gels capability of delivering the drug locally via a sustained release profile. This in turn prevented the toxicity against surrounding ocular tissue while providing sufficient drug loading to the target site. The gel provided superior efficacy compared to conventional 5-FU exposure making it a suitable candidate for the prevention of postoperative scarring formation[83].

Another design strategy is transforming a drug into its own delivery system. This approach removes the need for additives and permits the release of the drug through the degradation of the gel system. Yu et al. formulated a hydrogel that presents controlled release of ibuprofen into the eye for the topical treatment of anterior uveitis[84]. The gel design consists of ibuprofen conjugated to a GFFY peptide via a cleavable ester bond linkage (hydroxybenzoic acid). This type of design permitted the slow release of the drug via esterase exposure without compromising the biological activity of ibuprofen. In-vivo studies showed that the hydrogel was cytocompatible and had excellent ocular biocompatibility. Despite ibuprofens lower anti-inflammatory efficacy than diclofenac, 0.3% (wt/vol) of the hydrogel had similar therapeutic efficacy to that of the clinical product 0.1% (wt/vol) diclofenac eyedrops in a lipopolysaccharide-induced rabbit uveitis model. With both the diclofenac eyedrops and hydrogel treatments decreasing IL-6 and TNF-α production dramatically[84].

In another study, Li's group turned the steroidal drug dexamethasone into a prodrug hydrogel (succinated dexamethasone) which gels via pH hydrolysis[85]. The thixotropic hydrogel was instilled into the lower conjunctival sac of a rabbits eye without causing irritation. In-vivo release studies indicated that the viscous nature of the hydrogel improved drug bioavailability compared to dexamethasone solution by providing improved corneal permeability and reduced drug clearance. And finally, in-vitro stability tests, demonstrated that the lyophilized hydrogel possesses excellent stability in storage at −20°C up to 30 days. Hydrogel ocular delivery systems may have great prospects in the advancement of ocular treatment.

Cancer is the highest cause of morbidity and mortality rates worldwide. Treatment involves multiple methods including chemotherapy, radiotherapy, immunotherapy, and their combinations. Although they have been successful to some extent, treatment is an exhaustive procedure due to the associated complications and side effects. Complications and side effects

arise, as high doses are required for sufficient bioavailability to be reached which results in poor cell targeting and elevated toxicity. Ongoing research is focusing on improving treatment by enhancing drug bioavailability, therapeutic index, drug tolerance, and targeted cytotoxicity. Hydrogels have been explored for their use as platforms for these chemotherapeutic cargos, with the aim of delivering the drugs without eliciting toxicity towards healthy cells and improving bioavailability leading to the ability to apply lower drug concentrations of the antineoplastic agents[86].

Strategic design is essential in the development of hydrogels for such localised delivery. LMWG's tunability is key as researchers can manipulate the gel according to the targets environment, as shown in the study by Zhong's group. By incorporating a non-steroidal anti-androgen drug (Bicalutamide (BLT)) through a cleavable ester bond with the lysine residue of a indomethacin-Gly-Phe-Phe-Lys-Glu-His gelator, a smart drug releasing reservoir was produced (ID-1-BLT)[87]. The gel can self-assemble with the assistance of zinc ions which are abundant in prostate cancer environments[88]. Once in the cancerous region the weakly acidic environment triggers disassembly of the fibrous network due to the protonation of histidine, that in turn disrupts the coordination interactions between histidine and zinc ions. This is followed by the internalization of nanofibers into tumorous cells where carboxylic-ester hydrolase (CES) cleaves the ester bond between ID-1 and BLT, activating BLT's chemotherapeutic activity. In-vitro drug release studies at pH values of 7.4, 6.5 and 5.5 demonstrated a higher release rate in the order of 5.5 > 6.5 >7.4. This is quite favourable as tumours tend to have acidic environments. A sustained release profile was achieved with the ID-1-BLT over 96 hours in the prostate gland of rats (Figure 16), in contrast to the rapid clearance (4 hours) if a simple BLT aqueous solution was injected[87]. The selective cytotoxicity of ID-1-BLT in a human-derived prostate cancer cell line DU145 was measured by using a MTT assay. The hydrogel provided improved selective cytotoxicity towards prostate cancer cell DU145 over normal fibroblast cell NIH3T3, compared to BLT alone.

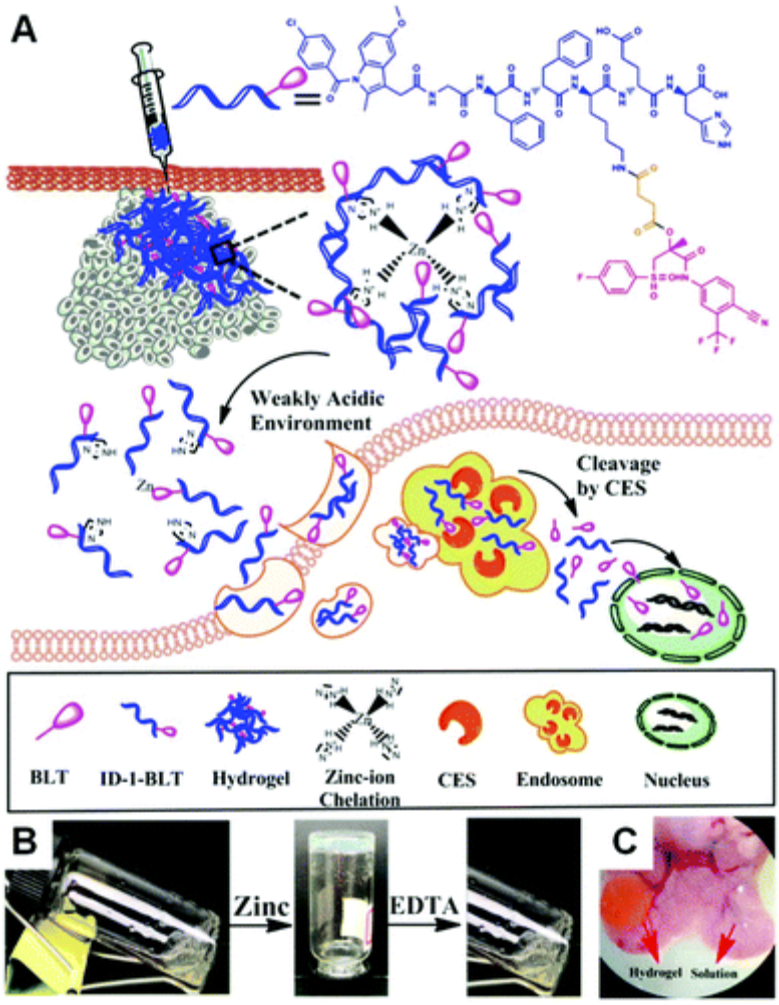

Figure 16. A) Schematic illustration of ID-1-BLT hydrogels acting as a drug depot for cancer treatment. B) optical images of sol–gel transitions of ID-1-BLT with zinc ions (0.27 equiv.) and EDTA (0.20 equiv.). C) intra-gland injections of ID-1-BLT spiked with dox orubicin (right) at the prostate site for 2 h. Adapted from He, S.[87]

CD8+ cytotoxic lymphocytes (CD8+ T) cells are anti-tumour cells which directly recognise and breakdown antigen-presenting tumour cells while inducing systemic immune responses[89]. Inosine promotes the proliferation and function of $CD8^+$ T cells and enhances programmed cell death protein ligand-1 (PD-L1) blockade therapy. Unfortunately, high doses of inosine and an immune checkpoint inhibitor (anti-PD-L1 antibody (aPDL1)) are needed for immunotherapy due to their low bioavailability. Zhao's group employed an inosine-based hydrogel, inosine-phenylenediboronic-isoguanosine (IPBisoG), linked via reversible borate ester bonds.[90] The hydrogel can successfully encapsulate aPDL1 to achieve dual release of the two biological agents. The self-healing hydrogel displayed biodegradability, biocompatibility, and stability. Injected into mice, the IPBisoG hydrogel acted as a reservoir of inosine and

aPDL1, providing a gradual release to the tumour site. In-vivo studies demonstrated the gels efficacy in enhancing PD-L1 blockade therapy. The gel has promising prospects for tumour-local immunotherapy in the future.[90]

Chen's group designed an isoguanosine-borate-guanosine (isoGBG) supramolecular hydrogel in which guanosine and isoguanosine are linked with reversible and dynamic borate ester bonds[91]. This design was an advancement to their previous work[92] in which an injectable hydrogel was made with guanosine (G) and isoguanosine (isoG) in the presence of K^+. The guanosine (G) and isoguanosine (isoG) hydrogel displayed anticancer activities and injectability, but had a short lifetime stability[92]. This led to the development of the isoguanosine-borate-guanosine (isoGBC) gel system with a dynamic borate ester bond which displayed excellent stability and self-healing properties as well as good biocompatibility and degradability. The boronic acid reversibly reacts with the diol and hence provides the gel with its self-healing mechanism. The isoGBG hydrogel's demonstrated anticancer activity in OSCC cells in vitro and in vivo. Figure 15 represents the self-assembly of the system with isoGBG 4-quartet stacking and its local injection to induce tumour cell apoptosis. The hydrogel displays dual functionality in which it combines a drug delivery platform and an anti-cancer compound in one system[91].

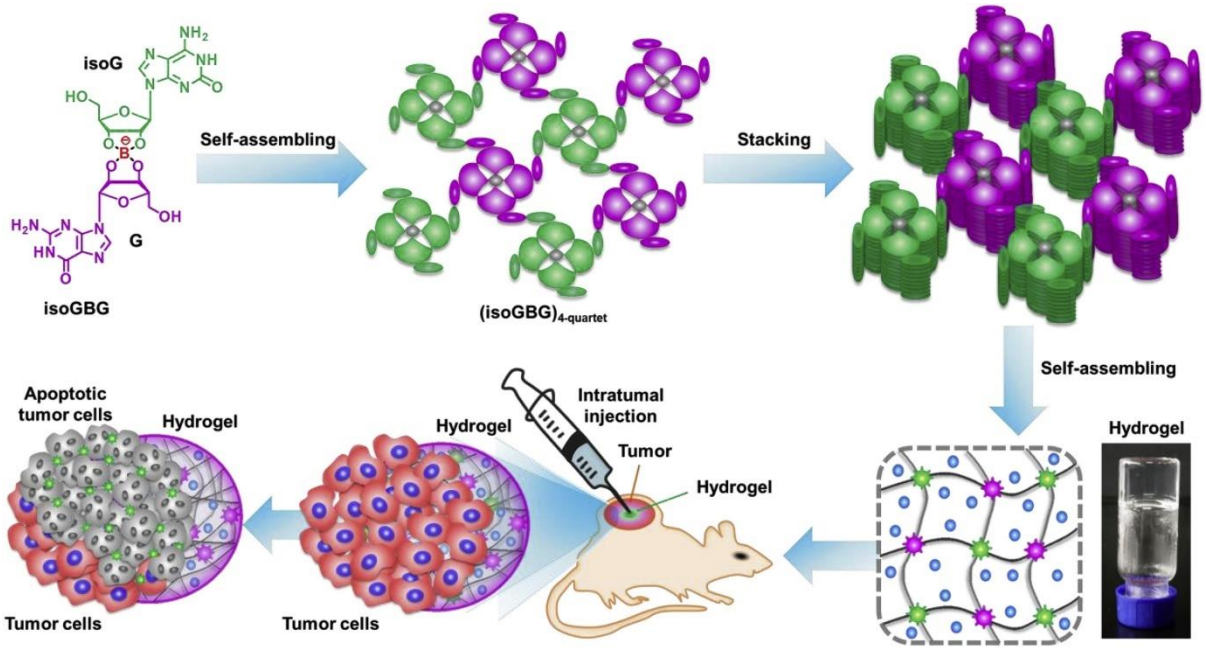

Figure 17. Schematics of the self-assembly of isoGBG hydrogels and its administration as an intratumoral injection for cancer therapy. Adapted from reference 53[53].

Overall, hydrogels are excellent candidates for drug delivery and their on-going development may soon greatly improve common problems associated with this field. We explored the different mechanisms drugs can be encapsulated into gels which results in various release profiles (ex. Rapid and Sustained release). We also discussed studies utilising hydrogels for localised delivery in which their properties can increase drug uptake and prevent systemic side effects.

1.3.3 Tissue Engineering

In vivo tissue engineering requires three-dimensional constructs that can be implanted into the body to substitute or repair diseased or damaged tissues. These structures are typically constructed using cells and biomaterials. Tissue engineering involves a number of steps, such as cell selection and isolation, the creation of a scaffold or matrix to support the cells and direct tissue formation, and the use of biochemical and physical cues to encourage the cells to grow and differentiate into functional tissue. The tissue can be implanted into the patient and integrated with the surrounding tissues after it has been engineered to re-establish normal function. It offers a potential solution to diseases that cannot be treated with conventional methods.

Hydrogels are ideal scaffolds for cell attachment and growth[93-95]. The soft nature of the hydrophilic self-assembled material mimics the properties of tissues and the extracellular matrix,[96] providing a similar environment for the cells to flourish and differentiate. Gels can also be tailored to obtain certain physical and chemical properties such as stiffness, shape, etc. for specific types of tissues.

Interesting work by Zhang and co-workers involved the use of a peptide hydrogel to promote the reconnection of an injured optic tract in the midbrain of a hamster[97]. Unlike other materials the injected gel can fill in the irregular shaped void as a solution and then assemble to form a gel in the shape of the gap. This is a great example of how gels unique properties

can be utilised for specific applications. The close contact between the nanofibers and the extracellular matrix promotes self-healing. The study demonstrated the peptide gels ability to regenerate the optic tract by knitting together tissue in the mammalian central nervous system and return the hamsters vision. The gel was also found to be almost completely excreted within 3-4 weeks[97]. Stupp et al designed a system that contained high-epitope density nanofibers by conjugating a pentapeptide epitope isoleucine-lysine-valine-alanine-valine to a peptide amphiphile hydrogel[98]. The pentapeptide epitope promotes the growth of central nervous system cells. The nanofibers present an artificially high density of epitopes to the surrounding cells compared to the extracellular matrix to encourage an intense signal presentation to cells leading to faster cell differentiation. The pentapeptide epitope was in direct contact with the tissue leading to the growth of large neurites within a day. Besides acting as a mechanical supportive matrix the gel is made up of 99.5 wt % water, and can therefore act as a medium for soluble factors and the migration of cells.

A recent study by Li et al involved the synthesis of three tripeptide hydrogels by coupling 4-biphenylacetic acid (BPAA) with tripeptides[99]. Altering amino acid arrangements of the tripeptides led to hydrogels that can be triggered through different stimuli, with one capable of being triggered by all methods - temperature switch, ion induction and pH switch respectively. Cell viability tests demonstrated the ability of BPAA-βAFF and BPAA-FFβA hydrogels to support cell attachment and spreading with more than 80% of L929 cells surviving after 72 hours with an MTT assay. BPAA-βAFF was chosen for further tests as it had a more appropriate gelation time and lower MGC. To explore cartilage repair, chondrocytes were encapsulated and were investigated in-vitro for a duration of 21 days. Live/dead staining showed spreading of a large number of chondrocytes and an increase of chondroid matrix surrounded by round cells. SEM confirmed typical round chondrocyte morphology. Further studies confirmed an increased secretion of collagen and glycosaminoglycan. This suggested that the hydrogel can contribute to hyaline cartilage formation. The hydrogel has a promising future in cartilage engineering as it can promote chondrocyte proliferation as well as specific matrix secretion, and facilitates the phenotype maintenance of hyaline cartilage[99].

Cell compatibility with a hydrogel platform is essential for the cells to attach and proliferate. In a study by Najafi et al. Fmoc-phenylalanine-valine was investigated as a 3D platform for the

cultures of WJ-MSCs (mesenchymal stem cells), HUVECs (primary cells), and MDA-MB231 (tumour cell line)[100]. After 72-hour incubation, the hydrogel gave a cell type-dependent growth with the HUVEC and MDA-MB231 cells exhibiting fewer cell deaths than for WJ-MSCs as these stem cells had a low cell–matrix attachment. These results were in line with an alamar blue essay in which cell proliferation was greater with HUVEC and MDA-MB231, and was confirmed in the MTT cytotoxicity assay where a concentration dependent toxicity was acquired with all cell lines but significantly more with WJ-MSCs[100]. This demonstrates that achieving stem cell growth in biomaterials can be particularly challenging as these cells are less robust than cancer cell lines. It is therefore important to assess reports of cell growth in gel materials critically bearing this in mind.

Growing specific cells requires unique biomaterial characteristics with each cell needing special types of environments to thrive. Rheological properties of hydrogels must be customised for each cell type to promote its growth for example, Hu et al demonstrated this by seeding mesenchymal stem cells (MSc) on the surface of phenylboronic acid derivatives with different rheological stiffness[101]. It was found that the gels that mimic bone stiffness with higher rigidity (G′ 20–60 kPa) directed MSCs to differentiate into osteoblastic cells, while chondrocytic differentiation was achieved with softer gels that mimic cartilage rigidity (G′0.1–10 kPa)[101]. Therefore, tuning stiffness can be a valuable tool in achieving particular cell growth and must be considered with the use of hydrogels for tissue engineering. Stupp's group focused on the development of peptide amphiphiles rheological properties by playing with the amount of valine and alanine moieties in the system for potential regenerative medicine use. It was found that additional valine molecules in the structure led to increased stiffness on the contrary addition of alanine produced softer gels. The study exhibits how hydrogels offer ease of tunability for this application[102].

In 2020, Godbe et al. investigated the tuning of rheological stiffness of an anionic peptide amphiphile nanofibers using oligo-l-lysines to act as an extracellular matrix for the growth of neural cells (figure 16)[103]. By altering the chain length of the Oligo-l-lysine (Kn) structure, it was found that adding a single lysine unit to the oligomeric gelator increases G' by 10 Pa. This exact control of 3D gel stiffness without altering other significant factors may provide an essential tool for enhancing the function, phenotypic, and outgrowth of dopaminergic neuron

transplants, important in terms of utilising hydrogels for the treatment of Parkinson's disease[103].

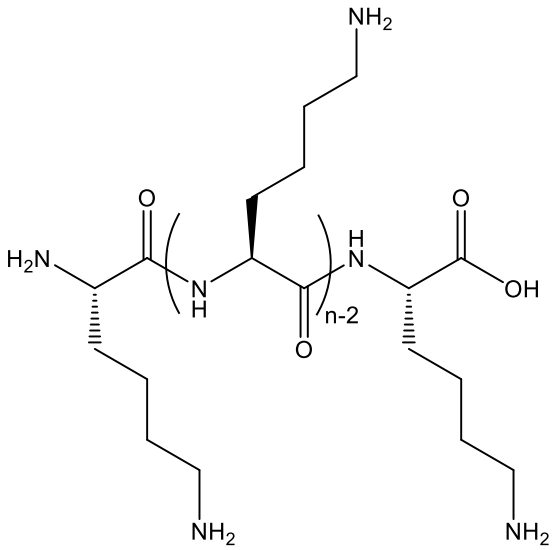

Figure 18. Chemical structure of Oligo-l-lysine (Kn)[134].

Besides altering the nature of LMWG's to tune the gels stiffness, an alternative method can be used in which the LMWG can be combined with polymer gels. Our group has produced multicomponent gel beads with enhanced stiffness and stability. The fabrication involved the use of DBS-CONHNH$_2$ with gellan gum to produce multicomponent gel beads. The beads had improved resistance against shear strain compared to agarose alone, and overall had higher stiffness as they become two interwoven networks in one system. A cell viability test showed the hybrid beads ability to support mesenchymal cell growth for a period of 21 days. The approach can make a platform suitable for the growth of a variety of cell types[104].

Interactions between gels and biological systems can be a delicate process. Other than changing rheological properties for cell differentiation and growth, other parameters need to be enhanced for gels to act as platforms.

Perez's group tried to enhance the characteristics of their gelator through structural manipulation[105]. The printable guanosine-boric acid hydrogel exhibited sustained cell survival, proliferation, and migration as a 3D platform for tissue engineering. Unfortunately, it had the drawback of short-term stability of at least 7 days in McCoy 5A medium at 37°C limiting its use. The group's hypothesis was that a more stable hydrogel can be acquired by increasing π-

π interactions associated with aromatic groups. However, the opposite was achieved as the new gels not only contradicted the hypothesis but also gave less stable gels in the culture medium with stabilities of 4 hours. This is believed to be due to steric hindrance induced by adjacent groups, preventing the formation of π-π stacking interactions between the added aromatic rings[105]. This demonstrates how it can be challenging to predict *a priori* the way in which LMWGs will behave in biological systems, making it important to perform careful structure-activity relationship studies in each case and avoid assumptions that may be over-simplistic.

Another issue with gel platforms is poor cell adhesion. Tsutsumi's group encountered this with their $(FFiK)_2$ peptide hydrogel containing two diphenylalanine (FF) units interconnected by a urea bond at the centre and lysine residues at each terminus through isopeptide bonds[106]. The pH-responsive hydrogel demonstrated excellent biocompatibility and can be easily produced in large scale. Unfortunately, this gel system had poor cell adhesion needed to stimulate cancer cell growth. To overcome this issue the peptide was conjugated to several bioactive sequences (Figure 20) derived from extracellular matrix (ECM) proteins (Fibronectin and laminin) known for cell adhesion and proliferation.

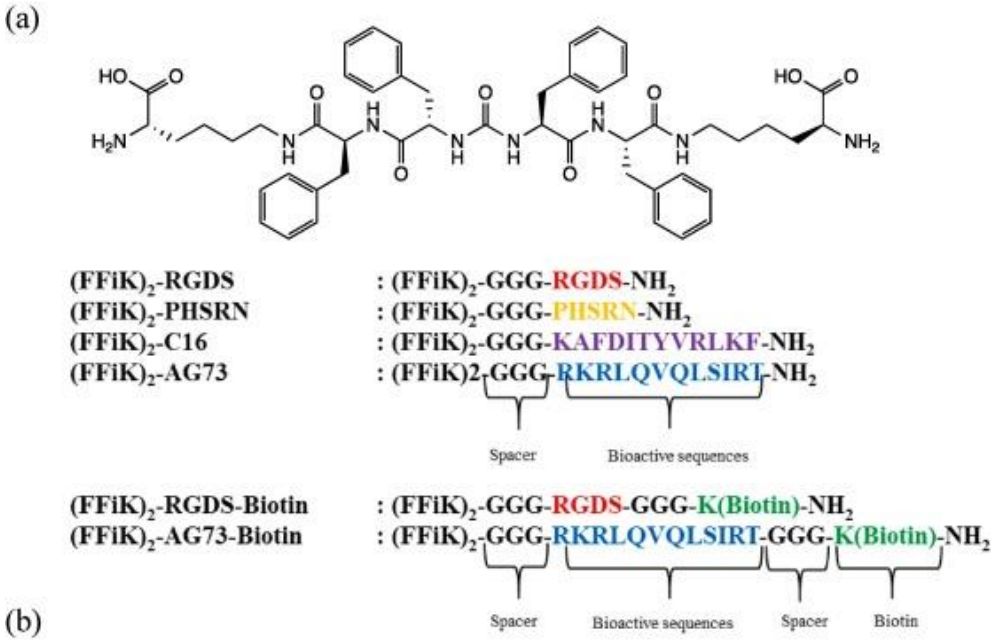

Figure 19. a) Chemical structure of (FFiK)2. b) Peptide sequences of (FFiK)2 derivatives. Obtained from Chia, J. Y.[137].

The gels were then investigated for their gelation abilities and were tested with the breast cancer cell line, MCF-7. The functionalised peptide hydrogels all had excellent stability in the cell culture medium, and all gave better adhesion to the cancer cell line than the $(FFiK)_2$ peptide alone. Spheroid formation was observed with $(FFiK)_2$, $(FFiK)_2$-RGDS, $(FFiK)_2$-C16 and $(FFiK)_2$-PHSRN. $(FFiK)_2$-RGDS and $(FFiK)_2$-PHSRN can therefore be used to control spheroid formation in drug screening. Spheroid formation did not occur with $(FFiK)_2$-AG73, however it was found it can induce metastatic activity of MCF-7 cells which is useful for drug screening tumour cells in their metastatic state. Overall, the study demonstrated how functionalization of peptides can enhance the performance of gels in tissue engineering[106].

The studies presented in this section demonstrate hydrogels ability to facilitate cell growth and differentiation as a result of their resemblance to the extracellular matrix. It also shows how the gels can be structurally altered for specific functions such as altering the rheological properties to induce cell differentiation. Although, the hydrogels do have their limitations they are promising tools for advancing in this field.

1.4 Conclusions and Project Aims

This review highlights different types of LMWG's based on bioderived building blocks and the role of non-covalent interactions taking place during self-assembly. It also discusses the efforts taken to advance the properties of hydrogels for specific biomedical applications, with a particular focus on the use of structural manipulation or the development of a multicomponent system to acquire desired properties. As a result, the rheological stiffness can be altered, the gel can gain thixotropic and shear-thinning properties, boost its stability, and can even become stimuli responsive to certain stimuli - light, pH. Hydrogels are highly tuneable and their biocompatible nature make them ideal in biomedical applications including drug delivery and tissue engineering. In this Introduction, there is a particular focus on reviewing recent progress in these areas.

There has also been a considerable amount of interest in the use of peptides and amino acid-based hydrogels due to their flexibility – antibacterial activity, stimuli responsiveness (enzymes, pH, and light), and self-healing and injectable properties. We will explore the synthesis of simple hydrogelators based on LMWGs developed in York, specifically the amino acid-based two-component hydrogel - Benzyl glutamine. The hydrogel is composed of glutamine amide (containing an alkyl chain) coupled with benzaldehyde via a Schiff base which self assembles in water. By tuning the hydrophilic and hydrophobic domains of the structure, a stronger understanding of self-assembly will be achieved. Those molecules capable of forming gels will be characterised and their properties will be compared to the original hydrogelator to assess whether the exchange of functional groups influences the gelation characteristics. The hydrogel has already been previously investigated for the application of drug delivery by our group. Patterson investigated the use of benzyl glutamine as a delivery platform for the drug levodopa[2]. The design of delivery utilised the self-healing properties of this novel gel by injecting the drug-loaded hydrogel intranasally through which it reassembled in the nasal cavity. This type of localised drug delivery improves bioavailability as a result of two variables. The first is, the nasal route skips the extensive metabolism associated with oral delivery in which most of the drug would be deactivated upon reaching its target. While the second is due to the viscous nature of the gel, in which it resides on the nasal cavity and increases residence time. Rheological studies performed using parallel plate geometry demonstrated that the soft gel breaks at a strain of 12.5 % which was reduced to 7 % upon drug loading. Which is appropriate for forming a thin coating on the walls of the nasal cavity. Further rheological studies involved testing its self-healing properties. Of which, the system managed to recover much of its original performance within 10 seconds. NMR studies indicated that levodopa is mostly mobile within the gel network which corresponds to the rapid kinetic release of the drug. By assisting in retention of the drug in the nasal cavity, the hydrogel limited passage of the drug into the GI tract and enhanced blood and brain uptake of the drug as tested in-vivo on mice. The gel achieved greater uptake into the brain and blood compared to intravenous delivery of an equivalent dose by 4 and 2 folds respectively. It was also found to be significantly more effective than the intranasal administration of levodopa solution[2].

Therefore, it is of interest to further examine the hydrogel Benzyl glutamine for the application of drug delivery. The investigation will involve testing the hydrogels ability to encapsulate drugs of different molecular weights and functionalities. The studies will also involve determining the extent of drug uptake and the kinetics of drug release.

To enhance the shaping and moulding of Benzyl glutamine class LMWGs, two techniques will be applied:

1) Formation of multicomponent hydrogels by introducing polymer gels (alginate and agarose) into the gel matrix.
2) Triggering gelation through a solvent switch directed to form gel filaments and 3D printed gel scaffolds via wet spinning.

The multicomponent hydrogels will be characterised to study the effects of combining two systems with distinctive properties. The gels will be moulded into a variety of shapes and applied in several applications. They will also be tested for their drug encapsulating and drug release abilities compared to the multicomponent gel systems of our groups sorbitol-based LMWG's - DBS-$CONHNH_2$ and DBS-COOH[42, 107].

Wet spinning is a novel exciting approach for self-assembly of filaments and 3D printed gels that may hold a great role in future advancement in biomedical applications. The study will focus on determining the appropriate conditions for this technique on Benzyl glutamine and its derivatives. Creating 3D printed patterns will also be investigated with the Benzyl glutamine gel as well as DBS-COOH. In addition, the study will involve exploring these fabrications in the applications of drug delivery and tissue engineering.

Chapter 2 Synthesis of Glutamine Amide Derivatives

2.1 Introduction

The development of a new gelator through design is quite a challenge. There are various guidelines on how to design hydrogels[108, 109] and theoretically they should work. Actually, however, most hydrogels are found through serendipity. As just one example, during studies on organocatalysis, Hawkins, Clarke and Smith discovered a new gelator based on a simple glutamine amide[110]. This gelator was based on the modification of the glutamine amino acid coupled through its carboxylic acid group with a hydrophobic chain. When the compound reacted through its amine with an aromatic aldehyde it formed effective multi-component hydrogels in situ via Schiff base formation (Figure 21). Self-assembly is mediated through the hydrophobic effect, supplemented with strong directional hydrogen bond interactions between the amino acid head groups. The incorporated interactions complement one another to enable hydrogel formation. In the presence of water, the hydrophobic domain of the amphiphilic molecule is positioned in the core and surrounded by polar groups exposed to an aqueous environment. When sufficient concentration is reached (the minimum gelation concentration, MGC), the molecules aggregate and self-assemble into a hydrogel[111]. The gel was characterized through various techniques to determine its properties including thermal stability, rheological and self-healing properties, NMR, IR, pH sensitivity, etc. The notable characteristics of the hydrogel were its relative thermal stability as well as its self-healing properties which gave it potential applications in *in situ* gel formation and drug delivery.

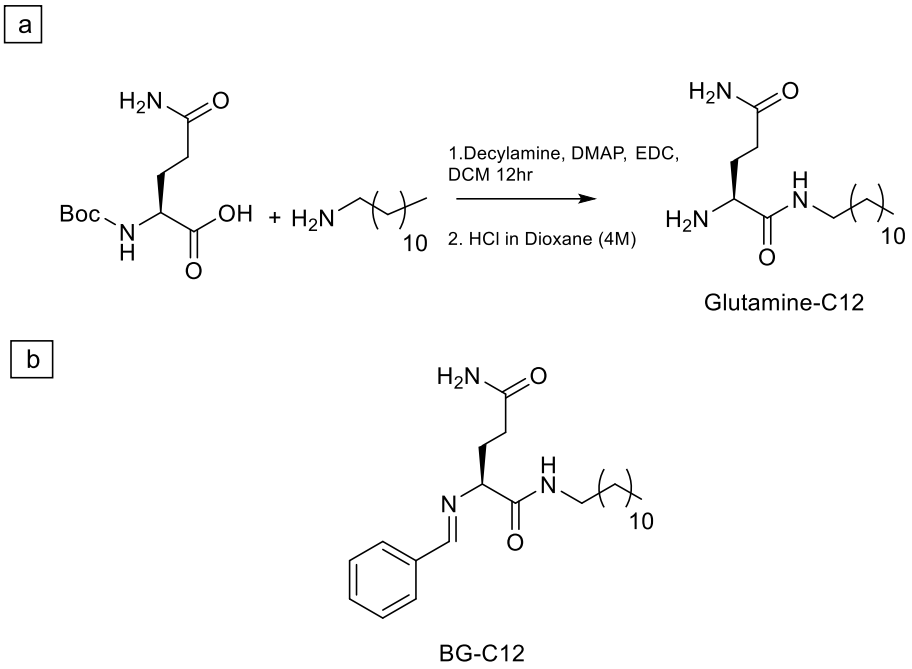

Figure 20. a) Synthesis of glutamine-C12 b) Benzyl glutamine gelator (BG-C12).

The discovery of the novel gelator opens doors to the development of various types of gels. Some unpublished work had previously been conducted on the optimization of the gelator structure. This included some changes to the amino acid and aldehyde regions of the structure. Similar gelator optimisation work has been reported by Willemen who worked on an organogelator composed of cholic acid linked to an alkyl tail[112]. The linker group between those components was varied and a solvent screen was performed with each gelator. The results led to the discovery of a two-component gel and several other one component gels. Furthermore, by characterising each modified gelator and comparing their results, the researchers were able to identify what influences the gelation process of these gels.

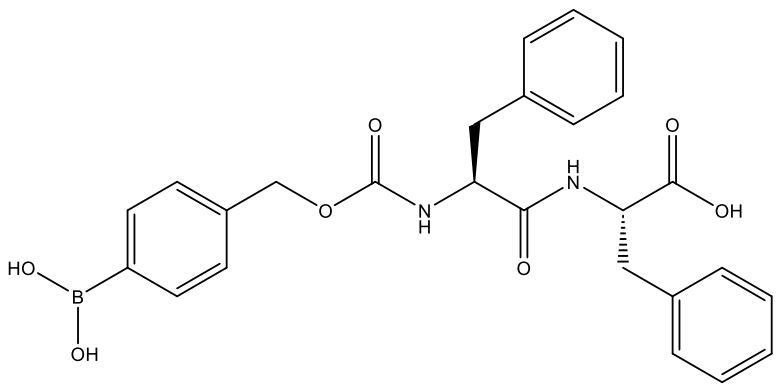

Figure 21. Chemical structure of BPmoc-FF.

Shigemitsu et al integrated specific functional groups to supramolecular hydrogels to initiate responses to stimuli (thermal, optical, pH, and metal ion)[113]. One of those modifications involved exploiting the idea that hydrophobic entities on a molecule provide stability and can induce degradable hydrogels. A *p*-borono-phenylmethoxycarbonyl (BPmoc) group was added to the dipeptide hydrogel (BPmoc-FF); this hydrogen peroxide responsive functional group reacts to give *p*-quinonemethide and carbon dioxide. This completely disrupts the interactions involved in the gel network leading to its degradation[113]. A library of nucleo-tripeptides was synthesized based on the previously reported hydrogel. The study aimed to improve their gel system for tissue engineering applications as the pH-triggered system required a low pH for self-assembly which was not compatible with viable cells. By the addition of several amino groups to the molecule, the group noticed different gelation behaviour, such as change in the rate of gelation. Hydrophobicity was the driving factor for self-assembly as it improved gelation efficiency, as well as increasing the pKa of the terminal carboxylic acid group leading to an increased pH of gelation[114].

In this chapter, we will demonstrate structural manipulation of the one-component portion, glutamine-C12 (G-C12), of the novel two-component hydrogel Benzyl glutamine (BG-C12) (Figure 18 (a)). We will reference glutamine-C12 (G-C12) as the original scaffold. The manipulations involve the addition/removal of hydrophobic and hydrophilic interactions. Designing our hydrogel systems require a solubility balance which prevents the molecules from fully aggregating or fully dissolving in the solvent. Hydrogen bonds and the hydrophobic effect are key elements for gelation. The strength of the supramolecular interactions are influenced by the nature of constituent atoms, the bond geometry, and their neighbouring atoms. The challenge will be to balance the supramolecular interactions involved in these systems and to study their effect on the structural properties of the gels. The ability to tune the gel systems to our desired application, drug delivery, will be an exciting tool for future projects.

2.2 Altering the Length of the Alkyl-Chain

2.2.1 Method of synthesis

2.2.1.1 Synthesis of Glutamine-C10

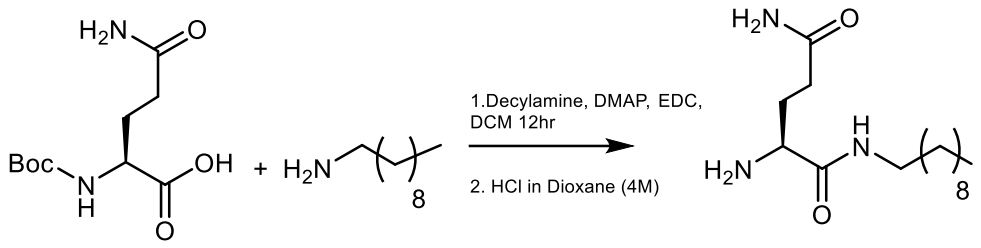

Figure 22. Synthesis of glutamine-C10.

To synthesize glutamine-C10, Boc protected glutamine was coupled with decylamine in the presence of coupling agents 1-ethyl-3-(3-dimethylaminopropyl) carbodiimide and 4-dimethylaminopyridine. To remove impurities of the hydrophilic molecule, a work-up with 1 M HCl, deionised water, 1 M NaOH, and brine was performed. Due to its relatively high solubility in water, there was a relatively large amount of product loss. Column chromatography was used as an extra step to remove impurities. The Boc group was then removed by the addition of 4 M of HCl in dioxane. The molecule was not deprotonated in the same way as the original scaffold with sodium hydroxide in the presence of dichloromethane via the separatory technique to circumvent product loss as the molecule favoured the aqueous layer leading to a significant loss of product. The molecule was characterised by ^{1}H NMR and was produced in a yield of 20%.

2.2.1.2 Synthesis of Glutamine-C11 and Glutamine-C14

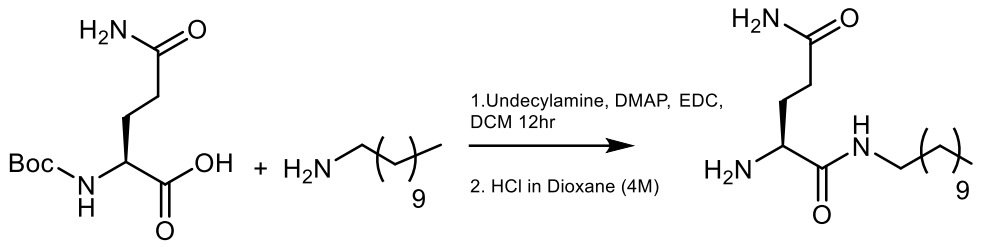

Figure 23. Synthesis of Glutamine-C11.

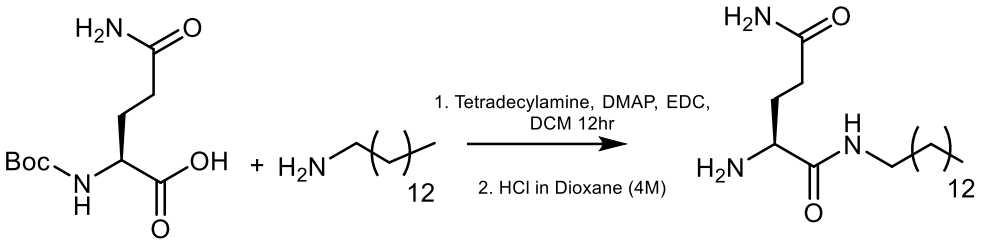

Figure 24. Synthesis of Glutamine-C14

Boc protected glutamine was also coupled with undecylamine and tetradecylamine respectively in the presence of coupling agents 1-ethyl-3-(3-dimethylaminopropyl)carbodiimide and 4-dimethylaminopyridine. A work-up was performed on both separate molecules with 1 M HCl, deionised water, 1 M NaOH, and brine. The Boc protecting group of the molecules was removed through the addition of 4 M of HCl in dioxane. Deprotonation of the molecules was performed by the addition of sodium hydroxide in the presence of DCM via a separatory technique. The molecules in the organic media were collected and dried to give white powders with yields of 54% and 55% respectively. The new molecules were characterised by ^{1}H NMR, ^{13}C NMR, HRMS, and FT-IR. We therefore had a small family of molecules with different alkyl chain lengths, which we hoped would provide an insight into the impact of the hydrophobic chain on the self-assembly of this class of gelator.

2.2.2 Solvent Screen

A key element for gelation is for the solvent to be engulfed within the self-assembling network. Making up around 99.7% of the weight of the gel, this component must maintain a balance in

terms of the solubility of the gelator. High solubility in the chosen solvent means the gelator will form a solution, whereas if the gelator is too insoluble, it will simply precipitate. In other words, the gelator should be able to form some sort of interactions with the bulk solvent but not dissolve in it, instead forming a one-dimensional assembly held together with supramolecular forces. Other aspects to consider are the biocompatibility, toxicity, and availability of the solvent to be used. The solvent should be readily available and affordable, have a relatively low impact in the disruption of the environment, and most importantly for our applications in drug delivery and tissue engineering, be biocompatible.

To find a new gel system, the novel amino acid derivatives were exposed to solvents of different polarities and attempts to initiate gelation were made. This typically involved sonication, direct heating, or sonication then heating until dissolution. Different volumes of solvents and quantities of gelators were used according to the solubility of each molecule.

2.2.2.1 Solvent Screen of Glutamine-C10

The synthesis of glutamine-C10 (G-C10) as previously mentioned, had issues regarding its low yield. This was mainly due to the high-water solubility of the target molecule, which resulted in a significant loss of product. To avoid this problem the last step, neutralization with NaOH, was avoided. The solvent screen therefore involved the use of water with varied alkaline conditions to ensure deprotonation and hence potentially induce gelation. The samples were prepared in glass vials in which equal quantities of the gelator and solvent were heated with a heat gun until dissolution. The vials were left to cool overnight, and a tube inversion test determined the presence of a gel.

Table 1. pH screen to test the gelation of glutamine-C10.

Quantity of gelator (mg)	**Quantity of water (mL)**	**pH**	**Did it gel?**
3.0	0.30	11	No
3.0	0.30	12	No
3.0	0.20	13	No

3.0	0.30	13	No
3.0	0.15	14	No
3.0	0.30	14	No

Unfortunately, the molecule was incapable of forming any gels. We can therefore propose that replacing the C12 chain with a C10 chain led to the inability of the molecule to self-assemble as the apolar functional group and its associated hydrophobicity were essential for stabilising gelation. This is in-line with the enhanced solubility of the molecule in water observed during the synthesis. Decreasing the alkyl chain length decreases the hydrophobic effect, increases solubility, and tips the balance of the molecule away from gel formation. It is perhaps surprising that such a small change can have such a significant effect, but this demonstrates how carefully the gelation of low-molecular-weight systems can be balanced on a knife-edge[115].

2.2.2.2 Solvent Screen of Glutamine-C11

The synthesis of glutamine-C11 (G-C11) produced a good yield without avoiding the end neutralization step as the molecule was not so soluble in the aqueous medium as G-C10. We were therefore optimistic that this system may have greater gelation potential than the C10 derivative. The gel was exposed to numerous solvents, and gel activation was tested using different methods (heat, sonication, or both) to increase the chances of gel discovery. The samples were left overnight, and a tube-inversion method was used to determine gel formation.

Table 2. Solvent screen to test gelation of glutamine-C11 (0.3% wt/vol).

Solvent	Quantity of Solvent (mL)	Quantity of Gelator (mg)	Sonication	Heat	Sonication + Heat
Water	1	3	No - ppt in solution	No - ppt in solution	No - ppt in solution
Methanol	1	3	No - Clear solution	No - Clear solution	No - Clear solution
Acetone	1	3	No - ppt in solution	No - ppt in solution	No - ppt in solution
Ethyl Acetate	1	3	No - ppt in solution	No - ppt in solution	No - ppt in solution
THF	1	3	No - Clear solution	No - Clear solution	No - Clear solution
Diethyl Ether	1	3	No - ppt in solution	No - ppt in solution	No - ppt in solution
Toluene	1	3	No - Foggy solution	No - Foggy solution	No - Foggy solution
Cyclohexane	1	3	No - ppt in solution	No - ppt in solution	Yes - Opaque gel

The solvents displayed in Table 2 are organised in descending order of polarity to demonstrate the relationship between the gelator and the polarity of the solvent. With the majority of solvents, the gelator formed a precipitate in the solvent, with the gelator only dissolving completely in solvents of intermediate polarity. Cyclohexane did manage to form a gel with this gelator, just like the original scaffold, as reported in previous work[116]. This demonstrates that although a carbon atom was removed, the molecule holds similar properties to the original scaffold. The opaque organogel however, cannot be used for drug delivery due to cyclohexane's toxicity and so we did not pursue these studies any further.

2.2.2.3 Solvent Screen of Glutamine-C14

As with glutamine-C11, glutamine-C14 (G-C14) synthesis was not problematic in regard to product loss and impurities. The molecule was therefore simply exposed to several solvents of descending order of polarities and attempts were made to trigger gelation using various methods. The samples were left overnight, and gel formation was determined as with previous solvent screens.

Table 3. Solvent screen to test gelation of glutamine-C14 (3% wt/vol).

Solvent	Quantity of Gelator (mg)	Quantity of Solvent (mL)	Sonicate	Heat	Sonicate then Heat
Water	3.0	0.1	No - White ppt	Yes - White Gel	Yes - White Gel
Methanol	3.0	0.1	No - White ppt in solution	N/A	N/A
Acetonitrile	3.0	0.1	No - White ppt	No - White ppt	No - White ppt
DMSO	3.0	0.1	No - Opaque solution	No - Opaque sol with ppt	No - ppt
DMF	3.0	0.1	No - White ppt	No - White ppt	No - White ppt
Acetone	3.0	0.1	No - White ppt	N/A	N/A
Ethyl Acetate	3.0	0.1	No - White ppt	No - White ppt	No - White ppt
THF	3.0	0.1	No - White ppt	No - White ppt	No - White ppt
Diethyl Ether	3.0	0.1	No - White ppt	No - White ppt	No - White ppt
Toluene	3.0	0.1	Yes - Opaque Gel	Yes - Opaque Gel	Yes - Opaque Gel
Cyclohexane	3.0	0.1	Yes - White Gel	Yes - White Gel	No - White ppt

Integrating two additional carbon atoms to the original scaffold should lower solubility in water and promote increased hydrophobic interactions. The close packing and increased supramolecular interactions of the long alkyl chain elevated the strength of the assembly process and thus resulted in the formation of a reproducible hydrogel in the presence of water. This is quite interesting as the original C12 scaffold only produced irreproducible hydrogels in water and required an aldehyde as a reactive second component for stability and consistency of gelation. Clearly the addition of a C2 unit leads to the consistent formation of a hydrogel even in the absence of an aldehyde – presumably as a result of the more significant hydrophobic effect. The molecule also gelled the solvents toluene and cyclohexane, which are not applicable for drug delivery purposes and were not further investigated.

2.2.3 Aldehyde Screen

As mentioned previously, the original scaffold could only produce reproducible gels via Schiff base formation with an aldehyde, a process which was thoroughly discussed and

investigated[116]. In this work, we therefore screened a range of aldehydes with our newly synthesized molecules. Given the aldehyde provided the original scaffold with additional gelation potential, as a result of modifying the hydrophobicity/hydrophilicity, we reasoned the same would be true for the new molecules. We tested a variety of aldehydes, with particular focus on those previously successful with G-C12 (nitrobenzaldehydes and benzaldehyde), as well as a variety of aldehydes selected from sustainable sources.

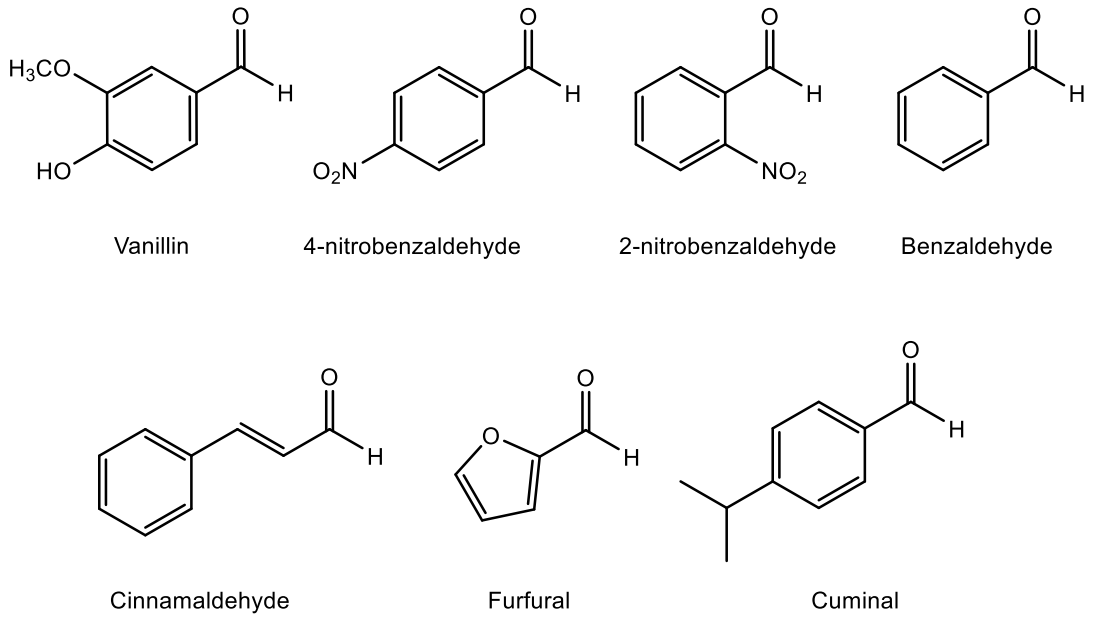

Figure 25. Structures of aldehydes used in aldehyde screens.

2.2.3.1 Glutamine-C10

Since glutamine-C10 was not capable of forming a gel on its own, we considered whether glutamine-C10 could form gels in the presence of aldehyde additives. To form two component gels, solutions of the gelator and aldehydes were used with the addition of 0.1 mL of water. The samples were activated through sonication and heating (Table 4). The vials were left undisturbed to fully self-assemble and a tube inversion method was used to determine gel formation.

Table 4. Aldehyde screen on 3% (wt/vol) glutamine-C10 in 0.1 mL water.

Aldehyde	Quantity of Aldehyde	Equivalents of Aldehyde	Quantity of Gelator (mg)	Did it gel? Sonicate	Heat
Benzaldehyde	10 µL	9.0	3.0	No	No
2-nitrobenzaldehyde	1.4 mg	1.0	3.0	Yes	Yes
4-nitrobenzaldehyde	1.4 mg	1.0	3.0	No	No
Furfural	10 µL	11.0	3.0	No	N/A
Glycolaldehyde Dimer	1.4 mg	1.0	3.0	No	No

The molecule had largely lost the ability to form two-component hydrogels with the aldehydes compared with the C12 system[116]. It did, however, form irreproducible hydrogels with 2-nitrobenzaldehyde. It therefore seems that by shortening the alkyl chain the ability of the system to form two-component gels with aldehydes has been decreased. Unfortunately, the molecule was difficult to prepare due to its hydrophilic nature giving economically inefficient yields. In the light of these results, we did not pursue the C10 system further, but note that it probably represents the lower limit of alkyl chain length at which any type of hydrogelation might reasonably be expected for this class of gelator.

2.2.3.2 Glutamine-C11

As gelation with glutamine-C11 on its own did not occur in the solvent screen besides with cyclohexane, we then examined the ability of this molecule to form gels in the presence of an aldehyde. Equal quantities of the molecule were used in 1 mL of water with various aldehydes in glass vials. Each mixture was sonicated, heated until dissolution, and left to cool to detect gel formation via the tube-inversion method.

Table 5. Aldehyde screen on the BG-C11 molecule (0.3% wt/vol) in 1 mL water.

Aldehyde	Quantity of Aldehyde	Equivalents of Aldehyde	Quantity of Gelator (mg)	Did it Gel?
Benzaldehyde	10.0 µL	10.0	3.0	Yes - Partial gel
Furfural	10.0 µL	12.0	3.0	Yes - Brown gel
4-Nitrobenzaldehyde	0.77 mg	0.50	3.0	Yes- White gel
Vanillin	1.00 mg	1.50	3.0	No gel – clear solution with brown oil droplets
2-Nitrobenzaldehyde	0.74 mg	0.50	3.0	No gel- opaque solution
Cuminal	10.0 µL	7.0	3.0	No gel – White solution
Glyceraldehyde Dimer	0.64 mg	0.50	3.0	No gel – White solution

The molecule gelled via Schiff base formation with some of the aromatic aldehydes - benzaldehyde, 4-nitrobenzaldehyde, and furfural. This therefore suggests the beginning of the retrieval of the original scaffold's capabilities. Studies with furfural will not be continued here due to the molecule's known toxicity[117], although it is noted that this compound can be generated from biorenewable resources and may have some applications as a 'green' gelator[118]. White gels were formed with benzaldehyde and 4-nitrobenzaldehyde, of which benzaldehyde produced more reliable gels and was therefore particularly targeted for further investigations.

2.2.3.3 Glutamine-C14

Equal quantities of glutamine-C14 were dissolved in water (1 mL) with various aldehydes. Each mixture was heated until dissolution. The hot solutions were left to stand overnight to determine which aldehyde promotes gelation. The tube inversion method was used to determine gel formation.

Table 6. Aldehyde screen of 0.3% (wt/vol) glutamine-C14 in 1 mL water.

Aldehyde	Quantity of Aldehyde	Equivalents of Aldehyde	Quantity of Gelator (mg)	Did it Gel?
Benzaldehyde	1.13 µL	1.0	3.0	Yes - White gel
Cinnamaldehyde	1.16 mg	1.0	3.0	No – White ppt
Furfural	0.986 µL	1.0	3.0	No – ppt in orange solution
4-Nitrobenzaldehyde	1.33 mg	1.0	3.0	No – White ppt
Vanillin	1.34 mg	1.0	3.0	No – White fibres
2-Nitrobenzaldehyde	1.33 mg	1.0	3.0	Yes – Opaque gel
Glyceraldehyde Dimer	1.06 mg	1.0	3.0	No gel – White ppt

The new gelator formed gels with benzaldehyde and 2-nitrobenzaldehyde forming white and opaque hydrogels respectively. Fibres were formed with the addition of vanillin and this system was therefore further investigated. By adding various concentrations of vanillin to the molecule we found that a green tinted gel formed only after > 48 hours. Although vanillin has fewer toxic properties compared to benzaldehyde, the relatively slow gelation compared to gels formed with benzaldehyde (20 minutes gel formation) were felt to make it less suitable for practical applications. Therefore, we continued to characterize the benzaldehyde-based two-component systems in more detail. It is worth noting that vanillin is a significantly more hydrophilic aldehyde than benzaldehyde. With the C11 and C12 systems, vanillin did not induce gel formation. We suggest that the more hydrophobic nature of the Glutamine-C14 system means that the somewhat more hydrophilic vanillin can be better tolerated hence leading to some tendency for gel formation.

2.2.4 Minimum Gelation Concentration

The minimum gelation concentration (MGC) is the lowest gelator concentration that can form gels in a given solvent. Obtaining this value is a good indicator of gelator efficiency. Gels with MGC's lower than 1% wt/vol are considered to show great efficiency[119], as their low concentrations can immobilise high percentages of solvent compared to their actual low weight.

2.2.4.1 Benzyl Glutamine-C11

The minimum amount of benzaldehyde required to induce the gelation of Benzyl glutamine-C11 (BG-C11) was investigated. To determine this value, equal quantities of the gelator and distilled water were used with multiple concentrations of benzaldehyde. All of the vials were exposed to sonication preceded by heat until dissolution. The gels were left to form, and the results are recorded below.

Table 7. Finding the minimum quantity of benzaldehyde needed to form a gel with 0.15% (wt/vol) glutamine-C11.

Quantity of Benzaldehyde (µL)	Equivalents of Benzaldehyde	Quantity of Gelator (mg)	Quantity of Water (mL)	Did it Gel?
0.10	0.1	3.0	2.0	No
0.20	0.2	3.0	2.0	No
0.30	0.3	3.0	2.0	No
0.40	0.4	3.0	2.0	Inconsistent weak gel
0.50	0.5	3.0	2.0	Weak gel
0.60	0.6	3.0	2.0	Yes
0.70	0.7	3.0	2.0	Yes
0.80	0.8	3.0	2.0	Yes
0.90	0.9	3.0	2.0	Yes
1.00	1.0	3.0	2.0	Yes

The gel was just capable of gelling with the use of 0.4 µL of benzaldehyde making this the minimum quantity of benzaldehyde needed for gelation. Below that concentration, no gels were formed. Above the minimum aldehyde concentration, the gels become more and more

reproducible and durable (through physical observation). Reliable gels could be formed using 0.7 µL of benzaldehyde. This is due to the formation of a Schiff base, which supports assembly into the hydrogel network. Now that this value is acquired, we can further investigate and determine the minimum amount of gelator needed to immobilise water.

By using the same quantity of gelator and aldehyde, and varying the quantity of solvent, the minimum gelation concentration (MGC) of the two-component system in water was determined (Table 8).

Table 8. Minimum gelation concentration of two-component gel system (BG-C11 with 0.7 molar equivalence of benzaldehyde).

Quantity of Water (mL)	**Quantity of Gelator (mg)**	**Quantity of Benzaldehyde (µL)**	**Did it Gel?**
2.0	3.0	0.7	Yes
2.1	3.0	0.7	Yes
2.2	3.0	0.7	Yes
2.3	3.0	0.7	Yes
2.4	3.0	0.7	Yes
2.5	3.0	0.7	Yes - Inconsistent weak gel

As the volume of water was reduced the reproducibility of gel formation increased. The most reproducible homogenous-looking gel had 2 mL of water. Meanwhile, 2.5 mL was the maximum amount of water that 3 mg gelator + 0.7 µL benzaldehyde could immobilise. At this volume, the gel does not always form, so we consider this to be the maximum limit of water content. The gel with 2.4 mL water was more reproducible, therefore the MGC could be determined by:

Total weight of gelator = (0.73 mg benzaldehyde) + (3 mg glutamine-C11) = 3.73 mg

Weight per volume = $(3.73\times10^{-3}$ g)/ 2.4 mL = $1.55\times10^{-3}\times100\%$ = 0.155%

Therefore, the gelator can form a gel at a 0.155% (wt/vol). This is higher than BG-C12 which formed a gel at a 0.074% (wt/vol). This probably reflects the one carbon atom shorter hydrophobic chain giving a slightly lower hydrophobic driving force for assembly. Nonetheless, this is still highly effective gelation – very significantly below 1% wt/vol[119].

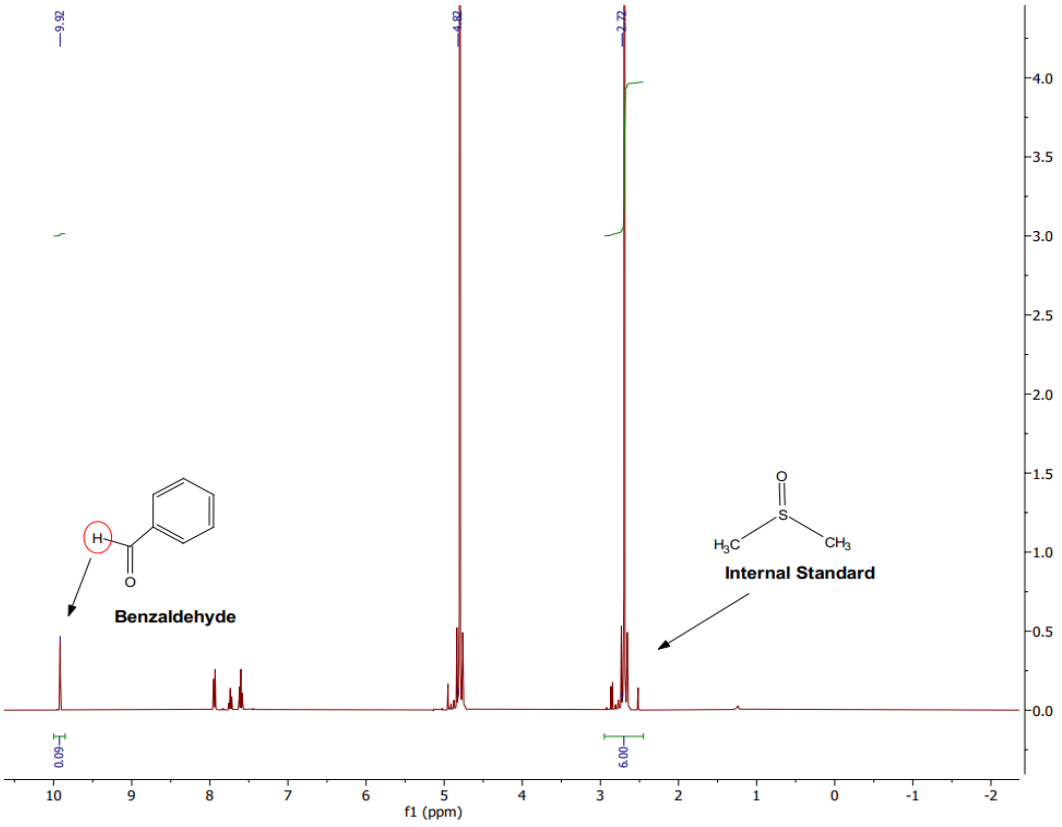

Figure 26. ^{1}H NMR spectra of BG-C11 hydrogel in D_2O with DMSO as an internal standard used to quantify the free-flowing benzaldehyde in the gel network.

^{1}H NMR spectroscopy was performed on the new gel to determine the percentage of benzaldehyde involvement in the 3D network. ^{1}H NMR spectroscopy can only detect mobile or soluble substances, and hence any gelator that is self-assembled into a 'solid-like' network will not be detected. If the aldehyde is mobile it will give a peak in the ^{1}H NMR spectrum. To quantify how much free aldehyde is in the gel, a mobile internal standard, dimethyl sulfoxide, was used as a solvent spike in the gel. Integration of the internal standard and the gelator peaks can hence quantify the amount of mobile component. The glutamine-C11 gel was prepared using 1 mg gelator with 0.5 µL Benzaldehyde in 0.7 mL D_2O with the addition of 2 µL DMSO as the internal standard. By comparing the integral peaks of DMSO (δ = 2.70 ppm) and benzaldehyde (δ = 9.92 ppm) it was found that 51.6% of the aldehyde is free flowing in the network and 48.4% is integrated into the solid-like self-assembled network. This relatively large quantity of mobile aldehyde compared with the original system is in-line with the view that the BG-C11 is more soluble than the original BG-C12 system.

2.2.4.2 Glutamine-C14

Glutamine-C14 (G-C14) self-assembled on its own as well in the presence of benzaldehyde. We therefore determined the MGCs of both the one and two component gel systems. Equal quantities of glutamine-C14 were loaded into various volumes of distilled water and were heated to initiate gelation, see Table 9. As for the two-component system involving benzaldehyde, equal quantities of glutamine-C14 and distilled water were heated in the presence of multiple concentrations of benzaldehyde as shown in Table 10. To determine the maximum water content the gel system (BG-C14) can engulf, gels with equal quantities of gelator and aldehyde concentration were added to various volumes of water (Table 11). The gels were induced as previously reported. For all experiments, an inversion test was performed, in which a gel is determined based on its ability to retain its shape as it is inverted. If it forms but falls, it is considered a weak gel.

Table 9. Determining the minimum gelation concentration of glutamine-C14 hydrogels.

Gelator (mg)	Water Volume (mL)	Did It Gel?
3.0	0.1	Yes – White gel
3.0	0.2	Yes – Partial gel
3.0	0.3	No – White ppt
3.0	0.5	No – White ppt
3.0	1.0	No – White ppt

Table 10. Determining the minimum aldehyde concentration for gelation of the two-component hydrogel (BG-C14).

Gelator (mg)	Water Volume (mL)	Benzaldehyde Volume (µL)	Equivalents of Aldehyde	Did It Gel?
3.0	1.0	0.20	0.2	No – White ppt
3.0	1.0	0.30	0.3	No – White ppt
3.0	1.0	0.40	0.4	No – White ppt
3.0	1.0	0.50	0.6	Yes – White gel
3.0	1.0	0.80	0.9	Yes – White gel

3.0	1.0	1.00	1.1	Yes – White gel
3.0	1.0	1.13	1.3	Yes – White gel
3.0	1.0	2.00	2.2	Yes – White gel

Table 11. Determining the minimum gelation concentration of two-component hydrogel (BG-C14).

Gelator (mg)	**Water Volume (mL)**	**Benzaldehyde Volume (µL)**	**Did It Gel?**
3.0	1.0	1.13	Yes – White gel
3.0	1.2	1.13	Yes – White gel
3.0	1.4	1.13	Yes – White gel
3.0	1.6	1.13	Yes – White gel
3.0	1.8	1.13	Yes – White gel
3.0	1.9	1.13	Yes – White gel
3.0	2.5	1.13	Yes – Weak gel
3.0	2.8	1.13	Yes – Weak gel
3.0	3.0	1.13	Yes – Weak gel
3.0	3.5	1.13	Yes – Weak gel
3.0	4.0	1.13	Yes - Weak gel
3.0	4.5	1.13	Yes – Weak inconsistent gel

The glutamine-C14 one component gel system (3 mg) could immobilise a maximum volume of 0.2 mL. The new gelator had an MGC 3% (wt/vol), which is not ideal as it is >1% (wt/vol)[119]. However, the new molecule nonetheless possesses a greater assembly capacity compared to the original scaffold as it managed to self-assemble without an additional aldehyde. This indicates the possible improvement in assembly stability when increasing the chain length, presumably a result of the greater hydrophobic effect. The gelation efficiency of the new gelator is dramatically improved with the addition of the aromatic aldehyde. Increasing the volume of immobilised water 19-fold (from 0.1 mL to 1.9 mL water). To form a gel in 1 mL of water, the minimum quantity of benzaldehyde needed to self-assemble the two-component network is 0.5 µL.

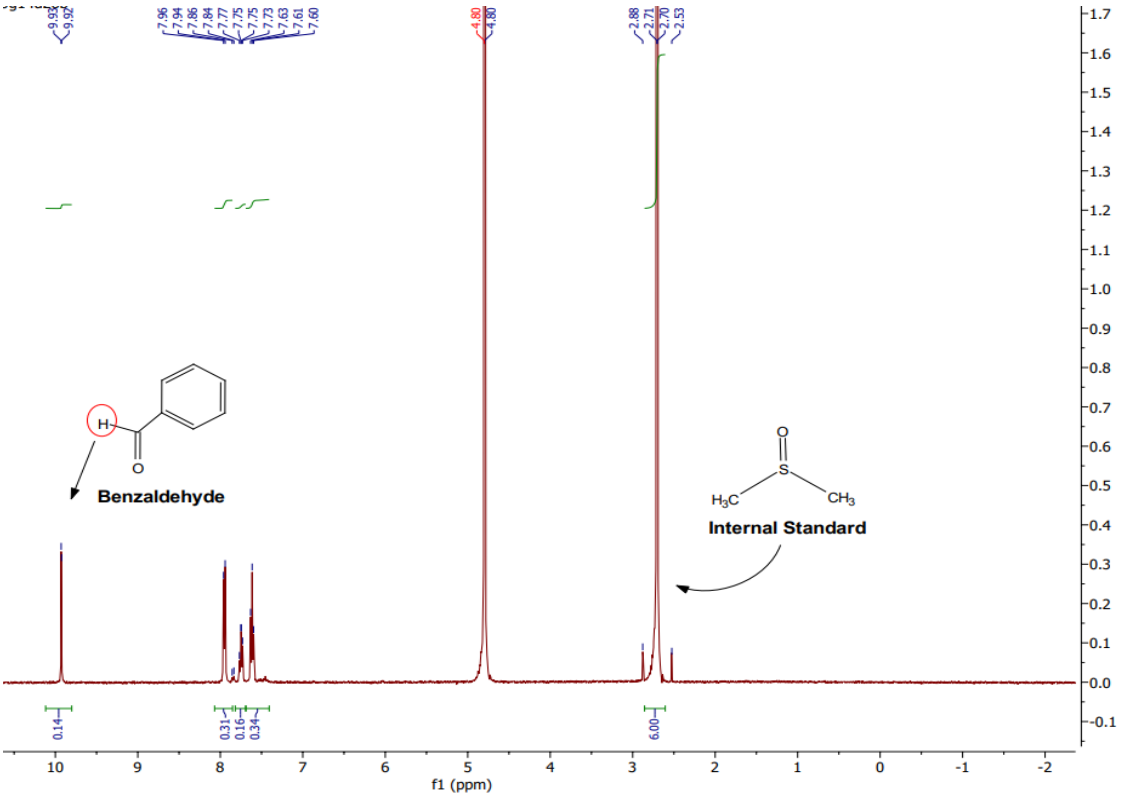

Figure 27. ^{1}H NMR spectra of BG-C14 hydrogel in D_2O with DMSO as an internal standard used to quantify free-flowing benzaldehyde in the gel network.

To further quantify benzaldehyde in the two-component system and determine how much has been incorporated into the solid-like network, ^{1}H NMR was utilised. Glutamine-C14 (3 mg) and benzaldehyde (1.13 µL) were added to D_2O (1.0 mL) with DMSO (2 µL) as an internal standard. The hot mixture was poured into an NMR tube and left undisturbed until self-assembly was complete. The peak of DMSO (δ = 2.70 ppm) was compared to the carboxyl group of benzaldehyde (δ = 9.92 ppm) obtained from the NMR spectrum. BG-C14 has 35.5% benzaldehyde freely flowing in the network and 64.5% integrated into the network. This means that of the total volume of benzaldehyde added with 3 mg of glutamine-C14 in this experiment, 0.73 µL is intimately involved in stabilising the hydrogel, broadly in-line with the minimum aldehyde concentration required for gelation reported above.

2.2.5 Thermal Stability

The T_{gel} value is the temperature at which a gel becomes a sol on heating. Being a measure of thermal stability, the T_{gel} is an important property as it can predict the temperature range the gel can withstand and keep its structural integrity. It is also a good indicator of whether these new molecules possess increased thermal stability compared to the original gels based on Benzyl glutamine (BG-C12). By applying heat to the gel sample in a thermoregulated oil bath, we could determine the T_{gel} value. The ability of the gel to retain its shape on sample inversion was monitored, and once this was lost, the temperature was recorded.

Table 12. Thermal stability Study of BG-C11 hydrogels performed in triplicate.

Quantity of Benzaldehyde (µL)	Equivalents of Aldehyde	Quantity of Water (mL)	Quantity of Gelator (mg)	T_{Gel} (°C)
1.0	1.0	2.0	3.0	53
1.0	1.0	2.1	3.0	53
1.1	1.1	2.1	3.0	24
1.2	1.2	2.1	3.0	37
1.3	1.3	2.1	3.0	28
1.4	1.4	2.1	3.0	25
1.5	1.5	2.1	3.0	21

As with BG-C12, for BG-C11 as the concentration of benzaldehyde is increased the gels lose their ability to maintain their shape at higher temperatures. The gel withstanding the highest amount of thermal energy was that of 1.0 µL benzaldehyde. In other words, this quantity of benzaldehyde is the ideal amount to form the most stable gel from all of the concentrations tested. This suggests that excess benzaldehyde actually makes the gel less stable as the extra aldehyde is not incorporated into the network leading to its disruption.

Table 13. Thermal stability Study of BG-C14 hydrogels - Performed in duplicate.

Quantity of Benzaldehyde (µL)	Equivalents of Benzaldehyde	Quantity of Water (mL)	Quantity of Gelator (mg)	T_{Gel} (°C)
0.50	0.6	1.0	3.0	65
0.80	0.9	1.0	3.0	70

1.13	1.3	1.0	3.0	79
1.13	0.6	1.0	6.0	77
1.13	1.5	1.0	2.5	68
2.00	2.2	1.0	3.0	75

As for the two-component gels formed by BG-C14, the maximum thermal stability was 79°C. Gel breakdown at a temperature of 53°C (BG-C11) and 79°C (BG-C14) implies that the gels in question would not be affected by the body's temperature of 37°C. BG-C14 proved to have superior thermal stability compared to BG-C11. The increased hydrophobic effect in BG-C14 provides enhanced assembly of the gel molecule, making it more resistant to thermal disruption. Even reducing the chain length by one group (12C to 11C) reduced the stability of the gel compared to BG-C12 (83°C – 0.35 % glutamine-C12 with one molar equivalent of benzaldehyde in 1 mL water). However, it should be noted that experimental conditions such as the volume of the vial used and the set rate of temperature change/time may also influence results[120].

This quality is valuable when considering the use of the gel for sustained release of a drug molecule. The gel would release the drug over a period of time and the temperature would not be considered a factor affecting this release.

2.2.5 Rheology

The next step was to study and compare the rheological robustness of the newly synthesized gels. Rheology studies the deformation of a material upon exposure to a certain stress. The method involves measuring the response of the gel placed between a stationery and force-applying plate. The experiment is a tool to confirm that the materials investigated are in fact gels. Elastic (G') and viscous (G'') moduli are observed with an increase of frequency or magnitude. Elastic modulus is the elasticity of a material once deformed, and therefore represents the energy storage of a material – the solid-like behaviour. Conversely, the viscous modulus is the flow of a material during deformation, and thus represents the loss of energy – the liquid-like behaviour. Rheology can indicate gel-like behaviour (viscoelastic properties)

when G’ > G’’. If the viscous modulus is equal to or greater than the elastic modulus, the material is considered a liquid. It is therefore interesting to see the role of the added/removed functional groups had on rheological performance. To perform this study, the viscoelastic region (LVR) must be determined. The region is defined by the independence of G’ and G’’ from the magnitude of stress (amplitude sweep). This was performed for each gel and its value was then used for the frequency sweep. The gels were prepared on the rheometer plate, with the use of 1 mL of BG-C11 (0.15% (wt/vol) glutamine-C11 with 0.61 molar equivalent of benzaldehyde) and BG-C14 (0.3% (wt/vol) with 1.26 molar equivalent of benzaldehyde) respectively. Once fully formed the gels were ready for analysis.

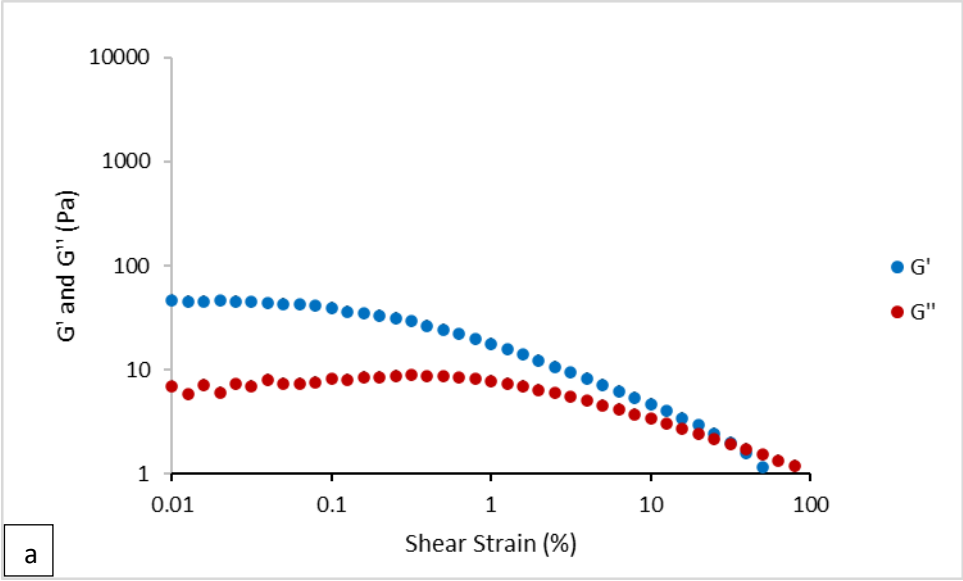

a

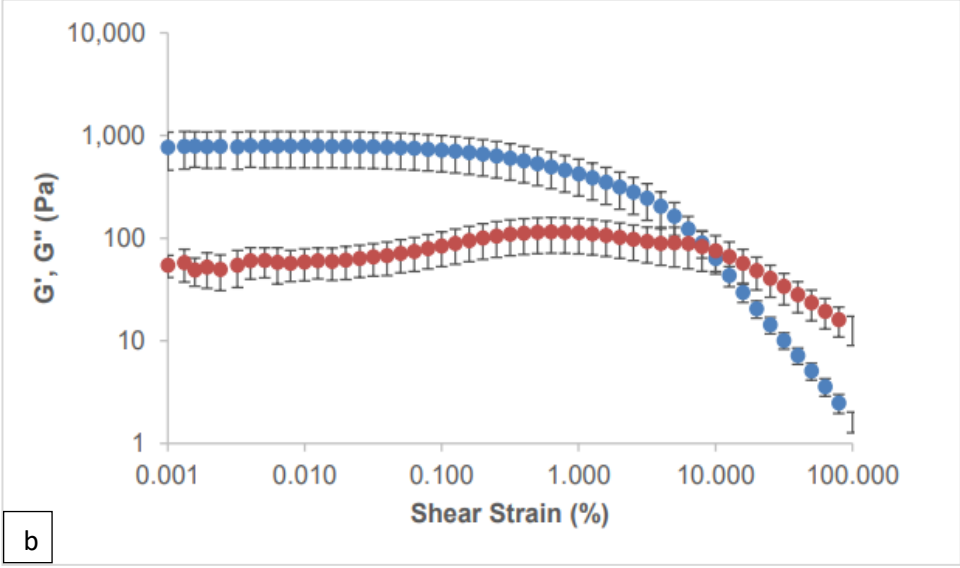

b

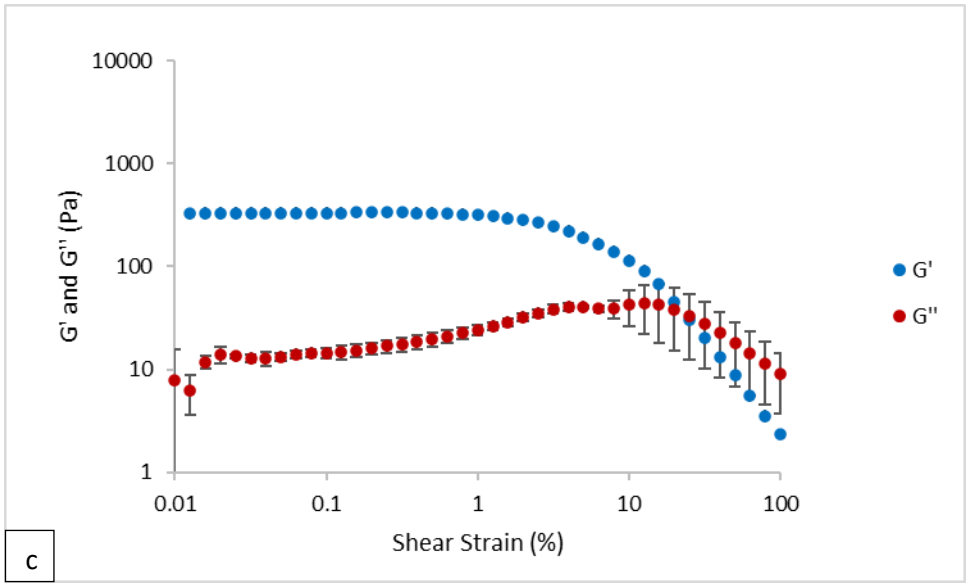

Figure 28. Viscous(G') moduli and elastic (G') moduli with increasing shear strain performed using parallel plate geometry at 25°C a) BG-C11 (0.15% (wt/vol) glutamine-C11 with 0.61 molar equivalent of benzaldehyde) hydrogel b) BG-C12 hydrogel (glutamine-C12 (0.4% (wt/vol)) with equimolar amount of benzaldehyde) obtained from K. Hawkins et al[142] c) BG-C14 (0.3% (wt/vol) glutamine-C14 with 1.26 molar equivalent of benzaldehyde) hydrogel. Error bars in the graph represent the standard error of the mean.

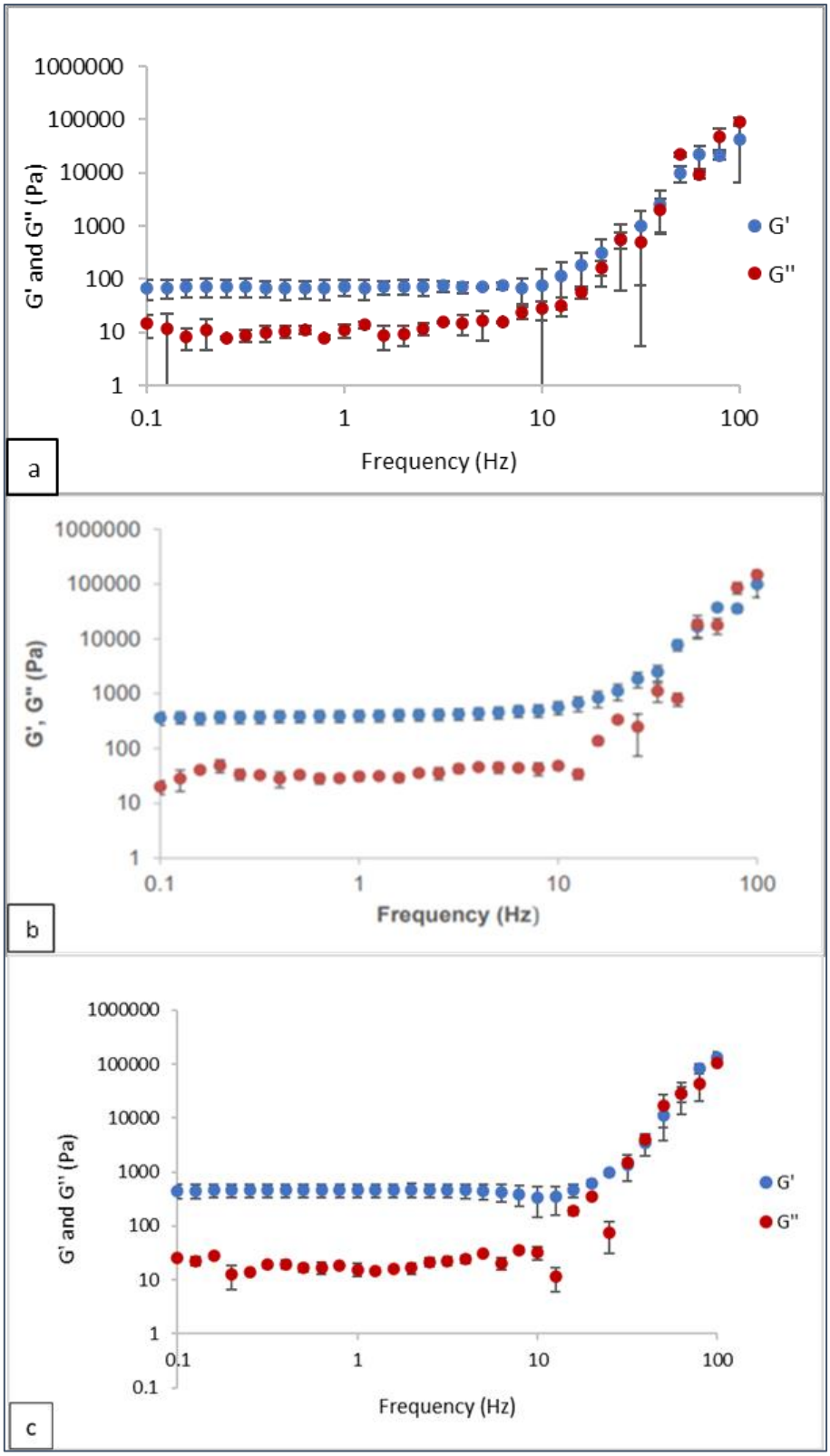

Figure 29. Viscous(G') moduli and elastic (G') moduli with increasing frequency performed using parallel plate geometry at 25°C a) BG-C11 (0.15% (wt/vol) glutamine-C11 with 0.61 molar equivalent of benzaldehyde) hydrogel b) BG-C12 hydrogel (glutamine-C12 (0.4% (wt/vol)) with equimolar amount of benzaldehyde) obtained from K. Hawkins et al[142] c) BG-C14 (0.3% (wt/vol) glutamine-C14

with 1.26 molar equivalent of benzaldehyde) hydrogel. Error bars in the graph represent the standard error of the mean.

It is clear from the amplitude and frequency sweeps shown in Figure 28 and 29 that the molecules are capable of forming gels as G' > G''. For BG-C11, the new molecule has less stored energy (elastic modulus) compared to BG-C12, meaning the gel is softer. This reflects the results described above in which it was noted that the system with the shorter chain length is less effective at forming gels, presumably due to the greater solubility of the molecular-scale building block (see above). For BG-C14, the G' value is similar to that of BG-C12 and there is slight variation in response to a change of strain. However, the differences may be due to sample handling as the rheological data for the original scaffold was obtained from K. Hawkins et al.[110] We can therefore conclude that neither gel possesed enhanced rheological properties compared to BG-C12. However reducing the length of the carbon chain of the original scaffold results in the reduction of the gels structural integrity, whereas increasing it beyond 12 carbon atoms did not significantly increase the stiffness any further.

2.2.6 Self-Healing

Low molecular weight gelators (LMWGs) are particularly desirable if they have self-healing properties. It is beneficial in drug formulation as the gel could be administered in the form of an injection and then reform a gel *in situ*. Drug administration through injection causes minimal invasive damage and can fill cavities of various shapes[121]. Once injected, the broken network could retain its structure and begin drug release. For example, Laurenti et al. produced a biocompatible LMWG composed of magnesium phosphate nanosheets. The thixotropic and self-healing properties of the gel enabled its use in high gauge needles. Used to improve bone healing, this system could minimize the invasiveness of orthopaedic and craniofacial interventions associated with bone recovery[122]. Zang reported the Nap-GFFYGGKOGEOGKOGSO hydrogel that can self-assemble via the heat/cool cycle. The gel displayed self-healing ability after being converted to a solution by either shaking, pipetting, or vortexing. Upon being converted to a viscous solution, the gel reassembles after being left

sitting at room temperature for a period of time. Rheological recovery studies indicated that the gel required an hour for the gel to fully recover[123].

BG-C12 has this self-healing ability[110] and it was shown to be essential for the effective delivery of levodopa in the intranasal cavity[2]. Rheology can be used to demonstrate the ability of a gel to reform once it has been broken. Supramolecular interactions are heavily involved in this property as they can easily be broken and reformed. However, it is also important that on disassembly, the gelator does not precipitate from solution, as many do, otherwise a thermal/ultrasound treatment would be required to reinitiate gel formation, preventing the observation of thixotropy. The use of two component systems, in which the individual components, unlike the two-component complex, have good solubility, is an effective strategy for avoiding gelator precipitation, and hence enabling self-healing type behaviour.

To understand the effect of altering the length of the alkyl chain on thixotropy we conducted a study on the two new gels, BG-C11 and BG-C14. Due to the delicate nature of the gels, they were made on the rheometer plate by heating the gel solutions and injecting them into bottomless vials attached to the rheometer plate. Once formed, the gels were independently exposed to a shear force of 0.0126% at a frequency of 2 Hz for 30 seconds. The frequency was then increased from 2 Hz to 100 Hz for 30 seconds (breaking the gel). Finally, the frequency was returned to 2 Hz and the recovery monitored over time. This variation in frequency is designed to mimic the way in which devices such as spray inhalers stress materials in order to spray them into the nasal cavity.

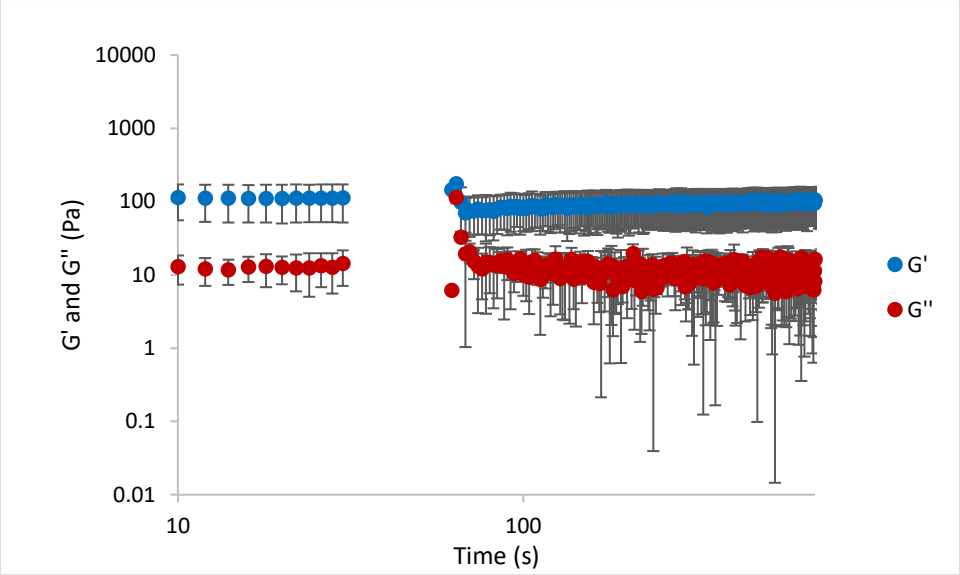

Figure 30. Recovery test on BG-C11 (0.15% (wt/vol) glutamine-C11 with 0.61 molar equivalent of benzaldehyde) hydrogel via rheology (performed at 25°C). Error bars in the graph represent the standard error of the mean.

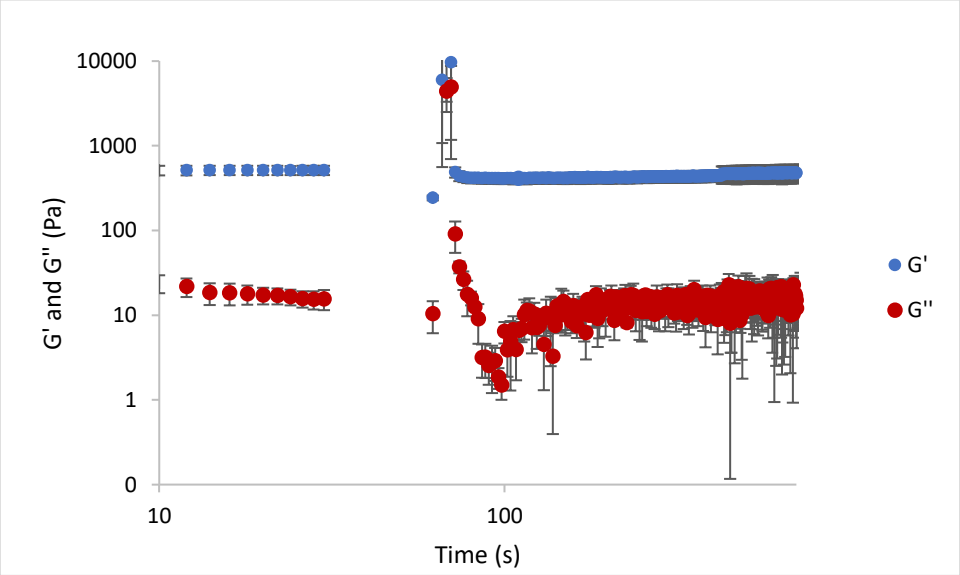

Figure 31. Recovery test on BG-C14 hydrogel (0.3% (wt/vol) glutamine-C14 with 1.26 molar equivalent of benzaldehyde) BG-C14 via rheology (performed at 25°C). Error bars in the graph represent the standard error of the mean.

We were pleased to discover that as with BG-C12, both gels were capable of recovering from breakage. The G' remained greater than the G'' indicating the maintenance of gel properties upon exposure to stress. As with previous rheology studies, the difference between G' and G'' is greater for BG-C14 compared to BG-C11 suggesting greater rigidity and self-standing stability of the BG-C14 molecule. We can conclude that the desired thixotropic property remains even with manipulations of the length of the alkyl chain. We therefore suggest that, for the reasons outlined above, this is an inherent (and useful) property of these two component gelator scaffolds.

2.2.7 pH Screen

Throughout the human body, the pH of fluids varies. The variation is associated with certain physiological functions that occur in the body. Metabolism in the body relies on these specific pH values as it affects (e.g.) enzyme activity. In this experiment we tested the pH range across which the gels could form. We aimed to observe whether the pH alteration will interfere with the hydrogen bond potential of the gels functional groups, and if this leads to competitive hydrogen bond formation between the gelator and water molecules that will destroy gel formation. To achieve this, the pH value of distilled water was changed with the addition of HCl or NaOH solutions to obtain the desired pH. The study was conducted with the use of 0.15% (wt/vol) BG-C11 (with 0.61 molar equivalent of benzaldehyde), 0.3% (wt/vol) BG-C14 (with 1.26 molar equivalent benzaldehyde), and 3% (wt/vol) glutamine-C14. All factors such as aldehyde concentration and volume of solvent were standardised.

Table 14. pH screen of BG-C11 (with 0.61 molar equivalent of benzaldehyde) and BG-C14 (with 1.26 molar equivalent benzaldehyde) in 1 mL solvent respectively and glutamine-C14 in 0.2 mL solvent.

pH	**Did it gel?** **BG-C11**	**BG-C14**	**Glutamine-C14**
1	No	No – Clear solution	Yes- White (marble like) gel
2	No	No – Clear solution	Yes – White gel
3	Yes - White gel	Yes - White gel	Yes – White gel

4	Yes - White gel	Yes - White gel	Yes – White gel
5	Yes - Very Weak gel	Yes - White gel	Yes – White gel
6	Yes - Weak gel	Yes- White gel	Yes – White gel
7	Yes - White gel	Yes - White gel	Yes – White gel
8	Yes - White gel	Yes - White gel	Yes – White gel
9	Yes - White gel	Yes - White gel	Yes – White gel
10	Yes - White gel	Yes - White gel	Yes – White gel
11	Yes - Very weak gel	Yes - Weak white gel with ppt	Yes – White gel
12	No	Yes - Weak white gel with ppt	Yes – White gel
13	Yes - Partial gel	Yes - Weak white gel with ppt	Yes – White gel
14	No	Yes - partial gel on top of solution	Yes – Partial gel

Table 14 describes the gel formation of BG-C11, BG-C14, and glutamine-C14 across a range of pH values. Overall, both two-component gels gave similar results in the different pH environments. BG-C14 was slightly better able to self-assemble across a wider range of mediums, which was no surprise due to its increased stability from its longer alkyl chain. The most robust looking gels were formed at pH 3-4, giving reproducible white gels. It is known that mildly acidic pH values can promote the reaction to give the Schiff base derivative[124] – this may help give more robust gels. Below pH 3, the forward reaction is less favoured and this is reflected in the inability to form gels. Above pH 10, the gels were either extremely weak or did not form at all – given the forward reaction to generate the Schiff base is catalysed by H^+, this is not surprising. For the one component system, a gel was formed in all pH environments, with the exception of pH 14 where precipitate was prevalent. At pH 1 the glutamine-C14 gelator formed the most homogenous-looking gel. We suggest this reflects the high level of protonation of the amine group improving the hydrophilic nature of the amino acid head group, and potentially assisting self-assembly. Table 14 clearly indicates that these gels could be quite compatible with the fluids found in the body. We can expect the gels to keep their integrity in the presence of bodily fluids and gel structure may not be completely disrupted by pH.

2.2.8 SEM and TEM

To gain a full understanding of the newly-discovered gels, it is necessary to study the nanoscale morphology of the networks. The morphology could, for example, be in the shape of tubules, strands, tapes or chiral ribbons[125]. The junction zones and branching between these fibres are responsible for the rigidity of the microstructure of the gel matrix[126]. These junction zones connect the 1D fibres to form a 3D network that entraps the liquid component macroscopically by capillary forces and surface tension[125]. Scanning electron microscopy (SEM) displays the 3D structural arrangement of the network, while transmission electron microscopy (TEM) gives more detailed information on fibre morphology. Both approaches involve sample drying which can lead to morphological change[127]. However, comparing equivalent samples produced from a family of related gelators in the same way is at least useful for comparative purposes.

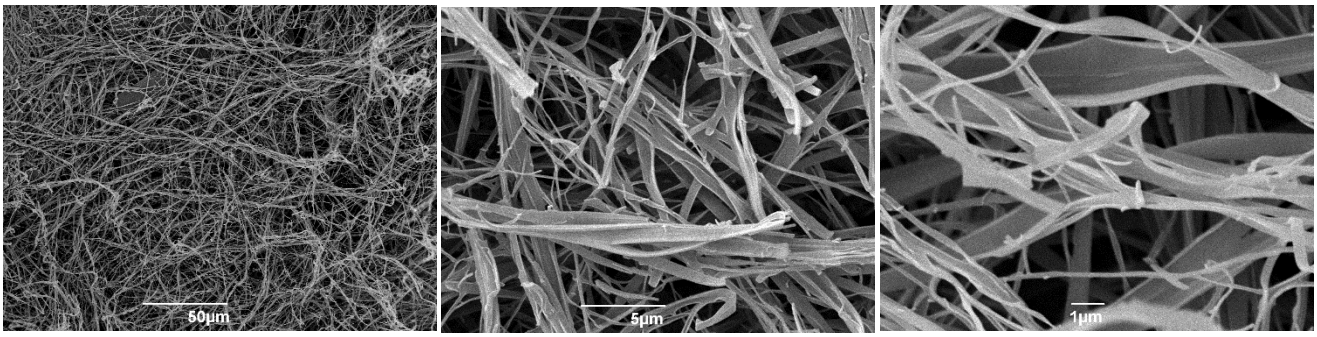

Figure 32. SEM images of BG-C11 (glutamine-C11 (0.15% (wt/vol)) with 0.8 molar equivalent of benzaldehyde) - (magnified by 1K and 5K).

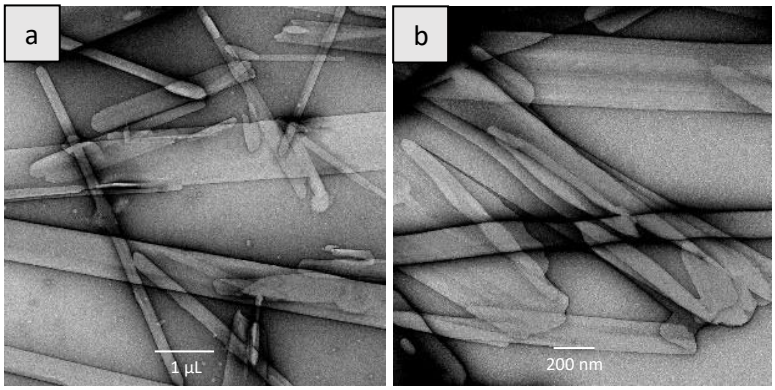

Figure 33. TEM images of BG-C11 (glutamine-C11 (0.15% (wt/vol)) with 0.8 molar equivalent of benzaldehyde) - (magnified by 6.8K(a) and 23K(b)).

The fibres of BG-C11 shown in figure 32 are flat and strand shaped, with various sizes of strands connected at junction points. This confirms the presence of 1D fibres in this gel system. The morphology is somewhat tape-like and crystalline in nature, at least under these sample preparation conditions, with some relatively large tapes (ca. 1.40 - 0.50 µm diameter) and smaller fibres (ca. 0.35 – 0.10 µm diameter). This is consistent with the opaque nature of the gels – larger aggregates have a tendency to scatter light. Figure 33 displays the TEM images of the network which have fibres of varying thickness overlapping one another – once again, these images indicate a degree of rigidity and crystallinity.

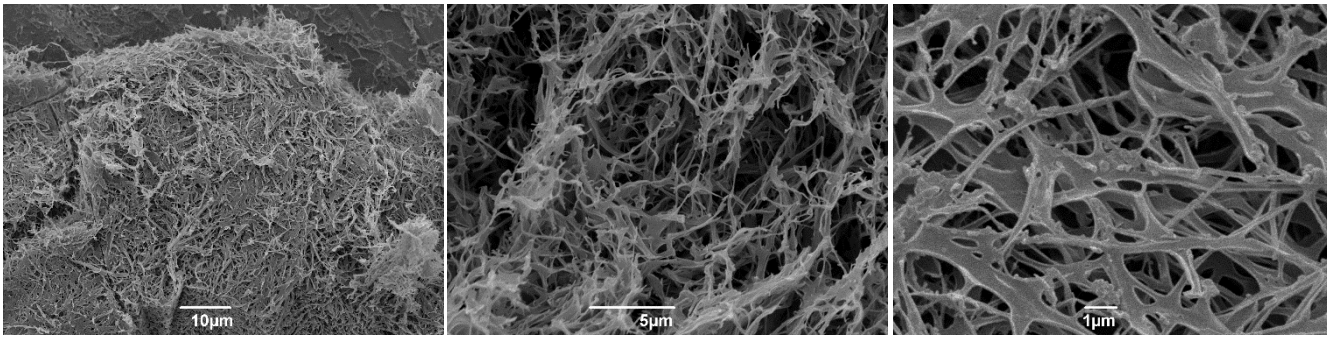

Figure 34. SEM images of BG-C14 (0.3% (wt/vol) glutamine-C14 with 1.26 molar equivalent of benzaldehyde) - (magnified by 1.5K, 5K, and 10K).

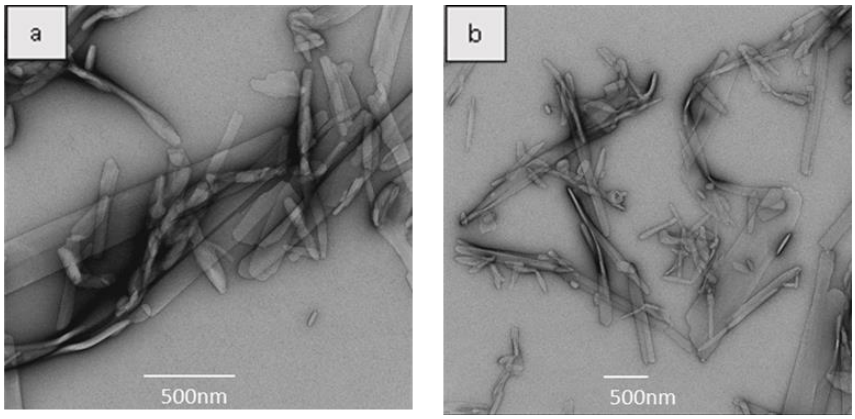

Figure 35. TEM images of BG-C14 (0.3% (wt/vol) glutamine-C14 with 1.26 molar equivalent of benzaldehyde - (magnified by 18.5K(a) and 9.3K(b)).

The densely packed structure of BG-C14 is displayed in Figure 34. Examining the structure more closely, the fibres are compact and in close proximity to one another. The fibres range in diameter, which link up together throughout the network. The diameter of the thicker fibres ranges from 1 – 0.5 µm and the thinner fibres have diameters of 0.4 – 0.1 µm. They appear to be slightly folded and somewhat stretched within each other. Figure 35 shows the TEM images of the network. The different thickness of the crystalline looking fibres which overlap each other is also exhibited in these images – the fibres appear significantly broken in TEM, which may likely be a sample-drying effect The morphology of this network and its highly entangled structure, most evident from the SEM imaging, may explain the rheological and thermal stability of the gel.

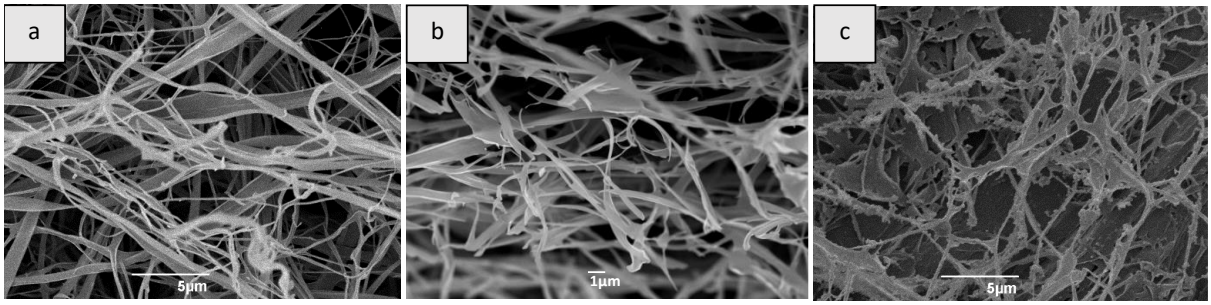

Figure 36. SEM image comparison (magnified by 5K) of a) BG-C11, b) BG-C12 (image obtained from Kirsten Hawkins[147]), c) BG-C14.

To further consider any structural variations in the nanoscale morphology, SEM images of gels formed by the newly synthesized molecules, BG-C11 and BG-C14, are compared to those of the previously reported BG-C12[116]. The gels were prepared in the same method (described in the experimental section), meaning the sample preparation protocol should not contribute to any structural variations. From Figure 36 it is clear that the removal of the methylene group (BG-C11) or addition of an ethyl group (BG-C14) on the original gelator (BG-C12) did not significantly affect the shape of the fibres.

2.3 Altering the Amino Acid

After demonstrating the character change of the original scaffold (G-C12) by manipulating the hydrophobic component of the molecule, we were interested to consider the more complex region of the molecule, the amino acid. By altering this functional groups, we aimed to continue our search for new gelation systems and improve our understanding of the key functional groups that encourage gelation. Clearly, changing the amino acid causes a larger perturbation on the system than modifying the hydrophobic chain, as it alters the hydrogen bonding groups present within the molecule, which play an intimate role in the self-assembly of the LMWG.

2.3.1 Method of Synthesis

2.3.1.1 Synthesis of Alanine-C12

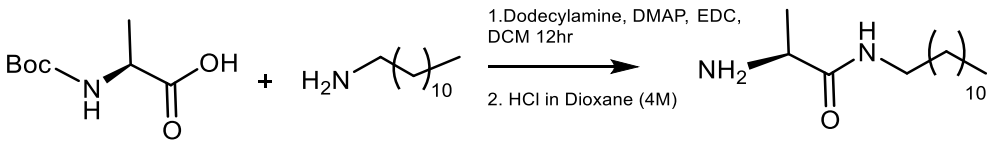

Figure 37. Synthesis of alanine-C12.

Coupling of dodecylamine and Boc-Alanine was performed in dichloromethane in the presence of 4-dimethylaminopyridine and 1-ethyl-3-(3-dimethylaminopropyl)carbodiimide. A workup was performed with 1 M HCl, water, 1 M NaOH, and brine. The product was dried with magnesium sulfate and dried in vacuum. The Boc group was deprotected with 4 M HCl in dioxane. Deprotonation of the molecule was achieved by the addition of NaOH, and the molecule was obtained by the collection of the organic layer (dichloromethane) from a separatory apparatus. The yield produced was 48% and the characterisation of the molecule used ^{1}H NMR, ^{13}C NMR, mass spectrometry, and IR.

2.3.1.2 Synthesis of Proline-C12

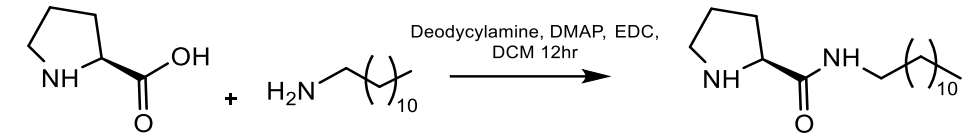

Figure 38. Synthesis of proline-C12.

The coupling of proline with dodecylamine was achieved in the presence of 4-dimethylaminopyridine and 1-ethyl-3-(3-dimethylaminopropyl)carbodiimide as coupling agents and dichloromethane as the solvent. The molecule was washed with 1 M HCl, water, 1 M NaOHl, and brine. The product was dried with magnesium sulfate and dried in vacuum to give a white powder. The molecule was obtained in a yield of 65 %, and was characterised by ^{1}H NMR, ^{13}C NMR, mass spectrometry, and FT-IR.

2.3.1.3 Synthesis of Asparagine-C12

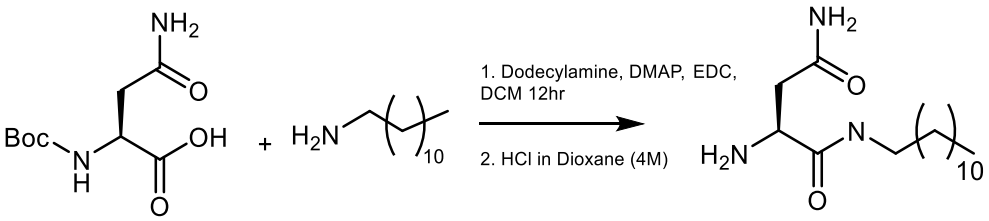

Figure 39. Synthesis of asparagine-C12.

Coupling of dodecylamine and Boc-asparagine was performed in dichloromethane in the presence of 4-dimethylaminopyridine and 1-ethyl-3-(3-dimethylaminopropyl)carbodiimide. A workup was carried out with 1 M HCl, water, 1 M NaOH, and brine. The product was dried with magnesium sulfate and dried in vacuum. Column chromatography was performed to remove further impurities associated with the molecule's hydrophilic nature. The Boc group was removed by deprotection with 4 M HCl in dioxane. As with glutamine-C10, the yield was extremely low and product isolation difficult, therefore, the water-soluble molecule was not deprotonated with NaOH and dichloromethane in a separatory funnel as a large quantity of

the molecule favours the aqueous later leading to low yield. We suggest that this difference to the C12-glutamine system reflects the fact that asparagine has one fewer carbon atom in the amino acid side chain, raising the polarity. Instead, this compound was deprotonated in the gelling process to avoid loss of product during synthesis. The yield produced was 44% and characterisation was performed by ^{1}H NMR, ^{13}C NMR, mass spectrometry, and FT-IR.

2.3.2 Solvent Screen

A solvent screen was performed with these new molecules. Alanine is the simplest molecule to be discussed in this chapter. Compared to the original scaffold it does not possess a side chain amide group. This group promotes hydrogen bonding and is potentially a major contributor to the balance of hydrophilicity/hydrophobicity of the original scaffold. It is interesting to consider the role of this functional group by studying this structure. The samples were prepared in glass vials in which the gelator and solvent were subjected to various gel activation methods. The vials were left undisturbed, and a tube inversion test determined the presence of a gel.

Table 15. Solvent screen of alanine-C12 (3% wt/vol).

Solvent	Quantity of Gelator (mg)	Quantity of Solvent (mL)	Sonicate	Heat	Sonicate then Heat
Water	3.0	0.1	No - White solution	No - ppt in solution	No - ppt in solution
	3.0	1.0	No - White solution	No - ppt in solution	No - White solution
Methanol	3.0	0.1	No - Clear solution	N/A	No - Clear solution
Ethanol	3.0	0.1	N/A	N/A	No - Clear solution
Acetonitrile	3.0	0.1	N/A	No - ppt with oil droplets in solution	No - ppt in solution
DMSO	3.0	0.1	N/A	N/A	No - Clear solution
DMF	3.0	0.1	N/A	N/A	No - Clear solution
Acetone	3.0	0.1	N/A	N/A	No - Clear solution
Ethyl Acetate	3.0	0.1	No - Opaque Solution	N/A	No - Clear solution
Diethyl Ether	3.0	0.1	N/A	N/A	No - Opaque solution

Toluene	3.0	0.1	No - Clear solution	N/A	No - Clear solution
Cyclohexane	3.0	0.1	N/A	N/A	No - Opaque solution
	3.0	1.0	No – Clear solution	No - Clear solution	No - Clear solution

The solvents displayed in table 15 are in an approximate descending order of polarity to demonstrate the relationship between the gelator and the polarity of the solvent. From table 15, it is evident that the alanine derivative failed to produce any gels. This outcome signifies the important role of the missing amide group in the molecule for gelation. If we also compared the new molecule to another gelator synthesized by Kirsten Hawkins, Serine amide[116] (serine-C12), we can exemplify the claim that the molecules solubility balance has been disrupted. The amino acid serine is similar in structure to alanine (Figure 38) but has an additional hydroxyl group. Studies conducted by Hawkins showed that Serine amide formed gels in acetonitrile, toluene, cyclohexane, and water[116]. The extra hydroxyl group has therefore now been proven to play a role in those gel forming events as removal of this hydroxyl group in alanine-C12, resulted in precipitate, an opaque solution, and a clear solution with those respective solvents. This indicates the importance of this functional group and its impact on solubility and any associated supramolecular bonds involved in the process of gelation.

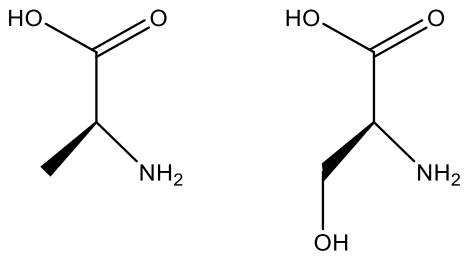

Figure 40. Structures of alanine and serine amino acids.

Table 16. Solvent Screen of proline-C12.

Solvent	Quantity of Gelator	Quantity of solvent	Sonicate	Heat	Sonicate then heat
Water	3 mg	0.1 mL	Oil droplets in clear solution	Oil droplets in clear solution	Oil droplets in opaque solution
Methanol	3 mg	0.1 mL	Clear solution	N/A	N/A
DMF	3 mg	0.1 mL	Clear solution	Clear solution	Clear solution
Ethyl Acetate	3 mg	0.1 mL	Clear solution	Clear solution	Clear solution
Diethyl Ether	3 mg	0.1 mL	N/A	White crystals	White Crystals
Toluene	3 mg	0.1 mL	Clear solution	Clear solution	Clear solution
Cyclohexane	3 mg	0.1 mL	Clear solution	N/A	N/A
Hexane	6 mg	0.1 mL	Clear solution	N/A	N/A

Table 16 demonstrates the solvent screen of the molecule proline-C12. The samples were prepared in glass vials in which the gelator and solvent were subjected to different gel activation methods. The vials were left to allow for gel formation, and a tube inversion test determined the presence of a gel. From Table 16 we can conclude that the proline derivative also failed to produce any gels. The molecule was interestingly soluble in most solvents. The hydrophobic interactions from the pyrrolidine ring did not substitute the supramolecular bonds formed from the missing amide group found on the original scaffold (glutamine-C12).

The low yield of asparagine-C12 was avoided by removing the final deprotonation step in its synthesis. Thus, to initiate gelation the protonated molecule was tested with pH altered water (with NaOH). The samples were prepared in glass vials in which equal quantities of the gelator and solvent were heated with a heat gun until dissolution. The vials were left to cool overnight and a tube inversion test determined the presence of a gel.

Table 17. pH screen of asparagine-C12.

pH of Water	Quantity of Gelator (mg)	Volume of Water (mL)	Did it Gel?
10.1	3.0	0.3	No
11.1	3.0	0.3	No
12.0	3.0	0.3	No
12.5	3.0	0.3	No

13.0	3.0	0.3	Yes
13.5	3.0	0.3	Partial gel

The optimum pH at which the molecule gelled was pH 13. Any pH value above or below 13 did not promote self-assembly. The molecule has one less methylene group compared to the original scaffold but has managed to form a white hydrogel. The molecule will therefore be further investigated by several characterization techniques later in this chapter. Overall, however, this observation would confirm the view that the side chain hydrogen bonding group (in this case an amide) plays an important role in promoting the gelation of this class of molecule in water.

2.3.3 Aldehyde Screen

Although the alanine and proline derivatives could not initiate gelation in their own right, we reasoned that they may be able to form gels on addition of an aldehyde, like the original scaffold. As with previous molecules, the new derivatives were therefore screened with multiple aldehydes.

Various concentrations of aldehydes were tested with alanine-C12 and proline-C12 in the presence of water respectively. The gels were exposed to various techniques to trigger gelation (sonication and heat). The vials were left undisturbed overnight and gel formation was determined through physical observation and the tube inversion test.

Table 18. Aldehyde screen of alanine-C12.

Aldehyde	**Quantity of Gelator (mg)**	**Equivalents of Aldehyde**	**Quantity of Aldehyde**	**Quantity of Water (mL)**	**Sonication**	**Heat**	**Sonication + Heat**
Benzaldehyde	3.0	1.2	1.40 µL	0.1	No – White ppt in solution	N/A	No - White solution with oil droplets

2-Nitrobenzaldehyde	3.0	0.5	0.88 mg	0.2	No – Pink oil droplets in white solution	No – Orange oil droplets in white solution	No – Orange oil droplets in white solution
Vanillin	3.0	1.0	1.77 mg	0.2	Yes – Irreproducible yellow gel with yellow droplet	Yes – Irreproducible light-yellow gel	No – Green solution with droplets
Furfural	3.0	1.0	0.95 µL	0.3	No – Brown oil droplets in clear solution	No – Brown oil droplets in clear solution	No – Orange oil droplets in clear solution
Cuminaldehyde	3.0	1.0	1.70 µL	1.5	No - Oil droplets in clear solution	No - Oil droplets in clear solution	No - Oil droplets in clear solution

Unfortunately, the addition of a range of aldehydes to alanine-C12 did not induce gelation via Schiff formation as shown in Table 18. The molecule did produce a gel with vanillin however it was irreproducible. It is worth noting that vanillin is the most hydrophilic of the aldehydes tested, and this may therefore be acting to offset the relative hydrophobicity of the methyl side chain of the alanine and shift the solubility into the region where hydrogelation becomes possible. For all samples, however, the aldehyde is apparent in the solution as it separates from the aqueous solution, suggesting relatively ineffective Schiff base formation in each case.

Table 19. Aldehyde screen of proline-C12 (2% (wt/vol)) in 0.3 mL.

Aldehyde	**Quantity of Aldehyde**	**Equivalent of Aldehyde**	**Sonication**	**Heat**	**Sonication then Heat**
Benzaldehyde	0.54 µl	0.25	No - White solution	No – White solution with oil droplets	No – white solution with oil droplets
Glycolaldehyde Dimer	0.64 mg	0.25	No – clear solution with oil droplets	No – clear solution	No – clear solution with oil droplets

				with oil droplets	
Furfural	0.44 µL	0.25	No – Orange solution with oil droplets	No – Clear solution with brown oil droplets	No – Orange solution with orange oil droplets
Cuminaldehyde	0.80 µL	0.25	No – White solution with oil droplets	No – Clear solution with oil droplets	No – Milky solution with oil droplets
Vanillin	0.80 mg	0.25	No - Milky solution	No – White solution with oil droplets	No - Milky solution with oil droplets
2-Nitrobenzaldehyde	0.8 mg	0.25	No – White solution with yellow oil droplets	No – Opaque solution with yellow oil droplets	No – Opaque solution with yellow oil droplets
4-Nitrobenzaldehyde	0.8 mg	0.25	No – White solution with yellow oil droplets	No – White solution with yellow oil droplets	No – White solution with yellow oil droplets

As demonstrated in Table 19, gels were also not produced with Proline-C12. There is a trend in the incompatibility between the aldehyde and gelator with the use of heat. Applying heat to the mixtures gave larger oil droplets, which constitute the aldehyde added to the mixture. In this case, it should also be noted that the amine in proline is a secondary amine and will not give rise to a Schiff base derivative in the same way as a primary amine. We therefore suggest that the lack of reactivity between proline and aldehyde means that there is no ability for the aldehyde to be incorporated into the system and hence fully solubilised in the water, leading to the observation of highly biphasic mixtures.

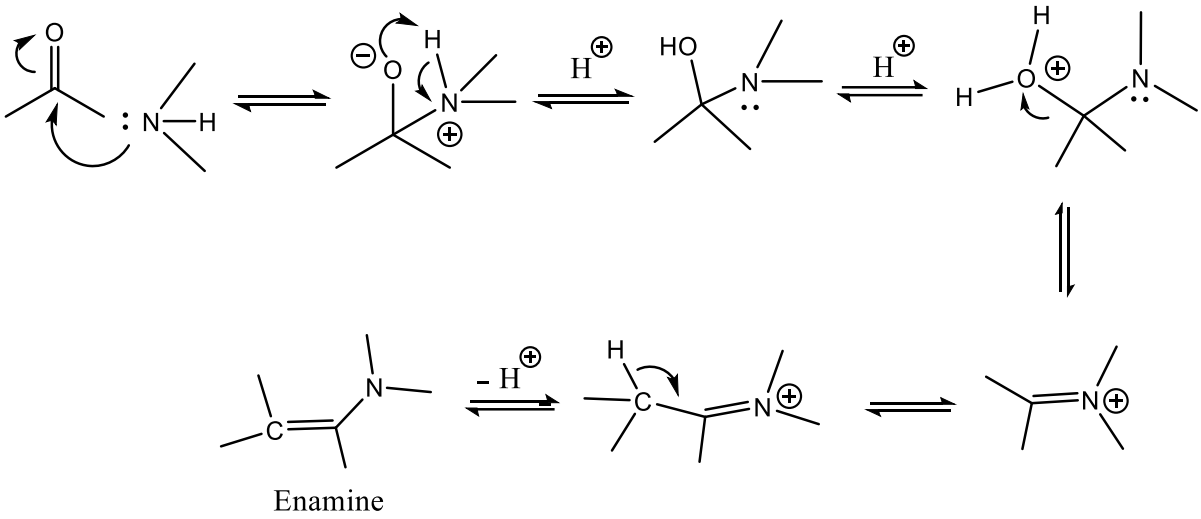

Figure 41. Scheme of enamine Formation.

We might expect proline to form an enamine in a reversible reaction as described in figure 41, however, we saw little evidence that this was occurring, and it certainly did not result in any gel formation.

Unfortunately, owing to the relatively low quantities of asparagine-C12 obtained from synthesis, a full aldehyde screen could not be obtained. We therefore continued with the characterization of the asparagine-C12 hydrogel in water.

2.3.4 Characterization of Asparagine-C12

2.3.4.1 Minimum Gelation Concentration

In order to determine the MGC, we made up samples with various quantities of the gelator and added equivalent volumes of water to each sample. The samples were activated by the heat/cool method and the results are shown in Table 19.

Table 20. Determining the minimum gelation concentration of asparagine-C12.

Quantity of gelator (mg)	Volume of water (mL)	Did it gel?
0.2	0.1	No
0.3	0.1	No
0.4	0.1	No
0.5	0.1	No
0.7	0.1	No
0.8	0.1	No
0.9	0.1	Yes
1.0	0.1	Yes

As the concentration of the gelator increased, the solubility of the molecule decreased giving rise to a network complex. The network developed at the quantity of 0.9 mg in 0.1 mL, which gives a minimum gelation concentration (0.9% wt/vol). Although it may seem as that this molecule is efficient at gelation considering the relatively low concentration, the gelator could not produce reproducible gels above 1.0% (wt/vol), as a result of incomplete solubilisation. As such, the concentration range at which gelation occurs is very limited (see below).

2.3.4.2 Thermal Stability

To determine the T_{gel} values, we prepared gels at different concentrations of the asparagine gelator. Using an oil bath, we recorded the temperature at which the gels lost their shape via the tube-inversion method (Table 21).

Table 21. Determining the T_{gel} of asparagine-C12 gels with varying concentrations.

Gelator Quantity (mg)	Volume of Water (mL)	Tgel (°C)	Appearance of Gel Before Experiment
2.70	0.30	34-36	Opaque gel
3.00	0.30	34-42	Opaque gel
3.60	0.30	N/A	Weak clear gel

3.90	0.30	N/A	No gel

The results showed that the 1% wt/vol gel was the most thermally stable as it withstood a higher temperature. Gels with higher concentrations gave weak gels (1.2% wt/vol) and, at higher concentrations, precipitation (1.3% wt/vol). This reflects the inability of all of the gelator to dissolve at these higher concentrations. As such, this gelator only forms gels in a limited range of ca. 0.9 - 1.1% wt/vol. It should be noted that after the gel-sol transition the gels did not reform a gel on simple cooling indicating that this gel is not thermo-reversible. However, it is interesting to note that the gel-sol transition temperature occurs at around body temperature, which could make this simple amino acid gelator of interest for use as a drug delivery vehicle *in vivo*.

2.3.4.3 Transmission Electron Scanning

To confirm the nanostructure of the asparagine-based gel, 1% (wt/vol) of asparagine amide with water was prepared to form a gel. A small sample was taken to give TEM images (Figure 42).

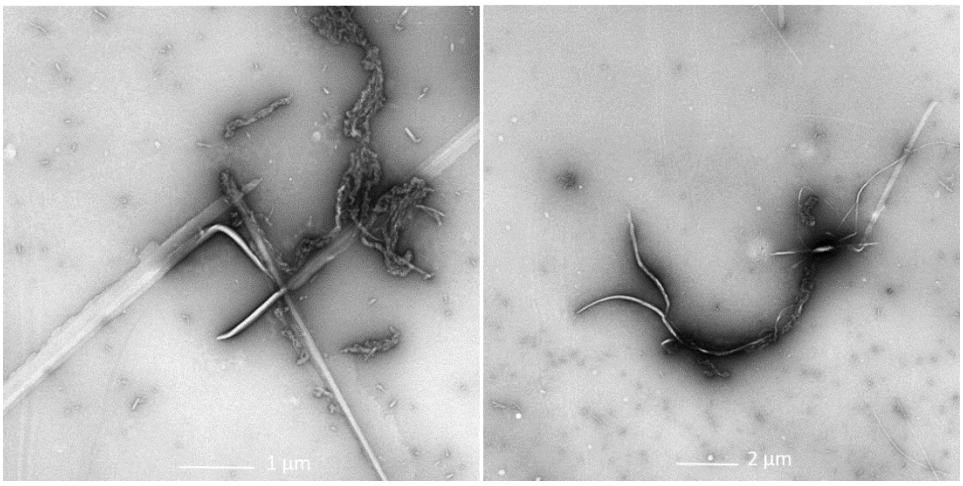

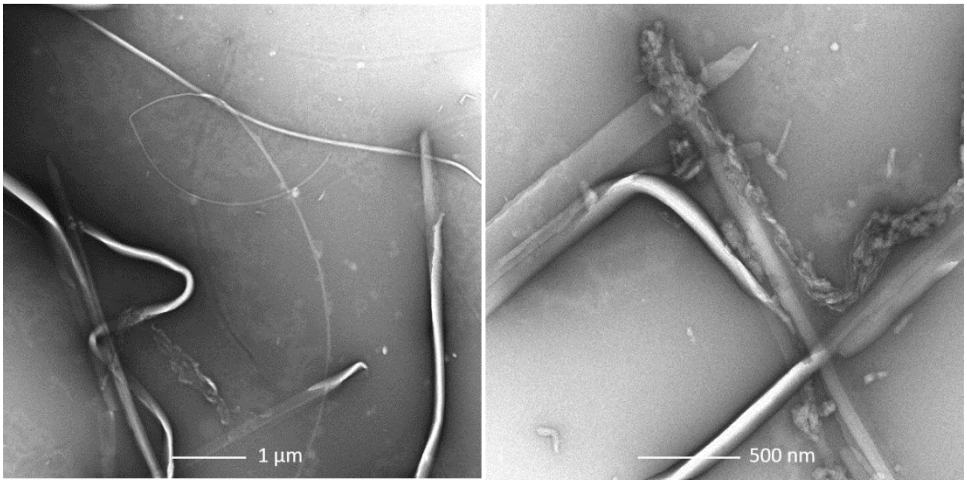

Figure 42. TEM images of asparagine-C12 (1% wt/vol) gel fibres.

These images confirm that some one-dimensional assemblies are formed. They vary in diameter (0.1 - 0.2 µm). The fibres are entangled within each other, with some fibres looking more crystalline, while others seem to have a softer braided-like structure, entangling with one another.

2.4 Summary and Conclusions

In this chapter, we successfully report the synthesis and investigation of some new amino-acid based lipids, and characterised their ability to form gels both in the absence, and presence, of a variety of aldehydes.

Firstly, we varied the length of the alkyl chain and to study the importance of the hydrophobicity associated with the alkyl groups. Reducing the chain to 10 carbons completely disrupted the formation of the 3D network. This indicates that the alkyl chain has a direct effect on self-assembly. Synthesizing BG-C11 hydrogels uncovers the shortest length of alkyl chain needed for self-assembly. The hydrophobic nature of the chain is essential for fibre formation leading to hydrogel self-assembly. The gel properties however are altered compared to the BG-C12 hydrogel with a decreased thermal stability as well as rheological stability. There is evidence that greater solubility of the gelator underpins this somewhat less effective gelation. The carbon chain was then increased from 12 to 14 carbons which successfully caused the gelator to form reproducible hydrogels in its own right, as well as a two-component hydrogel via Schiff base formation. The one-component hydrogel unlike the

glutamine-C12 was reproducible and can form in water at almost all pH values. The additional hydrophobic effect reinforced the self-assembly of the hydrogel. It is important to note that for the hydrogel to assemble without forming a Schiff base, it required a high concentration relative to the two-component hydrogel (BG-C14). The formation of Schiff bases with aldehydes stabilized the gel giving much more opaque gels and improving gelation efficiency. The two-component gel displayed similar thermal stability, rheological, and thixotropic properties as the original gel (BG-C12). The study confirms that the hydrophobic and amphiphilic domains both play key roles in underpinning the self-assembly of this class of molecule. The reproducibility of the BG-C14 hydrogel and its maintenance of the original properties of the BG-C12 suggest that perhaps increasing the length of the chain to >14 would produce more stable gels with improved qualities. There was some evidence that with the greater degree of hydrophobic modification, a more hydrophilic aldehyde, such as vanillin could potentially assemble into gels, although with a C14 chain, the gelation kinetics remained slow.

Manipulation of the original scaffold by varying the amino acid produced molecules which mostly lacked the ability to gel or achieve consistent gel formation. Notably, Alanine-C12 was unable to form gels, unlike the Serine-C12 analogue previously produced by Hawkins[116]. This indicates the importance of a single OH group in enabling gel formation. Asparagine-C12, although forming gels did not appear to offer significant advantages over the glutamine-based system, and its synthesis and isolation were more challenging.

Overall, in this study we have highlighted the role of functional groups in the process of gelation. We have confirmed the importance of hydrophobic/hydrophilic balance, and the way in which very small changes to functional groups (addition/removal of a single CH_2 group, or a single OH group) can significantly impact on self-assembly and gelation behaviour. This demonstrates the highly tuneable nature of supramolecular gels, and also outlines how this specific class of molecule only forms gels successfully in a relatively precisely defined area of chemical space.

Chapter 3 Benzyl Glutamine as a Drug Delivery Platform

3.1 Introduction

Supramolecular hydrogels consist of molecules that self-assemble in processes that lead to water-rich solid-like materials upon the application of stimuli. When the gelator molecules are exposed to drug moieties, possible interactions between the two may occur. Interactions are key components to the gel-drug compatibility and can have a significant influence on the drug loading and release profiles. The physical properties of the drug, such as lipophilicity, may also impact the gel-drug compatibility. The presence of interactions can result in strong forces preventing drug release, hence producing a slow-release system. In some instances, such interactions can prevent gel formation as the drug initiates instability. There is unfortunately no 'one-size-fits-all' type of gel for drug molecules, and therefore screening of drugs is usually carried out with a specific hydrogel.

For example, Friggeri et al studied the drug release profiles of two quinolone derivatives with a *N*,*N*'-dibenzoyl-L-cystine hydrogel[75]. It was discovered that the amine group of 8-aminoquinoline can interact with the carboxylic acid functional group of the hydrogelator forming acid-base interactions. This led to a better binding of the drug to the gel as well as a higher thermal stability compared to the other derivative investigated, 2-hydroxyquinoline, which can only interact with the gelator through weak hydrogen bonding or van der Waals interactions. This was reflected in the release profile of 8-aminoquinoline was significantly slower in its release compared to 2-hydroxyquinoline[75]. This underlines the important role of drug-gel interactions which can lead to control over release profile kinetics. In another study, bovine serum albumin (containing a thiol group) and polysaccharide dextran release profiles from two glycosylated nucleoside-based bola-amphiphile hydrogel derivatives (with/without disulfide groups) revealed that the thiol group of the drug integrated itself with the disulfide of the gel by forming a reversible covalent bond. This resulted in a slow onset of release whereas the lack of this combination gave faster drug release[128]. As described in the previous chapter, Benzyl glutamine (BG-C12) displayed desirable qualities that would make it suitable for applications in drug delivery, and this had previously been explored with regard to the

release of the Parkinson's Disease drug L-DOPA[2]. In this chapter, we will focus on the compatibility of the gel with various drug molecules and study their respective drug entrapment and release profiles. In the process, we will highlight any potential drug-gel interactions and determine the most suitable drugs for this gel system. We will also discuss the fabrication and application of multicomponent LMWG/PG gel networks formed from our LMWG (Benzyl glutamine) and natural seaweed-derived polymer gelators based on alginic acid, which were developed in order to overcome some of the weaknesses of Benzyl Glutamine (see below).

3.2 Benzyl Glutamine-Alginate Multicomponent Beads

One of the limitations of the Benzyl glutamine hydrogel, which is common with many LMWGs, is its mechanical strength and inability to generate self-standing objects. Indeed, Benzyl glutamine has particularly weak rheological performance, which was one of the reasons it had previously been developed for consideration as a nasal delivery gel. There have been reports of combining LMWGs with polymer gels to synergise the desirable properties of each gelator and hence produce a superior hybrid gel system[129]. Very often, the more robust rheological properties of polymer gels can enhance the mechanical performance of more fragile LMWGs. Indeed, this approach has been used by our group to convert DBS-COOH and DBS-$CONHNH_2$ fragile hydrogels into spherical multicomponent gel beads by the addition of calcium alginate. The new gel system makes it possible for these LMWGs to be easily transferred and held without damaging the network as the polymer provided structural support while maintaining the properties of the LMWGs[42]. This inspired the fabrication of multicomponent beads consisting of Benzyl glutamine with calcium cross-linked alginate. This new system was initially developed by a BSc project student Lauren Woolley in our research group.

Figure 43. BG-C12/Alginate hybrid beads (composed of 0.35% (wt/vol) glutamine-C12 with equimolar benzaldehyde, and 1% alginate) in a water bath.

Alginic acid is composed of alternating blocks of α-L- guluronic acid (G) and β-D-mannuronic acid (M). Upon mixing with multivalent cations such as Ca^{2+}, ionic interchain bridges form to produce an instant interconnected network through what is called the "egg box" model.[130] Alginic acid is a brown algae derived polymer, and is widely used in the food industry, as well as in environmental and biomedical applications[131, 132]. It was reasoned that by combining calcium alginate with Benzyl glutamine, robust multicomponent beads could potentially be fabricated for potential application in drug delivery.

Benzyl glutamine (0.35% wt/vol) was heated with alginic acid (1 % wt/vol) to initiate gelation of the LMWG. The solution was pipetted into a 40 mL calcium chloride bath (5% wt/vol) in droplets of 25 μL volume, to enable calcium cross linking, which gives rise to droplet-shaped hybrid beads (fig. 43) with diameters of 3 mm. The diameter of the bead being formed is in agreement with the droplet size.

3.2.1 Microscopy Imaging

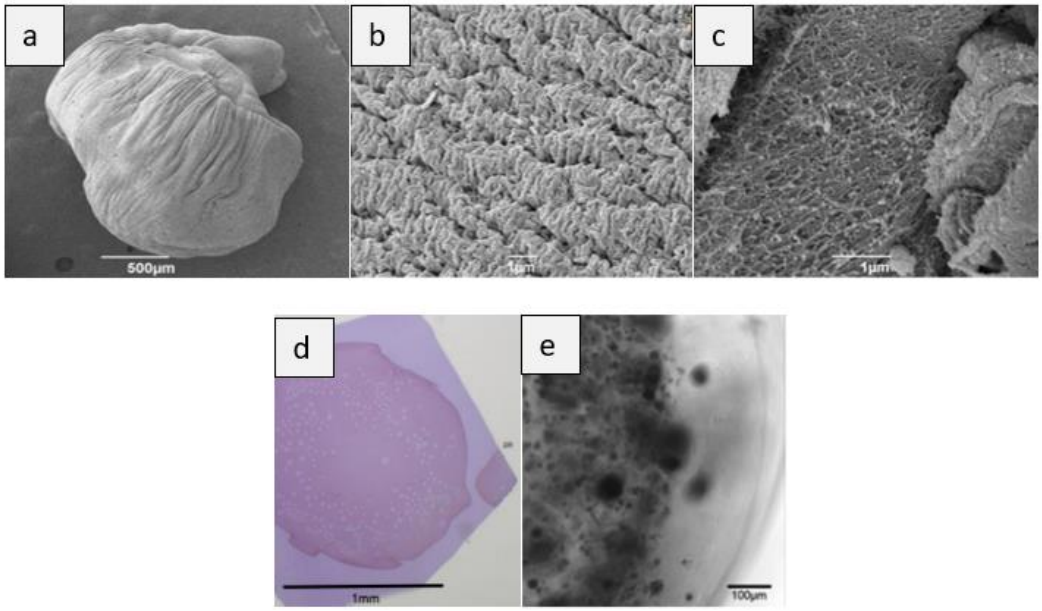

Figure 44. Images of Benzyl glutamine/Alginate beads - SEM (a-c), optical microscopy (d), and confocal microscopy (e).

Pipetting droplets of the multicomponent gel solution into a calcium chloride bath, likely results in core-shell beads with a LMWG core that is surrounded by a calcium alginate polymer outer shell as a result of rapid crosslinking of the exterior of the droplet on addition to the bath. To test this theory, microscopy was utilized to obtain a better understanding of the structuring of these beads. The nanoscale morphology of the hybrid bead arrangement was observed using SEM (figure 44). The outer surface of the bead was a densely wrinkled mass, while the cross-sectional images showed the extended nanofibrillar networks within the bead. This is in agreement with the previous characterisation of DBS-$CONHNH_2$/Alginate gel beads for which a core-shell morphology was proposed, with the self-assembled network of the LMWG being formed within the calcium alginate gel bead shell. The hybrid beads were then embedded in resin and dyed with toluidine blue prior to optical microscopy. There is a contrast in colour (figure 44 (d)) showing a thin outer shell (lighter colour) and thicker inner region (darker colour). The results however aren't very clear, an alternative method of imaging was therefore used, confocal microscopy. Figure 44 (e) provides a better display of the structure, with the outer region having less contrast than the inner region, promoting the idea that the

BG-C12 formed the self-assembled core while the outer shell is predominantly composed of crosslinked calcium alginate.

3.2.2 Thermal Stability

To determine the thermal stability of the multicomponent gels and the influence of the calcium alginate on this property, the gel-sol transition temperature (T_{gel}) was determined. The gel was made in a vial with BG-C12 (glutamine-C12 (0.35 wt/vol) with equimolar benzaldehyde) and 1% wt/vol alginic acid crosslinked with 5% wt/vol calcium chloride. By using a temperature-regulated oil bath, it was found that the hybrid gel had a T_{gel} value of >100°C. This was considerably higher than the LMWG gel alone (T_{gel} = 83°C) providing evidence that hybrid gels exhibit enhanced thermostability as a result of the presence of the calcium alginate.

3.2.3 FT-IR and NMR Studies

By comparing IR spectra (data found in section 7.2.5) of the gel bead xerogels with BG-C12 xerogels we could detect possible interactions between the two gelators. There is a shifted sharp peak in the C=O region (1652 → 1640 cm^{-1}) suggesting a potential interaction between the LMWG and polymer. This reinforces the idea of the collaboration between the two gels to produce an improved material carrying properties of both individual gels.

NMR was utilised to calculate the quantity of LMWG present in each hybrid gel bead (experimental details found in section 7.2.4). 10 beads were dissolved in DMSO-d_6, alginic acid is not soluble in DMSO and is therefore not observed in the spectrum. An internal standard, acetonitrile, was added to enable quantitative NMR. By comparing the integral peak of acetonitrile (δ = 2.07 ppm) and the end methyl group of the LMWG (δ = 0.71 ppm), we found that 98.3% of the added LMWG is located in the hybrid beads. This means the gel bead fabrication is a highly efficient process with minimal loss of the LMWG.

3.2.4 Rheology

An integral part of fabricating the novel multicomponent system was the additional mechanical stability associated with the additional polymer which allowed the beads to be handled. Other than visible observations (a self-standing gel bead), the ''robustness'' of the new system was quantified by rheological studies. Gels were made in vials to enable rheological study with Benzyl glutamine (0.35% (wt/vol) glutamine-C12 with equimolar amount of benzaldehyde)) and alginate (1.0 % (wt/vol)). They were prepared in bottomless glass vials held in place with a sealant. Once the gels had formed, the vials were removed, and the self-standing hydrogel placed on a rheometer plate. Figure 45 presents the frequency sweep of the hybrid gel.

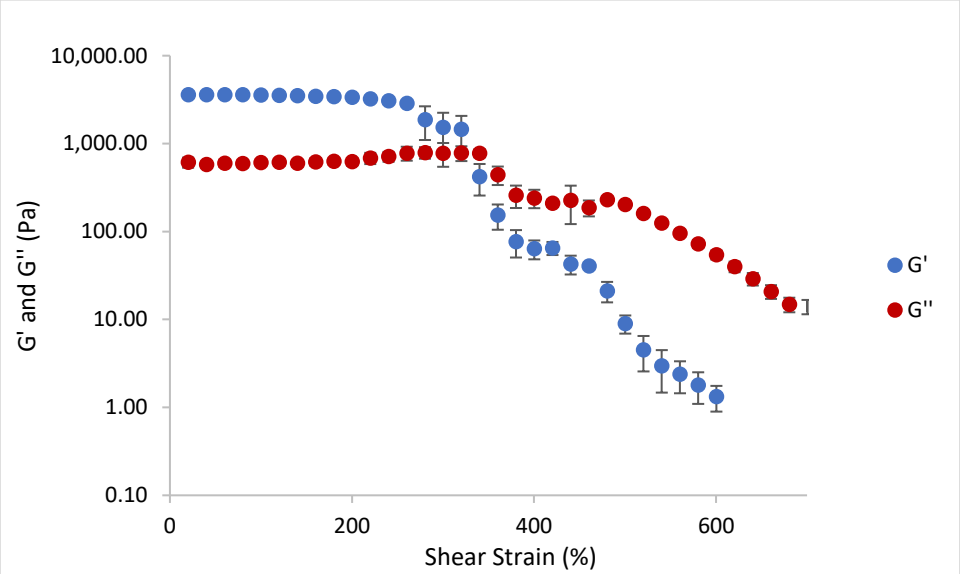

Figure 45. Elastic (Blue) and viscous (Red) moduli with increasing strain of BG-C12/Alginate (glutamine-C12 (0.35% wt/vol) with equimolar benzaldehyde, and alginate (1.0 % wt/vol)) hydrogel performed using parallel plate geometry at 25°C. Error bars in the graph represent the standard error of the mean.

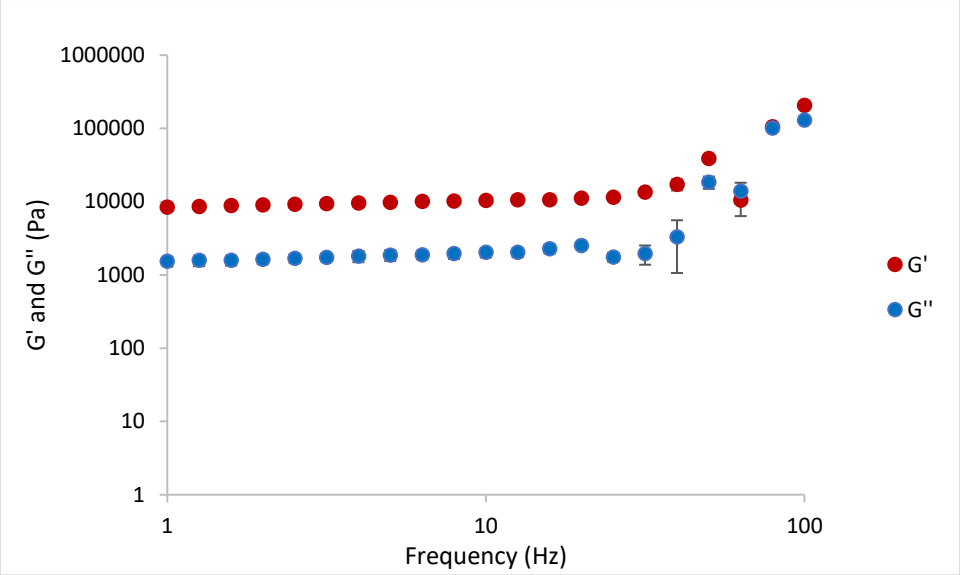

Figure 46. Elastic (Blue) and viscous (Red) moduli with increasing frequency of BG-C12/Alginate (glutamine-C12 (0.35% wt/vol) with equimolar benzaldehyde, and alginate (1.0 % wt/vol)) hydrogel. performed using parallel plate geometry at 25°C. Error bars in the graph represent the standard error of the mean.

We were not surprised to find that the elastic (G') and viscous (G'') moduli of the hybrid gel were much greater than the values of the LMWG alone[110]. Indeed the G' value of BG-C12/Alginate is 3610 Pa compared with 780 Pa for BG-C12 alone[110]. This means the LMWG gained additional stiffness and solid-like behaviour through the addition of the polymer, confirming the value of adding the polymer into this system. This indicates how the PG is capable of stabilising the network and is able to maintain the gel in its water droplet shape. The next step was to investigate both Benzyl glutamine and the new hybrid beads for their drug delivery applications with a range of active pharmaceutical agents.

3.3 Naproxen

Naproxen (NPX) is a non-selective non-steroidal anti-inflammatory drug (NSAID). Frequently used as an antipyretic and analgesic medication. The drug is commonly prescribed for patients with continuous pain such as rheumatoid arthritis. It is a non-selective COX-inhibitor meaning it inhibits both cyclooxygenase enzymes (1 and 2). COX 2 is inducible upon injury and is associated with prostaglandin production that promotes inflammation such as pain, fever, and

swelling of vessels.[133] The drug forms a reversible bond with the enzyme thus blocking prostaglandin synthesis. The outcome of naproxen's non-selectivity however leads to the blocking of COX 1, which is found in the mucosal stomach lining. Stimulation of gastrointestinal bleeding is the result of such a blockade, and this is the main side effect of this group of drug.[134] We started investigations with naproxen due to its structure and physical properties as well as being a familiar molecule in our group[39, 135].

In other research, Vilaca et al produced a dihydrodipeptide-containing naproxen N-capped tryptophan hydrogelator[136]. Li et al synthesized a group of naproxen-conjugated D-amino acid based supramolecular topical gels. Conjugation of the amino acids to the carboxylate end of naproxen did not deplete naproxen's potency and in fact increased COX 2 selectivity as a result of the structural modification. This resulted in a group of API hydrogelators with resistance to proteolysis due to the use of D-amino acids[136]. We therefore wanted to explore the use naproxen with our Benzyl glutamine gelator.

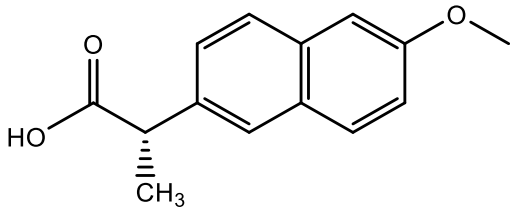

Figure 47. Structure of naproxen.

3.3.1 Drug Loading

There are two common practices to load a drug molecule into a hydrogel. The favoured choice is to formulate the gel in the presence of the drug. The drug would therefore be present during self-assembly and may possibly be intimately involved in the gelation event as it forms interactions with the gelator molecule. This approach offers an advantage as it avoids the need for methods to quantify the drug loading. If the drug is not compatible with this approach, for example preventing the gel from forming, then another method can be used - diffusion-based loading. The drug solution is added on top of the surface of the gel and the drug diffuses into

the gel network. This approach, however, requires quantitative methods to calculate drug loading, making it unfavourable. It can also limit the overall loading achieved, and requires high levels of drug solubility to achieve high loadings, which is not always possible.

Table 22. Gelation of BG-C12 (0.35% glutamine-C12 with one molar equivalent of benzaldehyde) in the presence of naproxen (pre-gelation).

Quantity of Naproxen (mg)	Quantity of Gelator (mg)	Volume of Water (mL)	Did it gel?
2.2	3.5	1.0	No
3.3	3.5	1.0	No
3.9	3.5	1.0	No

Gels were formulated using the same quantities of gelator and solvent to study the effect of the drug molecule on gelation (Table 22). Unfortunately, the gels could not form in the presence of naproxen. It was noted that naproxen has relatively poor solubility in water[137] which may be the reason for naproxen's disruption of the delicate 3D network. Naproxen is known to be nearly insoluble in water and is available commercially in salt form. It might therefore have just precipitated leading to disruption of gel formation. Alternatively, the naproxen may have interacted with the gelator, and disrupted the network assembly as a result of its hydrophobicity, which can also potentially interact with hydrophobic surfaces in the LMWG, that are required for effective assembly. Finally, it is possible that the carboxylic acid on naproxen may interact with the amine group, competing with the aldehyde, and hence limiting Schiff Base formation between aldehyde and amine, which would prevent the fabrication of an effective gel. To test this a little further, the experiment was performed with naproxen in the presence of sodium hydroxide, in which it is soluble. Multiple quantities of naproxen and equal quantities of BG-C12 were dissolved in 1 mL of water with NaOH (Table 23).

Table 23. Testing the gelation of BG-C12 (0.35% glutamine-C12 with one molar equivalent of benzaldehyde) with naproxen dissolved in NaOH (Pre-gelation).

Quantity of Drug (mg)	Quantity of Gelator (mg)	Volume of Water (mL)	Did it Gel?
10	3.5	1	No
9	3.5	1	No
5	3.5	1	Yes
1	3.5	1	Yes

As demonstrated in Table 23, reproducible gel formation could be achieved in the presence of sodium hydroxide at lower drug loadings, producing white gels. This promotes the theory that the insolubility of the drug in water led to precipitate and prevented self-assembly of the peptide gel. On deprotonation, the drug becomes more soluble and gel assembly is facilitated.

FT-IR studies on xerogels gelled with/without naproxen and pure naproxen were then used to probe the environment of the carboxylic acid group of naproxen within the gels (data found in section 7.2.2). There is a shift in the C=O region in the spectrum, in which pure NPX has a distinct peak of 1725 cm^{-1}. The C=O region of the naproxen-loaded xerogel had a broadened peak at 1659 cm^{-1} – this could reflect the deprotonated naproxen but may also indicate some interaction with the secondary amine group on the gelator.

An alternative method of loading naproxen, diffusion-based, was also tested. The gel was made by sonicating and heating 0.35% (wt/vol) BG-C12 in 1 mL water in a glass vial. The vial was left undisturbed for complete self-assembly to occur. Samples were then prepared with 1 mL of naproxen sodium solution (0.2 mg/mL naproxen and 0.7 mL 1M NaOH) being added to each vial. The vials were incubated at 37°C for >12 hours. The drug molecule was predicted to diffuse into the 3D network during incubation. The drug loading was measured by detecting the concentration of the drug supernatant post drug loading via UV-Vis. The drug loading efficiency was approximately 56% of the 0.2 mg/mL NPX sodium solution.

It is worth noting at this point, that even though gels could therefore be obtained, the acquired drug loadings (ca. 5mg/mL) does not correspond with the therapeutic dose (250-500 mg per dose). It is hard to see how this loading difference can easily be solved, and the gel would therefore seem to have low potential for use as a naproxen delivery platform. Nonetheless,

despite the extremely low loading outcome, we were interested in studying the variation in drug release between the gels loaded using the two different methods. It is also worth mentioning that the chosen dose in this study was based on naproxen's high UV-Vis spectroscopic signal, meaning this concentration was optimal for UV analysis.

3.3.2 Drug Release Studies

As the gel has been loaded with two different methods (pre-loading and diffusion loading), we studied the nature of release of the drug molecules from the 3D network in each case. For both naproxen-loaded gels, 4 mL 0.01 M tris buffer was added to the gel, and the diffusion of the drug out of the gel network monitored. The gels were placed in an incubator at 37°C, to imitate body temperature, hourly aliquots were removed and tested by UV-vis spectroscopy to measure the absorbance with time. Naproxen was monitored by following the absorbance at 329 nm. The studies were performed over a duration of 6 hours and were carried out in duplicate and triplicate. A control was also set up which was not loaded with naproxen.

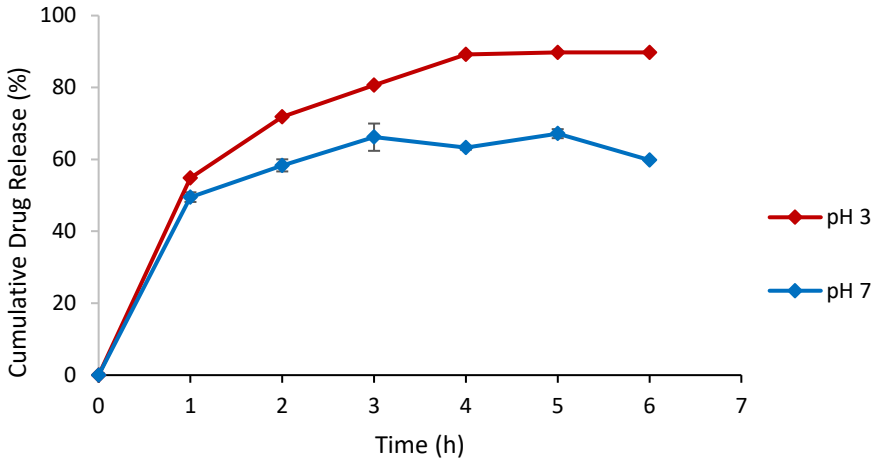

Figure 48. Naproxen sodium release profile from BG-C12 (0.35% glutamine-C12 with one molar equivalent of benzaldehyde) vial hydrogel (loaded with naproxen via diffusion) in tris buffer at varying pH's and at a temperature of 37°C. Error bars in the graph represent the standard error of the mean.

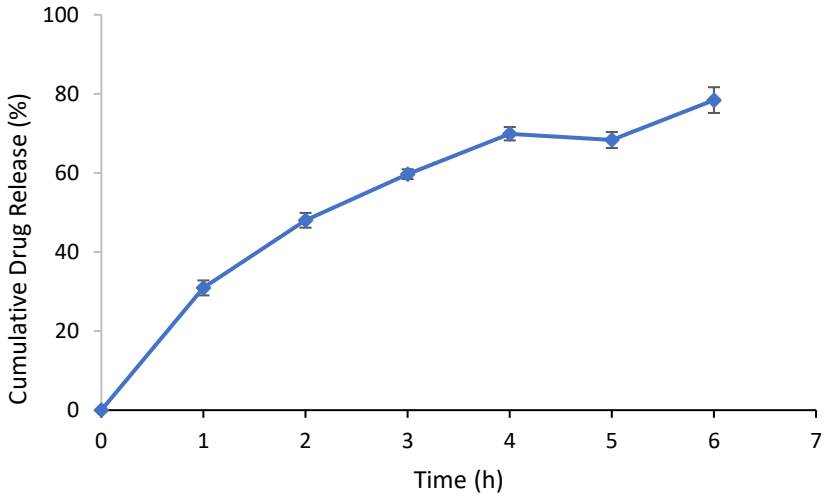

Figure 49. Drug release profile of naproxen from BG-C12 (0.35% glutamine-C12 with one molar equivalent of benzaldehyde) vial hydrogel (loaded with naproxen pregelation) in tris buffer (pH 7) and at a temperature of 37°C. Error bars in the graph represent the standard error of the mean.

For gels loaded by diffusion (Fig. 48), drug release at a pH value of 3 had an initial ca. 55% release which then slowly roughly doubles by the end of the 6-hour period, with a maximum drug release of 90%. The hydrogel showed a variation in release based on pH, with a greater sensitivity to pH 3 compared to pH 7 which, after 50% release in the first hour, only had a further 10% increase in drug release during the study. This event is due to the fragility of the gel towards acidic media, leading to the breakdown of the gel at pH 3, and consequently giving a greater release (erosion release mechanism). This will be exhibited in further drug release profiles throughout the chapter.

Figure 49 displays the release profile of naproxen released from naproxen-loaded gels prepared using the pre-gelation loading method. Unlike the diffusion-loaded gel, the drug diffuses out of the network at a steady rate. Roughly 80% of NPX has been released after 6 hours. By comparing the release profiles of both loading methods (pH 7) we can observe that the pre-gelation method produced a steadier release profile that the diffusion method which plateaued within the second hour. This may suggest that the pre-gelation approach distributes the drug throughout the gel for steady release, whereas the diffusion method is better at rapidly loading (and unloading) the more accessible sites of the gel network close to the surface of the gel, with most of the release then occurring in the first hour of the study. This

study therefore provides new insights into the ways in which drug loading mode can impact on the drug release mechanism – a factor rarely considered in the LMWG literature.

3.4 Rosuvastatin

With easy access to unhealthy food, and more sedentary lifestyles, much of the world is observing a rise of obesity. There are therefore increasing numbers of patients suffering with cardiovascular diseases (CVDs). CVDs are major contributors to morbidity and mortality rates. Statins have therefore been widely prescribed as a preventative measure as well as a first line of treatment to act as a lipid-lowering agent. The mechanism of action of statins relies on their action as HMG CoA reductase inhibitors[138]. We therefore chose to explore the combination of our LMWG with the drug Rosuvastatin (RSV). This highly insoluble drug[139] is found commercially in its calcium salt form to enhance its absorption and solubility in water. The structure of the drug is shown in Figure 50. The molecule is bulkier than naproxen, with more diverse functional groups that could potentially interact with the LMWG. Once again, there is a carboxylic acid group which may interact with the secondary amine on the Benzyl glutamine gelator.

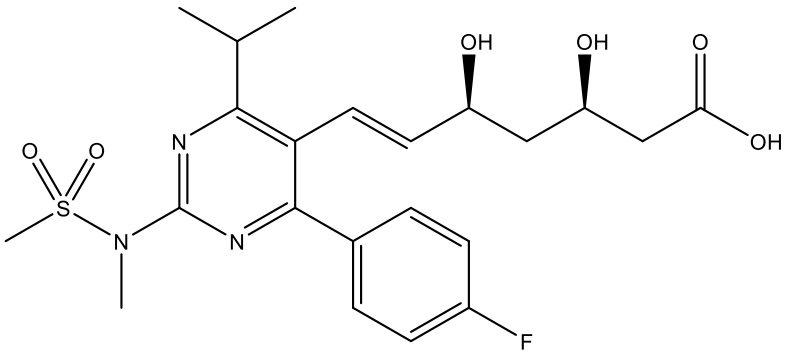

Figure 50. Structure of rosuvastatin.

3.4.1 Drug Loading

Initially, an attempt was made using 0.35% (wt/vol) Benzyl glutamine with various concentrations of rosuvastatin solution to form stable rosuvastatin-loaded hydrogels (Table 24). Gelation was attempted with the use of the heat/cool cycle and the gels were left to stand for 24 h.

Table 24. Rosuvastatin gelation with Benzyl glutamine (0.35% glutamine-C12 with one molar equivalent of benzaldehyde).

Drug concentration (mg/mL)	Did It Gel?
0.50	No
0.25	No
0.15	No

The results clearly show that the presence of the statin prevented the formation of the gel. There are several potential explanations for the lack of gel formation. Considering the drug is soluble in aqueous media, drug solubility is not the issue as with the previously described experiment with naproxen.

The high molecular weight drug may interact with the gel system and as a result disrupt equilibrium of the metastable network and prevent self-assembly. Alternatively, the drug may not interact with the gelator molecules but instead sandwich itself in between gelator molecules as a bulky molecule hindering their assembly, hence preventing an effective sample-spanning gel from being established. Tiwari et al. reported a study in which the molecular weight of drugs contributed to different release profiles with diphenylalanine hydrogels[140]. Stronger involvement with the gels was attributed by drugs of higher molecular weight (curcumin and doxorubicin) compared to smaller drugs (5-flouracil). Computational data explained the different drug-gel interactions, showing the different areas each drug occupies on the gel molecule which corresponds to their release profiles[140]. Benzyl glutamine also gave similar outcomes with another high molecular weight drug dexamethasone (figure 51). Benzyl glutamine (0.35% (wt/vol) glutamine-C12 with equimolar benzaldehyde) was prepared with dexamethasone sodium (0.3 mg/mL) through the heat/cool method. The solution was left overnight in which no gel formation was observed. Dexamethasone sodium

is a large molecule which dissolves in water. This provides another indication that the self-assembly of the gel could be prevented by larger molecules.

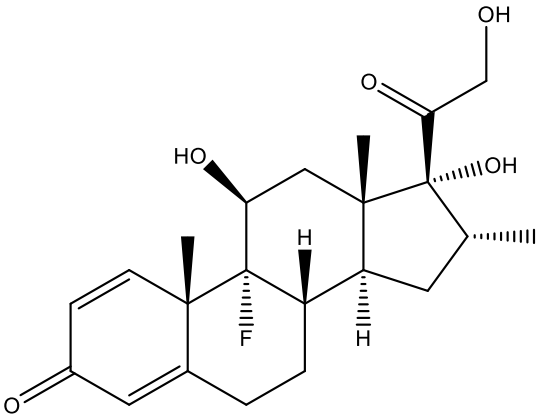

Figure 51. Structure of dexamethasone.

Given that Benzyl glutamine was unable to form a hydrogel in the presence of rosuvastatin, the alternative method of diffusion-loading was pursued. The hydrogel was soaked in 1 mg/mL rosuvastatin calcium solution. The hydrogel took up 65% of the drug, which was measured through quantitative ^{1}H NMR spectroscopy. To measure the drug loading, the drug supernatant was dried and redissolved post drug loading in D_2O with an internal standard DMSO. The calculation was performed by comparing the integrals of DMSO (δ = 2.7 ppm) and the alkene group of rosuvastatin (δ = 5.53-5.85 ppm) in the ^{1}H NMR spectra. FT-IR studies were performed on BG-C12 xerogels (loaded with and without rosuvastatin calcium through diffusion) as well as pure drug. By comparing their spectra no shifts in peaks were detected – suggesting no interactions between the two molecules. Although no interactions were found through FT-IR (data found in section 7.2.14), the results do not dismiss the idea of rosuvastatin interacting with the gelator molecules during self-assembly in the pre-gelation method via the heat/cool cycle. In the diffusion loading method, the pre-formed solid-like Benzyl glutamine gels network may have interactions that do not permit any further involvement with the rosuvastatin molecules in solution. Whereas in the pregelation method the addition of the drug prior to gelation may interact with Benzyl glutamine in the solution phase and hence disrupt the self-assembly of the metastable network.

3.4.2 Drug Release

The release study was conducted in the presence of 4 mL of 10 mM tris buffer at 37°C in an incubator. Rosuvastatin release was detected with the use UV-Vis spectrometry at its distinguishable wavelength of 244 nm. The study was conducted in duplicate and a control with no API loading was used.

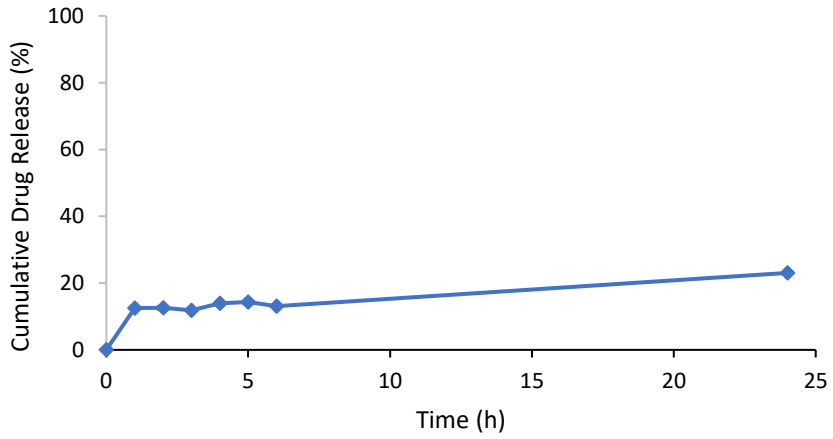

Figure 52. RSV release from Benzyl glutamine (0.35% glutamine-C12 with one molar equivalent of benzaldehyde) vial hydrogel in tris buffer during a 24-hour study at 37°C. Error bars in the graph represent the standard error of the mean.

Overall, the release profile shown in figure 52 was controlled and slow. An initial 11% release of the loaded drug solution within the first hour, which doubled by the time it had reached the 24-hour period. The outcome of this type of controlled release could be due to several reasons. The drug size could be a factor, molecules with dimensions smaller than the cross-linked fibres have more freedom of movement compared to molecules with similar or larger dimensions. Rosuvastatin could have a similar size to the pores of the hydrogel, making it difficult for the molecule to diffuse out of the entangled structure, and therefore would be trapped in between the pores. However, it is unlikely that the size of rosuvastatin reaches this threshold. It is also possible that the drug preferring to hydrophobically interact with the self-

assembled gel fibres with release being inhibited. This type of interaction would be difficult to detect by FT-IR as it is not associated with any specific bands in the IR spectrum.

It is worth briefly noting that slow controlled release of statins is of potential clinical use because these drugs are taken on a daily basis across a significant part of a patient's lifetime. Indeed, slow-release formulations can have particular value in the treatment of 'lifetime' diseases, as they can limit the dosing frequency and increase patient compliance.

3.4.3 Benzyl Glutamine/Alginate Beads

Given the intriguing results reported above, we decided to investigate the influence of calcium alginate on the release profile of our LMWG. Rosuvastatin was therefore loaded into and released from the previously described BG/Alginate beads. 20 beads were loaded with the API via the soaking/diffusion methodology using a 1 mg/mL rosuvastatin calcium solution. From ^{1}H NMR spectroscopy, quantitative analysis, the drug loading could be calculated by comparing the integrals of DMSO (δ = 2.7 ppm) and the methine group of rosuvastatin (δ = 5.53-5.85 ppm). The 20 beads managed to take-up 65% of the rosuvastatin. Drug release was tested with similar conditions as the LMWG-alone.

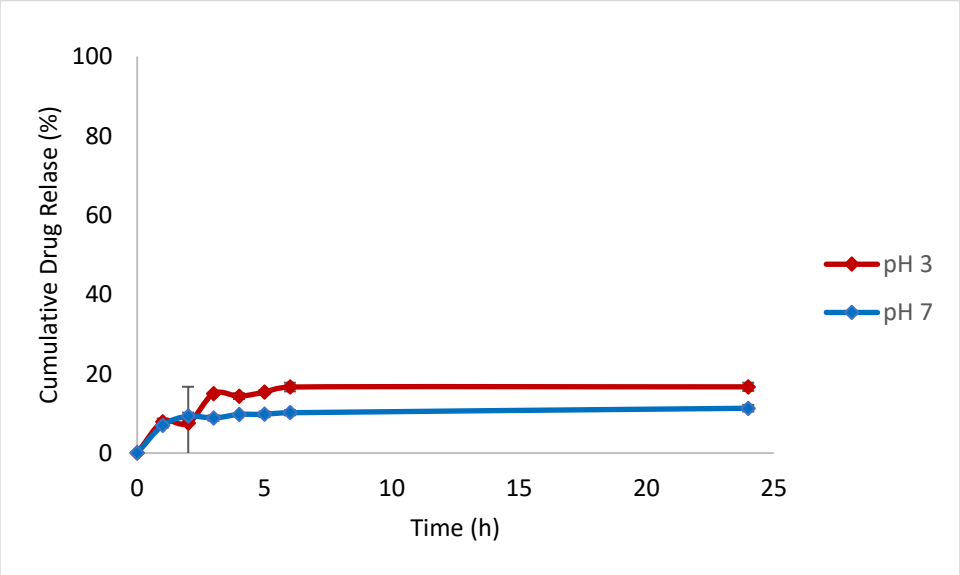

Figure 53. RSV release from Benzyl glutamine/Alginate beads (produced from glutamine-C12 (0.35% wt/vol) with equimolar benzaldehyde, and alginate (1.0 % wt/vol)) in tris buffer during a 24-hour study in tris buffer at 37°C. Error bars in the graph represent the standard error of the mean.

Once again, the release profile of Rosuvastatin is low and relatively controlled. There is a slightly larger extent of release at pH 3, this is suggested to result from the sensitivity of the LMWG to low pH which leads to some erosion of the gel as previously described in the naproxen release studies. As the gel breaks down, this enables the release of the drug from the beads. Comparing the release between the LMWG and hybrid beads we could see a similar initial release profile. However after 24 hours, unlike when the LMWG was used, the robust polymer gel appeared to prohibit further release of the API, with drug release stopping at ca. 11%, rather than rising to 23%. It is possible that the presence of the calcium alginate limits the drug release from the centre of the gel. Or alternatively, the PG maintains the robustness of the gel and prevents any slow release associated with the weakness of the LMWG. With regard to the drug loading, 20 beads achieved similar loading to 1 mL of Benzyl glutamine gel. With each 1 mL of the hybrid gel, 40 beads are formed giving a loading of 0.032 mg per bead. In this study, addition of a polymer has yielded an easily transferrable robust bead. Just as with naproxen the loading of the LMWG vial and hybrid beads therefore cannot fully accommodate the therapeutic dose required (10-40 mg per dose)[141].

3.5 Atropine

Atropine, an alkaloid derived from the plant Atropa belladonna as well as from other members of the Solanaceae family, has a great historical background for its use for aesthetic applications as it dilates the pupils as a beautification method. The drug is a non-selective antagonist of muscarinic receptors and is therefore indicated to be used as a mydriatic agent, anti-vagal agent, and for the blockage of atrioventricular conduction in the heart[142]. These properties have led to its use during surgery to block secretions from the body, being the first line of treatment for bradycardia, as well as for anticholinergic poisoning. Atropine is widely prescribed to inhibit the highly widespread eye condition, myopia[143]. Myopia also known as short sightedness is truly becoming a major health problem as it has become extremely prevalent particularly in east Asia[144, 145]. The condition is described as an extreme increase in

the length of the eye (axial length) relative to the eyes refractive power[146] and is caused by genetic and environmental factors such as exposure to a high screen time and low outdoor time. There has been a focus on the use of atropine in children to slow down its progression by increasing choroidal thickness to prevent myopia, which if it is not corrected will lead to drastic visual impairment potentially including retinal detachment, myopic maculopathy, macular retinoschisis, myopic optic neuropathy, and even blindness[147].

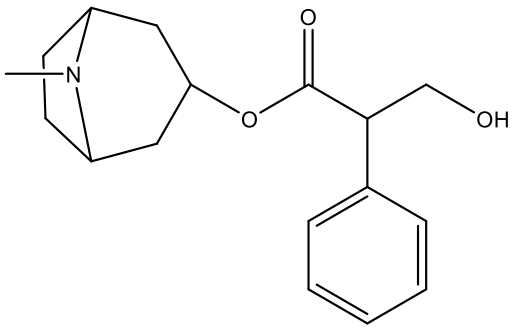

Figure 54. Structure of Atropine.

Research and clinical trials led to the conclusion that high doses of atropine are effective in controlling the condition, however, patients were unwilling to maintain this treatment for long periods of time as it accompanies light sensitivity known as photophobia. To surpass this hurdle young patients were treated with low concentrations of atropine[146]. The treatment involved the use of 0.01-0.05% atropine applied for several years and was found to be effective with slower myopic progression, minimal side effects, and reduced chance of rebound once treatment is halted[147-149]. Unfortunately, although atropine is frequently prescribed at such low doses, there are no FDA approved formulations with doses of 0.01-0.05%. Instead, the FDA-approved 1% atropine eye drops are diluted by pharmacists for the young patients.[150] Although a 1% atropine gel formulation composed of methylcellulose has been developed and is commercially available in China[151], to our knowledge there are no reports of the use of LMWG gels as thickening agents for this treatment[151]. We will therefore discuss the use of our thixotropic gel as a carrier of the anticholinergic agent.

Atropine is different to the other drugs investigated so far, as it is significantly more hydrophilic, exhibiting very good water solubility. It also does not include a carboxylic acid functional group, instead containing amine and alcohol groups as its main polar functionalities. We therefore anticipated that it might show different behaviour to the naproxen and rosuvastatin discussed previously.

3.5.1 Drug Loading

As with previous API's, loading of atropine sulfate was first tested with its addition to the gelator mixture. Therefore, 0.35% wt/vol Benzyl glutamine was added to multiple concentrations of 1 mL atropine solution (concentrations 2, 3, 5, 10, 12, and 15 mg/mL) in glass vials, and the mixture was heated until complete dissolution, and left to stand for 24 hours.

Table 25. Testing the maximum uptake of atropine by 1 mL of the Benzyl glutamine hydrogel (0.35% glutamine-C12 with one molar equivalent of benzaldehyde).

Concentration of Atropine (mg/mL)	**Did it gel? (Appearance)**
2	White gel
3	White gel
5	White gel
10	White gel
12	No – White precipitate
15	No – White precipitate

As predicted, the hydrophilic drug solution did not hinder the self-assembly of our gelator at concentrations up to 10 mg/mL. Instead, it formed reproducible atropine-loaded hydrogels. This is in contrast to what was seen for the more lipophilic drug rosuvastatin, which we believe potentially interacted with the hydrophobic domain of the LMWG, preventing self-assembly. Conversely, the more hydrophilic atropine allowed the Benzyl glutamine to form its self-assembled nanofibers, presumably as it remained in the solvent component of the gel and did not precipitate. Furthermore, it did not contain an acid group that could potentially interact

with the amine of the Benzyl glutamine LMWG, disrupting assembly. As the drug concentration was increased beyond 10 mg/mL, however, the saturated solution did eventually precipitate and then prevented gelation. A successful maximum drug loading of 10 mg/mL was therefore achieved, this corresponds to the doses required for the common ailments atropine is prescribed for. This makes our gel a potentially clinically relevant candidate for the enhancement of atropine delivery.

3.5.2 NMR and FT-IR Studies

By studying the gel by ^{1}H NMR spectroscopy, we can we further understand the possible relationship between the API and the gel system, as well helping us predict the type of release profile the gel will give. The atropine-loaded hydrogel was formulated in D_2O with the addition of an internal standard (sodium trimethylsilylpropanesulfonate, DSS). Anything that is mobile on the molecular scale in the gelled NMR tube will be detected. Therefore, if the drug is detected, we can hypothesize that the drug is freely mobile in the liquid-like phase of the 3D colloidal network. If no peaks are detected, then we can conclude that the drug is, in fact, bound to the solid-like gel nanofibers having formed some type of interaction with them. The integrated peak of DSS (δ = 0.00 ppm) was compared to the aromatic group of atropine sulphate (δ = 7.40 ppm). From these calculations, we found that almost 100% of the drug is mobile. This therefore proves that, as hypothesised above, there is therefore no binding of atropine to the gel network. FT-IR was employed to confirm the NMR results. By comparing the IR spectra of BG-C12 xerogel with an atropine loaded BG-C12 xerogel as well as the pure drug, there was no significant shift in any regions of the IR spectrum (data found in section 7.2.18). Once again, this suggests that there are no interactions involved between the two molecules.

3.5.3 Drug Release Study

Atropine-loaded Benzyl glutamine vial gels were then formulated to investigate the release profile of the drug from the amino acid-based gel. The release study was conducted in triplicate, in an incubator at 37°C. Since the pH of the fluids in the eye are roughly pH 7,[152] the

use of D_2O was selected as an appropriate release medium to perform our study. Aliquots (0.6 mL) were removed from the release medium (total volume of 2 mL) at hourly intervals and replaced with fresh solvent. An internal standard (sodium trimethylsilylpropanesulfonate) was added to each sample and ^1H NMR spectrometry was used to quantify the release of atropine over time.

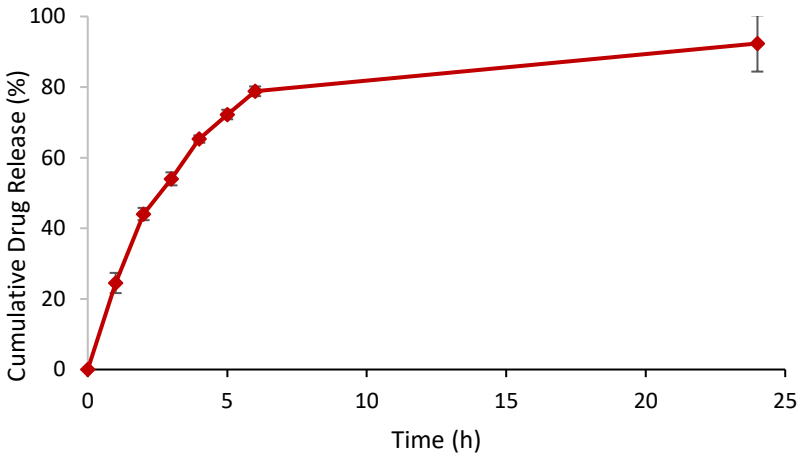

Figure 55. Release profile of atropine sulfate from Benzyl glutamine vial hydrogel (0.35% glutamine-C12 with one molar equivalent of benzaldehyde) vial in D_2O at 37°C. Quantified via ^1H NMR. Error bars in the graph represent the standard error of the mean.

The hydrogel released the drug at a steady regular pace, and within 24 hours the drug was completely released. Over the first 5 hours, 80% of the drug was released, with approximately linear drug release kinetics. Although NMR and FT-IR studies indicated no possible interactions between the gel and the API, we were pleased to find that there was not a completely uncontrolled rapid (burst) release of the drug. We suggest that in clinical use, the injected gel could reside on the outer surface of the eye and the drug would diffuse out of the 3D network to reach its target site. Using hydrogels for this line of treatment is based on the ability of the material to improve drug residence time and hence enhancing eye corneal drug penetration.

3.5.4 Rheology

The thixotropic property of this type of hydrogel may be of use for this application. To apply the gel into the cavity of the eye, we hypothesize that the atropine loaded hydrogel will re-self-assemble once pushed out through the nozzle of the container, in the same way it did in studies conducted by our group by injecting the same gel with L-DOPA into the nasal cavity[2], when, on contact with the nasal cavity, the gel reformed.

By performing a recovery test through rheological studies, we aimed to discover whether the gel retained its self-healing abilities in the presence of atropine. The hydrogel was made as previously described with 0.35% wt/vol Benzyl glutamine and atropine (1 mg/mL). The solution was heated and added to a bottomless vial attached on the rheometer plate. Once fully formed, a shear force of 0.0126% was applied to the gel at 2 Hz for 30 seconds, the frequency was then increased to 100 Hz for a duration of 30 seconds. After that, the frequency was returned to 2 Hz and the recovery of the materials performance monitored over time.

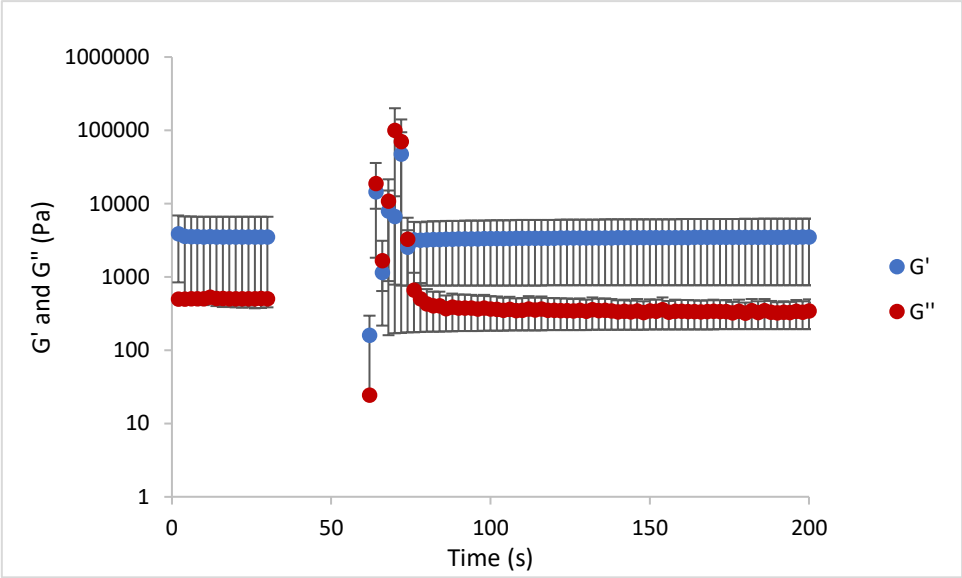

Figure 56. Creep recovery test of atropine loaded BG-C12(glutamine-C12 (0.35 wt/vol) with equimolar benzaldehyde, and (0.1 wt/vol) atropine) performed using parallel plate geometry at 25°C. Using a (shear force 0.0126%, with the frequency ranging in three phases 2Hz, 100 Hz, and 2 Hz. Error bars in the graph represent the standard error of the mean.

The gel successfully fully recovered after the decrease in frequency. With an initial G' of 3872 Pa which was fully preserved after roughly 16 seconds giving similar results demonstrated by the unloaded gel[2]. We can therefore conclude that the addition of atropine did not disrupt the self-healing property of the hydrogel and had no impact on this behaviour as it remains in the mobile phase. As such, this system could potentially be injected into the eye cavity where it would reform as an atropine-loaded hydrogel.

With this approach in mind, Liang et al. formulated a peptide hydrogel (Nap-GFFY) for the ophthalmic drug delivery of diclofenac sodium[153]. In-vivo pharmacokinetic studies conducted on rabbits in which the gel was inserted into the lower conjunctival sac of the rabbit's eye demonstrated an increase in ophthalmic bioavailability from the diclofenac loaded hydrogel compared to commercial DIC eye drops (DiFei®). This is believed to be due to the nanofibers of the gel which increased the pre-corneal retention time and corneal absorption of the drug[153]. Li's group prepared a prodrug supramolecular hydrogel derived from succinated dexamethasone (Dex-SA) for improved ophthalmic delivery of dexamethasone[85].

A few concerns with this application could be the effect of force applied on the gel during blinking and whether the gel can handle such a stress. The gels mechanical strength and adhesion properties determine this effect. If this were an issue, it may be solved by increasing the concentration of the gelator as it increases the gels stiffness. A commercial issue with our system is the lack of transparency. Being a white gel may not be accommodating to patients as it could hinder their vision during treatment. Further development of this system will therefore needs to be addressed.

3.6 Summary and Conclusions

We have explored the formulation of three different drugs into our Benzyl glutamine hydrogels – naproxen, rosuvastatin and atropine. In the case of naproxen and rosuvastatin, drug loading during gel formation proceeds to be impossible, which we assigned to poor solubility and/or interactions between the drug and the LMWG, hindering assembly. Drug loading had to be achieved using a diffusion-based approach into a pre-formed gel. Furthermore, the release of the drugs also appeared to be limited, presumably as a result of interactions with the gel

network – this was particularly marked for rosuvastatin. However, for hydrophilic drug atropine, the gel could be formed in the presence of the drug, and therapeutical levels of loading could be achieved. Furthermore, atropine release was well controlled from the gel over a period of hours, with all of the drug being released after a day.

We can conclude that the most compatible design of a drug to our LWMG, should be water soluble (naturally or in its crystal salt form), otherwise, the precipitation of the drug on cooling will inhibit self-assembly as shown with NPX. We also conclude that the gel is best compatible with drugs that have relatively low therapeutic doses such as with atropine sulfate, levodopa (previous work), and propranolol HCl (see Chapter 4), with good solubility in the mobile phase and which did not show any drug-gel interactions in FT-IR studies. In this way, disruption of gel assembly does not occur at therapeutically-relevant loading levels. It is worth noting however, that as a drug delivery system the gel holds limitations, particularly its rheological strength as well as the degree of gel degradation with time, which might constrain its use for sustained release applications. However, the breakdown of the gel is beneficial for administration routes such as nasal delivery (L-DOPA) or ocular delivery (atropine).

The most promising results in this chapter were obtained using atropine, a water-soluble alkaloid that is well known for its anticholinergic activity. The loaded gel system complied with the appropriate dose for the problematic condition myopia, as well as the other ailments for which atropine is prescribed. During in-vitro studies, atropine release was controlled with linear release of 80% of the drug over a 5 hour period. The gel has prospects in being a delivery vehicle for the 0.1% atropine solution used for the treatment and prevention of myopia in children. The gel nature of this platform may improve patient compliance as application will be eased as the gel sits on the surface of the eye to deliver atropine via slow diffusion. Further work with this platform may involve In-vivo studies of this system in an animal model system.[154] Key optimisation would be to work on the optical transparency of the gel system, and to ensure it could retain sufficient stability on the surface of the eye to achieve effective drug release over the required period of time.

The addition of polymers to the LMWG to form multi component gel beads produced gels with improved rheological robustness that could increase their versatility in terms of administration as a drug carrier. The beads demonstrated slow-release profiles of

rosuvastatin and the use of this approach as a drug delivery system will be further explored in the next chapter.

Chapter 4 Investigating Drug Release Profiles of LMWG's and their Hybrid Derivatives

4.1 Introduction

In this chapter, we will investigate the release profiles of the drugs Propranolol and Levodopa from a range of LMWG's and their hybrid gel derivatives. The LMWG's used in this work are two 1,3:2,4-dibenzylidene-D-sorbitol (DBS) based gelators, DBS-$CONHNH_2$ and DBS-COOH, as well as our amino acid based gelator, Benzyl glutamine. The sorbitol-based gels are economically-friendly, exhibit low toxicity, and have been demonstrated to be capable of several applications, such as binding to precious metals and pharmaceutical drugs, as well as supporting cell growth in tissue engineering applications[43, 155]. Gelation of DBS-$CONHNH_2$ and Benzyl glutamine is triggered by the elevation of temperature followed by slow cooling. The exposure of the insoluble molecules to a rise in temperature results in complete dissolution. As the temperature begins to decrease, self-assembly then directs gel formation. For DBS-COOH, gelation is achieved by the protonation of its carboxylic acid functional groups by reducing the pH below the functional group's pKa value. This in turn decreases the solubility of the molecule and leads to gelation. Slow acidification is required to ensure the formation of a homogeneous gel, with rapid acidification giving poorly controlled gelation and inhomogeneous materials. All LMWG's have been previously characterised by our group.[110] DBS-COOH and DBS-$CONHNH_2$ have been reported as having potential in several biomedical applications by our group[38, 45, 107].

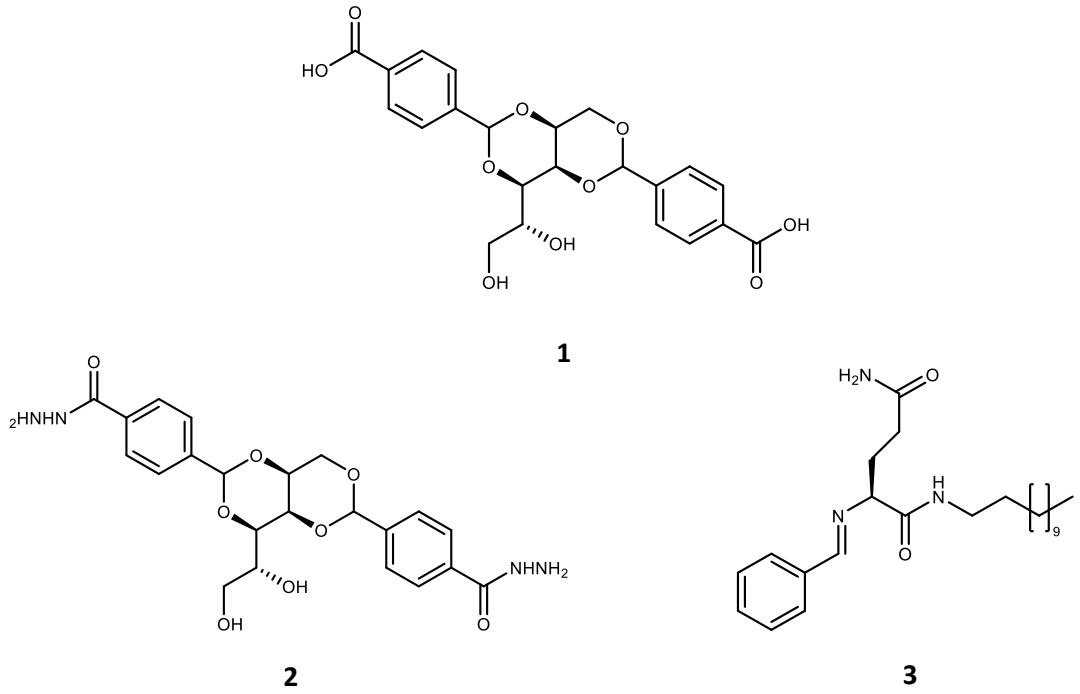

Figure 57. Structures of LMWG's - DBS-COOH (1) DBS-CONHNH$_2$ (2), and Benzyl glutamine (3).

Despite the unique properties of physical supramolecular gels, they suffer from the disadvantage of being rheologically weak. To overcome that problem, our group have combined LMWGs with polymer gels (PGs) and fabricated these multicomponent gels in the form of beads. The beads are composed of the LMWG's combined with either agarose or calcium alginate. The seaweed-derived polymers are frequently used in commercial and scientific applications and have desirable characteristics such as rheological robustness and excellent biocompatibility. Agarose, which has an average molecular weight of 100 KDa, is commonly used in protein separation chromatography and other applications mainly due to its unique porous structure and physical properties. The molecular structure of agarose is a copolymer consisting of 1,3-linked β-D-galactose and 1,4-linked 3,6-anhydro-α-L-galactose. It forms gels on heating and cooling as a result of hydrogen bond interactions and polymer entanglement. Alginic acid is a biopolymer made of β-D-mannuronic acid and α-L-glucuronic acid units linked through β (1–4) bonds. It can form hydrogels with multivalent cations by creating ionic inter-chain bridges[156]. The use of such polymers gives us the opportunity to impose shape onto our LMWG's and exploit their properties with significantly improved ease-of-handling. It was proposed here to use the resulting gels as carriers for the delivery of API cargoes.

Levodopa is a synthetic prodrug of dopamine, which was first derived from the plant *Mucuna pruriens*.[157] It is the most potent medication used in the treatment of the neurological disease known as Parkinson's. Pathologically, Parkinson's is the loss of dopaminergic neurons in the *substantia nigra*. This depletion of dopamine is associated with the common side effects such as bradykinesia, tremor, muscle rigidity, etc[158]. Elevation of dopamine levels leads to the improvement of the patient's condition. The drug molecule is required to cross the blood brain barrier to reach its target site and give its therapeutic effect, which is a downfall, as it limits its use in the oral route where it undergoes extensive metabolism. Our group has previously formulated a method to deliver L-dopa through the intranasal route, which has been demonstrated to achieve direct uptake into the brain. In this case, Benzyl glutamine acted as the carrier for Levodopa and was injected into the nasal cavity. The thixotropic properties of Benzyl glutamine allowed the gel to reform *in situ* and adhere to the lining of the nasal cavity. The *in vivo* studies proved that the LMWG enhanced levodopa's delivery compared to the intranasal delivery of a solution of levodopa, as it increased the retention time of the drug as well as its bioavailability. The rheological behaviour of the LMWG enabled it to adhere for longer in the nasal cavity and promote the diffusion of the drug. There was also less passage of the drug from the nasal cavity into the GI tract when administered in the form of the gel. This therefore limited the exposure to first pass metabolism and increased the bioavailability of the drug[2]. This study inspired us to investigate alternative gel systems to act as carriers for this drug. It is worth noting that like atropine sulfate in the previous chapter, L-DOPA is a highly soluble hydrophilic drug molecule, making it ideal for incorporation into hydrogel systems.

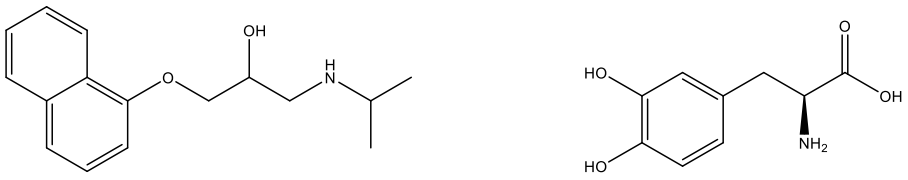

1 **2**

Figure 58. Structure of Propranolol (1) and Levodopa (2).

Propranolol is a synthetic beta blocker. The beta-adrenergic antagonist blocks β1 and β2 adrenoceptors with the same affinity and stops sympathetic stimulation of the heart. It is therefore often prescribed for irregular heartbeats, hypertension, and other cardiac related problems. Propranolol has also been the first line of therapy for the treatment of Infantile haemangioma (IH) since 2008[159-164]. IH is the most common soft tissue tumour found on infants, with locations varying on the neck, head, trunk, and extremities. After birth, proliferative rapid growth of the tissue begins up to 8-12 months of age which is followed by a slow regression of growth until the ages of 5-10 years. Although only 10% of cases are life-threatening, with the airway being obstructed, IH is a concern as it may cause functional impairment, permanent disfiguration, as well as influencing a person's emotional wellbeing. The pathogenesis of this tumour is not fully understood, but studies have shown that the cause could be due to an imbalance of angiogenic factors that stimulate the proliferation of endothelial cells, as well as cytokines and growth factors that promote the formations of capillary networks. Propranolol's mechanism of action in the treatment of IH is believed to be due to its beta blocking activity[165]. Vasoconstriction is a consequence of blocking beta-adrenergic receptors, this in turn leads to a decrease in blood supply to the cancerous lesion, decreasing the transfer of nutrients to promote cell growth. Propranolol also works by inhibiting angiogenesis, and inducing the apoptosis of endothelial cells[166]. This leads to the reduction of the vascular tissue on the skin. The drug is given orally at doses ranging from 1.5-3mg/kg/pd[162, 167]. Systemic application of propranolol, however, has resulted in cases with adverse effects such as bronchospasm, bradycardia, hypotension, and hypoglycaemia. There are a few reports discussing the effective use of topical propranolol for this indication, which may reduce its associated risk factors as the drug would be locally administered.[168-170] We therefore propose the use of a LMWG as carrier for the topical delivery of propranolol for infantile haemangioma. In this study, we explore the release of propranolol and levodopa from three LMWG's and their hybrid gel derivatives for various potential formulation prospects including topical gels, suppositories, and sublingual dosage forms.

4.2 Gel preparation and characterization

4.2.1 Gel Preparation

The LMWG's were fabricated into various forms. Bulk gels produced in vials was the standard approach for making gels and consisted of triggering the gelator while being dispersed in water in a vial. For bead fabrication, the LMWG was added to a polymer and one or two stimuli were imposed on the solution to initiate gelation of a bead shaped gel with controlled dimensions. These methods are discussed in more detail below.

4.2.1.1 Bulk gel preparation in vials

To formulate bulk gels (formed in 7 mL vial) triggered through the following methods:

Temperature change: 1 mL of 0.35% (wt/vol) glutamine amide with 1 molar equivalent benzaldehyde, or 1 mL of 0.4% (wt/vol) DBS-$CONHNH_2$ were heated until dissolution and were left to cool under ambient conditions to enable self-assembly into a gel.

pH induced gelation: 1 mL of DBS-COOH 0.3% (wt/vol) was dissolved with 0.5 M solution of NaOH (60 μL). Glucono-delta-lactone GdL (10 mg) was added as a pH activator and the sample was left overnight to self-assemble into a gel.

4.2.1.2 Gel Bead Preparation

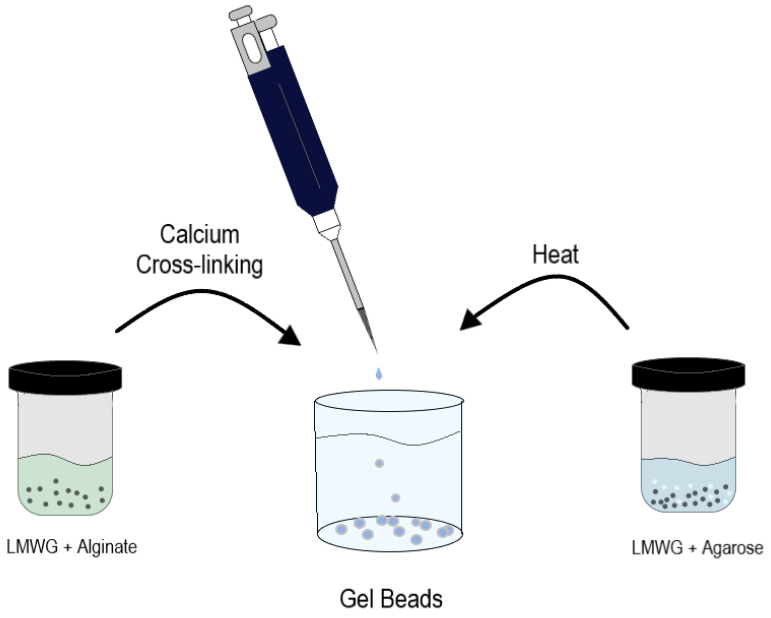

Figure 59. Illustration of the preparation method of alginate hybrid beads via calcium cross-linking and agarose hybrid beads via temperature change respectively. The mixtures are prepared in vials and are pipetted into the beaker containing the appropriate solvent to form hybrid bead networks.

Alginate hybrid beads:

The concept behind these beads revolves around the integration of alginate with the LMWG's, which are then pipetted into a bath of $CaCl_2$ to enable gelation of the polymer through calcium cross-linking. As the system cools (or the pH slowly lowers) the LMWG also assembles, resulting in multi-component structured beads. To achieve this, 0.4% (wt/vol) DBS-$CONHNH_2$ solution was added to 1% (wt/vol) alginate solution. The mixture was heated until complete dissolution, was pipetted into 40 mL solution of 5% (wt/vol) $CaCl_2$ and left to stand until gel bead assembly was complete. Alternatively, DBS-COOH 0.3% (wt/vol) was added to 0.94 mL water and 60 µL NaOH. Alginate 1% (wt/vol) was added, and the solution is pipetted into 5% (wt/vol) $CaCl_2$ (Acidified by the addition of 1M HCl) for complete crosslinking of alginate. Finally, the preparation of Benzyl glutamine alginate beads involved the direct heating of 0.35% (wt/vol) glutamine amide (with one molar equivalent of benzaldehyde) with 1 mL 1% (wt/vol) alginate solution. The solution was pipetted into a 5% (wt/vol) $CaCl_2$ solution to induce gelation of the multi-component bead. It is considered that this approach gives rise to a core-shell bead architecture, with the highest concentration of calcium alginate being

formed at the surface of the droplet where the two solutions interface with one another as demonstrated with microscopy in chapter 3[171].

Agarose hybrid beads:

These beads were made by heating a mixture of the two gelators and pipetting drops of the hot solution with defined volumes into cold paraffin oil, resulting in rapid formation of beads as the temperature is reduced. In this case, the gel networks are considered to be fully interwoven as both of them form simultaneously and throughout the gel bead on the cooling of the system. DBS-$CONHNH_2$ 0.4% (wt/vol) solution was added to 10 mg agarose. The mixture was heated until complete dissolution and pipetted into cold paraffin oil. DBS-COOH 0.3% (wt/vol) was dissolved with 60 µL NaOH and 0.94 mL water. 10 mg GDL was added, followed by 10 mg agarose. The solution was heated until complete dissolution and then pipetted into cold paraffin oil. Once fully formed, both DBS-based agarose hybrid beads were washed with petroleum ether, ethanol, and water to remove any remaining paraffin oil residues. Finally, 0.35% (wt/vol) glutamine amide with one molar equivalent of benzaldehyde was added to 10 mg agarose. The mixture was heated until complete dissolution and pipetted into 1:1 ratio of petroleum ether and paraffin oil. The use of petroleum ether in this case was developed because for these beads the hot solution did not maintain its droplet shape once exposed to paraffin oil to give a gel bead but rather the surface tension led to the flattening of the gel system to produce a sheet on its outer surface. To reduce the surface tension, petroleum ether was added and this resulted in reproducible gel beads. Once fully formed, the gels were washed with petroleum ether and water to remove any remaining residues of paraffin oil.

4.2.2 Characterization

All of the bulk gels and most of the gel beads have been previously reported and fully characterised by our group[42, 110, 172]. The characterisation of DBS-COOH/ Agarose beads was performed by Dr Carmen Piras and is found in the experimental chapter. The Benzyl glutamine/Alginate gel beads were described in Chapter 3. In this part, we will specifically discuss the characterisation of Benzyl glutamine/Agarose beads, which were new systems in this project.

4.2.2.1 Benzyl glutamine/Agarose beads

4.2.2.1.1 Quantifying the Self-assembled Benzyl Glutamine in Each Bead

To determine the proportion of Benzyl glutamine in each bead we conducted a ^{1}H NMR study on 9 dried beads. The beads were crushed and dissolved in DMSO-d_6 and spiked with acetonitrile as an internal standard. By comparing the integrals of acetonitrile *(*δ = 2.0 ppm*)* and the methyl group of Benzyl glutamine *(*δ = 0.80 ppm*)* from the NMR spectrum we could conclude that 58% of the LMWG was assembled in each bead. This is slightly less than the uptake that was observed for the DBS-based gelators. Some of the LMWG may have been lost in the paraffin oil during preparation, or the concentration may actually be greater but is not mobile in the NMR due to the interactions involved between the two gel systems preventing the LMWGs release.

4.2.2.1.2 FT-IR Studies on Benzyl Glutamine-Agarose Hybrid Gel beads

FT-IR was utilised to study any possible interactions involved between Benzyl glutamine and agarose (experimental data found in section 7.3.3.2). Xerogels of Benzyl glutamine/ Agarose beads and Benzyl glutamine hydrogels were prepared. By comparing the spectra, a degree of interaction between the LMWG and the polymer is suggested by shifts in the N-H region (3299 → 3337 cm^{-1}) and C=O region (1652→ 1645 cm^{-1}). The gel beads are therefore held together by involvement of both gel network systems, indicating a synergistic effort from both components to support this system. This is in-line with the view that both networks are formed simultaneously on cooling of the droplet during the fabrication method and extend in interpenetrated form throughout the gel beads.

4.2.2.1.3 Thermal Stability Studies

To study the temperature at which the two-component system breaks down, a bulk gel containing 0.35% Benzyl glutamine with 10 mg agarose was prepared in glass vials. The

temperature was elevated at a rate of 1°C/30 seconds in a thermally controlled oil bath. At each increase of one degree the vials were removed and inverted to test their ability to hold on to the surface of the glass. Once the gel fell in the vial, the temperature was recorded. The experiment was performed in triplicate, and the results indicate that the gel system loses it structural integrity at a temperature of ca. 100°C, unlike Benzyl glutamine alone which has been reported to be converted to a sol at 83°C. This value is around the boiling point of water, and it therefore should be considered that the gels are stable until the solvent vaporises. The results indicate that the agarose polymer gel contributes to the thermal stability of the system, in addition to enabling the system to maintain its shape, and thus the robust characteristics of agarose are effectively added to the new gel system.

4.2.2.1.4 Rheology

Given that the rheological robustness of agarose is the key purpose for this hybrid gel fabrication it was important to characterise this effect. Through physical observations, it was clear that agarose has stabilized the hybrid system, as with its addition the system could be more easily physically manipulated, and retained its shape once removed from the glass vials, which is very difficult to do with the LMWG alone. To quantify this change more accurately in rheological terms, experiments were conducted on the rheometer with the hybrid system and the agarose system as a control.

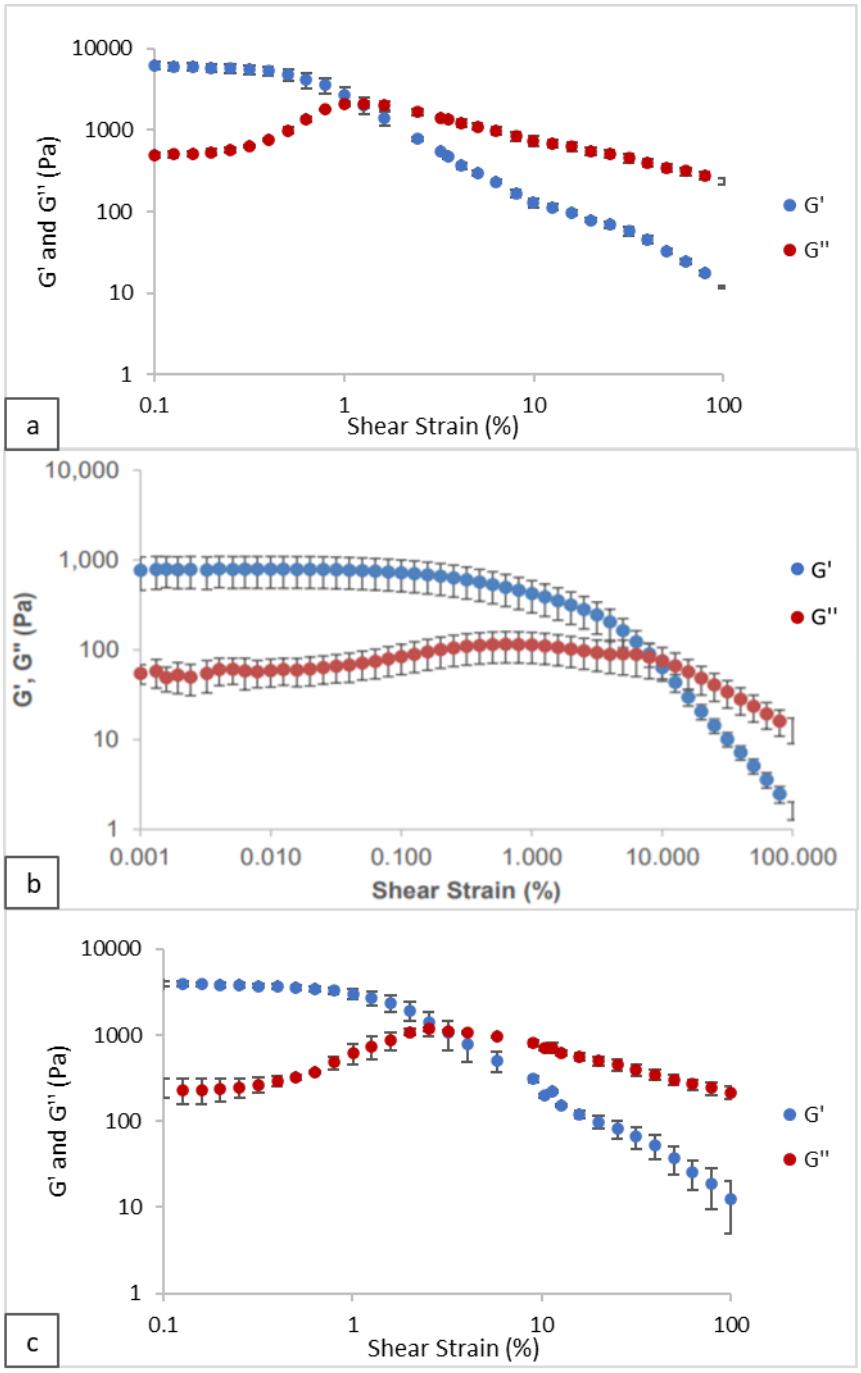

Figure 60. Elastic (Blue) and viscous (Red) moduli with increasing shear strain of a) Benzyl glutamine/ Agarose vial gel (glutamine-C12 (0.35% wt/vol) with equimolar benzaldehyde, and agarose (1% wt/vol)). b) Benzyl glutamine (glutamine-C12 (0.4% (wt/vol)) with equimolar amount of benzaldehyde) hydrogel (obtained from K. Hawkins et al[142]. c) Agarose vial gel (agarose (1% (wt/vol). All of which are performed using parallel plate geometry at 25°C. Error bars in the graph represent the standard error of the mean.

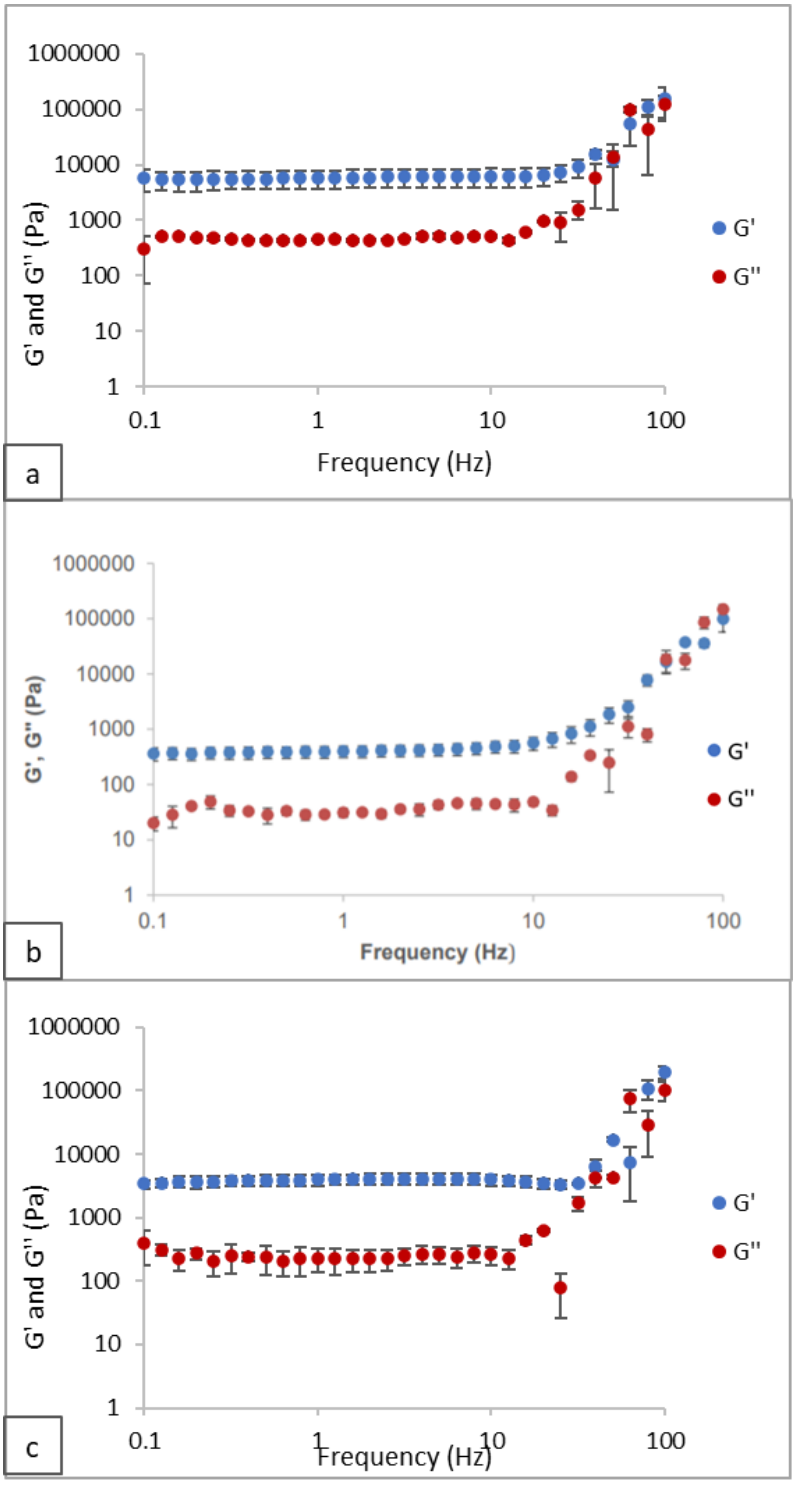

Figure 61. Elastic (Blue) and viscous (Red) moduli with increasing frequency of a) Benzyl glutamine/ Agarose vial gel (glutamine-C12 (0.35% wt/vol) with equimolar benzaldehyde, and agarose (1% wt/vol)). b) Benzyl glutamine (glutamine-C12 (0.4% (wt/vol)) with equimolar amount of benzaldehyde) hydrogel (obtained from K. Hawkins et al[142]. c) Agarose vial gel (agarose (1% (wt/vol). All of which are performed using parallel plate geometry at 25°C. Error bars in the graph represent the standard error of the mean.

To begin, G' is greater than G'' confirming that the addition of the two components together still produces a gel. The cross over of Benzyl glutamine/ Agarose, Benzyl glutamine, and agarose are 1%, 8% and 3% respectively which is in line with the results obtained by our groups DBS-$CONHNH_2$/ Agarose multicomponent gel system[172]. Furthermore, the G' value is stable across a range of frequencies. The G' in the multicomponent gel system is similar to that of the agarose gel, whereas the elastic modulus is slightly greater in the multicomponent gel, thus combining the two gels gives a more elastic gel system. The hybrid gel is therefore much stiffer than a gel only comprised of the LMWG Benzyl glutamine. This reflects the role played by the agarose PG in stiffening the gel system– hence allowing the gel macrobeads to be stable self-standing objects.

4.2.2.1.5 Microscopy

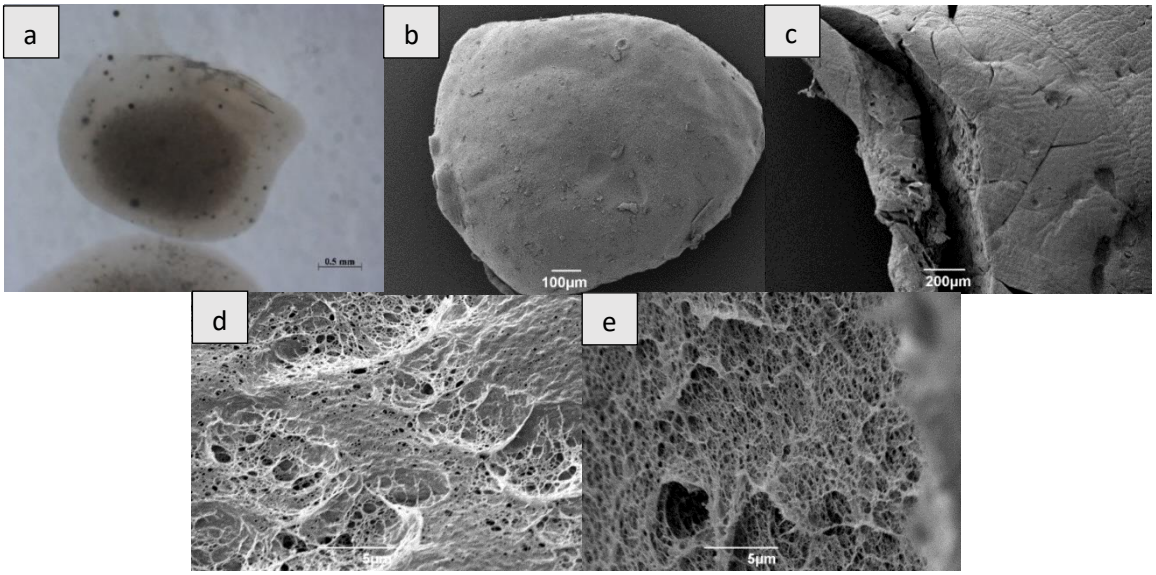

Figure 62. Optical microscopy (a) and SEM images (b-e) of multi-component Benzyl glutamine/ Agarose beads (glutamine-C12 (0.35% wt/vol) with equimolar benzaldehyde, and agarose (1% wt/vol)).

SEM and optical microscopy were used to examine the structure of the new beads. Images of the hybrid bead reveal the bead's outer smooth exterior. A closer look into the structure

(figure 62 (c-e)) shows complex intertwined fibres with no visible solid-like objects which might have indicated the presence of non-assembled material.

4.3 Drug Loading

All gels in vials and gel beads were loaded with 2.2 mg/mL levodopa solution via the soak method except for the Benzyl glutamine vial gel which was reported previously[2]. All gels in vials and gel beads were loaded with 1 mg/mL propranolol with the soak method, apart from Benzyl glutamine vial gels, which were prepared by the addition of propranolol pre-gelation. This is the preferred method of loading as it eliminates the difficulty of using quantitative methods to calculate the drug loading as it is quite challenging with this particular gelator. This is a result of Benzyl glutamine being released into the supernatant used to calculate the non-absorbed drug (post drug loading), which would be detected by UV-vis and as a result amplify the absorbance producing inaccurate results. It also may maximise the drug loading compared to the diffusion method which was shown to be less effective in the previous chapter with this gelator. For each experiment, the vials contained 1 mL of low molecular weight gels, or 20 multicomponent beads. Drug loading efficiency was calculated from the use of NMR spectrometry and UV-Vis on the gels in vials and the gel beads. In particular, we analysed the supernatant solution to determine how much of the API was left non-adsorbed. The hydrogels in the drug solution were incubated at 37°C to facilitate diffusion for >12 hrs. The table presents the drug loading as well as the drug loading efficiency.

Table 26. Calculated drug loading and drug loading efficiency of 1 mL vial gels and multicomponent gel beads (20 beads), and calculated drug loading of 1 mL of each system loaded with propranolol and levodopa respectively.

Gel System	**Propranolol**			**Levodopa**		
	Drug loading (mg)	Drug loading efficiency (%)	Drug loaded per 1 mL of gel (mg)	Drug loading (mg)	Drug loading efficiency (%)	Drug loaded per 1 mL of gel (mg)
DBS-$CONHNH_2$ vial gel	0.57	57	0.57	1.27	58	1.27

DBS-$CONHNH_2$ / Alginate beads	0.50	50	0.75	1.03	47	1.55
DBS-$CONHNH_2$ / Agarose beads	0.45	45	0.9	0.92	42	1.84
DBS-COOH vial gel	0.48	48	0.48	1.68	76	1.68
DBS-COOH / Alginate beads	0.54	54	1.35	0.97	44	2.43
DBS-COOH / Agarose beads	0.51	51	0.77	1.00	46	1.50
BG vial gel	0.50	100	0.50	N/A	N/A	N/A
BG / Alginate beads	0.66	66	1.32	1.42	65	2.84
BG / Agarose beads	0.36	36	0.54	1.02	46	2.13

The table demonstrates the loading efficiency of each gel system. We can conclude that DBS-$CONHNH_2$ vial gels gave similar loadings with both drugs. DBS-COOH vial gels however, had a greater uptake of levodopa compared to propranolol which may indicate possible involvement/interactions between the API and gel system which would favour partition of the drug into the gel. Benzyl glutamine vial gels, loaded via pre-gelation, will be discussed later in the chapter. As for comparing uptake by the vials and their respective alginate gel beads, the beads (total number of beads per 1 mL of gel as shown in table (26) displayed a greater absorption of the drugs. As for the agarose gel beads, in most cases agarose is slightly less efficient in loading the drugs compared to alginate. This may be due to possible interactions between the drugs with the outer alginate shell, or the porous nature of agarose which prevents the encapsulation of the drug. It should be noted that the therapeutic oral dose of levodopa is much greater than all of the results displayed in the table. However, our study will demonstrate the ability of these gels to act as drug delivery systems, and how the addition of polymers influences that ability.

4.3.1 Characterization of Propranolol Loaded Benzyl Glutamine

To understand the impact of the presence of propranolol in our system, a series of experiments involving NMR, microscopy, thermal stability, and rheology were conducted. To measure the thermal stability, a benzyl glutamine hydrogel ((glutamine-C12 (0.35 wt/vol) with equimolar benzaldehyde)

was formed in a glass vial and placed into an oil bath. The inversion test was used to determine the temperature at which the gel can no longer hold its weight. The propranolol loaded Benzyl glutamine hydrogel gave a T_{gel} value of 77-80°C. This value of thermal stability is similar to that observed for Benzyl glutamine alone (83°C) and indicates that the presence of the drug does not significantly disrupt the gel. This means that the drug-loaded gel will be stable to the body's internal temperature (37°C), although it should be noted here that the drug loading is quite low. This leaves other factors such as enzymes, pH, salt content as potentially being the main contributors to the breakdown of the gel in the body.

NMR was then used to quantify mobile propranolol in the system and detect any possible interactions between the drug and the gel carrier. ^{1}H NMR spectrometry could be used to detect how much of the propranolol is incorporated into the gel as well as the amount that is mobile within the gel matrix. This type of spectrometry only detects the drug if it is mobile and in the 'liquid-like phase', solids will not be detected and give no peaks. This means that any mobile propranolol hydrochloride in the gel matrix will be detected by NMR, whereas if the propranolol hydrochloride is chemically (or physically) bound to the gel, then no peaks will appear. The propranolol containing hydrogel was made in D_2O in an NMR tube with DMSO added as an internal standard. Integrals of DMSO (δ = 2.70 ppm) and the hydroxyl group on the propranolol molecule (δ = 6.99 ppm) were compared to calculate the quantity of propranolol visible or free flowing in the network. It was found that ca. 42±2% of the loaded propranolol was unbound in the gel system, with the remining ca. 58% being in the solid-like form and thus associated with the gel nanofibers. This outcome would perhaps lead us to predict a drug release profile in which sudden burst release is followed by a slow release of the API. It is possible that the interactions between the propranolol drug and the LMWG network involve non-covalent interactions.

4.3.1.1 Rheological Studies on Propranolol Loaded Benzyl Glutamine Hydrogel

The Benzyl glutamine hydrogel has already been tested by rheology (see above), and therefore we compared the performance of the propranolol-loaded Benzyl glutamine hydrogel to see if any changes occurred to the mechanical integrity of the gel. Therefore, a gel based on 0.35% (wt/vol) Benzyl glutamine was made with propranolol (0.5 mg/mL). The hot solution was added to a sealed bottomless glass vial attached to a petri dish. The gel was left for >24 hrs and was later placed on the rheometer plate.

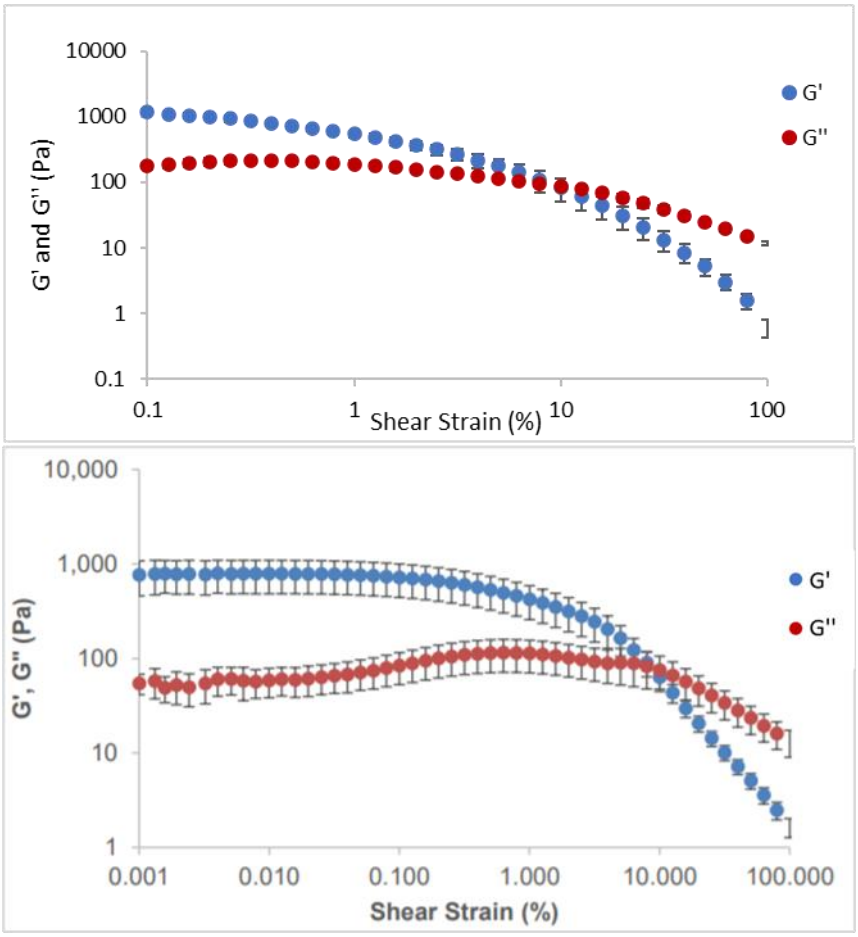

Figure 63. Viscous(G') moduli and elastic (G') moduli with increasing shear strain (%) performed using parallel plate geometry at 25°C. Of (top graph) propranolol loaded Benzyl glutamine hydrogel (glutamine-C12 (0.35% wt/vol) with equimolar benzaldehyde, and propranolol (0.05% wt/vol)) and (bottom graph) Benzyl glutamine (glutamine-C12 (0.4% (wt/vol)) with equimolar amount of benzaldehyde) hydrogel obtained from K. Hawkins et al[142]. Error bars in the graph represent the standard error of the mean.

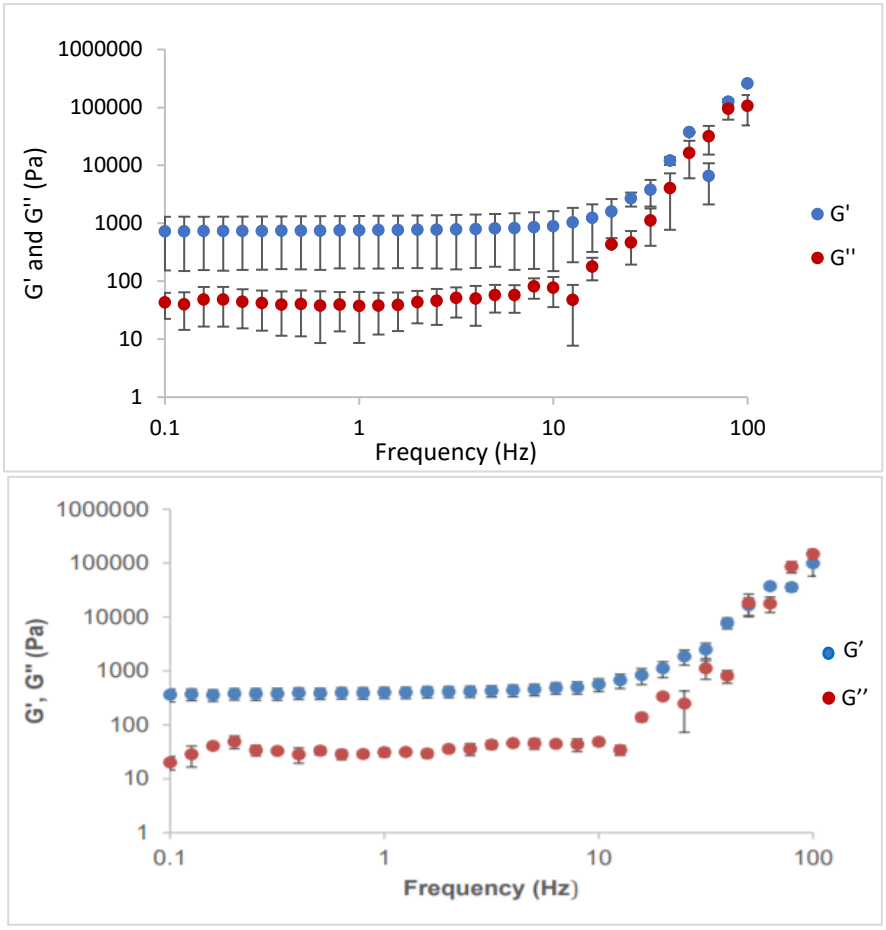

Figure 64. Viscous(G') moduli and elastic (G') moduli with increasing frequency performed using parallel plate geometry at 25°C. Of (top graph) propranolol loaded Benzyl glutamine hydrogel (glutamine-C12 (0.35% wt/vol) with equimolar benzaldehyde, and propranolol (0.05% wt/vol)) and (bottom graph) Benzyl glutamine (glutamine-C12 (0.4% (wt/vol)) with equimolar amount of benzaldehyde) hydrogel obtained from K. Hawkins et al[142]. Error bars in the graph represent the standard error of the mean.

The G' value had a greater magnitude than G'', meaning that the addition of the drug did not affect the gel characteristics of the Benzyl glutamine. In comparison to the unloaded Benzyl glutamine hydrogel (2.99 mg glutamine amide + 1.01 mg benzaldehyde in 1 mL deionized water)[110], both gels have a crossover point at ca. 8% strain. Furthermore, the G' and G'' values of both gels are generally similar indicating again that no significant rheological change has occurred on the addition of the drug, at least at these relatively low loadings.

4.3.1.2 Microscopy Imaging

To further understand the effect the drug molecule has on the 3D network of the gel SEM images were taken of the propranolol hydrochloride loaded gel in glass vials.

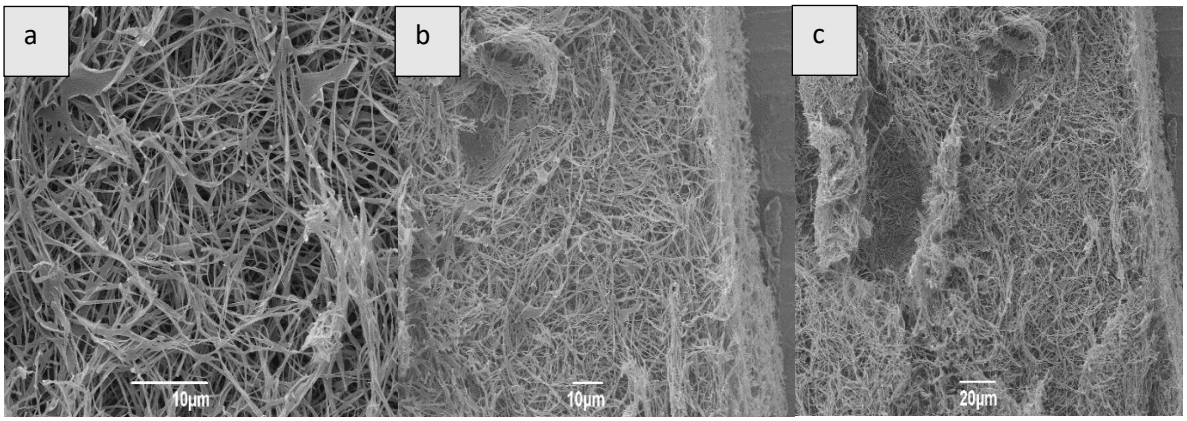

Figure 65. SEM images of propranolol HCl loaded Benzyl glutamine hydrogels (glutamine-C12 (0.35% wt/vol) with equimolar benzaldehyde and propranolol HCl (0.05% (wt/vol)).

.

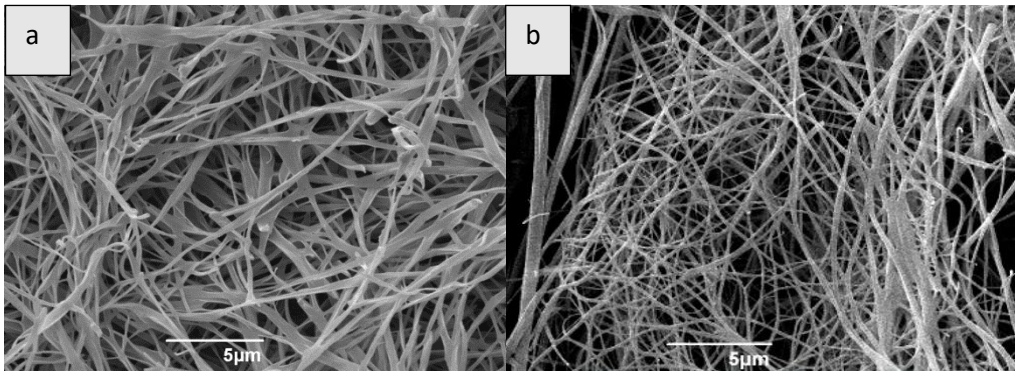

Figure 66. SEM images of a) propranolol hydrochloride loaded Benzyl glutamine (glutamine-C12 (0.35% wt/vol) with equimolar benzaldehyde and propranolol HCl (0.05% (wt/vol)) b) Drug free Benzyl glutamine (obtained from K. Hawkins et al)[141].

The images show a dense 3D network with a web-like connection of fibres. Comparing the shape of the fibres between the drug-loaded and drug-free hydrogel indicates that they look similar. However, the drug loaded gel may have flatter-shaped fibres and the fibres may be in

a closer proximity to each other compared to the drug-free gel. This may be due to the interaction between the propranolol drug and the LMWG. For example, the secondary amine of propranolol could also interact with the benzaldehyde component of the gelator, thus modifying the network somewhat. However, the evidence of this is not strong and it is possible that sample-to-sample drying effects may also have contributed to these differences.

To complete the characterization, TEM images were also taken of the drug loaded hydrogel.

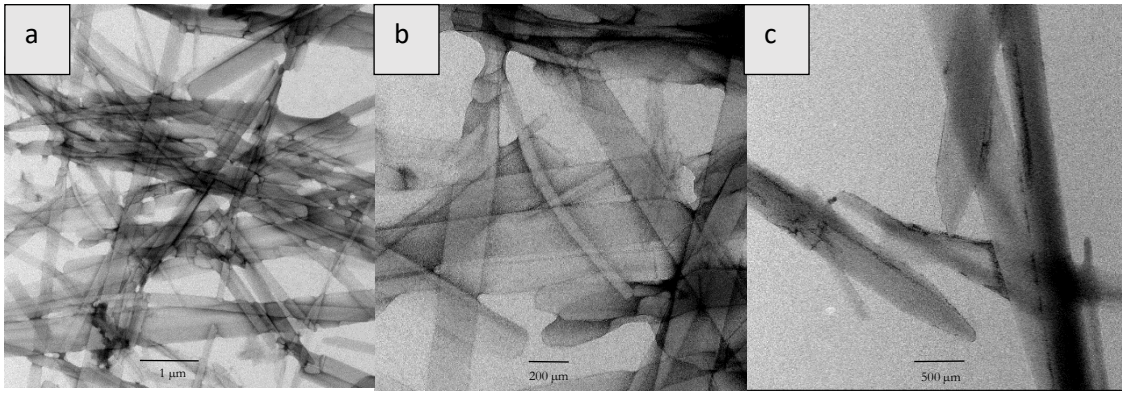

Figure 67. TEM images of propranolol loaded Benzyl glutamine (glutamine-C12 (0.35% wt/vol) with equimolar benzaldehyde and propranolol HCl (0.05% (wt/vol)).

The images display rod-shaped fibres clustered on top of each other. The images are similar to the drug-free Benzyl glutamine. Showing no significant difference with the addition of the drug molecule[110]. Overall, these studies show that the drug has effectively no impact on the ability of Benzyl glutamine to form a gel.

4.3.1.3 Maximum Drug Loading

The maximum concentration of propranolol that could be loaded into the Benzyl glutamine system was determined using a pre-gelation method. Various concentrations and volumes of propranolol HCl solution were added to Benzyl glutamine (0.35% (wt/vol) glutamine-C12 with one molar equivalent of benzaldehyde). The mixture was heated until dissolution and left to fully assemble into a drug-loaded gel.

Table 27. Finding the maximum drug loading of propranolol in Benzyl glutamine hydrogels (0.35% glutamine-C12 with one molar equivalent of benzaldehyde) pre-gelation – Performed in duplicate.

Propranolol concentration (mg/mL)	Water Volume (mL)	Did it Gel?
1	1	Yes
3	1	Yes
3	2	Yes
4	1	Yes
5	1	Yes
5	2	Yes
10	1	No
20	1	No
30	1	No
40	1	No

The table identifies the largest quantity of propranolol that can be added without disrupting gelation as 5 mg/mL. Importantly, this corresponds to the appropriate dosing of propranolol for the treatment of IH. The gel could also assemble at the same loading (5 mg/mL) in larger volumes (e.g. 2 mL), possibly providing us with a method to tune the drug release profile. When using higher concentrations of propranolol, a precipitate was observed, and the presence of the drug appeared to prevent gelation.

4.4 Drug Release Studies of Propranolol and Levodopa

We studied the release of the two therapeutic agents from our gel systems. The gels in vials and the gel beads were exposed to 4 mL of tris buffer to act as a model biological medium at pH 7 and 3. The gels were incubated at 37°C, samples removed each hour and drug release was quantified with the use of UV-Vis on the supernatant solution. The results are displayed in graphs showing the release profiles in pH 7 and 3. To investigate the interactions involved between the gel systems and the drugs, FT-IR studies were also conducted on the xerogels including the control gels, drug loaded gels, and the drug alone (data found in appendix).

Propranolol exhibited IR stretches for O-H (3275 cm^{-1}) and C=O (1579 cm^{-1}). Levodopa FT-IR stretches include O-H (3062 cm^{-1}), N-H (3195 cm^{-1}), and C=O (1651 cm^{-1}).

4.4.1 Propranolol Drug Release

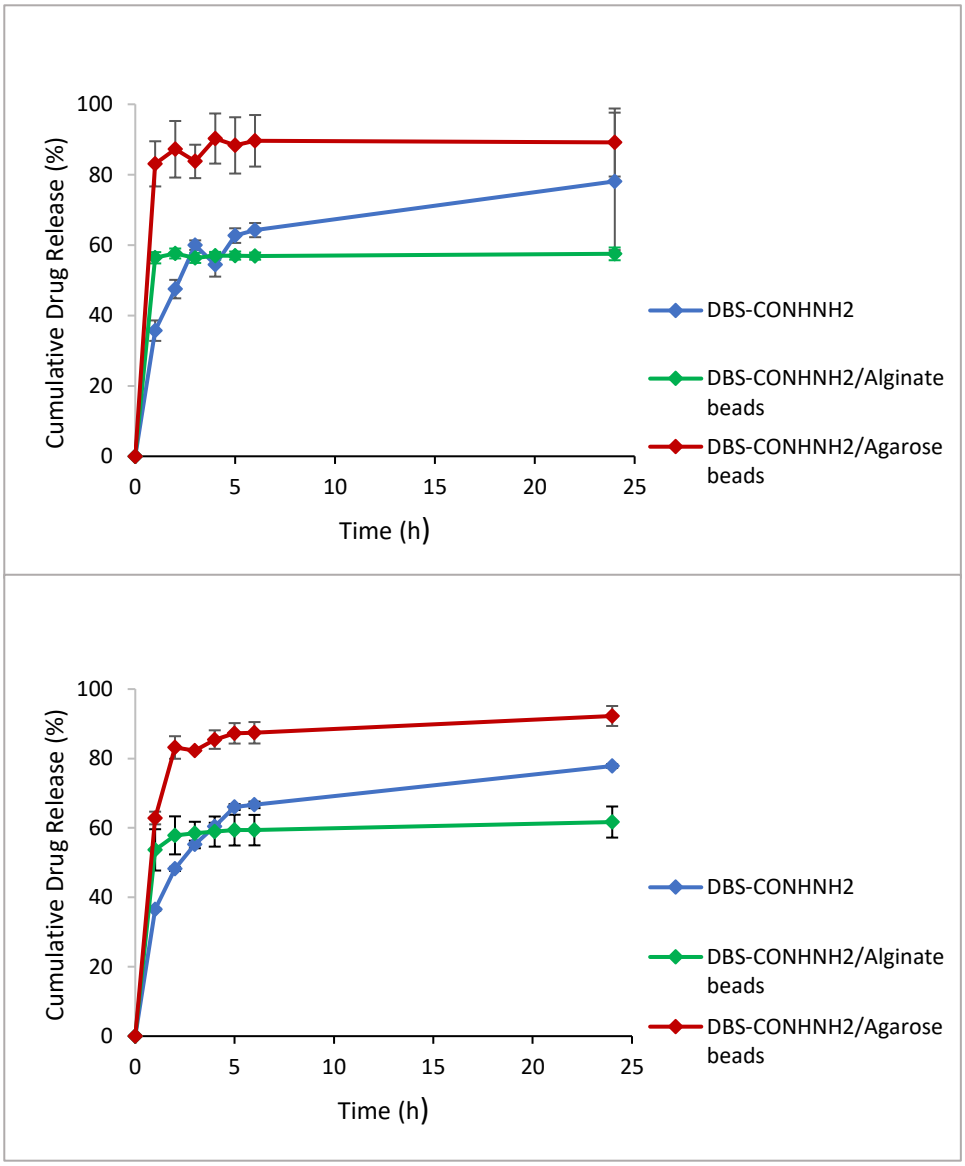

Figure 68. Propranolol release from DBS-CONHNH2 (0.4% (wt/vol) and its hybrid derivatives in tris buffer (0.1% (wt/vol)) at pH 7 (Top) and pH 3 (Bottom) respectively at 37°C. Error bars in the graph represent the standard error of the mean.

The release of propranolol at pH 7 from DBS-$CONHNH_2$ gels in vials was gradual with roughly 75% release over a 5 hour period. After 1 hour, the release was only 36%. In contrast, the multicomponent gel beads gave rapid, and effectively maximal release of propranolol within the first hour which plateaued immediately. It is possible that the smaller dimensions of the gel beads means that all of the drug can be released more rapidly, as it is not so far distant from the interface with the aqueous solution. Whereas for the bulk vial gel, some of the drug has to diffuse over longer distances to be released. It is also possible that interactions between agarose or alginate and DBS-$CONHNH_2$ may limit its ability to interact with the drug and hence control the rate of release. Similar results have been shown in our groups study on the release of rosuvastatin from DBS-$CONHNH_2$/Alginate beads[42].

Given that there may be possible interactions between the drug and gel system, FT-IR investigations were carried out. The FT-IR of the DBS-$CONHNH_2$ vial gel had a slight shift in its C=O region (1642 → 1637 cm^{-1}) on loading of the drug – this may indicate some interaction with the drug, which would correspond with the controlled release. However, these changes are very small. Agarose and alginate beads gave roughly 90% and 58% rapid release respectively. The agarose hybrid gel had no real shift in its C=O region but a shift in the O-H stretch (3324 → 3308 cm^{-1}) possibly due to propranolol-agarose interactions. The alginate hybrid gel displayed a slight shift in its C=O region (1586 → 1583 cm^{-1}). Clearly, the alginate gel beads are significantly less able to release the drug – it is possible that the calcium ions present within the calcium alginate shell can interact with the propranolol. Alternatively, it is possible that the more core-shell nature of the calcium alginate gel beads may more effectively limit release of the drug in comparison with the agarose hybrid gel bead system which is more fully interwoven throughout the architecture.

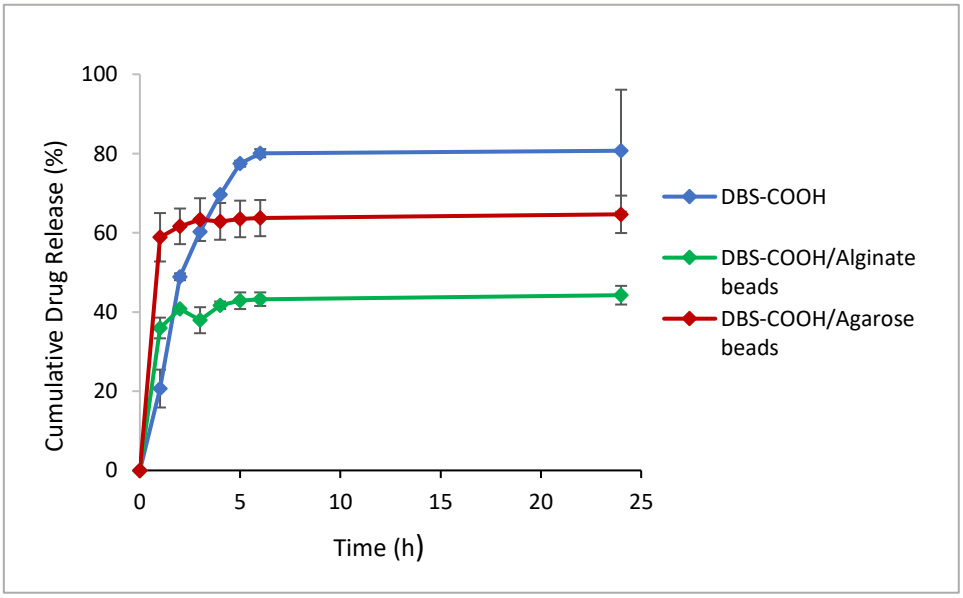

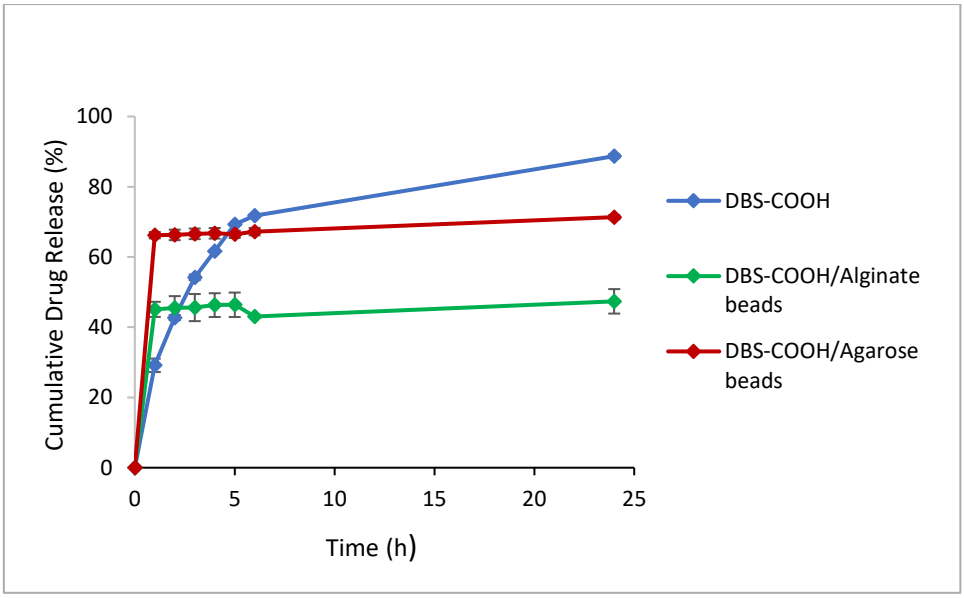

Figure 69. Propranolol release from DBS-COOH (0.3% (wt/vol)) and its hybrid derivatives in tris buffer (0.1% (wt/vol)) at pH 7 (Top) and pH 3 (Bottom) respectively at 37°C. Error bars in the graph represent the standard error of the mean.

At pH 7 (figure 69 – top graph), the DBS-COOH vial gel gave a slow release of the API reaching a plateau at ca. 80% release within 6 hours of release. The drug release was slightly faster than had been observed for DBS-$CONHNH_2$ in vials, which would support the view that the $CONHNH_2$/COOH group was important in mediating the interactions between the gelator and the drug. As was observed for DBS-$CONHNH_2$, the gel beads once again gave rise to rapid drug release – this may be due to their smaller dimensions, or the presence of the polymer gel limiting interactions between the LMWG and the drug. Once again, the agarose-based beads gave more complete drug release than the alginate-based beads, and we suggest this may be due to the presence of calcium ions in the alginate based system, interacting with the drug molecule. The release profile at pH 3 for all gel systems was slightly less compared to the values at pH 7.

FT-IR studies show that DBS-COOH and its agarose derivatives had a decrease in frequency in its O-H region (3308 → 3294 cm^{-1}), (3372 → 3341 cm^{-1}) respectively. While the agarose derivative had an increased shift of (3278 → 3303 cm^{-1}). DBS-COOH, showed a slight shift its in C=O region (1695 → 1690 cm^{-1}), while the hybrid gels with agarose and alginate showed effectively no change in this band, with changes of (1697 → 1695 cm^{-1}), (1695 → 1696 cm^{-1})

respectively. The resulting shifts suggest that the ionised propranolol (pKa 9.4)[173] may interact with the carboxylate ion of the DBS-COOH system. Meaning this interaction may play a role in the release profiles of propranolol. As the pH gets closer to the pKa value of propranolol, a reduced amount of ionised propranolol is available. Making the escape of the drug from the 3D network easier. This may support the variation in release between pH environments of 3 and 7. In the presence of the polymer gels, we suggest this interaction becomes less significant and therefore more rapid release of the drug occurs.

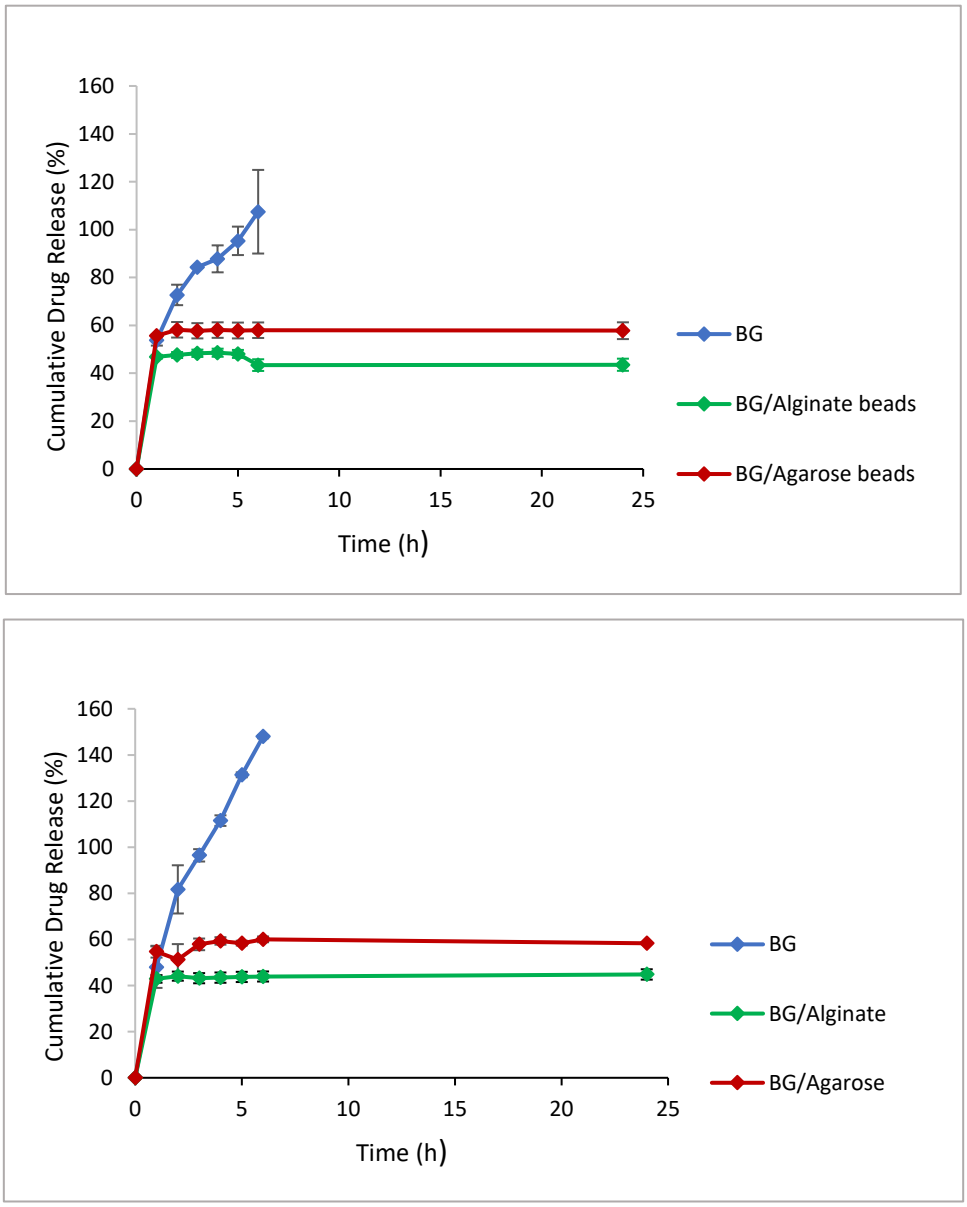

Figure 70. Propranolol release from Benzyl glutamine (glutamine-C12 (0.35% wt/vol) with equimolar benzaldehyde and propranolol HCl (0.05% (wt/vol)) and its hybrid derivatives in tris buffer (0.1%

(wt/vol)) at pH 7 (Top) and pH 3 (Bottom) respectively at 37°C. Error bars in the graph represent the standard error of the mean.

Benzyl glutamine hydrogel gave erosion-type release with a greater sensitivity to pH 3. The release appears to exceed 100% within the 6-hour time frame – this is a result of the Benzyl glutamine also being released as the gel erodes, giving rise to an additional UV signal that was difficult to correct for as both the drug and gel had overlapping signals. The addition of agarose resulted in a plateau of at 60% drug release within the first hour. Addition of calcium alginate to Benzyl glutamine gave rapid release of ca. 40-50% of the drug. Clearly in this case, the use of hybrid gels stabilises the Benzyl glutamine and prevents erosion of the system. It is also the case that once again, drug release from these beads is rapid, presumably because of their smaller dimensions. Also, the calcium alginate-based systems show less drug release, which might indicate interactions between the drug and the calcium ions in this particular polymer gel network.

Gels of Benzyl glutamine in vials displayed changes in peaks in its N-H region (3299 → 3285 cm^{-1}) and C=O region (1652 → 1656 cm^{-1}) suggesting that the gel network interacts with the drug and indicating a mechanism by which drug release may give rise to gel erosion, particularly for a very weak gel such as this one. The agarose derivative had a significant shift in its O-H region (3349 → 3369 cm^{-1}), similar to in other systems, while the alginate-based system only showed negligible changes (ca. 1 cm^{-1}) in its IR spectra, suggesting perhaps that the presence of Ca^{2+} may be responsible for interactions with the propranolol.

4.4.2 Levodopa Drug Release

We then moved on to look at the release of levodopa from the different gel systems to determine similarities and differences in trends and hence better understand the drug release process. It should be noted that L-DOPA release from Benzyl glutamine in vials was the subject of the previous publication from our group as mentioned in the introduction.

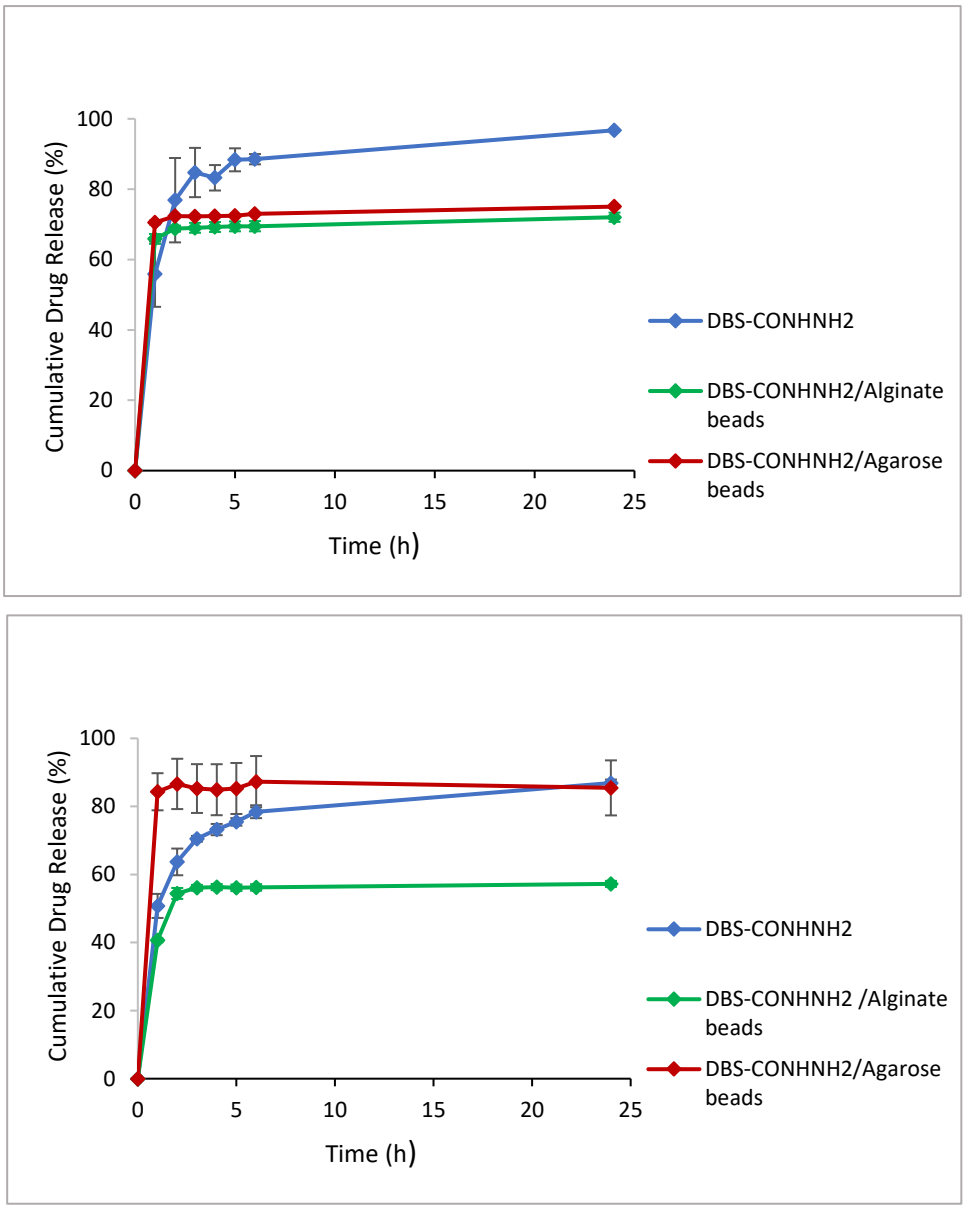

Figure 71. Graph of levodopa release in tris buffer (0.1% (wt/vol)) from DBS-$CONHNH_2$ (0.4%(wt/vol)) and its hybrid derivatives at pH 7 (Top) and pH 3 (Bottom) respectively at 37°C. Error bars in the graph represent the standard error of the mean.

On testing gels based on DBS-$CONHNH_2$, we found that L-dopa was gradually released from the DBS-$CONHNH_2$ gel in vial over time, with a greater release at pH 7 compared to its release in an acidic environment. Indeed, the release of this drug was highly effective under physiological conditions, reaching 97% after 24 hours, which may hint at some potential pharmaceutical uses. The hybrid beads once again gave rapid release profiles with a lower overall release compared to LMWG alone. The agarose gel beads gave slightly more release

than the alginate equivalents. There was also a sensitivity to pH 7 for both hybrid beads, giving roughly a 20% increase in release compared to the study at pH 3. FT-IR studies revealed that DBS-$CONHNH_2$ had a shift in its C=O region (1656 → 1640 cm^{-1}), N-H region (3195 → 3208 cm^{-1}), and in the O-H region (3283 → 3286 cm^{-1}), thus implying likely involvement between the drug and LMWG which may play a role in mediating the release kinetics. The agarose hybrid gel had a decrease in its C=O region (1643 → 1636 cm^{-1}) and in the O-H region (3324 → 3299 cm^{-1}). While the alginate beads had a shift in its C=O region (1586 → 1593 cm^{-1}). It is possible that interactions with the polymer gel network are preventing the complete release of this drug from the gel beads.

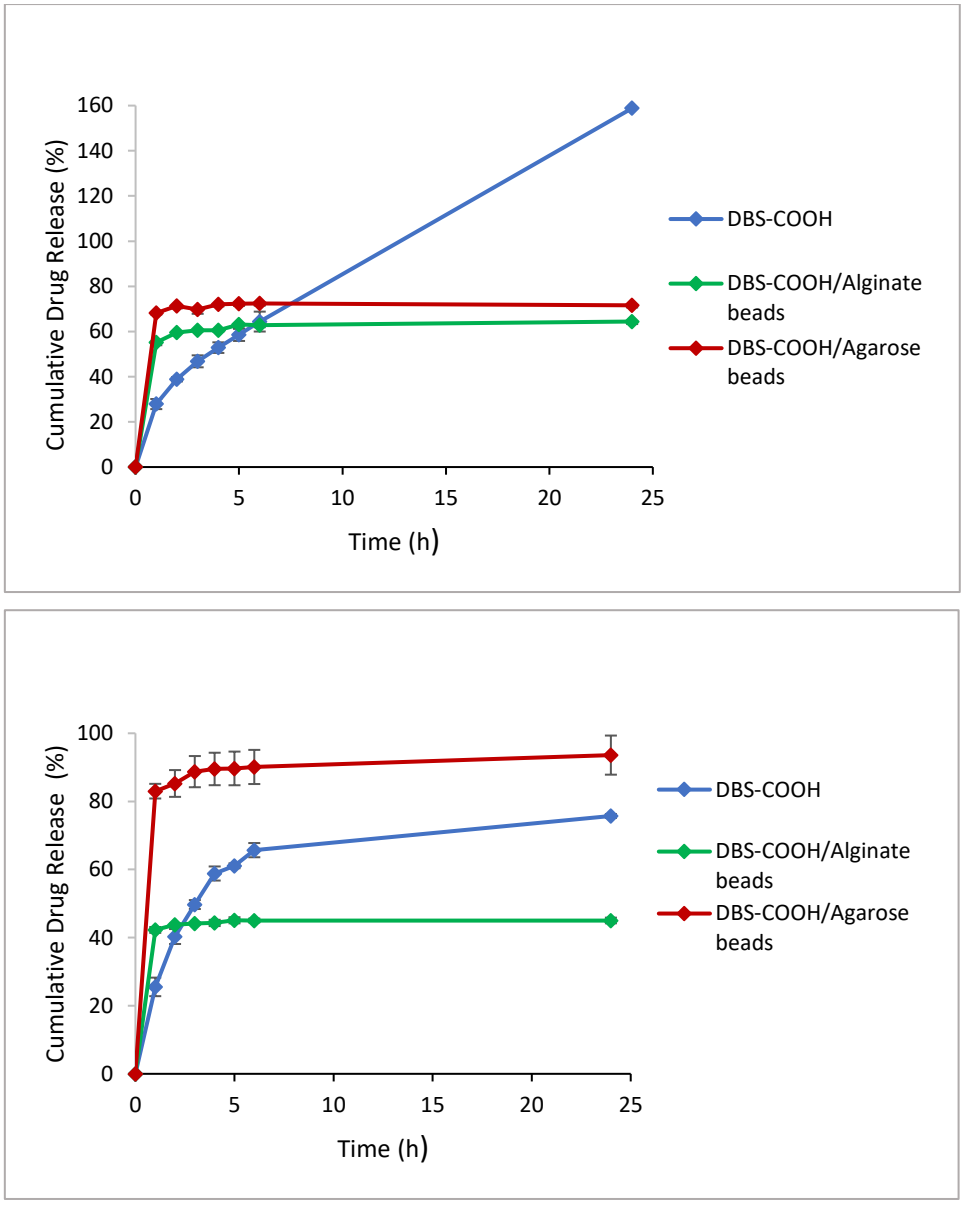

Figure 72. levodopa release from DBS-COOH (0.3% (wt/vol)) and its hybrid derivatives in tris buffer (0.1% (wt/vol)) at pH 7 (Top) and pH 3 (Bottom) respectively at 37°C. Error bars in the graph represent the standard error of the mean.

The DBS-COOH gel in a vial gel gave a sustained release profile at both pH 3 and 7, with an obvious pH sensitivity at pH 7 leading to gel breakdown over time which meant the apparent drug release exceeded 100. Interestingly, this is somewhat different to what was observed with propranolol, where gel breakdown was not evident in the data. This might suggest that propranolol was better able to mitigate the effects of pH-mediated gel breakdown. Once again, as for propranolol, DBS-COOH/Alginate beads and DBS-COOH/Agarose beads gave rapid release within the first hour of the study, perhaps as a result of their relatively small

dimensions. Also as previously, the DBS-COOH /Agarose beads gave a greater release (ca. 70%) compared to the DBS-COOH/Alginate beads (ca. 60%), which may suggest some interaction of the drug with calcium ions in the calcium alginate shell. Interestingly, alginate beads exhibited greater release at pH 7, while agarose beads had a greater release of the drug at pH 3. Highlighting the possible stability agarose contributes to the hybrid system as it is well known that DBS-COOH's stability is reduced as the pH is elevated.

FT-IR studies of DBS-COOH and its hybrid gels gave a trend of decrease in frequency for both C=O (1695 → 1691 cm^{-1}), (1643 → 1609 nm), (1594 → 1591 cm^{-1}), and the O-H region (3308 → 3271 cm^{-1}), (3372 → 3334 cm^{-1}), and (3278 → 3204 cm^{-1}) for the LMWG and its agarose and alginate derivatives respectively on loading with L-DOPA. As with the propranolol drug, the protonated levodopa molecule may be bound to the carboxylate ion of the DBS-COOH system inhibiting the APIs escape, although in this case, it seems likely that as it is released, the gel is damaged and begins to degrade.

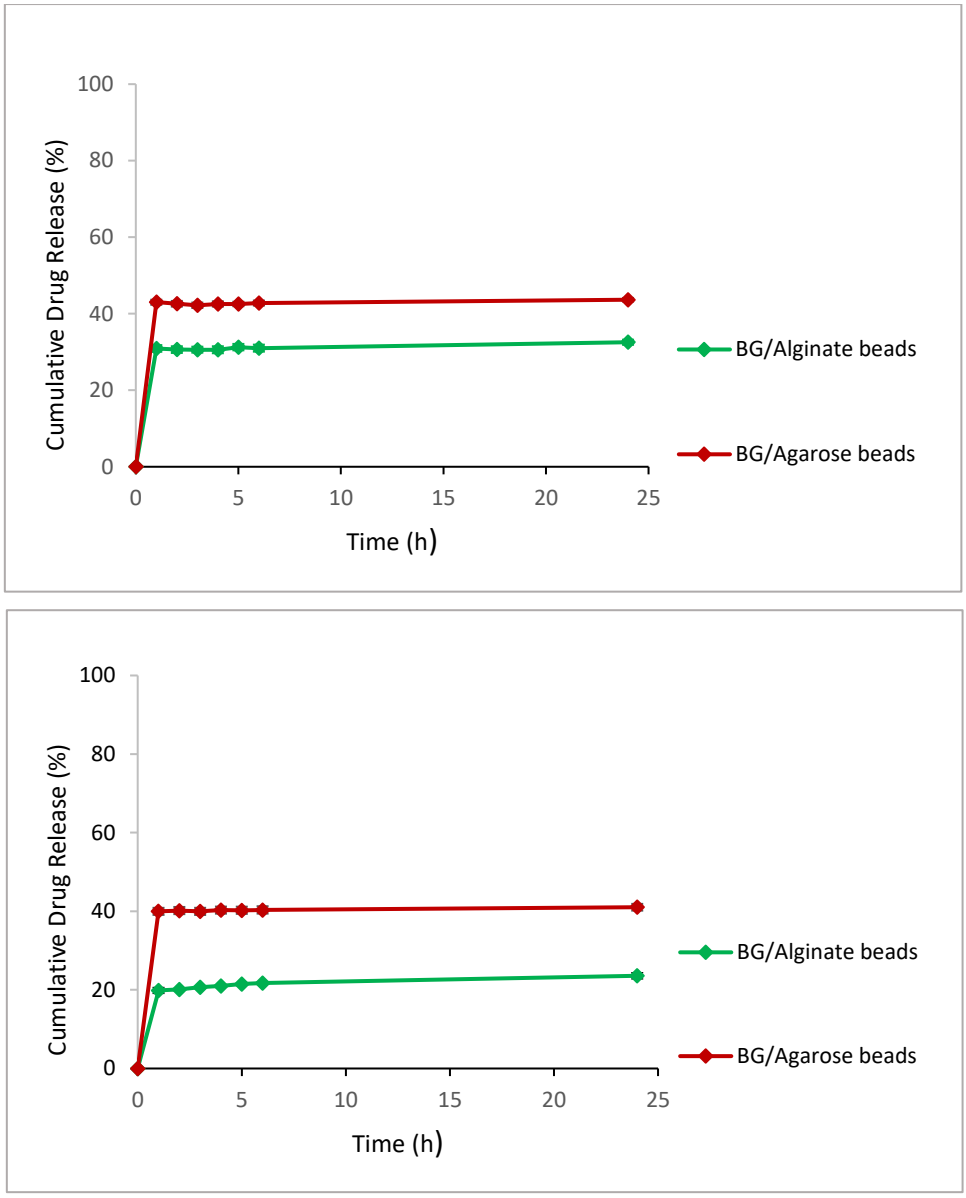

Figure 73. Levodopa release from Benzyl glutamines hybrid derivatives in tris buffer (0.1% (wt/vol)) at pH 7 (Top) and pH 3 (Bottom) respectively at 37°C. Error bars in the graph represent the standard error of the mean.

Levodopa release from Benzyl glutamine gels in vials has been previously reported by our group[2]. The release of L-dopa was studied in in-vitro and in-vivo. The gel system was loaded with levodopa pre-gelation which did not significantly influence the characteristics of the gel. In-vitro studies (investigated in a similar approach as these studies) at pH 7 produced a rapid release profile of 60% of the loaded drug (8.81 mg of levodopa) within the first two hours. A desired result for its intranasal application. The drug and gel system displayed no interactions which would explain this release profile. A further step was taken, and the gel system was

tested in-vivo on mice. To monitor the drug, radiolabelled [3H]l-DOPA was loaded into the gel. The gel was inserted into the nasal cavity and the concentration of the drug was detected on the brain, nasal cavity, and blood. The results showed that in 10 mins 27% of the drug was released into the nasal cavity, corresponding to the in-vitro studies which predicted a similar outcome[2].

Studying the drug release from its hybrid derivatives indicated rapid release within the first hour from both beads which plateaued for the remaining study. As in all other cases, there is greater release from the agarose beads (ca. 43%) than from the alginate-based beads (ca. 31%). There was a slight pH sensitivity shown from the alginate beads with ca. 30% release at pH 7 and ca. 20% release at pH 3. FT-IR studies showed that levodopa loaded Benzyl glutamine vial gels had only very slight changes in the C=O (1652 → 1651 cm^{-1}) and its N-H (3299 → 3302 cm^{-1}). Agarose and Alginate beads both gave a significant shift decrease in their C=O region (1645 → 1628 cm^{-1}) and (1595 → 1585 cm^{-1}) respectively. This is suggestive of some interactions between the robust polymers and the drug moiety. The alginate and agarose beads also had wavenumber increases in their O-H region (3297 → 3313 cm^{-1}) and (3337 → 3269 cm^{-1}) respectively.

4.5 Conclusions and Future Work

Three supramolecular LMWG's have been fabricated into bulk vial and hybrid polymer beads. The gels were tested to act as carriers for the important anti-tumour drug and dopamine prodrug, propranolol and levodopa respectively. A trend in release from the LMWG vial bulk gels is observed to give a slow gradual release where erosion release may be the main contributor. Combining agarose or calcium alginate combination with the physical gels in the form of gel beads resulted in burst release profiles which mostly plateaued within the first hour, preventing the full escape of the drugs from the entangled networks. It is possible that the smaller dimensions of the gel beads helped contribute to the rapid drug release profile. Clearly there was little capacity of the LMWG to mediate the release kinetics from these systems – possibly because the PG network limits interactions between the LMWG and the PG. In all cases, release was less from hybrid gel beads based on calcium alginate than those based on agarose. This may, most likely, be a result of drug interactions with the Ca^{2+} ion.

Alternatively, the core-shell nature of these gel beads may limit drug release slightly more compared to the agarose system which is more fully interwoven. Infrared spectroscopy was used to explore possible interactions between these systems and the drug molecules. However, these studies can be somewhat limited as both the LMWG, the PG and the drug all contain C=O, N-H and O-H bonds, which can make their detailed interpretation challenging. The study showed that the drug molecules are not only carried by our LMWG's but in many cases, appear to form interactions with the 3D network.

We believe that some of these gel systems have potential for carrying propranolol for the treatment of infantile haemangioma. There are several methods by which our LMWG's can be formulated. The drug could be administered topically in the form of the LMWG alone as studies have shown the effectiveness of topical application for IH[170]. This would be particularly appropriate for the Benzyl glutamine gels, as this gelator can hold the appropriate amount of drug for effective treatment. An alternative is to use the hybrid gel beads suspended in a cream[174]. The latter would provide drug stability, and application would involve the crushing of the gel in its suspended lotion. The beads could provide stability for the drug and increase its shelf-life. Local administration prevents any of the side effects associated with the drug as its delivery is mostly concentrated in the site of action, with a low serum level concentration. The gels also have potential to be formulated into a suppository form, particularly Benzyl glutamine as it gave the fastest release profile. Suppositories are regarded as the ideal formulation for infants as they eliminate many issues associated with drug administration[175]. The gel could be moulded in the standard shape of a suppository and be normally administered in the rectum which has a pH of 7-8, as studied in our release profiles. This mucous membrane delivery mode avoids first pass liver metabolism, and hence might be expected to require a lower dosage than the typical oral dosage, as a result of increased bioavailability.

Levodopa is typically administered to Parkinson's Disease patients orally via tablets. The drug is exposed to a vast amount of degradation, as it needs to pass through the digestive tract and extensive liver metabolism in order to reach the bloodstream and it then needs to cross the BBB. This leads to multiple doses being required per day with very little drug reaching the brain. Clearly one approach to this is the nasal delivery methodology previously developed for the Benzyl glutamine gel. However, sublingual delivery may be a solution to this problem. This

approach readily delivers the drug to the blood by passing first pass metabolism and only exposed to enzymatic attack in the mouth, reducing the required dosing for this treatment[176]. Sublingual dosage forms can be easily administered, are fast-acting, and are particularly beneficial for patients that are unconscious after surgery, etc. Our drug release studies do not consider the presence of enzymatic breakdown which we believe have the potential to increase the rate of release making it a suitable applicant for buccal delivery. Therefore, we hypothesize the use of our LMWG's and their hybrid derivatives can be fabricated into disc shaped sublingual formulations. In particular, the DBS-$CONHNH_2$ gel gave very effective L-DOPA delivery over a suitable timescale. It is also known from other work in the group that this gelator is non-toxic and compatible with human cells[177].The sublingual discs will encapsulate the drug, have the potential to protect it from enzymatic breakdown, while releasing it to the vascular area underneath the mouth. This potentially allows the drug to flow through the blood and reach its target site with reduced associated side effects as a high loading of drug would be unnecessary.

Chapter 5 Wet-Spinning and 3D Printing LMWGs For Biomedical Applications

5.1 Introduction

Wet-spinning is a technique typically applied to chemically cross-linked polymers, utilised to obtain thin thread-shaped constructs[178]. The concept is based on the extrusion of a gelator dissolved in a good solvent into a coagulant solution. The coagulation triggers the self-assembly of the gel fibres as the solvent and anti-solvent are dynamically exchanged leaving long thin filaments. The use of LMWG's in wet spinning is a new methodology, and there have only been a very limited number of reports, with the method being pioneered by Fitremann and co-workers[3]. As yet, the factors which control the extent to which a LMWG is amenable to the wet-spinning process are not well understood as only a very limited number of systems have been wet-spun[179]. Chalard et al demonstrated this method using their N-heptyl-D-galactonamide molecule. The new technique gave greater control over the self-assembly of the gel compared to the regular activation method, which was a heat/cool cycle[3].

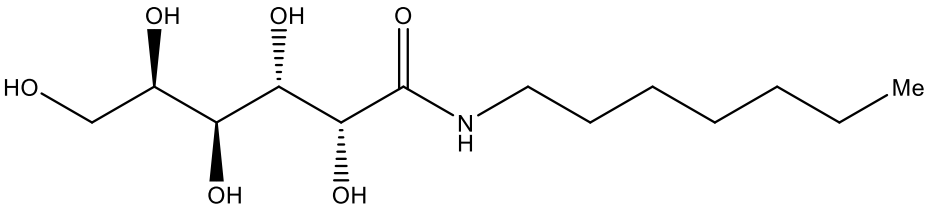

Figure 74. Structure of their N-heptyl-D-galactonamide[212].

Our group, in collaboration with Fitremann, has previously shown the ability of the DBS-$CONHNH_2$ LWMG to form this type of gel filaments by wet-spinning, to create 'printed' objects which could potentially be used as a platform for tissue engineering as well as drug delivery[177]. The wet-spinning of DBS-COOH was also then demonstrated. Furthermore, the two LMWGs

were then wet-spun in combination, to produce a stable and stimulus sensitive system. Individually, both gelators swiftly yield filaments with delicate networks. DBS-COOH is well known to be base sensitive and thus breaks down upon introduction to alkaline environments. DBS-$CONHNH_2$ however does not have such a characteristic, although it retains its desirable ability to reduce metals after wet-spinning. When wet-spun together, the gelators synergistically assembled leading to a multicomponent filament comprising both characteristics of the independent gelators. The filaments combined metal-reducing power and base sensitivity, and it was argued that they therefore may have promising potential applications for hosting cell growth[180].

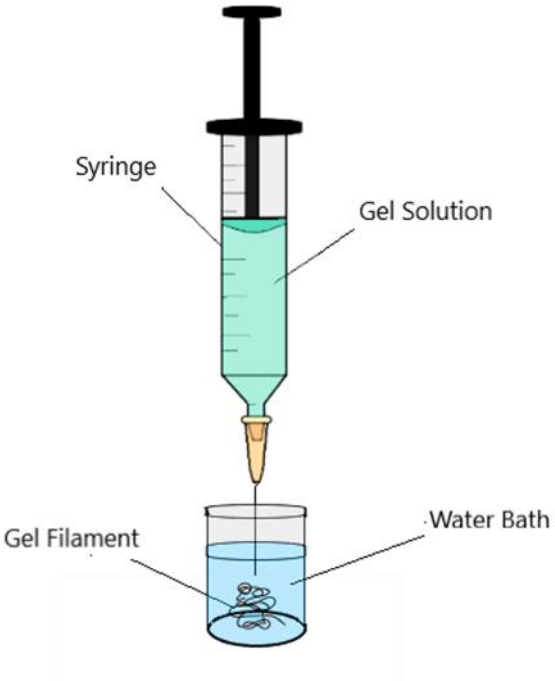

Figure 75. Wet Spinning apparatus.

To achieve the wet spinning of a gel, a high concentration of the LMWG is typically dissolved in a good solvent such as DMSO, and is then extruded into a water bath, rapidly resulting in long filaments. The high concentration removes the need for a supporting PG to be present during the fabrication process, instead the filaments are independently self-standing and do not require external support to sustain their shape. This is quite noteworthy as LMWG's are often inferior in terms of rheological robustness. DMSO is the solvent of choice, due to its

relatively low toxicity and high miscibility with water, meaning it exhibits fast-forming phase inversion resulting in a faster sol-gel transition. Wet spinning eliminates the need for thermal heating prior to gelation making it easier to form gels and would be beneficial when handling thermolabile drugs and loading them into shaped gel constructs. In this work, we focus on applying this method to our group of LMWG's to further understand the barriers and optimum conditions needed to pursue such a method, as well as pursuing its use in several applications. Further to extruding gel filaments, if this process is spatially controlled it is possible to use the wet-spinning approach to produce multiple layers of gel in a defined shape, and hence achieve effective 3D printing of shaped gel objects.

5.2 Wet Spinning of Benzyl Glutamine and its Derivatives

With the previously-reported success of gel filament formation of the sorbitol-based LMWGs[177], we were inspired to wet spin our novel, and much less explored LMWG – Benzyl glutamine. The thixotropic property of the novel gelator is unique amongst the gelators commonly used in the Smith group. We therefore reasoned that shaping the LMWG into a thin filament would have a high chance of success[177]. It was interesting to see if the Schiff base formation would trigger gel formation with this technique. We also wanted to enhance our understanding of the factors needed for optimum gel formation, and therefore wet spun a selection of gelators – Benzyl glutamine (BG-C12) and its derivatives BG-C11 and BG-C14.

5.2.1 Wet Spinning Benzyl Glutamine

Initially, various concentrations of glutamine-C12 with equimolar benzaldehyde were dissolved in DMSO. The gel solution was extruded from a syringe placed in a syringe pump, into a water bath at different rates with various needle sizes (Sizes are explained in table 28).

Table 28. Describing the inner diameter of each needle gauge size.

Needle Gauge (G)	Inner Diameter (mm)
15	1.372
20	0.603
23	0.337
25	0.260
28	0.184

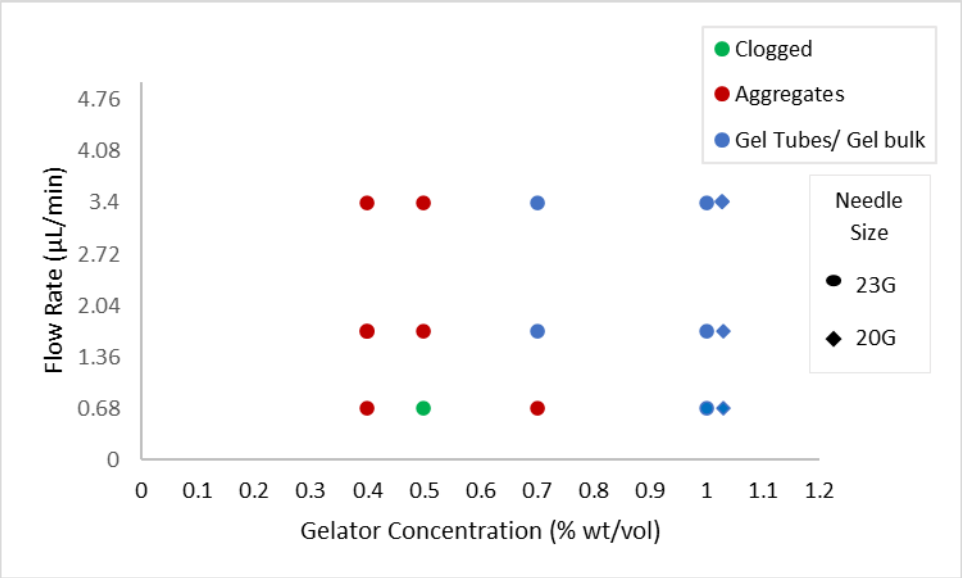

Figure 76. Wet spinning Benzyl glutamine (dissolved in DMSO) into a water bath at different concentrations, rates, and needle sizes.

At first glance, we can conclude that our gel system can be triggered through solvent exchange. Unfortunately, however, altering various parameters to achieve thin filament formation was not achieved but rather gel aggregates or tube-shaped/ bulk gels forming at the bottom of the vial were observed. Benzyl glutamine is a relatively slow-forming gel, and we therefore suspect gelation may be too slow for it to be able to acquire an immediate well-defined structure on extrusion. In part this is because the Benzyl glutamine has relatively good solubility in water compared with the DBS-based gelators. This will also limit it's ability to

rapidly form filaments on extrusion into a water bath. Indeed, the benefits of low water solubility were previously noted when comparing poorly soluble DBS-$CONHNH_2$ with Fitremann's more soluble N-heptyl-D- galactonamide[181].

Increasing the gelator concentration gave clearer indications of gel formation, however it became evident that the peptide-based gelator did not possess such good DMSO solubility as the previously reported DBS-$CONHNH_2$. The sorbitol gelator instantly formed thin filaments in part due to its high solubility in DMSO and low solubility in water – indeed, typical loadings for extrusion were 1.5-4.5% (wt/vol), with 3% (wt/vol) being optimal[177]. Such high concentrations of Benzyl glutamine could not be used, as for reproducible homogenous gel formation, the gelator must be fully soluble in the good solvent. High concentrations of gelator would give a greater chance of gel stability on extrusion, as more fibre/fibril entanglement is involved in the 3D network. Unfortunately, Benzyl glutamine could only be fully and reproducibly dissolved at a concentration of 0.5% (wt/vol) in DMSO. Above that concentration leads to precipitate in the gel solution and can result in clogging of the needle giving inconsistent release that produces unpredictable amounts of gel. We therefore elected to explore the use of different solvent systems in wet-spinning this molecule. Such studies have not previously been attempted for LMWG wet-spinning.

It was found that 3% (wt/vol) Benzyl glutamine was soluble in methanol. The gel solution was extruded from a 23G needle at various rates into different anti-solvent baths. The chosen solvent and anti-solvent are ideally required to be biocompatible for our desired biological applications, although there is potentially some opportunity to potentially wash any gel filaments obtained and exchange solvent.

Table 29. Wet spinning of Benzyl glutamine (3% wt/vol glutamine-C12 with equimolar benzaldehyde) in methanol extruded into various anti-solvent baths.

Solvent in Bath	Concentration of LMWG (%)	Rate (µL /min)	Appearance
Water	3.0	1.7	No gel formation
2-Propranol	3.0	1.7	No gel formation - Completely dissolved

Water acidified with HCl (pH 2.4)	3.0	1.7	No gel formation - Ppt
Petroleum Ether	3.0	1.7	No gel formation -Ppt
1 M HCl	3.0	1.7	No gel formation - Ppt on the top of the vial
Acetone	3.0	1.7	No gel formation - Completely dissolved

The gelator was readily dissolved in methanol, however no gel formation was triggered on extrusion into a solvent bath. Solvent exchange was inefficient for gelation and either a precipitate was formed, or the system completely dissolved due to solvent miscibility. This highlights the importance of solvent choice for triggering gelation. The solubility of Benzyl glutamine solubility in biocompatible reagents is limited, and the best solvent we could find for phase inversion gelation is DMSO and water.

We used ^{1}H NMR to characterise the gels created by extrusion of Benzyl glutamine in DMSO (0.5% wt/vol) into water. In particular, we calculated the remaining anhydrous DMSO left in the network after gelation. The amorphous gel was isolated, dried in a vacuum oven into a powder, and dissolved in D_2O. To quantify the DMSO the solution was spiked with an internal standard (acetonitrile), and integral peaks of the molecule (δ = 2.06 ppm) were compared to the peaks of DMSO (δ = 2.50 ppm). It was found that 99.9% of the injected DMSO escaped from the system as the water diffused into the hydrogel. Having a low quantity of residual DMSO eliminates the problem of DMSO-induced cell death in cell cultures and means that the gels created by this solvent switch extrusion method, although not spatially well-defined, should potentially be biocompatible.

5.2.2 Wet Spinning Benzyl Glutamine Derivatives

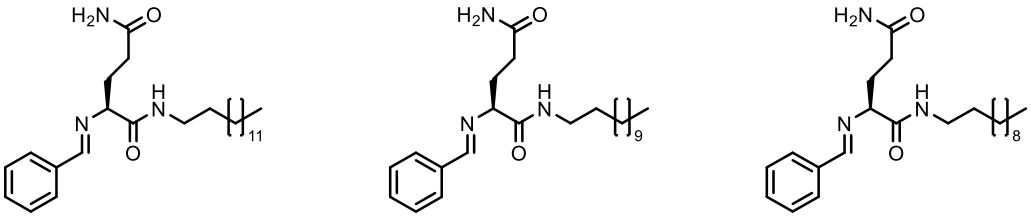

Figure 77. Benzyl glutamine (BG-C12) and its derivatives (BG-C14 and BG-C11).

Alkyl chain manipulation of Benzyl glutamine affects solvent solubility as a result of increased/reduced hydrophobic interactions as described in detail in Chapter 2. Both C11 and C14 derivatives have proven to form self-assembling hydrogels through the heat/cool method. It was therefore of interest to study the impact of structural modification in phase inversion triggered gelation as it may influence gel formation and stability. Using the same method described for wet-spinning Benzyl glutamine, its derivatives (BG-11 and BG-C14) were dissolved in 1 mL DMSO and extruded with a syringe pump into different bath mediums at various rates, and concentrations. In no case were well-defined gel filaments obtained, however, once again, under certain conditions, gel aggregates, tubes and/or bulk gels could be formed via this assembly mode.

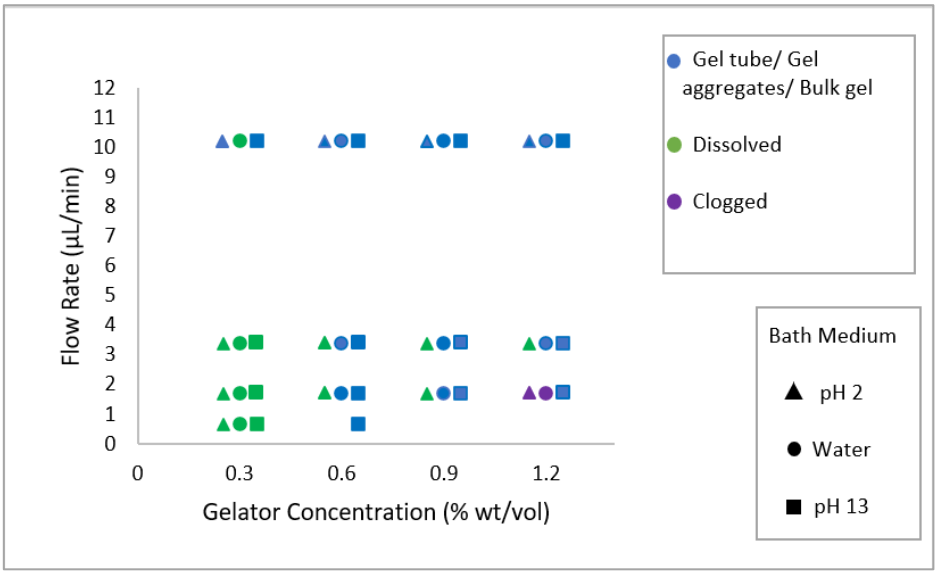

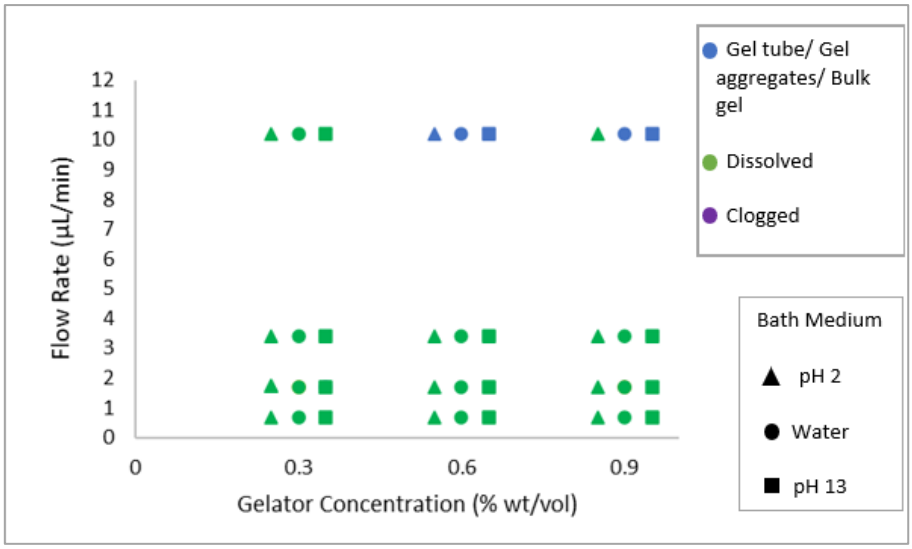

Figure 78. Wet spinning BG-C11 (Top) and BG-C14 (Bottom) dissolved in DMSO into different baths at different concentrations, and rates.

Reducing the length of the alkyl chain in BG-C11 elevated the affinity of the gelator for DMSO, while extending it in BG-C14 reduced its solubility. The BG-C11 gelator therefore easily dissolved in the solvent producing homogenous solutions, while BG-C14 was not completely soluble as the concentration rose. As shown in the graph, increasing the concentration from 0.3% (wt/vol) and above, the gelator went from being completely dissolved in the water bath after extrusion to forming self-assembled gels. The higher concentration promoted greater stability and withstood dissolving in the bath medium. Increasing the extrusion rate also promoted gelation as the gel solution quickly lands on the surface of the assembling gel which act as a form of support to form more gel. Gelation is established as the rate of solvent exchange is increased. Finally, gelation of the LMWG's was enhanced in an alkaline environment rather than in an acidic environment. Under acidic conditions, the gel solution dissolves in the water bath. It is known that Schiff bases are most likely to hydrolyse in acidic conditions[182-184], which would, in turn give rise to a protonated amine that would be soluble in water. We therefore suggest this is the reason for poor gelation performance at low pH. On extruding BG-C11 even at elevated concentrations of 1.2% (wt/vol), the gel formed at low pH values was relatively weak and broke down easily compared to gels formed in neutral or alkaline conditions.

Overall, therefore, the Benzyl glutamine derivatives triggered via phase inversion formed hydrogels, albeit not forming well-defined filaments. BG-C11's greater solubility in DMSO gave a significantly better success rate of producing 3D networks compared to the less soluble BG-C14. The reduced solubility of BG-C14 is due to increased hydrophobic interactions involved in the alkyl chain. This means BG-C14 provided inconsistent gel formation under these conditions with much less scope to alter the variables, as very specific conditions must be met for gel formation. Choosing a suitable anti-solvent to initiate gelation is also important. It is clear our systems have a sensitivity to low pH media as it increases their solubility and disrupts Schiff base formation. Although changing from a 12-carbon alkyl chain to a 11-carbon chain raises solubility in DMSO and allows higher loadings to be extruded, it also increases the solubility in water, which can cause problems with coagulation. Hence, the original Benzyl glutamine can formulate gels at significantly lower concentrations (e.g. 0.3% (wt/vol)) while the BG-C11 derivative requires a higher concentration as the gel assemblies are more soluble, and therefore less stable, in water. Nonetheless, both gelators could be extruded under the right conditions to give stable gels which lasted longer than one week.

5.3 Wet-Spinning LMWG's for Drug Delivery

Wet-spinning involves the rapid release of a gelator solution from a needle tip to gel upon exposure to an antisolvent. The rapid gel formation potentially makes it suitable for creating a depot type of formulation. The gel solution containing a therapeutic agent is injected through the skin. Once in contact with bodily fluids, solvent exchange triggers gelation of the drug loaded hydrogel. The released stream of the gel solution lands and layers on the forming gel to quickly grow a mass of the 3D network. The produced hydrogel may provide rapid or sustained release of the API depending on the required application. Drug delivery implants improve patient compliance, availability of tailored treatment, and localised drug delivery[185]. Indeed, in-situ gel formation is a common approach used with polymer gels, some of which are commercially available[185]. Despite their effectiveness molecules, we believe that LMWG's offer an advantage due to their biodegradability. Non-biodegradable systems may require invasive surgical intervention to the remove the implant from the site of injection once treatment is complete. The degree of instability of our self-assembled LMWG in aqueous

media can enable its breakdown over time, preventing the need for any surgical intervention. Indeed, Benzyl glutamine and DBS-$CONHNH_2$ are both biodegradable gels, that can form reproducible hydrogels via wet spinning, and therefore we proposed to investigate both of them for their ability to undergo this process in the presence of active pharmaceutical ingredient additives.

5.3.1 Wet-Spinning DBS-$CONHNH_2$ with Naproxen

The rapid gelation of DBS-$CONHNH_2$ and the stability of the filaments created via wet spinning promoted us to examine its ability to form such filaments in the presence of therapeutic agents. We hypothesize that the performance of an 'ink' would be indicated by its ability to form thin filaments rather than irregular shaped gels when wet-spun. Thin filament formation is therefore a good potential indicator for gel stability. As discussed above, there are several factors to consider when attempting to extrude well-defined filaments via wet spinning such as concentration of gelator, solubility of gelator, needle size, flow rate, and drug concentration, in order to obtain drug-loaded filaments. Naproxen, NPX, was the initial drug of choice in this study, given its good solubility in DMSO making it an appropriate drug model. We therefore aimed to establish the effect a therapeutic agent on the fabrication of thin gel filaments.

DBS-$CONHNH_2$ (1.5% (wt/vol)) was used with 10 mg naproxen in 1 mL of DMSO. The solution was extruded via syringe pump into a water bath at the following controlled rates – 3.4, 1.7, and 0.68 µL/min.

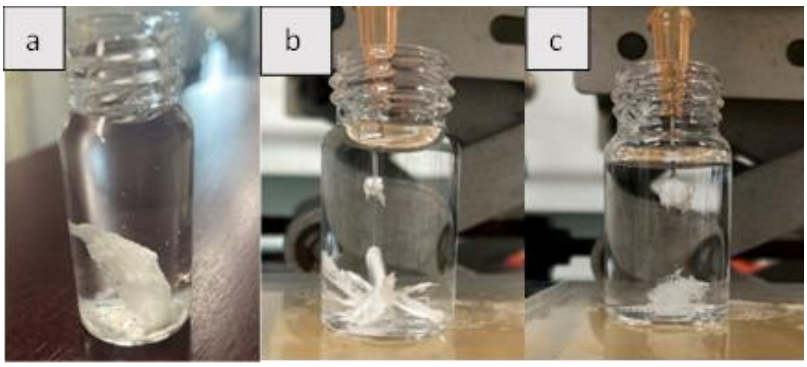

Figure 79. Wet spinning DBS-CONHNH2 with naproxen at rates a) 3.4 µL/min b) 1.7 µL/min c) 0.68 µL/min.

As shown in Figure 79 (a-c), the presence of NPX significantly limited the gelator's full potential to form extended flexible filaments. Reducing the pace of release gave the gelator the opportunity to self-assemble into the desired shape before landing at the bottom of the glass vial. The reduced extrusion rate in turn gave the extruded system more time for exchange between DMSO and water to occur, leading to sufficient self-assembly. From these studies 0.68 µL/min was found to be the optimum extrusion rate.

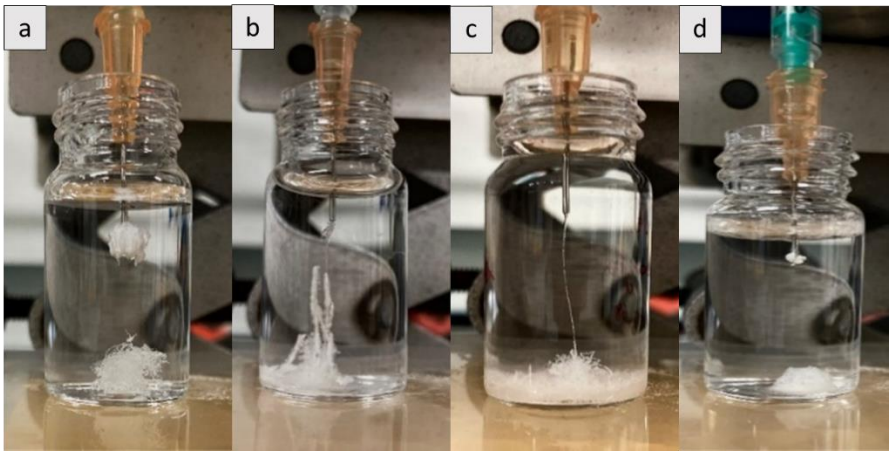

Figure 80. The effect of drug concentration on the formation of DBS-CONHNH2 filaments (10, 15, 20, 25 mg NPX- left to right).

While using the extrusion rate of 0.68 µL/min, 1.5% (wt/vol) DBS-$CONHNH_2$ in 0.2 mL DMSO was added to 10, 15, 20, 25 mg of Naproxen. On wet-spinning these solutions with different drug loadings, gel aggregates were obtained with 25 mg naproxen, irreproducible thin filaments at 20 mg, thick filaments at 15 mg, and reproducible thin filaments at 10 mg. This made 10 mg of Naproxen the most suitable drug concentration for achieving filament assembly, making it the maximum drug loading that does not appear to significantly disrupt the wet spinning of DBS-$CONHNH_2$.

5.3.1.2 SEM and Optical Microscopy

To gain better insight into the effect the presence of naproxen had on the DBS-$CONHNH_2$ filament, SEM and optical microscopy images were recorded. SEM images display the filaments in figure 81 (a, c, and d). The outer surface of the filaments resembles a collection of short rigid sticks which are the fibres of the 3D network. This is in strong contrast to the DBS-$CONHNH_2$ filaments formed without the presence of naproxen (figure 82), which have more of a coral like network. This therefore clearly indicated that the drug molecule affected the integrity and assembly of the gel structure from DBS-$CONHNH_2$, causing the nanofibers to be shorter and less flexible. This indicates that interactions between the naproxen and the gelator take place, but that they are not necessarily beneficial in terms of the wet spinning process. Such interactions have previously been proposed to exist between the COOH group on the naproxen and the acyl hydrazide functional group on the LMWG[40]. In the solvated gels this did not cause any apparent loss in integrity, but clearly the wet spun filaments are more sensitive to this kind of effect. This observation that the morphology was different in the presence of naproxen is consistent with the observation that larger amounts of naproxen disrupted the ability to wet-spin filaments of DBS-$CONHNH_2$. Optical microscopy images were difficult to obtain as the filaments were too delicate. However, in the figure, the images show fragments of the filaments consisting of irregular tubular shapes with various thicknesses.

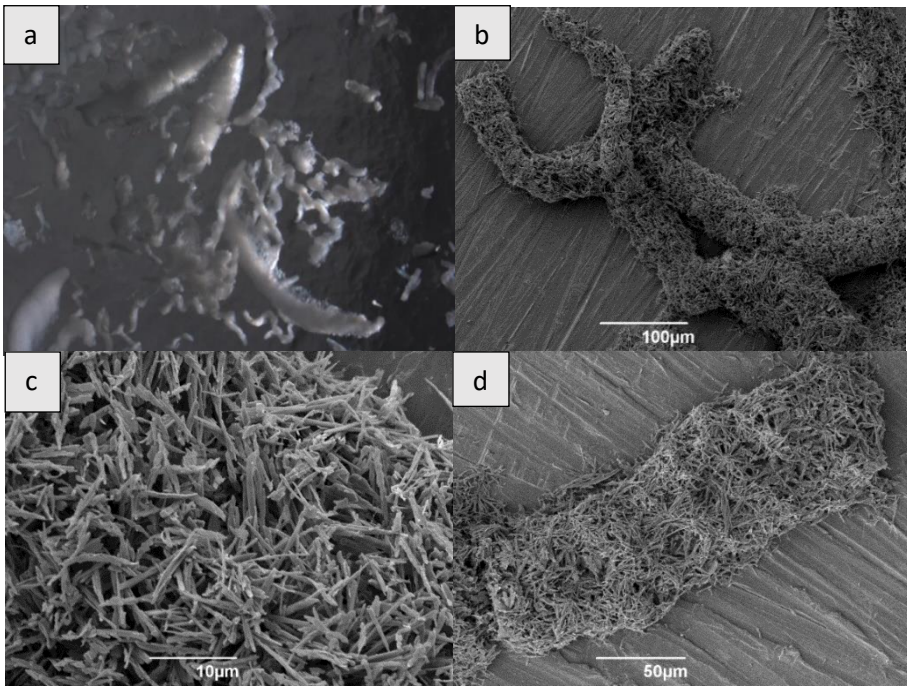

Figure 81. a) Optical microscopy image of DBS-$CONHNH_2$ NPX loaded filaments. b-d) SEM images of NPX loaded DBS-$CONHNH_2$ filaments.

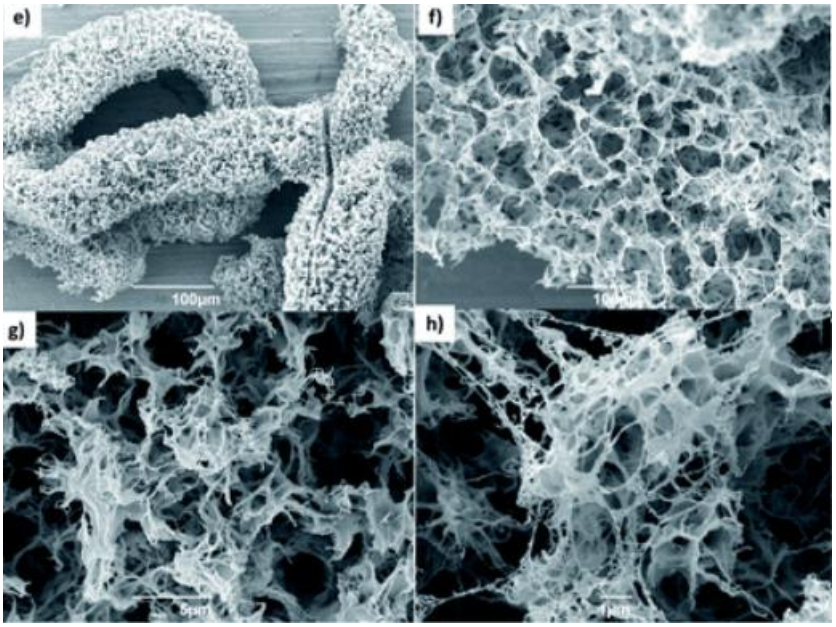

Figure 82. SEM images (e-h) of DBS-CONHNH2 filaments obtained by Carmen Piras “Self-assembled gel tubes, filaments and 3D-printing with in situ metal nanoparticle formation and enhanced stem cell growth”,Chemical science, 2022.

5.3.1.3 Drug Release Study

To gain a better understanding of the interactions between the wet-spun network and naproxen, a drug release study was then conducted. Although filament formation is a good indication of gel stability, gel formation with irregular shapes is still beneficial as the gel forms a densely packed network with increased resistance to water solubility. We therefore loaded the gel with naproxen and tested its ability to retain the molecule and its possible use as a depot drug delivery system. A 1.5% (wt/vol) solution of DBS-$CONHNH_2$ was extruded with naproxen (2 mg in 0.1 ml drug solution) at a rate of 10.2 µL/min into a 2 mL water bath. Once a gel was formed, 200 µL aliquots were removed from the water bath, tested by UV-Vis spectroscopy, and then discarded (The aliquots removed were not replaced with fresh buffer).

The gel system was placed in an incubator at 37°C for the remaining of the study, with aliquots being removed at fixed time periods.

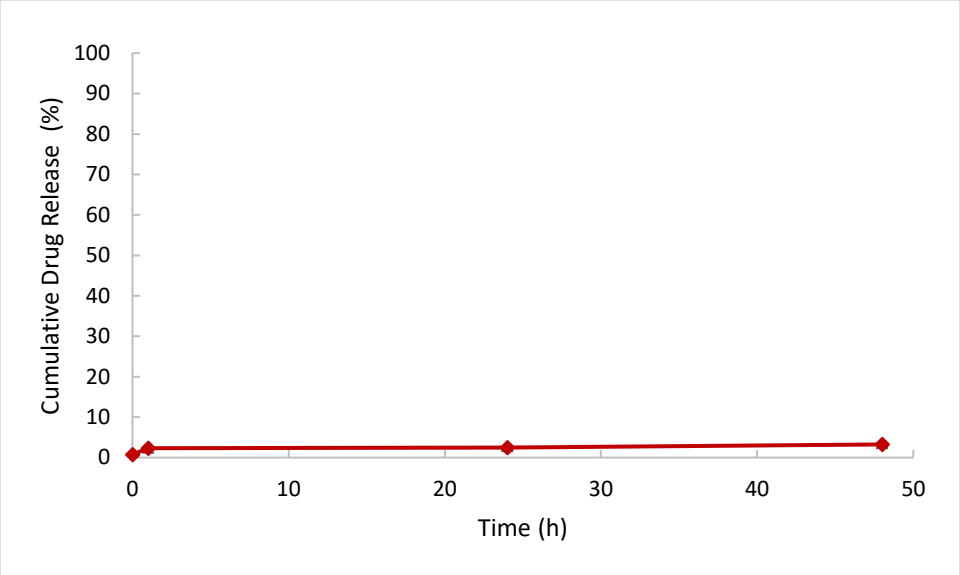

Figure 83. 48-hour drug release study of naproxen from wet-spun DBS-CONHNH2 hydrogels. Error bars in the graph represent the standard error of the mean.

The 48-hour study resulted in extraordinarily little release of the therapeutic agent, with a maximum observed release of 3%. This suggests that the maximum stable loading of NPX is 1.94 mg per 0.1 mL. We believe that drug-gel interactions, as reported previously[40], prevented the escape of the API. The retention of the API is more than reported previously, but in the wet-spinning method the ratio of drug:gelator is much smaller, which may contribute to its much more robust incorporation. If the drug concentration was increased, the gel became less stable (see discussion above), leading to the rapid release of NPX.[40] FT-IR studies on wet-spun gels with and without NPX were performed to test whether there is any evidence of gelator-naproxen interactions when the gel is triggered via wet spinning. FT-IR confirmed the presence of naproxen in the drug-loaded gel filament but did not exhibit any specific shifts (experimental data found in section 7.4.11).

It should be noted that that low loading of naproxen In these gels is a significant disadvantage in clinical terms, because the drug is well below the required therapeutic dose (ca. 0.5 g)[186]. However, we anticipate that this approach may be of value for depot release of other active

pharmaceutical ingredients that are active at much lower dose levels and could therefore be meaningfully incorporated. This would form the basis of future studies in this area.

5.3.2 Benzyl Glutamine Drug Delivery

Benzyl glutamine was then wet-spun with Naproxen and Propranolol HCl to test its ability to act as a carrier of the painkiller and chemotherapeutic. The study was conducted to understand the potential of LMWG's in the field of extrudable depot formulations. 0.5% (wt/vol) Benzyl glutamine (in 0.1 mL DMSO) was extruded with the drug (1 mg NPX or 2 mg propranolol HCl) into a 2 mL water bath at various rates, with samples being removed and discarded at different time intervals to monitor drug release via UV-vis spectroscopy (NPX - 329 nm) and (Propranolol - 289 nm).

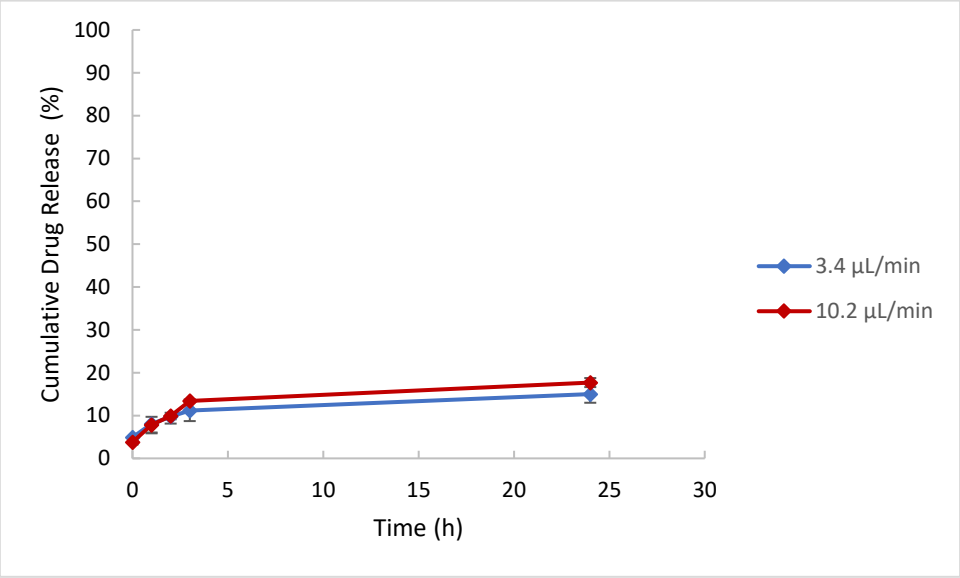

Figure 84. Monitoring naproxen release of wet spun with 0.5% (wt/vol) Benzyl glutamine extruded at rates - 3.4 µL/min and 10.2 µL/min. Error bars in the graph represent the standard error of the mean.

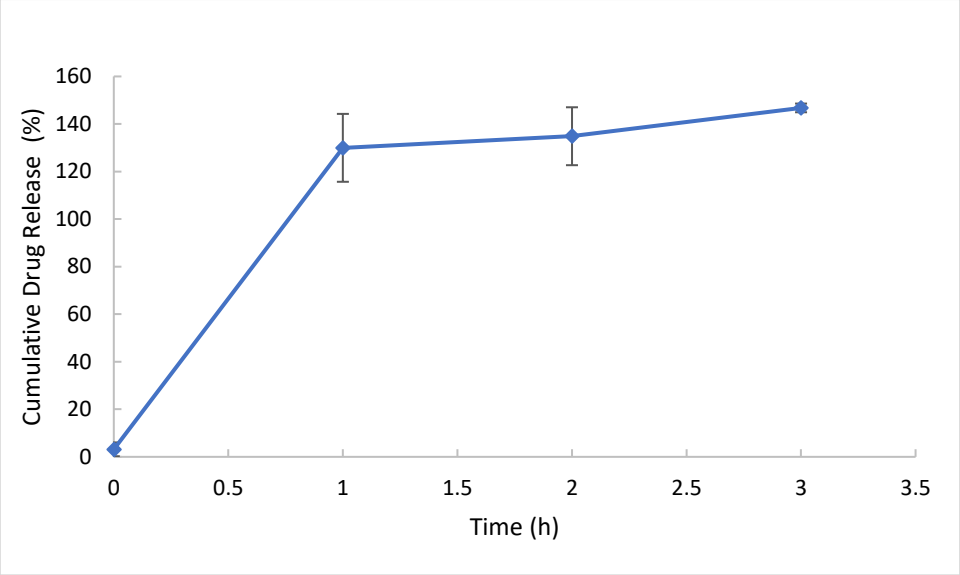

Figure 85. Monitoring propranolol release of wet spun with 0.5% (wt/vol) Benzyl glutamine. Error bars in the graph represent the standard error of the mean.

As the drug-gel solution undergoes its phase transition on extrusion into water, it generates fibres leading to entanglement. The drug can leach out during that lag period. The undesirable effect can cause serious harm with drugs of narrow therapeutic index as side effects can be activated in this type of situation. Benzyl glutamine has slightly shown this type of event with an initial ca. 3-6% release immediately after the completion of gel formation for both API's. We were, however, pleased to see that this occurrence is relatively negligible, and that most of the drug remained within the gel. The immediate entrapment efficiency of the gel is roughly 96% of the loaded naproxen (10 mg NPX per 1 mL gel solution) and 93% of the loaded propranolol HCl (20 mg propranolol per 1 mL gel solution). However, clearly the gel could not retain propranolol in its network, as within the 1st hour the gel released the entirety of the loaded drug. Propranolol's crystal form is highly water soluble and is therefore easily able to diffuse into the water bath. This is in contrast to Naproxen, which is relatively insoluble in water. This limits the driving force for it to transition into the aqueous phase. The NSAID slowly diffused out of the system over a 24-hour period, with 20% release. The Naproxen-loaded system was also extruded into the water bath at different rates as shown in figure 84, to monitor any impact of extrusion rate on the initial rate of release of the drug. From the results,

it is clear that changing this parameter has insignificant effect on the entrapment efficiency of the gel.

FT-IR studies were performed on xerogels of the wet-spun gels (Benzyl glutamine) loaded with and without the drugs propranolol and naproxen respectively (experimental data found in section 7.4.13). Addition of propranolol (IR peaks of C=O (1579 cm^{-1}) and N-H (3275 cm^{-1})) to the system resulted in a slight shift in the C=O peak (1654 → 1663 cm^{-1}) and N-H peak (3299 → 3284 cm^{-1}). This might suggest some interaction between the gel and the drug, however, clearly this does not significantly impact on release rate. Interestingly, however, no FT-IR shifts were observed with the comparative study of wet-spun xerogels in the presence/absence of naproxen. This suggests that there are not interactions between this drug and the gel, which seems counterintuitive given the large impact on drug release in this case. Further supporting the idea of the role drug solubility has on release rate. Alternatively, it is possible that the hydrophobic naphthalene unit of naproxen interacts with the hydrophobic part of Benzyl glutamine – an interaction which would not lead to significant IR shifts.

Overall, however, the results described above are exciting as the injectable gel remained stable during the study and did not immediately release the drug molecule. Compatibility of drug with solvent is a crucial factor to be considered, in this instance drugs with lower water solubility appear to favour remaining in the gel network, giving a prolonged release via diffusion and gel degradation. This technique suggests a possible way forwards to the use of biodegradable LMWG's for implant drug delivery.

5.4 3D Printing LMWG's

3D printing or direct ink writing, involves generating layers of gels with spatial resolution which stack one on top of another to form an acquired 3D construct. Printing gels in a designed shape holds great importance for applications such as tissue engineering and drug delivery. The soft material can be printed to accommodate cell growth, as well as being used for tailored therapy in which the gel is printed for each individual patient with specific needs. The technique permits the user to change the material being printed, the shape of the print, and the gel thickness (number of layers). This technique has been extensively explored with polymers[187-190] with the gels being triggered by chemical crosslinking, UV irradiation, etc[191-

[193]. While 3D printing polymer gels is effective, chemical crosslinking is a limitation as it can damage cells or reduce activity of therapeutic agents. However, conversely, most supramolecular gels have weak rheology, low viscosity, and non-thixotropic properties making them unsuitable for 3D printing with generic methods such as those used for polymer 3D printing. There have, however, been some emerging reports of 3D printing applied to LMWGs, mostly using extrusion of a pre-formed gel that then reforms after printing. Self-assembling Fmoc-dipeptide printed scaffold gels linked by electrostatic interactions gave tuneable mechanical property and biodegradability for cell growth[194]. Zhou printed a LWMG imidazolium-based supramolecular gelator. The properties of the gel permitted gel recovery once extruded to form a self-standing non-covalent hydrogel. Photopolymerization was subsequently utilised to form covalent bonds to reduce the brittleness of the gel and improve its overall rheology[195]. Adams group optimised the printing of LMWG 3-phenyl-2-[3-phenyl-2-[2-(5,6,7,8-tetrahydronaphthalen-1-yloxy)acetamido]propanamido]propanoic acid and Fmoc-diphenylalanine[196]. The group also constructed a 3D printed moiety containing layers of gels of alternating peptide based gels[197]. Triggering gels through solvent exchange potentially enables the printing of gelators which lack the standard requirements for 3D printing and thus opening doors to the production of 3D-scaffolds with unique properties associated with supramolecular bonds. The printing of physical gels via solvent exchange, as mentioned in the section describing wet-spinning methodology, is still considered a new field, and is only slowly getting recognized. *N*-alkyl-D-galactonamide gelators printed in 3D scaffolds were used for cell culture growth. The group also studied the effects of gelator solubility in water by altering the length of the molecule's alkyl chain. Although this method did enhance gel stability in water, it increased the fragility of the gel. Manipulating the structure of a gelator modifies the properties of a gel, as a result of changing the number of non-covalent interactions. Cryo-SEM images indicated that the new gelator no longer possessed self-assembled fibres but rather self-assembled flakes which may explain its increased fragility[181]. Insolubility in water is therefore an advantage for biological applications due to the greater stability that the gel will exhibit as a scaffold. Our group have fabricated a 3D printed hydrogel via phase inversion with DBS-$CONHNH_2$[177] which we believe was successful due to its water insolubility. We therefore wanted to compare the performance of our other LMWGs. Benzyl glutamine and DBS-COOH are reported to form bulk gels via a heat/cool cycle and pH switch respectively. The suitability of these gels for 3D printing was investigated as both gelators have distinctive properties.

5.4.1 Optimum Conditions for 3D Printing

We therefore performed experiments to explore the 3D printing of these two different gelators. In particular, we hoped to optimise the parameters required for effective 3D printing of the gels. DBS-COOH and Benzyl glutamine are sorbitol and amino acid based gelators respectively. As described previously, reproducible thin filaments of DBS-COOH can be achieved via the wet spinning technique, but Benzyl glutamine, although capable of forming gels using this technique could not retain a well-defined filament shape. We reasoned that the relatively high insolubility of DBS-COOH in water enabled faster gelation on extrusion with better spatial resolution and greater stability compared to the more soluble amino acid based gelator, which therefore assembles with less definition.

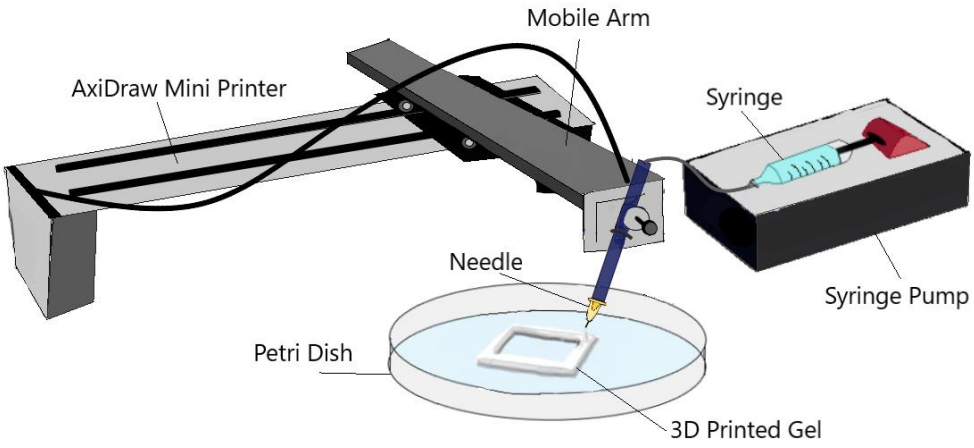

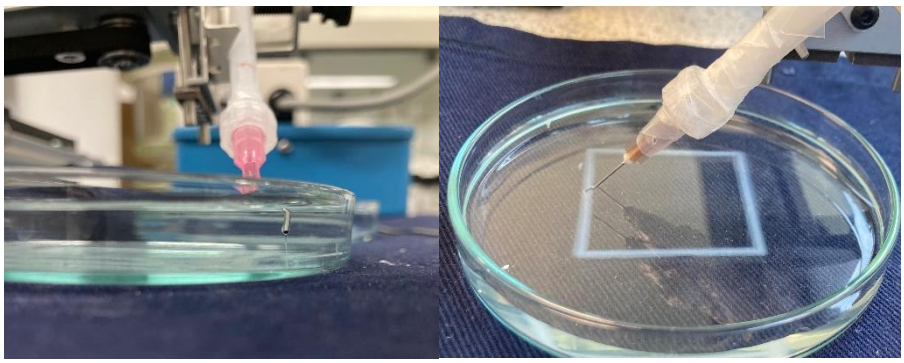

Figure 86. 3D printing setup (top) and 3D printed Benzyl glutamine (0.5% wt/vol with one molar equivalent of benzaldehyde) in a petri dish (bottom).

3D printing of gels involves the layering of the extruded gel triggered by solvent exchange. Ideally, the gel must land flat on the surface with minimal spreading which is then further stacked with additional layers to form a 3D object. This is achieved by moving the extrusion needle around a pre-programmed 2D path using x,y coordinate control. By circling around the path, a multi-layer object can be fabricated. The layers must be harmonized with very little variations in the printing path to achieve a specific pattern. We will highlight the necessary conditions needed to be optimised for this goal.

5.4.1.2 Concentration

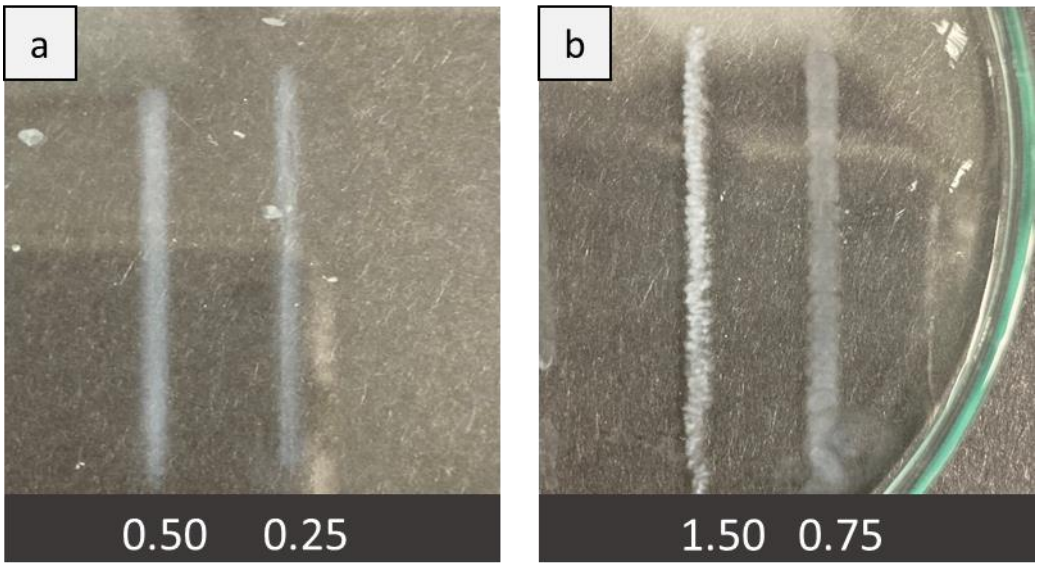

Figure 87. Comparing the effect of concentration on 3D printed platforms a) Benzyl glutamine (Concentrations of 0.25% and 0.5% wt/vol - with one molar equivalent of benzaldehyde) b) DBS-COOH (Concentrations of 0.75% and 1.5% wt/vol).

The effect of gelator concentration on 3D printing was determined based on physical appearance as displayed in Figure 85. Two layers of each gelator (Benzyl glutamine and DBS-COOH) with different concentrations were printed, with all other factors (Needle gauze size,

rate, and distance) being standardised and were compared. A high concentration (1.5% wt/vol) of DBS-COOH provides an instantaneous and visibly clear gel assembly in comparison to lower concentrations of DBS-COOH. Reduced loading of the gelator (0.75% wt/vol) gave more transparent prints. A greater concentration of gelator involved in the gel network leads to greater gel opacity and in turn increases the stability in the bath.

On printing Benzyl glutamine (figure 87, (a)), we again found that the lower the concentration the more transparent the print. Raising the concentration of this gelator above 0.5% wt/vol resulted in insolubility leaving precipitate and inconsistency in the printed gel and thus disrupting effective linkage between gel layers. Reducing below a concentration of 0.5% wt/vol reduces the defined shape of the gel, with increased gel spreading as the viscosity of the gel mixture is reduced and in turn a greater flow in the x-axis occurs. These problems and the slow gelation of Benzyl glutamine result in an expansion of the thickness of the printed object – i.e. the extruded solution spreads before gel assembly is complete. The degree of spreading will depend on the relative kinetics of diffusion and assembly. The optimum concentration therefore needed to be determined for improved stability and shaping of printed gels.

5.4.1.3 Needle Size

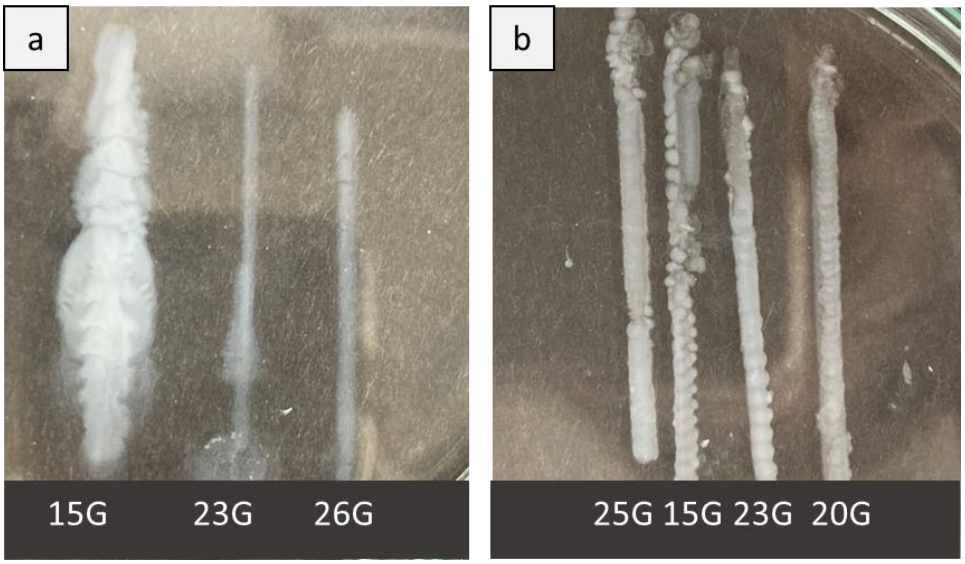

Figure 88. 3D printing of a) Benzyl glutamine (0.5% wt/vol with one molar equivalent of benzaldehyde) at a rate of 3.5 µL/min with needle gauge sizes of 15G, 23G, and 26G respectively. b) DBS-COOH (1.5% wt/vol) at a rate of 8.2 µL/min with needle gauge sizes 25G, 15G, 23G, and 20G.

In this case, the needle size played a key role in the extrusion process–- the thickness of the needle corresponds to a greater difficulty of release which may result in its clogging. Using a 26G needle (the narrowest needle), the flow of the fast-gelling DBS-COOH was somewhat pulse-like with little adhesion to the glass of the petri dish. Increasing the area of the needle tip to 23G led to smoother flow and increased adhesion of the gel to the glass surface (figure 88). The viscous gel mixture easily leaves the needle tip with a higher surface area promoting consistent release of the gel mixture, hence creating a consistent release of the ink. With the fast acting gel, smoothness of the print is dependent on both factors as in figure 88 (b) although all parameters are fixed with a high extrusion rate of 8.2 µL/min, the homogeneity and smoothness of the print varies greatly more than thickness.

The size of the nozzle can be used to provide various thicknesses of the printed gel. This is demonstrated with the use of Benzyl glutamine. In the case of this gelator, the diffusion of the gelator is faster than the kinetics of assembly (see above). Therefore, when the gelator was released into the water bath from needle sizes – 15G, 23G, and 26G (figure 88 (a)), this produced prints with width sizes of 0.7, 0.2, and 0.2 mm respectively. The needle size is clearly affecting the thickness of the print as it eases the release of the gelator. Gels with greater solubility and less stability are therefore more prone to sensitivity to needle size, which explains the dramatic variation between the results of Benzyl glutamine and DBS-COOH. This is therefore a powerful tool for printing different shapes that require specific thicknesses.

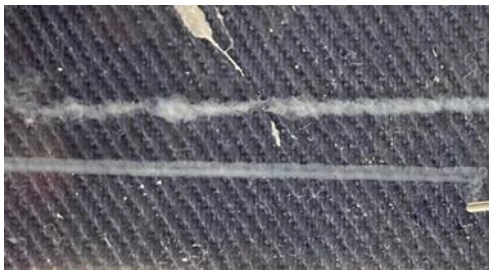

Figure 89. 3D printed 1.5% (wt/vol) DBS-COOH. Top line (Needle size 26G, rate of 5.1 µL/min), bottom line (Needle size 23G, rate of 3.4 µL/min).

5.4.1.4 Rate of Extrusion and time between prints

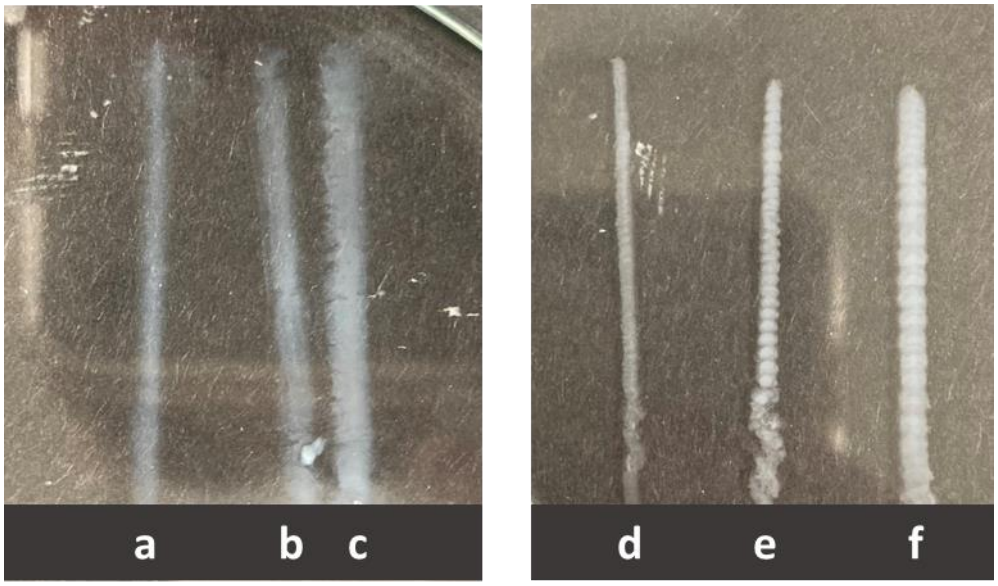

Figure 90. 3D printing of Benzyl glutamine (left image) - (0.5 wt/vol with one molar equivalent of benzaldehyde) at rates of a) 3.4 µL/min, b) 5.1 µL/min, and c) 8.2 µL/min (needle size 26G). And DBS-COOH (right image) - (1.5 wt/vol) at rates of d) 3.4 µL/min, e) 5.1 µL/min, and f) 8.2 µL/min (needle size 23G).

The extrusion rate regulates the amount of the ink released per second. Figure (90) demonstrates the effect of changing only the rate on 3D printed Benzyl glutamine and DBS-COOH respectively while maintaining other parameters. We can observe from both gels that the higher the rate, the thicker the print. Rates 3.4, 5.1, and 8.2 µL/min produce DBS-COOH prints (figure 90 (d-f)) with width sizes of 0.1, 0.2, and 0.4 mm respectively and Benzyl glutamine prints (figure 90 (a-b)) with width sizes 0.1, 0.2-0.3, and 0.3 mm respectively.

The extrusion rate and needle size work together as they are indirectly proportional to one another. If the needle size is reduced, the rate may need to be increased to prevent clogging and vice versa. Figure (89) displays prints of DBS-COOH, although a higher rate was used with the 26G needle, the small surface area did not facilitate such smooth passage into the water

bath as the larger nozzle with a lower flow rate. Similarly, to the needle thickness, the flow of the ink also controls the thickness of the gel, as more ink is released a greater surface will be covered. When dealing with a fast-acting gel like DBS-COOH, a higher extrusion rate may be required compared to a slower-acting gel system.

Another aspect to keep in mind is the time between printing each layer. Depending on the gelator, there must be a sufficient time-frame for each layer to stabilize and retain its shape and thickness before another layer is printed uses the first layer as a supporting platform. This time varies between gelators, which stabilize at different rates.

5.4.1.5 Distance Between Needle and Platform

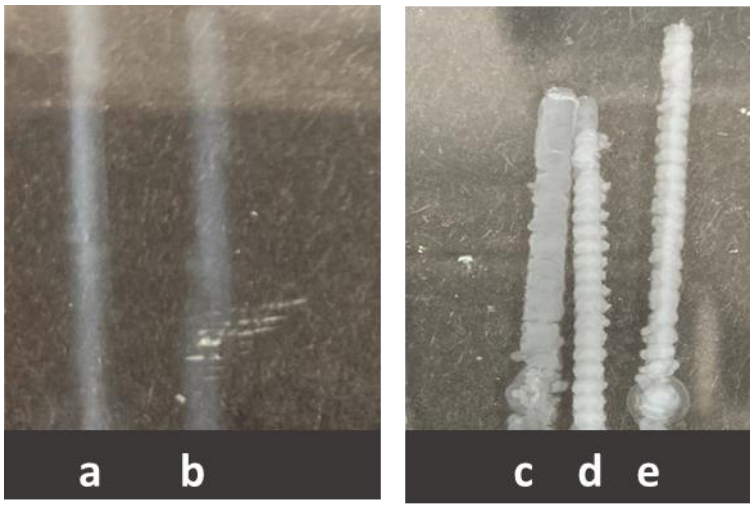

Figure 91. Displaying the effect of varying the distance between the nozzle and platform with 3D printed Benzyl glutamine (Left image) – a) 1 mm b) 0.4 mm and DBS-COOH (Right image) – c) 0.2 mm d) 0.4 mm e) 1 mm.

The movement of the bio-ink from the tip of the needle until it reaches the supporting platform must also be considered. As the ink falls and hits the surface, gelation occurs. It is found that reducing the distance between the needle tip and the platform provides more homogeneous gel formation with greater gel adhesion. Reduction of this height creates thicker gel prints as gel has time to spread on the surface before self-assembly is complete. Increasing this distance enables gelation to occur during its journey to the surface, providing

thinner prints. This means that vertical distance is another way of manipulating printed thickness.

From changing parameters as described above, we can conclude that the needle size can be used to manipulate the thickness of the printed gel, the greater the size the larger the thickness of the print. Increasing the rate of flow results in greater spreading of gel and thus a greater thickness. Increasing the space between the needle and the platform promotes thinner gel formation. The DBS-COOH gelator is an excellent candidate for 3D printing. It forms gels immediately with great stability. These qualities enable different variables to be used to alter the thickness of the printed ink to achieve a range of desired shapes, as well as being a valuable model to show the importance of finding the optimal conditions needed for 3D printing. Although Benzyl glutamine failed in terms of forming well-defined thin filaments via wet spinning, it could nonetheless be used for 3D printing of simple shapes under these solvent extrusion conditions. The gelator gave a slower onset of gelation compared to the sorbitol-based gel, which we believe is due to the greater solubility of Benzyl glutamine in water compared with DBS-COOH. We therefore concluded from this initial investigation of gel printing parameters that both gelators can potentially be used as inks for 3D printing capable of providing self-supported structures, albeit with very different characteristics. These differences may be valuable in providing access to printed objects with different types of behaviour.

5.4.2 Gel Printability

As described above, these gels proved their ability to be 3D printed. Although they were capable of forming straight lines and square shapes (see above), we then wanted to test their ability to form prints of different and more complex shapes. Inspired by Fitremann's filament fusion test[181], the test printing pathway involved an E shape with unique curves and lines distributed at varied distances within the shape. This design is an effective test of the performance of an ink for wet-spinning as it allows quantification of print thickness, resolution and ability to maintain both linear and curved structures.

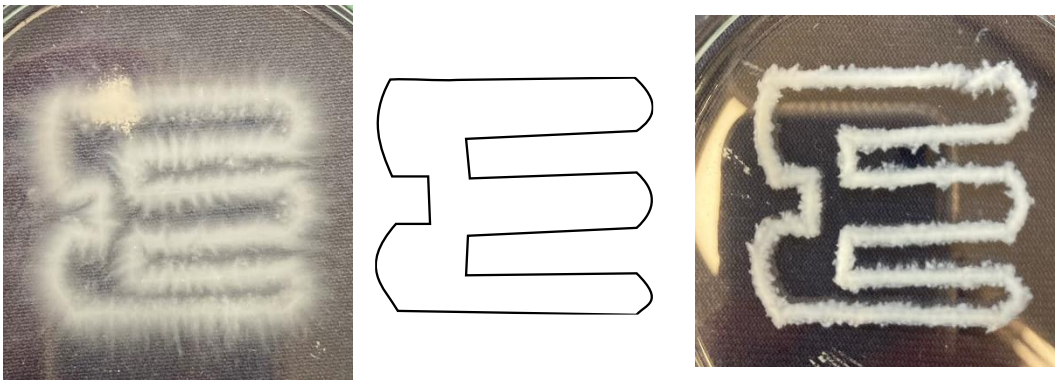

Figure 92. Testing the printability of Benzyl glutamine (a) and DBS-COOH (b).

The distance between the top two lines is 0.5 cm and the bottom two lines is 0.2 cm, allowing us to gain insight into print resolution. There are then curves and/or straight lines connecting these regions. DBS-COOH and Benzyl glutamine were printed in a water bath, at a rate of 8.5 µL/min and 5.1 µL/min with needle sizes 23G and 26G respectively. The 14-layered printed gels held their shape, with better resolution in straight paths compared to curvatures. DBS-COOH displayed significantly greater control compared to Benzyl glutamine in the curved sections as the highly insoluble gelator formed quickly as it was extruded into the bath, with no regard to fluid motion which would redirect the extruded stream slightly off the scaffold, as was seen with Benzyl glutamine. The slow-acting gelator needs time to form a gel, and as the printing arm moves the stream in these short distance movements, insufficient time is provided for the gelator to self-assemble leaving a less-structured, more widely spread 3D print. Indeed, there are multiple clear points on the Benzyl Glutamine print where assembly is extending outwards into the bath from the printed shape. Nonetheless both gel shapes were clear, indicating that the gels are capable of forming a variety of shapes, with DBS-COOH having significantly greater precision in terms of shape formation.

5.4.3 Self-Healing

The self-healing property of Benzyl glutamine is one of the key properties making it distinctive from our other gelators. Gels formed in vials through the heat/cool cycle have been shown to

be reformed once broken, with the process being observed both physically and using rheology[2]. Gelation through solvent exchange produces a meta-stable material with possible alternative qualities compared to the standard heat/cool cycle gelation. To demonstrate the ability of the gel to reform upon mechanical damage, several layers were printed in a square shape. The gel was punctured by a thin needle in several locations. The 26G needle passed through the layers leaving small visible holes in the gel.

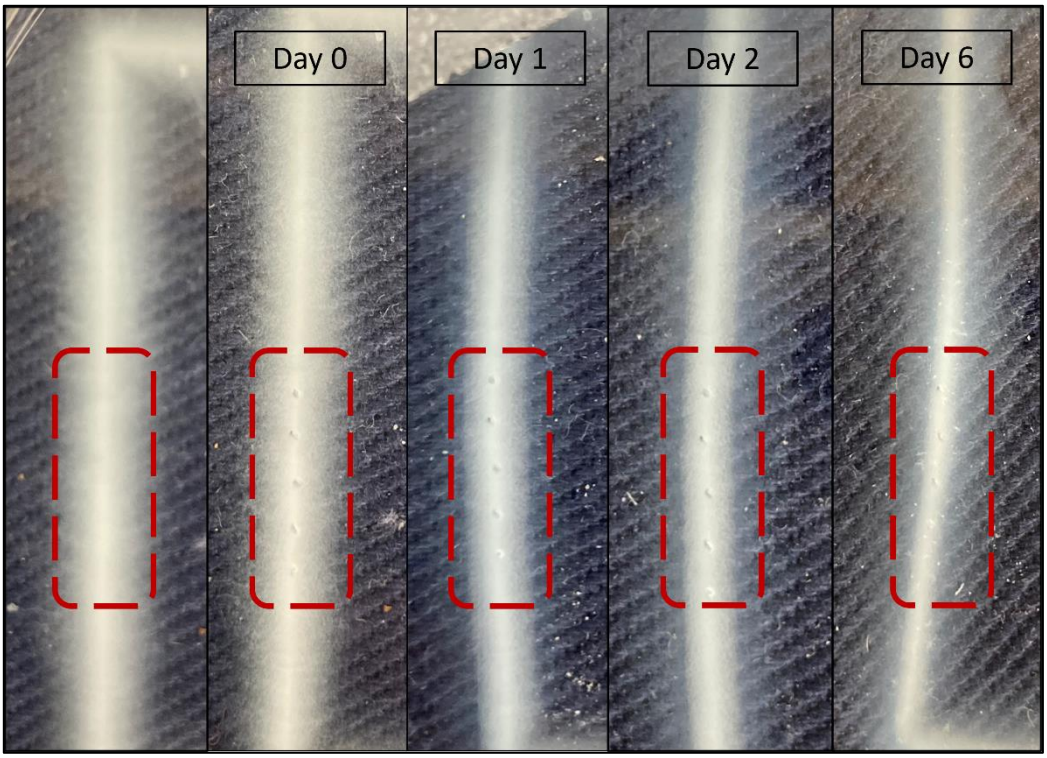

Figure 93. Investigating 3D printed Benzyl glutamine hydrogels self-healing properties by mechanical breakage.

As shown in figure 93, Benzyl glutamine was printed as usual (first image on the left), prior to damaging it with the needle (second image). The scarring produced by the needle was monitored for six days to ensure enough time was provided for the 3D printed scaffold to rebuild its network, which it failed it do. The puncture holes remained throughout the study with no indication of self-healing. This would suggest that the gel assembled rapidly via solvent switching is less dynamic and able to self-heal than the gels formed in previous studies

via a heat-cool cycle. This would be consistent with a more rapid gel assembly process on solvent extrusion, that is less reversible in nature.

Furthermore, we were interested to observe a progression in the stability of the gel in this study. The opacity of the gel slowly decreases with time, and the printed object appears to become narrower, making the original pathway of the ink become the most prominent component of the printed network. This is because this site is the least exposed to the water bath as well as being the most concentrated area of the gel. The surrounding gel is most exposed to the water bath and was roughly produced by the ink spreading outward during the printing process. Over time, we argue that the peripheral gelator is somewhat dissolved into the water bath. Despite losing this opacity and adhesion to the surface, the square shape of the gel was still intact – in fact if anything it had become better defined as the periphery of the printed object had been 'cleaned up'.

5.4.4 3D Printing for Tissue Engineering

3D printing of soft gel materials can promote cell growth, with the biofabricated platform resembling complex hierarchical tissue structure[198]. By providing a familiar environment for cells to thrive and replicate their respective biological environment, such materials can have significant potential applications in stem cell engineering and the creation of shaped synthetic tissues. The morphological and architectural structure of the gels must resemble the tissues for effective cell contact and interactions[199]. The high-water content, biodegradability, and stimuli responsive behaviour of hydrogels make them potentially ideal for tissue engineering. In collaboration with Chayanan Tangsombun within the Smith group, I therefore tested the application of 3D printed Benzyl glutamine for stem cell growth.

With this goal in mind, Benzyl glutamine (0.5% wt/vol glutamine-C12 with one molar equivalent of benzaldehyde) in anhydrous DMSO was extruded into non-adherent-96-wells plate, such that any cell growth could be ascribed to growth in or on the gel, rather than on the wells themselves. The gel solution was pumped into 300 µL autoclaved water through a sterile syringe and needle to form 100 µL hydrogels. The prepared Benzyl glutamine gels were then provided for Chayanan to conduct the cell growth study.

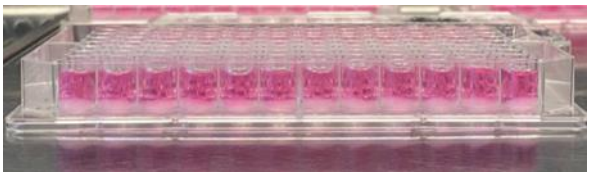

Figure 94. 96-well-plate containing 100 µL 0.5% (wt/vol) Benzyl glutamine in DMEM solution.

To remove any residual DMSO, the gels were washed with autoclaved water three times and left to stand in water overnight. The following day, the gels were washed with DMEM twice to ensure complete DMSO removal. A human mesenchymal stem cell line (Y201)[200] was seeded in each well with the addition of DMEM (10% FBS, 1% P/S). Cell viability was measured at days 0, 3 and 6. The spent medium was removed from each well and replaced with Alamar blue solution (100 µL, 10% in DMEM). The plate was incubated at 37°C for 4 hours. 20 µL aliquots were removed from each well and then transferred to a new 96-well plate containing 180 µL of DMEM (10% FBS, 1% P/S). Fluorescence microscopy was used to detect cell growth.

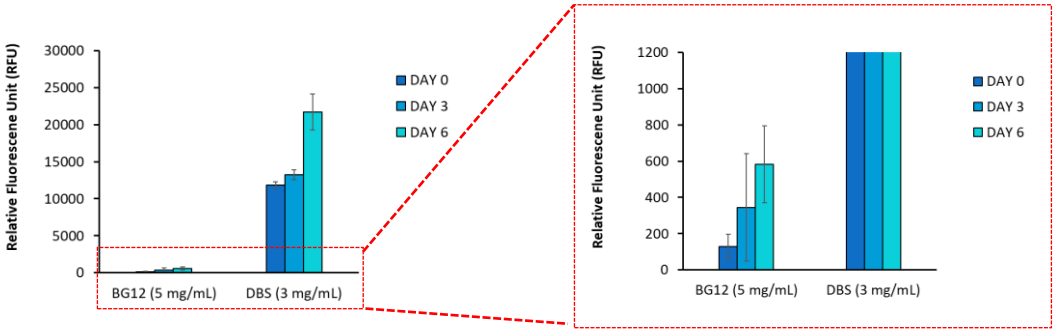

Figure 95. Cell viability of Y201-MSCs cultured onto the surface of DBS-$CONHNH_2$ (0.3% wt/vol) and BG12 (0.5% wt/vol).

As demonstrated in figure 95, the gel failed to provide an environment for cell growth compared to our positive control (DBS-$CONHNH_2$ - triggered via the heat/cool method). There may be two explanations for this lack of effective cell growth. The amino acid-based hydrogel may contain mobile surfactant-like molecules in the 3D network. The glutamine component of our dynamic hydrogel resembles cationic surfactants which are known to induce cell

apoptosis. The cell membrane is composed of two adjacent layers of neutral phospholipids, the phospholipid bilayer. On exposure to the cationic head of the gelator, the acidic phospholipid moves from the inner membrane to the outer membrane. The lipid flip flop leaves the surface of the intact plasma membrane to form a negative charge on the sialic acid residue of glycolipids and glycoproteins. The delocalized charge on the cationic gelator molecule may interact with this residue and as a result cause destabilization or destruction of the mammalian cell membrane[201, 202].

Another theory to the lack of cell viability, would be the presence of benzaldehyde, the other dynamic by-product from the gelator. The reversible nature of the Schiff base permits the release of benzaldehyde. Benzaldehyde and its derivatives are used in everyday products such as perfumes, pharmaceutical drugs, food, etc. They are also naturally formed in dairy products, fruit, coffee, and meat products. Although it is considered safe in low quantities, higher concentrations may lead to cytotoxicity, as benzaldehyde can be absorbed into the cell membrane to react with DNA and enzymes causing oxidative stress[203]. In our study a low percentage was used, but we cannot rule out this problem.

Alternatively, the Benzyl glutamine gel may just not be an effective medium to support stem cell growth or may be toxic in its own right to the growing stem cells. On balance, we reason the most likely explanation would be the surfactant-like nature of the Benzyl glutamine – this would agree with previous studies on nasal epithelial cells that demonstrated some issues with cell compatibility for this gelator[2].

Despite the outcome, 3D printing of LMWG's has exciting potential for tissue engineering. We propose the use of other LMWG's with this technique to print gels with the addition of cell lines to construct a complex self-standing network surrounded by growing cells.

5.5 Multicomponent Gel Tubes

Moving beyond filament spinning based solely on the LMWG, we decided to also make use of a polymer gelator to try and enforce an extended 1-dimensional architecture onto the LMWGs. After the successful formation of the Benzyl glutamine alginate beads described

previously, we reasoned that is should be possible to fabricate a worm shaped hybrid hydrogel using these two different gelators – benzyl glutamate as low-molecular-weight gelator (LMWG) and alginate as the polymer gelator (PG).

We therefore manufactured a hybrid material comprised of the LMWG in fibrillar form, coated with crosslinked alginate in order to form a cylindrical core-shell tube. To achieve this, Benzyl glutamine (0.35% wt/vol with one molar equivalent of benzaldehyde) was added to alginate solution (1.5% wt/vol). The heated mixture was quickly extruded manually through a syringe into a $CaCl_2$ solution (10% wt/vol). The hybrid system was left in the bath for the complete self-assembly of both gelators as shown in Figure 96. It is reasoned that the LMWG assembles on cooling and the PG forms as calcium ions crosslink the alginate polymers. A tubular system could thus be obtained. The thickness of the tubes can be controlled by connecting the syringe to a pump and altering the alginate viscosity, needle size, and jet flow of the ink. As shown in the image on the right of figure 96, Benzyl glutamine (0.35 wt/vol with one molar equivalent of benzaldehyde) was added with 1 mL of 0.1% wt/vol alginate and was heated as with the previous method. The heated solution however, was extruded via a pump at a rate of 33.7 µL /min (needle size of 26G) into a solution of 1.5% wt/vol $CaCl_2$. Leading to the generation of thin tubes of the multicomponent gel system. This process was limited as the strength of the pump was insufficient at preventing the clogging of the gel system at the tip of the needle, and therefore a stronger generating pump would be required. Gel tubes such as this could potentially be used in drug delivery or even tissue engineering.

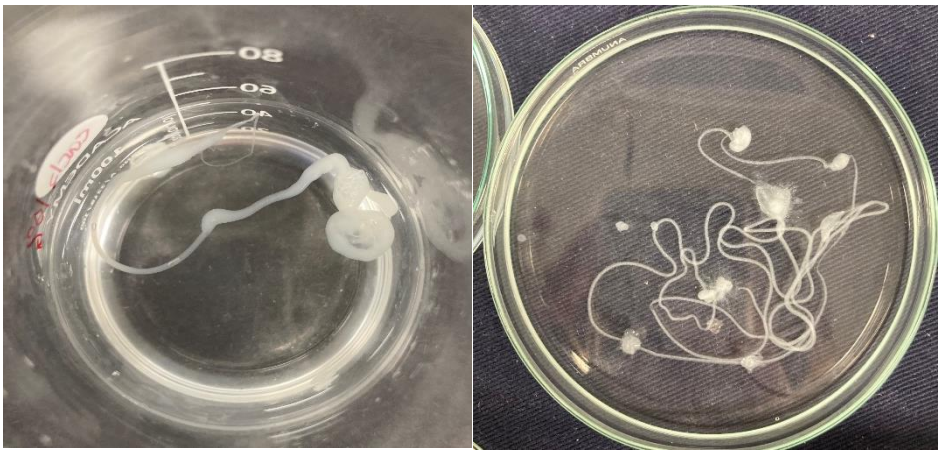

Figure 96. Benzyl glutamine-alginate tubes in $CaCl_2$.

5.4.1 Self-Assembly of the LMWG in the multicomponent Gel

Self-assembly of the gelators within the tubes was confirmed by taking a 1 - 2 cm length of the tube and performing an NMR study in D_2O spiked with an internal standard (DMSO). The ^1H NMR spectrum showed no signals either for the LMWG or the polymer, thus confirming the full self-assembly of both gelators into the solid-like state. Another NMR study was then conducted to quantify the self-assembly of the LMWG in the core-shell gel tubes. The dried Benzyl Glutamine/Alginate core–shell gel tube was dissolved in DMSO-d_6 with an internal standard of acetonitrile. The gel tube was prepared with 1 mL of water using 0.35% wt/vol of the LMWG (1.25×10^{-5} moles) and 1.5% wt/vol alginate solution crosslinked with 10% wt/vol calcium chloride solution. By comparing integrals of acetonitrile and the methyl group of the glutamine amide gelator, we could conclude that 88% of the LMWG was incorporated within the gel tube. This indicates an effective fabrication process with little loss of gelator.

5.4.2 SEM and Optical Microscopy

To further inspect the structure of the tubes, SEM and optical microscopy images were taken of the sample. Optical microscopy images of the cross-section of the tube (figure 97) shows two distinct layers which suggests a core-shell structure for this tube, similar to that of the hybrid beads described previously. SEM images are also similar to the previously fabricated hybrid beads displaying a rough outer surface with layers and fibres tangled in a web-like shape. The images in figure (97 (b and d) display an extended nanofibrillar network suggesting incorporation of both gel systems in the network.

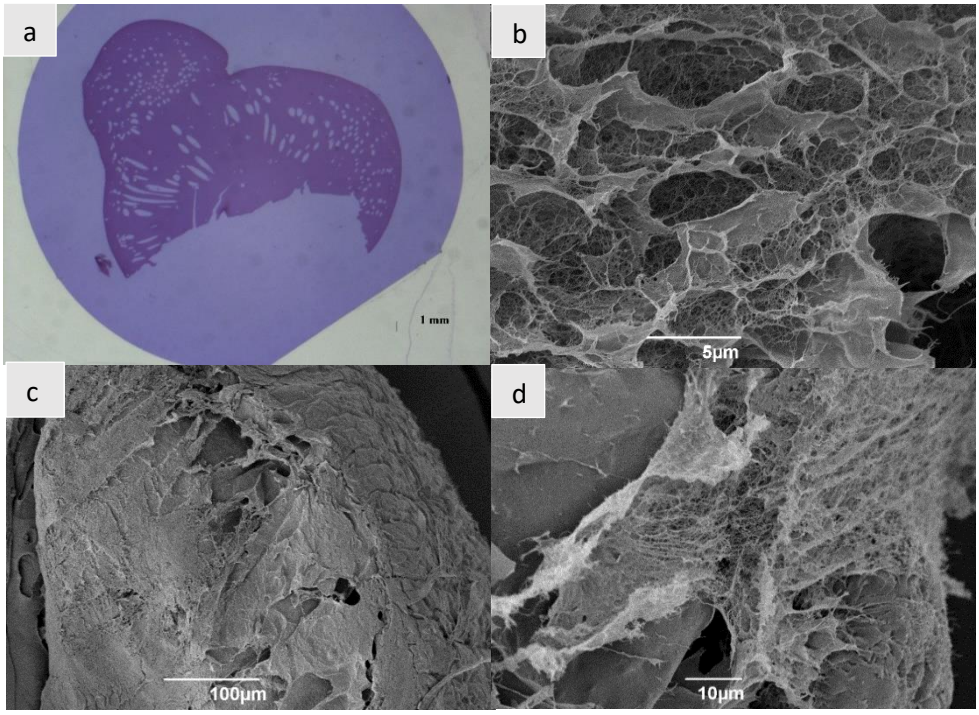

Figure 97. a) Optical microscopy image of the Benzyl glutamine/ Alginate gel tube cross-section embedded in resin and stained with toluidine blue. b and d) SEM images of the inner section of the Benzyl glutamine/Alginate tubes. c) SEM images of the Benzyl glutamine/Alginate tube outer edge.

5.4.3 Reduction of the Imine Functional Group in Benzyl Glutamine

Given that the dynamic nature of the Schiff base linkage may be contributing to the failure of promoting cell growth, reduction of this functional group may offer a way of 'fixing' this dynamic bond, stabilising the gelator within the self-assemble gel fibres, and hence preventing problems associated with surfactant-like behaviour or aldehyde leaching.

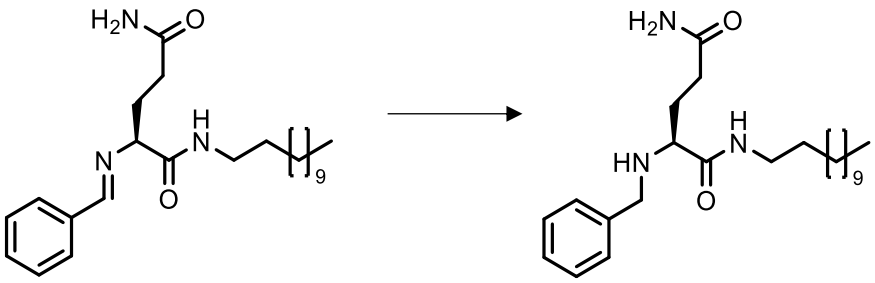

Figure 98. Imine to amine conversion with the addition of sodium borohydride.

Our group has previously reported this reaction, and it is known that the resulting amine is a highly effective hydrogelator[110]. We therefore experimented with an innovative approach which revolves around the use of the calcium alginate polymer to coat the LMWG as the reaction takes place. The beads were prepared as previously described with Benzyl glutamine (0.35% wt/vol glutamine-C12 with one molar equivalent of benzaldehyde) and alginate (1% wt/vol). Once ready, 2 mL of sodium borohydride solution (7 mg/mL) was added to 27 beads. The solution was left overnight to allow diffusion into the multicomponent gel beads. It was reasoned that the sodium borohydride would reduce the imine into a secondary amine while the calcium alginate acted to retain the shape of the gel. ^{1}H NMR spectroscopy was utilised to study this conversion. The beads were removed and dried with a vacuum oven. DMSO-d_6 was added to dissolve the LMWG (Alginate is insoluble in DMSO and will not appear in the spectrum). Methanol (2 µL) was added as internal standard to quantify imine reduction. By comparing the integral peaks of methanol (δ = 4.12 ppm) with the hydrogen on the imine (δ = 8.30 ppm) we can calculate how much imine remained in the hybrid gel beads after the reaction. It was found that 0.52 mg of the imine remained in the 27 hybrid beads. This quantity of beads would be predicted to contain 2.31 mg of the imine considering 98.3% of the added LMWG remains in the hybrid beads via regular preparation (40 beads produced in total). Therefore an 78% conversion was successfully acquired through the described method.

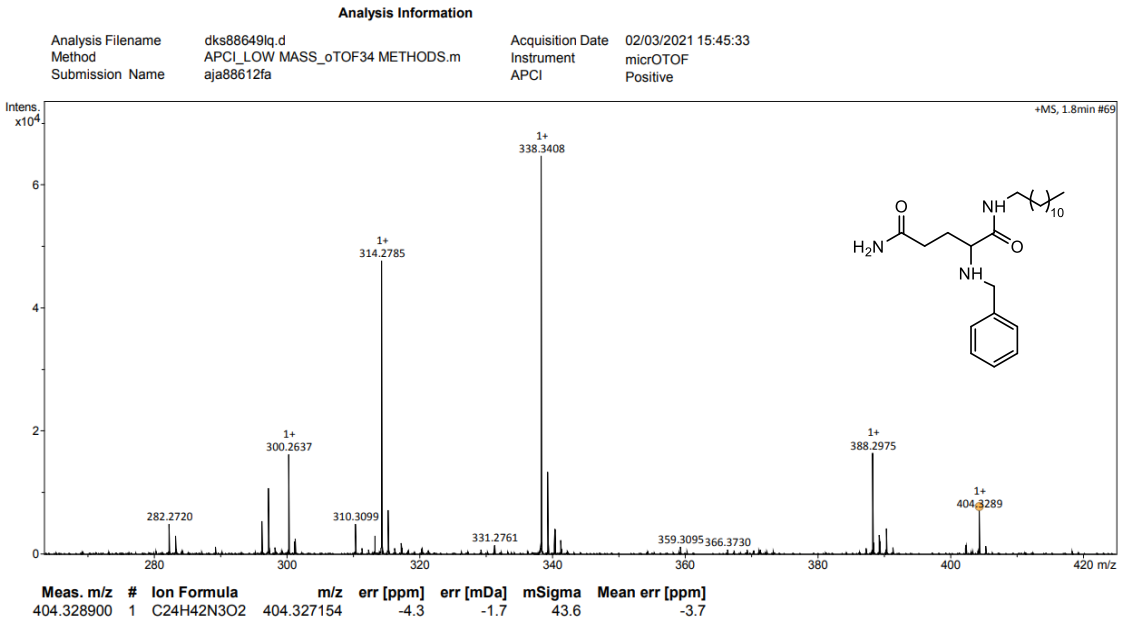

Figure 99. Mass spectrum of the amine formed in the LMWG/PG beads (Exact Mass: 403.32).

Further NMR studies involved the analysis of mobile species in the gel beads. The modified beads were added to D_2O in an NMR tube. DMSO (δ = 2.50 ppm) was added as an internal standard. The spectrum did not possess any mobile molecules indicating no presence of mobile benzaldehyde as would normally be observed in these beads in the absence of reduction. This suggests that reduction has taken place and effectively 'captured' the structure of the two-component system, preventing its dynamic behaviour. It should be noted that there may be small traces of benzaldehyde that do not appear in the spectrum as the previous ^1H NMR study indicated the presence of 22% of the original imine.

Finally, mass spectrometry was also used to prove the formation of the amine during the reaction (figure 99). A peak of the molecule was observed at 404 to the ion [H^+]. This is an exciting result, as it indicates that the LWMG gel system can undergo chemical reactions while it is in the form of a hybrid gel bead. In some ways, the alginate shell can almost be considered as a reaction vessel for this process. The concept of creating hybrid gels and then chemically modifying them is potentially extremely powerful. We hope that in the future, these reduced materials may prove better compatible to (e.g.) cell growth.

5.6 Conclusions and Future Work

Wet-spinning, extruding a concentrated solution of LMWG in a 'good' solvent into a 'bad' solvent, is an exciting new approach for triggering gelation in LWMG's as it offers the opportunity for gels to be self-standing materials without external support. Benzyl glutamine and its derivatives can be activated to form gels with this method. By studying the conditions needed for gelling these molecules, we obtained a better insight into using this technique with supramolecular gels. Using three molecules with different hydrophobic natures highlighted the role of solvent choice for triggering gelation.

DBS-$CONHNH_2$ and Benzyl glutamine were extruded to form drug loaded self-assembling hydrogels. Importantly, we noted that the presence of naproxen significantly changes the nanoscale morphology of the filaments assembled by DBS-$CONHNH_2$ as a result of interactions between the components. The drug release studies suggest a possible future of using LMWG's forming depot injections via phase inversion. Key factors to facilitate such a low release system with our LMWG's are drug-gel interactions as well as water insolubility of the drug (e.g propranolol's faster release into the water phase compared to the slower release of the less soluble naproxen).

We described the optimum conditions needed for 3D printing of these gelators. DBS-COOH and Benzyl glutamine were printed in various conditions to help us understand the role each factor has on the produced print. The main factors that dictated the condition of the print were needle gauze size, rate of extrusion, concentration of gelator, and distance between the platform and needle tip. Insolubility in water is an important characteristic of DBS-COOH, which provided the gelator with greater stability and well-defined prints compared to the more soluble Benzyl glutamine. Benzyl glutamine was further explored by using the printed gels as a tissue engineering platform. The gel did not support cell growth which we believe is due to the chemical nature of the gelator rather than the printing method used – however, this would need testing by ensuring that cell growth can still take place on 3D printed DBS-$CONHNH_2$.

We considered that forming a permanent bond between the glutamine amide and benzaldehyde, rather than a reversible Schiff base linkage may ultimately offer greater cell compatibility. This was achieved, in a preliminary experiment, by reducing the gelator *in situ* within a multicomponent hydrogel comprised of both the gelator and calcium alginate (to retain its structural integrity). Evidence indicated good conversion of the Schiff base to the reduced amine form. Future work would involve testing the toxicity of this reduced multicomponent system towards cells, and then using it for cell culture and other applications.

6.0 Conclusions

The work presented in this thesis begins with the novel amino acid based hydrogel Benzyl glutamine. The first chapter focuses on gel design and discovery, in which the gelator is structurally altered by changing components of the gel system (the amino acid, and the length of the alkyl chain). It was found that key components for gelation of this system are the amine groups on the amino acid portion of the structure and an alkyl chain of no less than 11 carbons. Going below the 12 carbon chain diminished properties of the gel (rheological and thermal properties). While going above to 14 carbons kept the gels properties. We established a stronger understanding of the importance of each component involved in gelation and are interested in the effects of increasing the length of the chain beyond 14 carbons for future work.

In the following chapters, Benzyl glutamine was investigated in its use as a delivery platform for the drugs naproxen, rosuvastatin, dexamethasone, and atropine. The study involved using different approaches to loading the drugs and using analytical techniques (NMR and FT-IR) to find any interactions between the drugs and the Benzyl glutamine gel. In-vitro drug release studies were conducted with the use of UV-Vis to describe the kinetics of release. The study led to the conclusion that the gel is most suitable with drugs of low molecular weight and have high water solubility. Atropine provided great compatibility with the gel system, we therefore suggest its use in the ocular treatment of Myopia.

Benzyl glutamine was combined with alginic acid and agarose respectively to form multicomponent gel beads. The beads were characterised by rheology, thermal stability

studies, and microscopy. The new fabrications provided new gel systems with enhanced rheological performance. Levodopa and propranolol were used to investigate and compare the performance of the drug delivery systems - Benzyl glutamine, DBS-COOH, DBS-$CONHNH_2$ and their respective multicomponent gel beads. The comparative study suggests several involvement of the drugs with the gel systems which provided different release profiles. Future work can involve the use of these systems for the treatment of HI and Parkinson's.

And finally, a new approach of forming thin filaments with rheologically weak LMWG's was investigated. The technique uses a solvent switch method to develop these constructs. We explored forming thin filaments with Benzyl glutamine (BG-C12) and the newly discovered gelators (BG-C11) and (BG-C14). The study focused on the different variables that need to be controlled for a successful formation of filaments. It was found that BG-C12 was the most stable, however was not capable of forming thin filaments. This is believed to be due to the gels slow acting gelation and its water solubility. Nonetheless, Benzyl glutamine and DBS-$CONHNH_2$ were investigated for their use as bulk depot delivery systems respectively. The design involves injecting the gel/drug mixture into the body where a solvent switch can initiate gelation and thus form a bulk gel acting as a depot system. In-vitro release studies indicated that the two gel systems provided controlled release of naproxen.

Benzyl glutamine and DBS-COOH were 3D printed via solvent switch to form various shapes on a platform. The study described the optimum conditions (needle gauze size, rate of extrusion, concentration of gelator, and distance between the platform and needle tip) needed for 3D printing of these gelators. DBS-COOH provided more defined prints compared to Benzyl glutamine, which is believed to be due to DBS-COOH's insolubility in water. 3D printed Benzyl glutamine was later used as a tissue engineering platform. Unfortunately, the gel was incapable of supporting cell growth which may be due to the chemical nature of the gel. And finally, to eliminate the potential toxicity associated with benzaldehyde freely flowing in the gel system. We designed an in-situ reaction within the multicomponent Benzyl glutamine/Alginate beads to remove the reversible Schiff base and form an amine. The reaction was proven successful with a good conversion within the gel beads. Future work may involve investigating the toxicity of the new gel system.

7.0 General Experimental Methods

All compounds required for synthesis and analysis were purchased from standard chemical suppliers and used without further purification. ^{1}H and ^{13}C NMR were recorded on a Jeol 400 spectrometer (1H 400 MHz, 13C 100 MHz). Coupling constants (J) are recorded in Hz. Mass spectrometry was performed by the University of York Mass Spectrometry Service. FT-IR were recorded on a ThermoNicolet Avatar 370 FT-IR spectrometer and data was analysed with Spectrus processor (ACD/ Labs) software. All rheological measurements were carried out using a Malvern Instruments Kinexus Pro+ rheometer with data analysed with the software MestReNova. T_{gel} values were recorded using a high precision thermoregulated oil bath. UV-vis absorbance was measured on a Shimadzu UV-2401 PC spectrophotometer. TEM images were taken on a FEI Technai 12 G2. SEM images were taken on either a JEOL JSM-7600f field emission SEM, or a JEOL JSM-6490LV by Karen Hodgkinson. Compounds DBS-$CONHNH_2$ and DBS-COOH were synthesized and purified by Liansong Yang and Anna Rodrigo.

7.1 Synthesis of Glutamine Amide Derivatives

7.1.1 Synthesis of Glutamine-C12

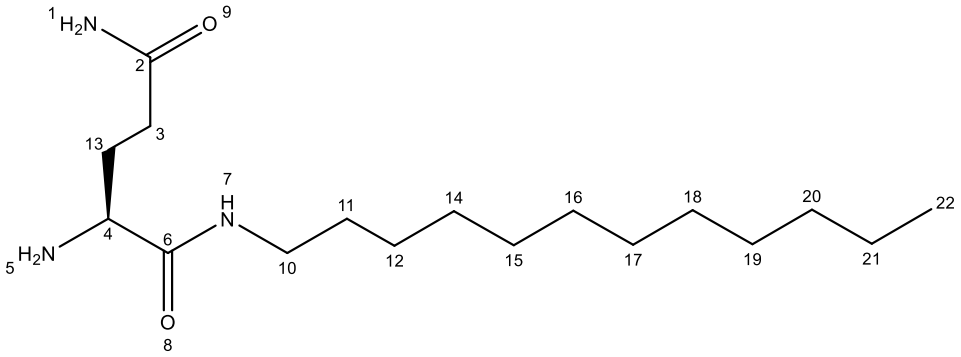

Figure 100. Structure of glutamine-C12.

Boc protected glutamine (482 mg, 1.97 mmol) was coupled with dodecylamine (362 mg, 1.96 mmol) with 4-dimethylaminopyridine (239 mg, 1.96mmol) and 1-ethyl-3-(3-dimethylaminopropyl)carbodiimide (660 mg, 3.87 mmol) in dichloromethane (50 mL). The

reaction was stirred in an ice bath for two hours and then overnight. A workup was performed with 1 M HCl (40 mL), deionised water (40 mL), 1 M NaOH (40 mL), and brine (40 mL). The Boc protecting group of the molecule was removed through the addition of 4 M HCl in dioxane (6 mL). The acidic solution was removed via vacuum. Deprotonation was performed by the addition of sodium hydroxide (40 mL) in the presence of dichloromethane (40 mL) via a separatory technique. The organic media was collected and evaporated to dryness to give the target compound as a white powder with a yield of 69%. **^{1}H NMR (400 MHz, DMSO-*D*$_6$):** δ 7.78 (s, H7, 1H), 7.24 (s, H1, 2H), 6.69 (s, H5, 2H), 3.33 (s, H4, 1H), 3.06 (m, H3, 2H), 2.08 (m, H13, 2H), 1.77 (m, H10, 2H), 1.53 (m, H11, 1H), 1.38-1.22 (m, H12-21, 18H), 0.84 (t, H22, *J* = 7.5 Hz, 3H). **^{13}C NMR (100.53 MHz, DMSO-d$_6$) δ ppm:** 175.25 (H_2N-C=O), 174.76 (NH-C=O), 54.99 (C-4), 54.99 (C-10), 38.79 (C-3), 32.27 (C-13), 31.84 (C-11), 31.69 (C12-C20), 29.72 (C12-C20), 29.60 (C12-C20), 29.56 (C12-C20), 29.31 (C12-C20), 29.26 (C12-C20), 22.64 (C-21), 14.50 (C-22). **IR ν_{max} (cm^{-1}):** 473 w, 485 w, 494 w, 531 w, 557 w, 618 m, 666 m, 720 m, 772 w, 811 w, 865 w, 875 w, 906 w, 1104 w, 1118 w, 1153 w, 1163 w, 1190 w, 1207 w, 1227 w, 1237 w, 1276 m, 1314 w, 1327 w, 1339 w, 1372 m, 1413 m, 1428 m, 1469 m, 1525 s, 1646 vs, 2850 s, 2872 w, 2917 s, 2956 w, 3194 w, 3300 m, 3358 w, 3399 m. **ESI-MS (m/z)** calc. $C_{17}H_{35}N_3NaO_2$ 336.2617, found 336.2621 (100% $[M+Na]^+$) and calc. $C_{17}H_{35}KN_3O_2$ 352.2366 found 352.2361 (8% $[M+K]^+$).

7.1.2 Synthesis of Glutamine-C14

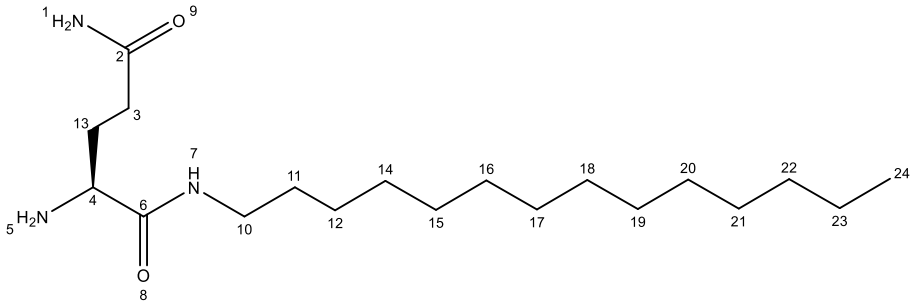

Figure 101. Structure of glutamine-C14.

Boc protected glutamine (482 mg, 1.96 mmol) was coupled with tetradecylamine (418 mg, 1.96 mmol) with 4-dimethylaminopyridine (239 mg, 1.96mmol) and 1-ethyl-3-(3-dimethylaminopropyl)carbodiimide (660 mg, 3.87 mmol) in dichloromethane (50 mL). The reaction was stirred in an ice bath for two hours and then overnight. A workup was performed with 1 M HCl (40 mL), deionised water (40 mL), 1 M NaOH (40 mL), and brine (40 mL). The Boc protecting group of the molecule was removed through the addition of 4 M HCl in dioxane (6 mL). The acidic solution was removed via vacuum. Deprotonation was performed by the addition of sodium hydroxide (40 mL) in the presence of dichloromethane (40 mL) via a separatory technique. The organic media was collected and evaporated to dryness to give the target compound as a white powder in a yield of 55%. **^{1}H NMR (400 MHz, DMSO-d_6) δ:** 7.72 (t, H7, *J* = 5.6 Hz, 1H), 7.20 (s, H1, 2H), 6.75 (s, H5, 2H), 3.80 (m, H4, 1H), 3.03 (m, H3, 2H), 2.06 (m, H13, 2H), 1.78 (m, H10, 2H), 1.39-1.21 (m, H11-23, 24H), 0.86 (t, H24, 3H). **^{13}C NMR (100.53 MHz, DMSO-d_6) δ ppm:** 174.89 (H_2N-C=O), 174.13 (NH-C=O), 54.53 (C-4), 54.53 (C-10) 38.36 (C-3), 31.75 (C-13), 31.31 (C-11), 31.19 (C12-C22), 29.22 (C12-C22), 28.75(C12-C22), 26.43 (C12-C22), 22.13 (C23), 14.04 (C-24). **IR ν_{max} (cm^{-1}):** 1644*vs*, 2917*vs*, 2850 s, 1522s, 622 s, 720 s, 1431m,1421 m, 1469 m, 3386 m, 3302 m, 1370 m, 667 m, 3194 m, 1294 m, 2873 m, 1342 w, 788 w, 1327 w, 2956 w, 1277 w, 1267 w, 810 w, 850 w, 866 w, 578 w, 1131 w, 471 w, 3364 w, 1153 w, 1190 w, 556 w, 1147 w, 1245 w, 1220 w, 1232 w, 532 w, 1104 w, 490 w. **ESI-MS (m/z)** calc. $C_{19}H_{40}N_3O_2$ 342.3115, found 342.3116 (9% $[M+H]^+$), and calc. $C_{19}H_{39}N_3NaO_2$ 364.2934, found 364.2943 (100% $[M+Na]^+$), and calc. $C_{19}H_{39}KN_3O_2$ 380.2674 found 380.2669 (13% $[M+K]^+$).

7.1.3 Synthesis of Glutamine-C11

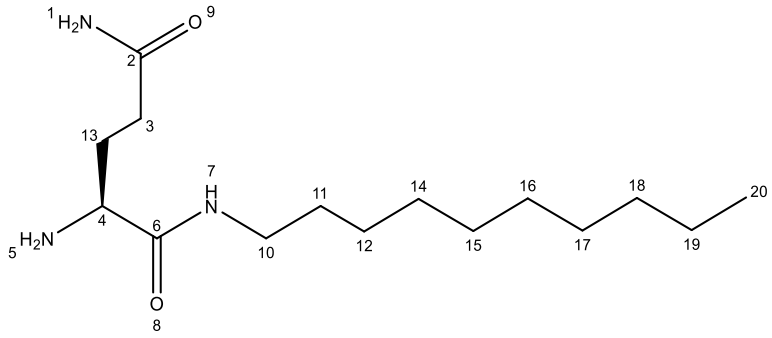

Figure 102. Structure of glutamine-C11.

Boc-Glutamine (482 mg, 1.96 mmol) was dissolved in dichloromethane (50 mL) with 1-ethyl-3-(3-dimethylaminopropyl)carbodiimide (660 mg, 3.87 mmol), 4-dimethylaminopyridine (239 mg, 1.96 mmol) and undecylamine (0.4 mL, 1.72 mmol) were added. The mixture was stirred for 2 hours at 0°C in an ice bath, followed by 12 hours stirring at room temperature. A workup was performed on the molecule with 1 M HCl (40 mL), deionised water (40 mL), 1 M NaOH (40 mL), and brine (40 mL). The Boc protecting group of the molecule was removed through the addition of 6 mL of 4 M HCl in dioxane. The acidic solution was removed via vacuum. Deprotonation of the molecule was performed by the addition of 40 mL sodium hydroxide in the presence of 40 mL dichloromethane via a separatory technique. The molecule in the organic media was collected and was dried to give a white powder of yield 53.6 %. **^{1}H NMR (400 MHz, DMSO-d_6) δ**: 7.80 (t, H7, 1H), 7.24 (s, H5, 2H), 6.69 (s, H1, 2H), 3.04 (m, H4, 1H), 3.04 (m,H10,Hz, 2H), 2.10 (m, H3, 2H), 1.68 (m, H13, 3H), 1.55 (m, H11, 1H), 1.40-1.24 (m, H12-20, 16H), 0.85 (t, H21, *J* = 6.66 Hz, 3H). **^{13}C NMR (100.53 MHz, DMSO-d_6) δ ppm:** 174.74 (H2N-C=O), 174.26 (NH-C=O), 54.47 (C-4), 54.47 (C-10), 38.28 (C-3), 31.76 (C-13), 31.34 (C-11) (C18-C9), 31.19 (C18-C9), 29.22 (C18-C9), 29.00 (C18-C9), 28.76 (C18-C9), 26.43 (C18-C9), 22.13 (C-19), 13.99 (C-20). **IR ν_{max} (cm^{-1}):** 3398 m, 3358 w, 3297 m, 3194 m, 2956 w, 2917 s, 2872 w, 2850 s, 1646 vs, 1624 s, 1525 s, 1467 m, 1429 m, 1412 m, 1372 m, 1365 m, 1338 m, 1327 m, 1314 w, 1279 m, 1273 m, 1245 w, 1233 w, 1224 w, 1212 w, 1200 w, 1191 w, 1164 w, 1153 m, 1118 w, 1105 w, 1045 vw, 987 vw, 963 w,930 w, 916 w, 903 w, 891 w, 874 m, 850 w, 786 m, 735 m, 721 m, 667 m, 617 s, 558 m, 530 m, 481 m, 465 m. **ESI-MS (m/z)** calc. $C_{16}H_{34}N_3O_2$ 300.2646, found 300.2646 (4% $[M+H]^+$), calc. $C_{16}H_{33}N_3NaO_2$ 322.2465, found 322.467 (100 % $[M+Na]^+$), and calc. $C_{16}H_{33}KN_3O_2$ 338.2204 found 338.2205 (8 % $[M+K]^+$).

7.1.4 Synthesis of Glutamine-C10

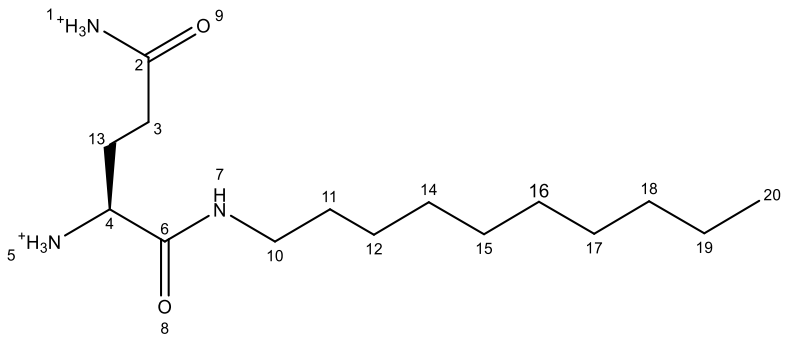

Figure 103. Structure of glutamine-C10.

Boc protected glutamine (482 mg, 1.96 mmol) was coupled with decylamine (0.39 mL, 1.95 mmol) with the addition of coupling agents 4-dimethylaminopyridine and (239 mg, 1.96 mmol) and 1-ethyl-3-(3-dimethylaminopropyl)carbodiimide (660 mg, 3.87 mmol) in dichloromethane (50 mL). The reaction was stirred in an ice bath for two hours and then overnight. A workup was performed with 1 M HCl (40 mL), deionised water (40 mL), 1 M NaOH (40 mL), and brine (40 mL). The Boc protecting group of the molecule was removed through the addition of 6 mL of 4 M HCl in dioxane. The acidic solution was removed via vacuum. Producing a white powder with a yield of 20%. **^{1}H NMR (400 MHz, DMSO-d_6) δ:** 8.57 (t, H7, *J* = 5.30 Hz, 1H), 8.31 (d, H5, *J* = 6.06 Hz, 2H), 7.50 (s, H1, 3H), 6.93 (s, H1, 1H), 3.75 (m, H4, 1H), 3.75 (m, H10, 2H), 3.13-3.07 (m, H3, 2H), 2.16 (m ,H13, 2H), 1.93 (m, H11,2H), 1.43-1.23 (m, H12-19, 14H), 0.85 (t, H20, *J* = 5.7 Hz, 3H).

Deprotonation of the molecule was performed by the addition of 40 mL sodium hydroxide in the presence of 40 mL dichloromethane via a separatory technique. The molecule in the organic media were collected and was dried to give a white powder· **^{1}H NMR (400 MHz, DMSO-d_6) δ:** 7.82 (s, H7, 1H), 7.26 (s, H5, 2H), 6.70 (s, H1, 3H), 3.03 (m, H4, 1H), 3.03 (m, H10, 2H), 2.06 (m, H3, 2H), 1.73 (m ,H13, 2H), 1.53 (m, H11,2H), 1.34-1.23 (m, H12-19, 14H), 0.85 (t, H20, *J* = 7.0 Hz, 3H). **ESI-MS (m/z)** calc. $C_{15}H_{32}N_3O_2$ 286.2489, found 286.2486 (50% $[M+H]^+$), calc. $C_{15}H_{31}N_3NaO_2$ 308.2308, found 308.2306 (100 % $[M+Na]^+$), and calc. $C_{15}H_{31}KN_3O_2$ 324.2048 found 324.2046 (15 % $[M+K]^+$).

7.1.5 Synthesis of Alanine-C12

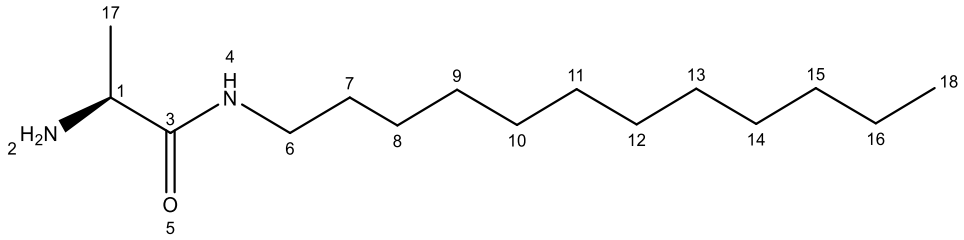

Figure 104. Structure of alanine-C12.

Boc-Alanine (373 mg, 1.97 mmol) was dissolved in dichloromethane (50 mL) with 1-ethyl-3-(3-dimethylaminopropyl)carbodiimide (660 mg, 3.87 mmol), 4-dimethylaminopyridine (239 mg, 1.96 mmol) and dodecylamine (362 mg, 1.95 mmol) were added. The mixture was stirred for 2 hours at 0°C in an ice bath, followed by 12 hours stirring at room temperature. A workup with 1 M HCl (40 mL), water (40 mL), 1 M NaOH (40 mL), and brine (40 mL). The product was dried with magnesium sulphate and dried in vacuum. The Boc group was deprotected with 4 M HCl (6 mL) in dioxane > 2 hrs. The acidic medium was removed by vacuum. Deprotonation of the molecule was achieved by the addition of NaOH (40 mL), and the molecule was obtained by the collection of the organic layer (dichloromethane) from a separatory apparatus. The product was dried in vacuum to give a yield of 48%. **^{1}H NMR (400 MHz, DMSO-d_6) δ:** 7.72 (s, H4, 1H), 3.30 (s, H2, 2H), 3.19 (q, H1, *J* = 4.6 Hz , 1H), 3.02 (q, H6, *J* = 6.01 Hz, 2H), 1.74 (s H7, 2H), 1.37-1.24 (m, H8-16, , 18H), 1.08 (d, H17, *J* = 3.8, Hz, 3H), 0.85 (t, 18H, *J* = 6.8 Hz, 3H). **^{13}C NMR (100.53 MHz, DMSO-d_6) δ ppm:** 175.55 (C-3), 50.30 (C-1), 38.20 (C-6), 31.31 (C-17), 29.10 (C-7), 29.01 (C15-C8), 28.76 (C15-C8), 26.36 (C15-C8), 22.10 (C15-C8), 21.81 (C-16), 13.96 (C-18). **IR ν_{max} (cm^{-1}):** 3382 w, 3342 w, 3282 m, 2958 m, 2918 vs, 2871 m, 2851 s, 1641 vs, 1606 m, 1531 vs, 1468 m, 1379 w, 1368 w, 1320 m, 1288 w, 1265 w, 1234 w, 1221 m, 1179 w, 1158 w, 1132 m, 1087 w, 1064 vw, 1043 vw, 1022 vw, 937 w, 898 w, 868 m, 781 w, 722 s, 644 w, 541 w, 500 vw. **ESI-MS (m/z)** calc. $C_{15}H_{33}N_2O$ 257.2587, found 257.2590 (70% $[M+H]^+$), and calc. $C_{15}H_{32}N_2NaO$ 279.2407, found 279.2407 (100 % $[M+Na]^+$).

7.1.6 Synthesis of Proline-C12

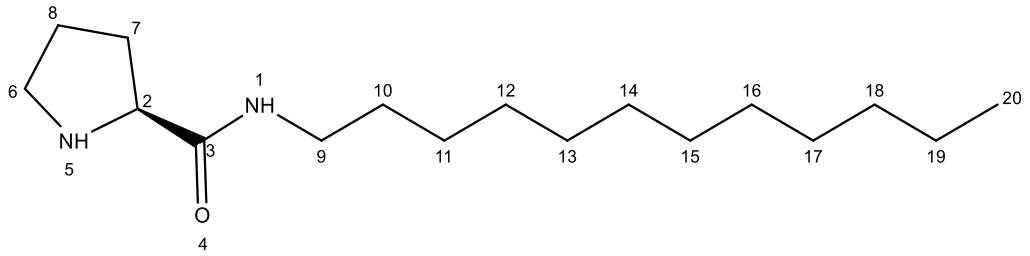

Figure 105. Structure of proline-C12.

D-Proline (421.24 mg, 1.96 mmol) was dissolved in DCM (50 mL) with 1-ethyl-3-(3-dimethylaminopropyl)carbodiimide (660 mg, 3.87 mmol), 4-dimethylaminopyridine (239 mg, 1.96 mmol) and dodecylamine (362 mg, 1.95 mmol) were added. The mixture was stirred for 2 hours at 0°C in an ice bath, followed by 12 hours stirring at room temperature. The molecule was washed with 1 M HCl (40 mL), water (40 mL), 1 M NaOH (40 mL), and brine (40 mL). The product was dried with magnesium sulphate and vacuum dried. Once cooled down a yellow oil was produced. Ethyl acetate (10mL) was added to the oil and placed under vacuum. A white solid product was yielded 65%. **^{1}H NMR (400 MHz, DMSO-d_6) δ:** 7.80-7.71 (t, H1, *J* = 6.1 Hz, 1H), 4.00 (q, H5, *J* = 3.1 Hz, 1H), 3.35 (m, H2, , 1H), 3.01 (m, H9, 2H), 3.01 (m, H6, , 2H) 2.04 (m, H10, 2H), 1.74 (m, H7, 2H), 1.74 (m, H8, *J* = 4.3 Hz, 2H), 1.38 – 1.22 (m, H11-19, 18H), 0.85 (t, 20H, *J* = 5.9 Hz, 3H). **^{13}C NMR (100.53 MHz, DMSO-d_6) δ ppm:** 174.13 (C-3), 60.27 (C-2), 46.73 (C-6), 38.07 (C-9), 29.05 (C-7), 31.32 (C18-C10), 30.55 (C18-C10), 29.22 (C18-C10), 29.04 (C18-C10), 28.72 (C18-C10), 25.81 (C-8), 22.12 (C-19), 13.97 (C-20). **IR vmax (cm^{-1}):** 3300 m, 2958 m, 2918 vs, 2872 m, 2850 s, 1665 m, 1632 vs, 1552 s, 1523 s, 1470 s, 1433 w, 1376 w, 1311 w, 1290 w, 1265 w, 1250 w, 1242 w, 1206 w, 1179 w, 1159 w, 1132 w, 1102 m, 1095 m, 1066 w, 1046 w, 1034 w, 1021 w, 974 vw, 949 w, 927 w, 910 w, 889 m, 871 w, 719 m, 664 m, 596 w, 549 w, 514 vw, 500 vw, 487 vw, 474 vw, 465 vw. **ESI-MS (m/z)** calc. $C_{17}H_{35}N_2O$ 283.2744, found 283.2745 (100% $[M+H]^+$), and calc. $C_{17}H_{34}N_2NaO$ 305.2563, found 305.2563 (6 % $[M+Na]^+$).

7.1.7 Synthesis of Asparagine-C12

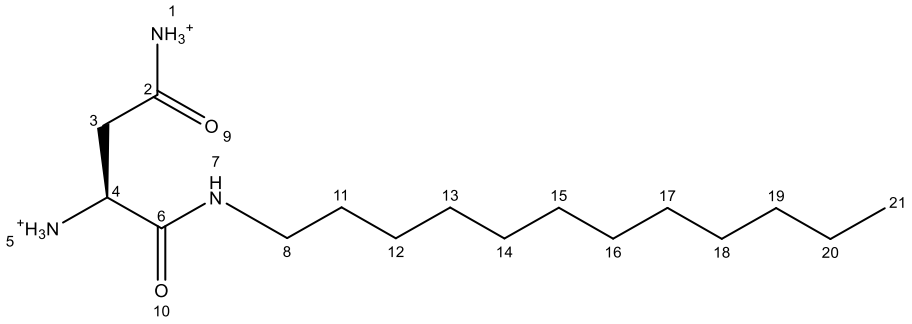

Figure 106. Structure of asparagine-C12.

Deodyclamine (362 mg, 1.95 mmol) and Boc-Asparagine (465 mg, 2.00 mmol) were coupled in dichloromethane (50 mL) in the presence of 4-dimethylaminopyridine (239 mg, 1.95 mmol) and 1-ethyl-3-(3-dimethylaminopropyl)carbodiimide (660 mg, 3.87 mmol). A workup was performed with 1 M HCl (40 mL), water (40 mL), 1 M NaOH (40 mL), and brine (40 mL). The product was dried with magnesium sulphate and dried in vacuum. Column chromatography was performed to remove further impurities associated. The Boc group was deprotected with 6 mL of 4M HCl in dioxane. The solution was left >2 hrs and the acidic medium was dried via vacuum. The produced yield is 44%. **^{1}H NMR (400 MHz, DMSO-*d*$_6$) δ** 8.45 (s H7, 1H), 8.18 (s, H5, 2H), 7.80 (s H1, 2H), 7.22 (s, H1, 2H), 3.90 (t, H4, *J* = 2.0 Hz, 1H), , 3.08 (m, H3, 2H), 2.63 (m, H11, 2H), 1.39-1.23 (m, H12-20, 18H), 0.86 (t, H21, *J* = 2.2 Hz, 3H).

Deprotonation of the molecule was performed by the addition of sodium hydroxide (40 mL) in the presence of dichloromethane (40 mL) via a separatory technique. The organic media were collected and evaporated to dryness to give the target compound as a white powder. **^{1}H NMR (400 MHz, DMSO-*d*$_6$) δ** 7.88 (s, H7, 1H), 7.41 (s, H5, 2H), 6.87 (s, H1, 2H), 3.03 (m, H4, 1H), (dd, H3,J= 10.3 Hz, 2H), 2.19-2.11 (m, H11, 2H), 1.37-1.23 (m, H12-20, 18H), 0.85 (t, H21, *J* = 6.36 Hz 3H). **^{13}C NMR (100.53 MHz, DMSO-d$_6$) δ ppm:** 170.80 (H2N-C=O), 167.91 (NH-C=O), 49.46 (C-4), 49.46 (C-8), 35.24 (C-3), 31.10 (C11 -C19), 28.82 (C11 -C19), 28.56 (C11 -C19), 26.08 (C11 -C19), 21.91(C20), 13.77 (C-21). **IR ν_{max} (cm^{-1}):** 3323 m, 3226 m, 3070 m, 2954 m, 2920 s, 2873 m, 2851 s, 2727 w, 1671 vs, 1643 m, 1619 m, 1554 m, 1519 w, 1494 s, 1476 s, 1469 s, 1432 m, 1405 m, 1397 m, 1378 m, 1339 w, 1290 w, 1278 w, 1259 m, 1239 m, 1215 m, 1159 w, 1138 w, 1114 w, 720 m, 632 m, 612 m, 583 m, 567 m, 547 w, 459 m. **ESI-MS (m/z)** calc. $C_{16}H_{34}N_3O_2$ 300.2646, found 300.2655 (100% $[M+H]^+$), calc. $C_{16}H_{33}N_3NaO_2$

322.2465, found 322.2469 (12% $[M+Na]^+$), and calc. $C_{16}H_{33}KN_3O_2$ 338.2204, found 338.2213 (12% $[M+K]^+$).

7.1.14 NMR Studies to Quantify the Free-flowing Benzaldehyde in the Self-assembling Networks of BG-C11 and BG-C14

NMR study of BG-C11:

Glutamine-C11 (1 mg) and benzaldehyde (0.5 µL) were added to D_2O (0.7 mL) with DMSO (2 µL) as an internal standard. The hot mixture was poured into an NMR tube and left undisturbed for self-assembly to occur. The DMSO resonance (δ = 2.70 ppm) was compared to the carboxyl group of benzaldehyde (δ = 9.92 ppm) in the ^{1}H NMR spectrum.

To begin, the number of moles of the internal standard, DMSO, needs to be calculated:

The mass of DMSO is determined by m=p **×** V = (1.1 g/mL) × (2×10^{-3} mL)

$m = 2.2\times10^{-3}$ g

Moles of DMSO used = Mass/Molar Mass = (2.22×10^{-3} g)/ (78.13 $g.mol^{-1}$)

$n = 2.82\times10^{-5}$ mol

Moles for 1 H = 2.82×10^{-5} moles

Moles of mobile aldehyde detected by NMR:

The integral of DMSO is multiplied by 6

Integral for mobile aldehyde = 0.09

Therefore, moles of mobile aldehyde = moles of internal standard × integral of mobile aldehyde

n = (2.82×10^{-5} mol) × 0.09 = 2.5×10^{-6} moles

2.5×10^{-6} moles of mobile benzaldehyde are free in 0.7 mL D_2O

From the moles of mobile aldehyde, the concentration of free aldehyde can be calculated:

Concentration = Moles of mobile aldehyde × Molar mass of benzaldehyde

C = (2.5×10^{-6} mol) × (106.12 $g.mol^{-1}$) = 2.69×10^{-4} g in 0.7 mL

(2.69×10^{-4} g)/0.7 mL = 3.84×10^{-4} g/mL

Conc. = 0.384 g/L

To calculate the % of mobile aldehyde:

Concentration of Aldehyde added:

Mass= Density × Volume

M= (1.044 g/mL) × (5×10^{-4} mL) = 5.22×10^{-4} g in 0.7 mL

= (5.22×10^{-4} g)/ (0.7 mL) = 0.745 g/L

Percentage of mobile aldehyde = (0.384 g/L)/ (0.745 g/L) × 100= 51.6%

From these calculations we can conclude that 48.3% of benzaldehyde is involved in forming the Schiff base in the solid-like network, while the remaining 51.6% is freely flowing in the gel network.

NMR study of BG-C14:

Glutamine-C14 (3 mg) and benzaldehyde (1.13 µL) was added to D_2O (1.0 mL) with DMSO (2 µL) as an internal standard. The hot mixture was poured into an NMR tube and left undisturbed for self-assembly to occur. The peak of DMSO (δ = 2.70 ppm) is compared to the carboxyl group of benzaldehyde (δ = 9.92 ppm) obtained from the ^{1}H NMR spectrum. The integration of DMSO was set at 6 (6H) and the integral of benzaldehyde was 0.14 and the same calculations were performed to quantity the free-flowing aldehyde in BG-C14. BG-C14 has 35.5% benzaldehyde freely flowing in the network and 64.5% integrated into the network.

7.1.15 Rheological Studies on BG-C11 and BG-C14

All studies were carried out using parallel plate rheology at 25 °C. For amplitude sweeps, the frequency was kept constant at 1 Hz. As for each frequency sweep, the shear strain was kept constant at a value determined by the amplitude sweep for that hydrogel.

BG-C11:

Glutamine-C11 (1.5 mg) was dissolved in 1 mL water (acidified with HCl (pH 3-4)) with 0.5 µL benzaldehyde by heating the solution and pipetting into a bottomless vial attached to the

rheometer plate to allow gel formation. The gel was left for 3 hours to fully form, once ready the vial was removed an amplitude and frequency sweep was conducted. The experiment was performed in duplicate.

BG-C14:

Glutamine-C14 (3 mg) was dissolved in 1 mL water with 1.13 µL benzaldehyde by heating the solution and pipetting into a bottomless vial attached to the rheometer plate to allow gel formation. The gel was left for 3 hours to fully form, once ready the vial was removed and an amplitude and frequency sweep conducted. The experiment was performed in duplicate.

7.1.16 Thixotropic Study of BG-C11 and BG-C14

BG-C11: Glutamine-C11 (1.5 mg) was dissolved in 1 mL water (acidified with HCl (pH 3-4)) with 0.5 µL benzaldehyde by heating the solution and pipetting into a bottomless vial attached the rheometer plate to allow gel formation. The gel was left for 3 hours to fully form, once ready the vial was removed.

BG-C14: Glutamine-C14 (3 mg) was dissolved in 1 mL water with 1.13 µL benzaldehyde by heating the solution and pipetting into a bottomless vial attached the rheometer plate to allow gel formation. The gel was left for 3 hours to fully form, once ready the vial was removed.

For both gel systems a thixotropic creep recovery test was conducted at 25°C. A shear force of 0.0126% at a frequency of 2 Hz was applied. After 30 seconds, the frequency was increased to 100 Hz for 30 seconds (breaking the gel). The frequency was then lowered back to 2 Hz and the recovery was monitored over time. The experiments were performed in duplicate.

7.1.17 pH Screen of BG-C11, BG-C14, and Glutamine-C14

BG-C11: Glutamine-C11 (1.5 mg) and Benzaldehyde (0.5 µL) were placed in glass vials with 1 mL water. Each vial was exposed to sonication and heat until complete dissolution and were left overnight. The experiment was performed in triplicate.

Glutamine-C14: Glutamine-C14 (6 mg) is added to water 0.2 mL. The mixture is sonicated and heated until dissolution. The vials were left overnight.

BG-C14: Glutamine-C14 (3 mg) and 1.13 µL benzaldehyde are added to 1 mL water. The mixture is sonicated and heated until dissolution. The gels were left to form overnight. The experiment was performed in duplicate.

The pH of the solvent for all gel systems was varied by adjusting the pH of water with either NaOH and HCl and was recorded with a pH probe. The tube inversion test was performed after 24 hrs.

7.1.18 Thermal Stability Studies of BG-C11

The gels were prepared with glutamine-C11 (3 mg) with various volumes of aldehydes and water. All vials were sonicated for 10 seconds and heated by a heat gun until dissolution. The samples were allowed to cool down until the formation of the gel occurred. After 24 hours, the gels were placed into the automated oil bath (Huber Ministat 230) with a starting temperature of 19.8°C (Rate 1°C/min). The gels were inverted vertically with each temperature increase. Once the gel no longer held its shape the temperature was recorded. The experiment was performed in triplicate.

7.1.19 Thermal Stability Studies of BG-C12

The gel samples were prepared with glutamine-C12 (3.5 mg) with benzaldehyde (1.13 µL) in 1 mL water. The samples were sonicated for 10 seconds and heated by a heat gun and were allowed to cool down until the formation of the gel occurred. After 24 hours, the gels were placed into the automated oil bath (Huber Ministat 230) with a starting temperature of 19.8 (Rate 1°C/30 seconds). The gels were inverted vertically with each temperature increase.

Once the gel no longer held its shape the temperature was recorded. The experiment was performed in triplet.

7.1.20 Thermal Stability Studies of BG-C14

The gels were prepared with glutamine-C14 (3 mg) with various volumes of aldehydes and 1 mL of water. All vials were heated by a heat gun and were allowed to cool down until the formation of the gel occurred. After 24 hours, the gels were placed into the automated oil bath (Huber Ministat 230) with a starting temperature of 19.8°C (Rate 1°C/30 seconds). With every increase of temperature by 1 degree Celsius, the gels were inverted vertically. Once the gel no longer held its shape the temperature was recorded. The experiment was performed in triplicate.

7.1.21 Thermal Stability Studies of Aspragine-C12

The gels were prepared by using 0.3 mL of alkaline deionized water (prepared by the addition of NaOH to deionized water to adjust a pH of 13) as the solvent and variable concentrations of the gelator inside a small glass vial. The gels were all activated by the use of heat and were allowed to cool down until the formation of the gel occurred. All the gels were placed into the automated oil bath (Huber Ministat 230) with a starting temperature of 19.8°C (Rate 1°C/min). With every increase of temperature by 1°C, the gels were inverted vertically. Once the gel no longer held its shape, the temperature was recorded.

7.1.22 SEM and TEM of BG-C11, BG-C14, and Asparagine-C12

<u>Gel Preparation</u>

BG-C11: Glutamine-C11 (3 mg) was dissolved with benzaldehyde (0.8 µL) in 2 mL water by heating until dissolution. The sample was left overnight in a glass vial.

BG-C14: Glutamine-C14 (3 mg) was dissolved with benzaldehyde (1.13 µL) in 1 mL by heating until dissolution. The sample was left overnight in a glass vial.

Asparagine-C12: Asparagine-C12 (3 mg) was dissolved in 0.3 mL of water in a glass vial. The mixture was heated until dissolution with a heat gun and was left overnight to fully self-assemble.

SEM

Samples of BG-C11 and BG-C14 (10 µL of each gel (200 µM), in H_2O) were respectively spread using a mounted needle on a thin piece of copper shim (to act as support); excess liquid was removed with filter paper. The gel was frozen on the copper support by submersion in nitrogen slush (ca. -210°C); after this water was removed from the gel by lyophilising on a Peltier stage, with a maximum temperature of -50°C. Once dry, the gel was knocked off the shim with a mounted needle, and the shim was mounted on an SEM stub using a carbon sticky tab. The sample was then sputter-coated with a thin layer (< 12 nm) of gold/palladium coating to prevent sample charging, before SEM imaging.

TEM

Each gel sample (BG-C11, BG-C14, and asparagine-C12) was prepared with 10 µL of each gel (200 µM), in H_2O, that were placed on a copper grid (standard) with Formvar and carbon support film and allowed to set for 5 minutes. A stain (1% uranyl acetate) was applied to the grid while wet (1% in water, pH 4.5) to allow the stain to run across the grid, then most of it was wiped off with a filter paper. The grid was left to rest for 20 minutes before taking the images.

7.2 Benzyl Glutamine as a Drug Delivery Platform

7.2.1 NPX Sodium Drug Loading and Release Studies with BG-C12 Hydrogel

Drug Loading

Diffusion method: A solution of BG-C12 (0.35% wt/vol with one molar equivalent of benzaldehyde) in 1 mL distilled water was prepared in a glass vial (4 mL). The vials were sonicated and heated with a heat gun until dissolution. The samples were left to cool for >12

hours. Once a gel had formed, 1 mL of naproxen sodium solution (0.2 mg/mL) was added to the vial and the vial was placed in an incubator (37°C) to increase the rate of diffusion. After >12 hours the solution was removed.

Pre-gelation method: BG-C12 (0.35% wt/vol) was added to 1.13 µL Benzaldehyde and NPX solution (1 mg naproxen + 33.3 µL 1 M NaOH + 0.966 mL water) solvent in a glass vial (4 mL). The vials were sonicated and heated until dissolution. The samples were then left to cool for >12 hours and tested for gelation.

Drug Release:

Tris buffer (4 mL) was added on top of each gel. The vial was placed in an incubator at 37°C. 2 mL aliquots were taken each hour, and UV-Visible spectra recorded before the aliquot was returned to the top of the gel. Each experiment was performed in triplicate. A control was set up in which the gel was not loaded with naproxen solution. The drug release was normalised with reference to the UV-Vis spectrum of the control gel.

7.2.2 FT-IR Studies of NPX Loaded Gels

Pre-gelation method - BG-C12 (0.35% wt/vol with one molar equivalent of benzaldehyde) was prepared as previously described with/without 3 mg naproxen and 100 µL NaOH in a total volume of 1 mL of water. The gels were dried in a vacuum oven to form xerogels. The naproxen-loaded xerogel, control xerogel, and naproxen dry powder were all analysed by infrared spectroscopy (Figure 107).

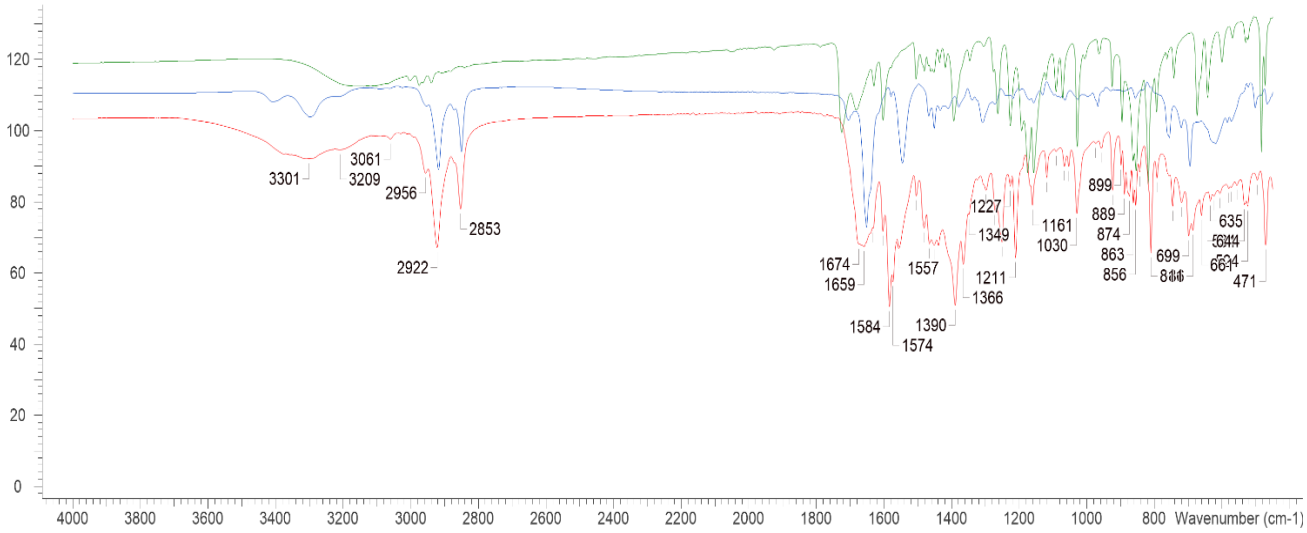

Figure 107. Comparison of IR spectra of BG-C12 xerogel (blue), NPX-loaded BG-C12 (using the pre-gelation method) xerogel (red), and NPX dry powder (green).

7.2.3 Gel Bead Preparation

Glutamine-C12 (3.5 mg) and benzaldehyde (1.13 µL) were dissolved in 1 mL alginate (1% wt/vol) by heating until dissolution. The solution was pipetted (25 µL) into a 40 mL calcium chloride bath (5% wt/vol) in which calcium cross linking occurred to form droplet shaped hybrid gel beads (diameter of 3 mm). The beads were left for 15 minutes for complete cross-linking and washed with water to remove any excess calcium chloride solution.

7.2.4 Quantification of LMWG Self-assembly in Multicomponent (BG-C12/Alginate) Gel Beads

10 beads were dried in a vacuum oven and were dissolved in 0.7 mL DMSO-d_6. The solution was sonicated to ensure that the LMWG fully dissolved. A spike of acetonitrile (2 µL) was added to quantify the concentration of Benzyl glutamine in the hybrid bead. By comparing the integrals of acetonitrile (δ = 2.07 ppm) and the terminal methyl group of the LMWG (δ = 0.71 ppm) this value can be obtained.

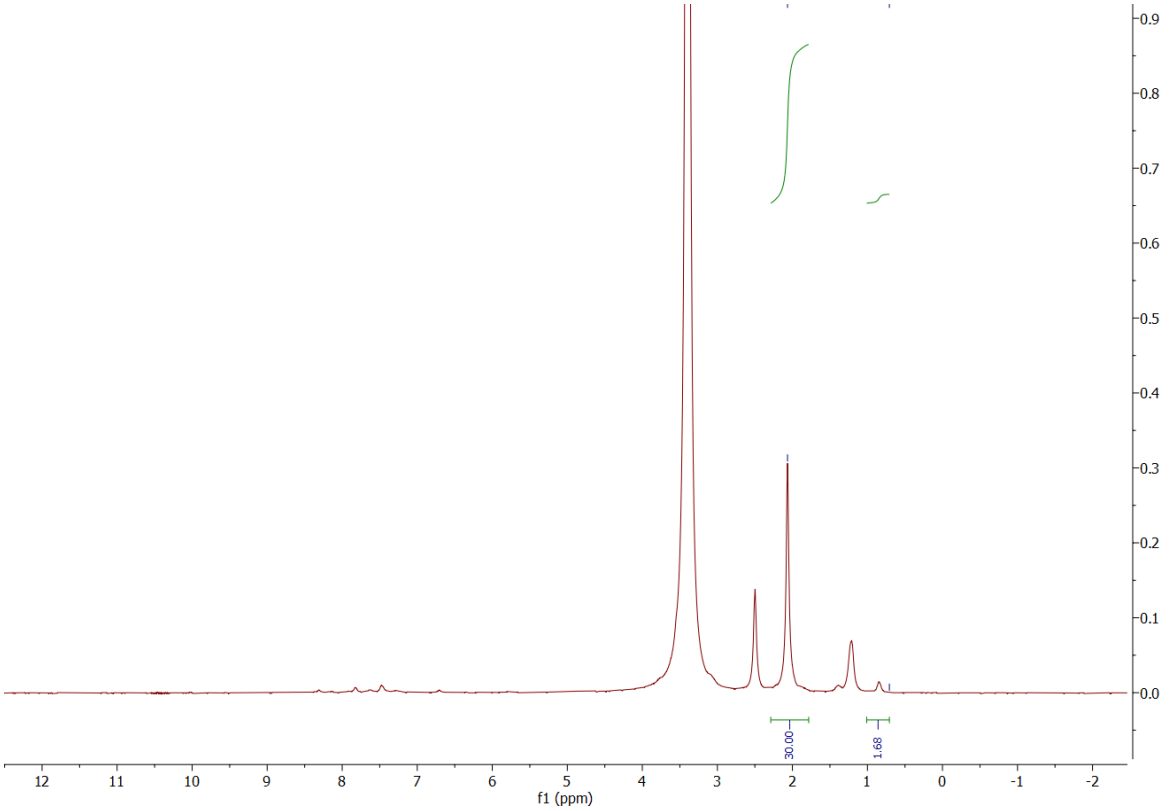

Figure 108. ^{1}H NMR of BG/Alginate dried beads in DMSO-d_6 with an internal standard of acetonitrile to quantify the LMWG concentration in the hybrid beads.

7.2.5 Infrared (IR) Spectroscopy of BG-C12/Alginate Beads

Gels were prepared as previously described and dried under vacuum to form xerogels. The IR spectra of the resulting powders were recorded in the range of 450 – 4000 cm^{-1}.

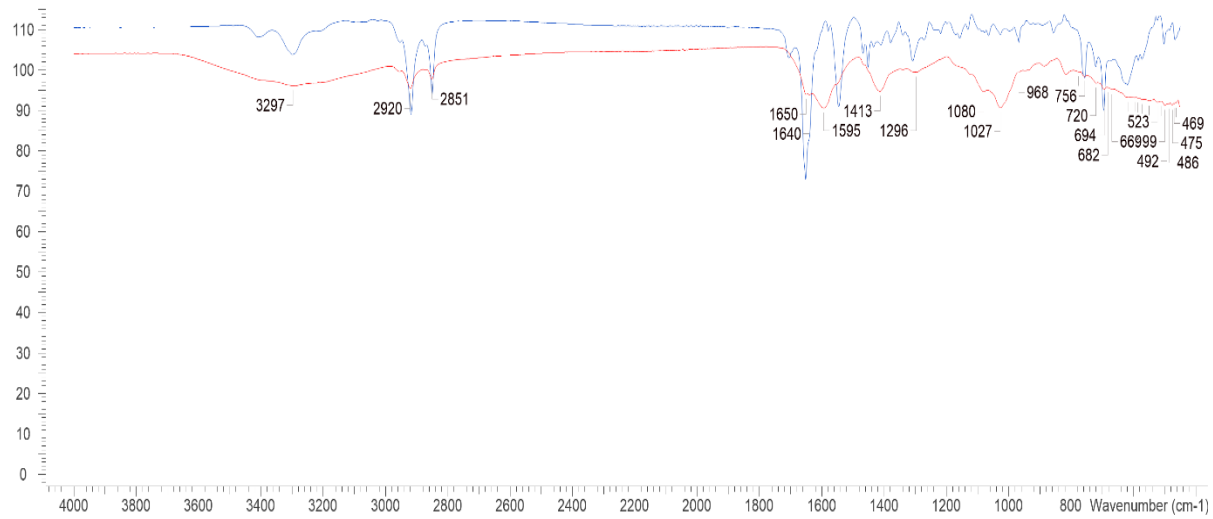

Figure 109. IR spectra comparison of BG-C12/Alginate gel bead xerogel (Red) with BG-C12 xerogel (Blue).

7.2.6 Microscopy imaging of BG-C12/Alginate Beads

Optical Microscopy

The beads were prepared and dehydrated through an ethanol series then embedded in LR white resin. Sections (0.5 µm) were taken and dried on a microscope slide then stained with Toluidine Blue (0.6% with 0.3% Na_2CO_3).

Scanning Electron Microscopy (SEM)

The gel beads were transferred to a piece of copper shim, then freeze-dried and mounted on a stub. The beads were critical point dried (acetone and liquid CO_2) and mounted on stubs either whole or halved using a razor blade. The mounted sample was sputter-coated with Au/Pd prior to analysis.

7.2.7 Rheological Studies of BG-C12/Alginate Beads

All studies were carried out using parallel plate rheology at 25 °C. For amplitude sweeps, the frequency was kept constant at 1 Hz. As for each frequency sweep, the shear strain was kept constant at a value determined by the amplitude sweep for that hydrogel.

Hybrid gels were prepared in bottomless vials for ease of transfer to the rheometer plate. Amplitude sweep experiments were conducted to determine the linear viscoelastic region. Experiments were performed in triplicate or quadruplicate and average data presented.

7.2.8 Thermal Stability Studies of BG-C12/Alginate Beads

The gels were prepared in vials and placed in a thermoregulated oil bath. The temperature was increased by 1°C per minute. Gel thermal stability was then tested using the tube

inversion method. The T_{gel} value was recorded as the point at which the gel could no longer fully support its own weight.

7.2.9 Drug Loading of Rosuvastatin into BG-C12 Hydrogels (Vials)

BG-C12 samples (0.35% wt/vol with one molar equivalent benzaldehyde) were prepared in 1 mL of water with various quantities of rosuvastatin via a heat/cool cycle. The hot solution was left to cool overnight to permit gelation to take place. Physical observations and the tube inversion test were performed to determine the presence of a gel.

7.2.10 Drug Loading of Dexamethasone Sodium into BG-C12 Hydrogels (vials)

BG-C12 samples (0.35% wt/vol with one molar equivalent of benzaldehyde) were prepared in 1 mL of dexamethasone sodium solution (0.3 mg/mL). The solutions were sonicated and heated with a heat gun until dissolution. The vials were then left overnight for complete self-assembly.

7.2.11 Quantifying Drug Loading of Rosuvastatin in BG-C12 Hydrogels (Vial)

BG-C12 hydrogel (0.35% wt/vol with one molar equivalent of benzaldehyde) was prepared in 1 mL water via sonication and the heat/cool cycle. The gel was left to form overnight. A solution of 1 mL of rosuvastatin calcium (1 mg/mL) was added onto the top surface of the hydrogel. The drug solution was left on the gel overnight in an incubator at 37°C to facilitate diffusion. The following day the drug solution was removed and dried in vacuum. The residue was redissolved in D_2O (1 mL) and 4 µL DMSO added as an internal standard. ^1H NMR was then used to quantify the remaining drug concentration in the supernatant. By quantitative analysis, the integrals of DMSO (δ = 2.7 ppm) and the alkene group of rosuvastatin (δ = 5.53 - 5.85 ppm) as shown in Figure 110. By subtracting the concentration of the drug in the supernatant from the total drug concentration originally added to the gel, the drug loading of

the gel was determined to be 65% of the total drug concentration. The experiment was performed in triplicate.

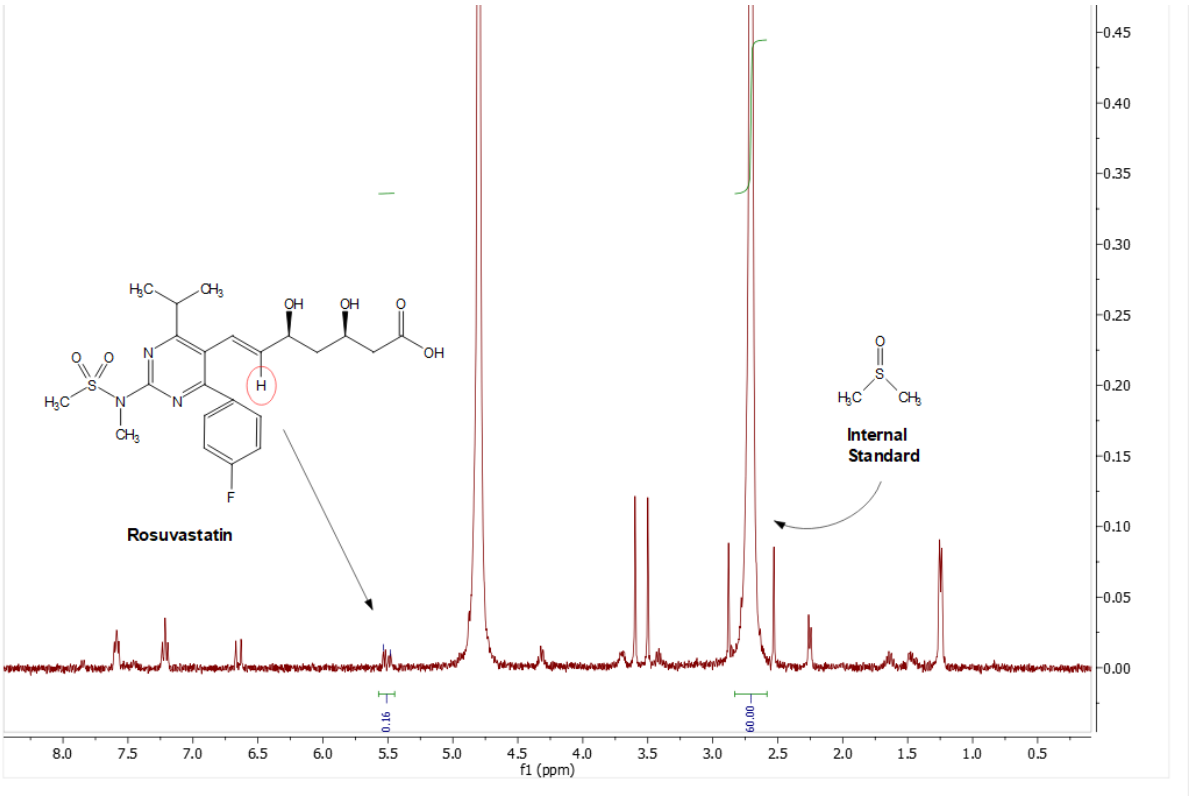

Figure 110. ^{1}H NMR spectra for quantitative analysis of rosuvastatin drug loading in BG-C12 hydrogels.

7.2.12 Quantifying Drug Loading of Rosuvastatin in BG-C12/Alginate Beads

Gel beads were prepared as previously described. The beads (20 beads per vial) were submerged in 1 mL rosuvastatin calcium solution (1 mg/mL) overnight in an incubator at 37°C The following day, the drug solution was removed and dried in vacuum. It was then redissolved in D_2O (1 mL) and 4 µL DMSO added as an internal standard. ^{1}H NMR was used to quantify the concentration of drug remaining in the supernatant. By quantitative analysis, the integrals of DMSO (δ = 2.7 ppm) and the alkene group of rosuvastatin group (δ = 5.53-5.85 ppm) as shown in Figure 111. By subtracting the concentration of the drug in the supernatant from the total drug concentration originally added to the gel, the drug loading can be

determined. The concentration in the diluent was 0.35 mg/mL and therefore 65% of the drug diffused into the gel. The experiment was performed in triplicate.

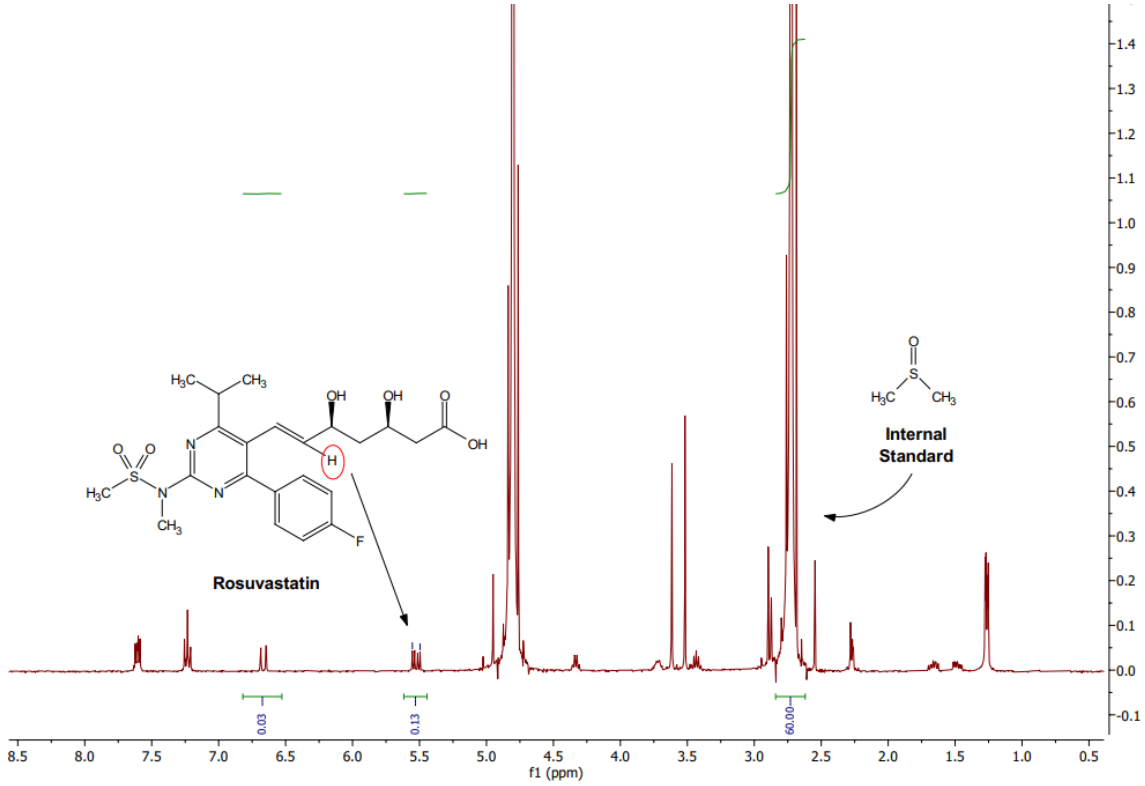

Figure 111. ^{1}H NMR spectra for quantitative analysis of rosuvastatin drug loading in BG-C12/Alginate beads.

7.2.13 Drug Release Studies of Rosuvastatin

Studies were conducted with gels in vials or hybrid gel beads prepared as previously described. For gels in vials and gel beads (20 per vial), 1 mL of rosuvastatin calcium solution (1 mg/mL) was added to each of the gels and the gels were incubated at 37°C overnight. The following day the solution was removed, and 4 mL tris buffer was added to the gel samples. The samples were then placed back into the incubator and each hour 2 mL aliquots were removed and tested by UV-Vis at the wavelength 224 nm. Once the value had been determined, the 2 mL aliquots were returned to the gel. The experiment was performed in duplicate.

7.2.14 FT-IR of Rosuvastatin Loaded Gels

A BG-C12 hydrogel (0.35% wt/vol) was prepared in 1 mL water via a heat/cool cycle. The gel was left to form overnight. A solution of 1 mL of rosuvastatin calcium (1 mg/mL) was added onto the top surface of the hydrogel in the glass vial. The drug solution was left overnight in an incubator at 37°C to facilitate diffusion. The following day the drug solution is removed and dried via vacuum. The spectrum was compared to BG-C12 xerogels that are not loaded with rosuvastatin calcium and rosuvastatin dry powder.

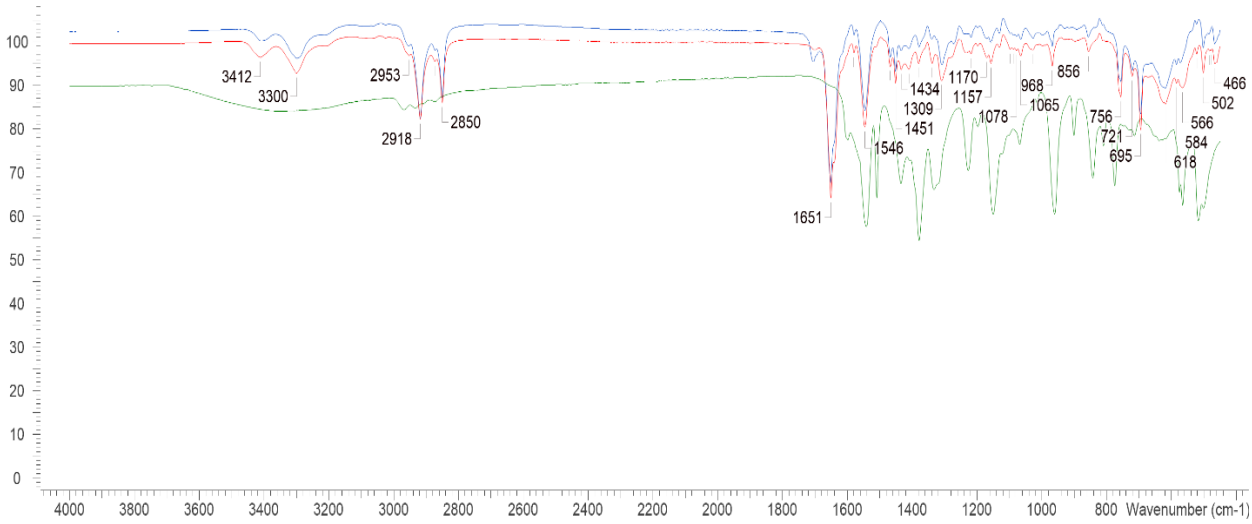

Figure 112. FT-IR spectra comparison of BG-C12 xerogel loaded with rosuvastatin calcium (red), BG-C12 xerogel control (blue), and rosuvastatin dry powder (green).

7.2.15 Drug Loading of BG-C12 with Atropine

In glass vials, glutamine-C12 (3.5 mg) and benzaldehyde (1.13 µL) were dissolved with various concentrations of atropine sulfate in 1 mL water. The solution was sonicated, heated until dissolution, and left overnight for complete self-assembly. The experiment was performed in duplicate.

7.2.16 Quantifying the Concentration of Mobile Atropine in a BG-C12 Gel

Glutamine-C12 (3.5 mg) with benzaldehyde (1.13 µL) and atropine sulfate (1 mg) were dissolved in D_2O (1 mL). 3.1 mg of sodium trimethylsilylpropanesulfonate (DSS) was added as an internal standard. The hot solution was added to an NMR tube which was left overnight for gel formation. Once fully formed, the gel was ready for ^1H NMR spectroscopic analysis. The integrated peak of DSS (δ = 0.00 ppm) was compared to the aromatic group of atropine sulfate (δ = 7.40 ppm) as shown in Figure 123. The integral was set at 90 (representing the 9H (DSS molecule) multiplied by 10). Calculations indicate that 100% of atropine is immobilised in the solid-like network.

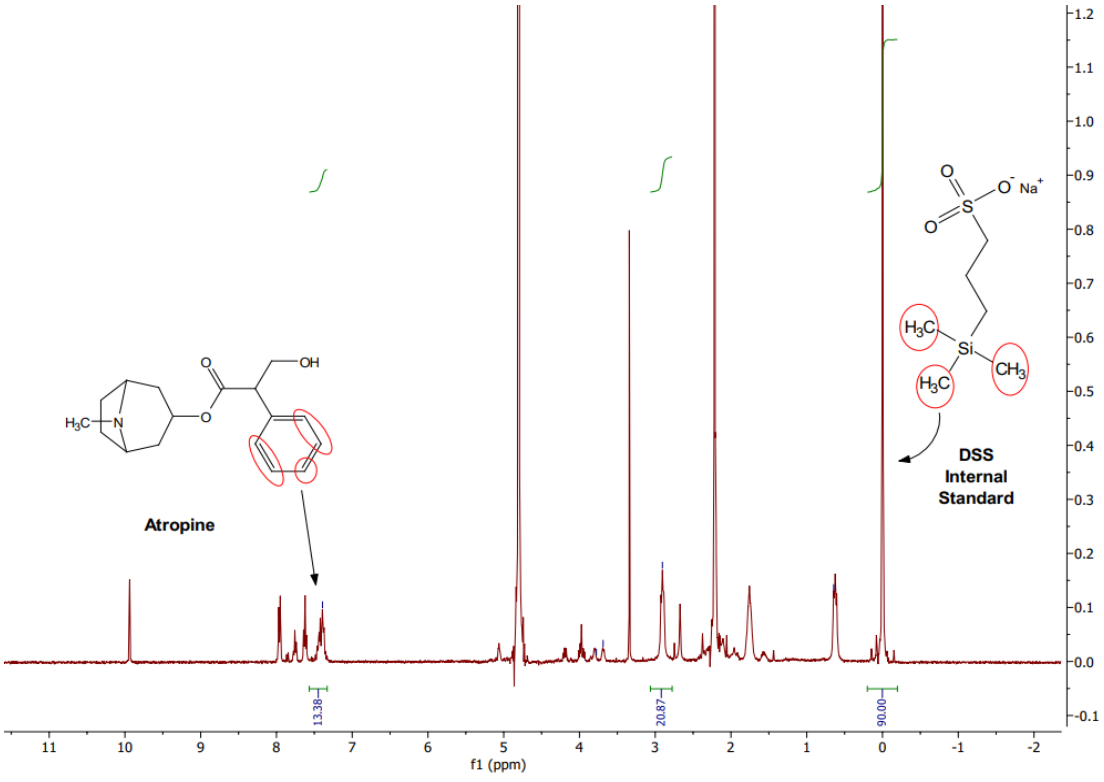

Figure 113. ^1H NMR spectrum of atropine loaded BG-C12 made in D_2O with DSS as an internal standard.

7.2.17 Drug Release Studies of Atropine

Glutamine-C12 (3.5 mg) with benzaldehyde (1.13 µL) and atropine sulfate (1 mg) were dissolved in D_2O. The vial was left undisturbed overnight for gel assembly. Once fully formed, 2 mL of D_2O was added on top of the gel. The gel was incubated at 37°C and samples (0.6 mL) were removed at hourly intervals and were replaced with fresh D_2O solvent (sink conditions). An internal standard, DSS, was added (0.1 mL of 10 mg/mL) to each removed sample (0.6 mL) before analysis. By comparing the integrated peaks of DSS (δ = 0.00 ppm) with the benzene ring of atropine (δ = 7.40 ppm), the drug released per hour could be calculated. The experiment was repeated in triplicate.

7.2.18 FT-IR of Atropine Loaded Hydrogels

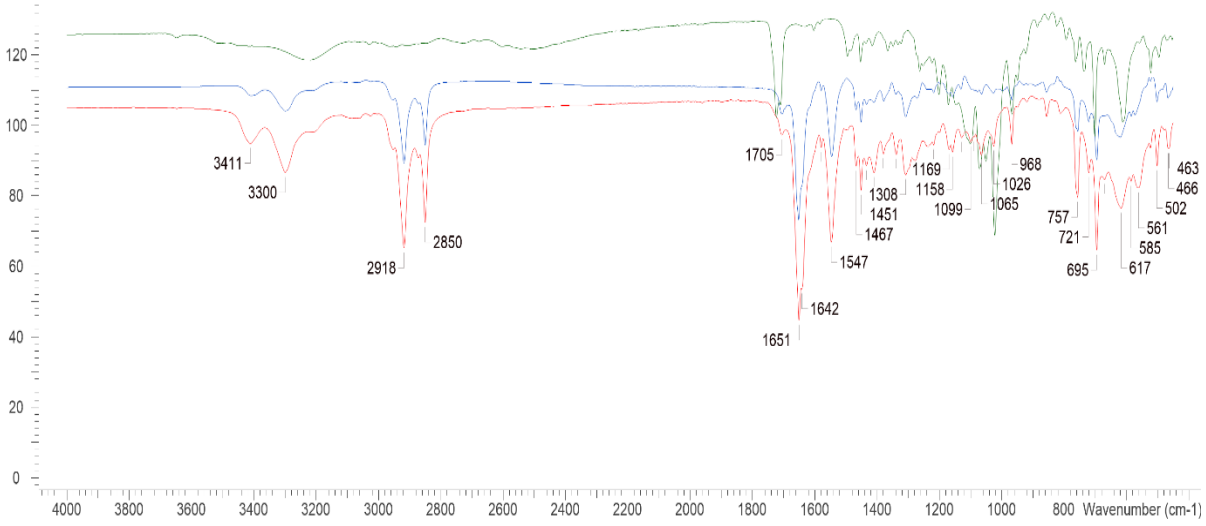

Figure 114. Comparison of atropine loaded BG-C12 xerogel (red), BG-C12 xerogel control (blue), and atropine sulphate powder (green).

Glutamine-C12 (3.5 mg) and benzaldehyde (1.13 µL) were dissolved with atropine sulfate (1 mg) in 1 mL water. The solution was heated until dissolution and the vial was left overnight for complete self-assembly. A control was set up as described, but in the absence of atropine. The gels in vials were dried in a vacuum oven and analysed. FT-IR spectra of both samples and a sample of atropine sulphate dry powder were compared as shown in Figure (124).

7.2.19 Rheology of Benzyl Glutamine Hydrogels Loaded with Atropine

The hydrogel was made by the addition of 0.35% wt/vol glutamine-C12 with equimolar benzaldehyde and atropine (1 mg) in 1 mL water. The mixture was heated and added to a bottomless vial attached on the rheometer plate. Once fully formed (after 3 hours), the bottomless vial was removed. A shear force of 0.0126% was applied to the gel at 2 Hz for 30 seconds, the frequency was increased to 100 Hz for a duration of 30 seconds. After that, the frequency was returned to 2 Hz and the recovery was monitored over time. The experiment was performed in duplicate at 25°C.

7.3 Comparative Study of Propranolol and Levodopa Drug Release from LMWG's and their Hybrid Derivatives

7.3.1 Gel Preparation

1. BG vial gels – 0.35% (wt/vol) glutamine-C12 (with one molar equivalent of benzaldehyde) was added to 1 mL water in a 7 mL glass vial. The sonicated solution was heated until dissolution and left to cool for gelation to form >12 hrs.

2. BG/Alginate beads – 0.35% (wt/vol) glutamine-C12 (with one molar equivalent of benzaldehyde) was added to 1 mL of 1% (wt/vol) alginate. The solution was sonicated and heated until complete dissolution. Once fully dissolved the solution was pipetted (20 µL/drop) into 40 mL 5% (wt/vol) $CaCl_2$. The beads were left for >30 mins for complete cross-linking and were thoroughly washed with water.

3. BG/Agarose – 0.35% (wt/vol) glutamine-C12 (with one molar equivalent benzaldehyde) and 10 mg agarose were dissolved in 1 mL water. Gelation was triggered through sonication and heating. The hot solution was dropped via a 20 µL pipette into an oil bath placed in an ice bath. The cold oil bath contained 20 mL paraffin oil and 20 mL petroleum ether. The beads were left to from for >30 minutes, after which the beads were left in petroleum ether (30 mL) for >30 minutes and then 30 mL water >12 hours.

4. DBS-$CONHNH_2$ vial gel– 0.4% (wt/vol) DBS-$CONHNH_2$ was dissolved in 1 mL water in a 7 mL glass vial. The solution was sonicated and heated until complete dissolution. The vial was left undisturbed for complete self-assembly for >12 hrs.

5. DBS-$CONHNH_2$ /Alginate beads – 0.4% (wt/vol) DBS-$CONHNH_2$ is dissolved in 0.5 mL water and sonicated >15 mins. 0.5 mL 1% (wt/vol) alginate solution was added, and the solution was heated until dissolution. The hot solution was pipetted (20 µL/drop) into 5% (wt/vol) $CaCl_2$ solution (40 mL). Once formed the beads were left for >30 mins and were washed several times in water.

6. DBS-$CONHNH_2$ /Agarose beads – 0.4% (wt/vol) DBS-$CONHNH_2$ and 10 mg agarose are dispersed in 1 mL water The solution was heated until dissolution, and the hot solution was pipetted (20 µL/drop) into a 40 mL cold paraffin oil placed in a ice bath. The beads were left to form for >30 minutes, after which the beads were left in petroleum ether (30 mL) for >30 minutes ethanol (30 mL) >30 minutes and then 30 mL water >12 hours.

7. DBS-COOH vial gel– 0.3% (wt/vol) DBS-COOH was suspended in water (1 mL) and dissolved by addition of a 0.5 M solution of NaOH (60 µL). The solution was then transferred into another sample vial containing 10 mg GdL and left undisturbed overnight to allow gel formation.

8. DBS-COOH/Alginate beads – 0.3% (wt/vol) DBS-COOH was suspended in water (0.5 mL) and dissolved by addition of a 0.5 M solution of 60 µL NaOH. Alginate solution (1.0% wt/vol - 0.5 mL) was subsequently added. The solution was pipetted (20 µL/drop) into 40 mL acidified $CaCl_2$ (5.0% wt/vol - 40 mL, acidified with 400 µL of HCl 1M). The gel beads were left to form overnight and washed with water several times.

9. DBS-COOH/Agarose beads – 0.3% (wt/vol) DBS-COOH was suspended in water (1 mL) and dissolved by addition of a 0.5 M solution of NaOH (60 µL). 10 mg agarose and 10 mg GdL is added to the solution, and the sample is heated until dissolution. The hot solution is pipetted (20 µL/drop) into a 40 mL cold paraffin oil placed in a ice bath. The beads were left to form for >30 minutes, after which the beads were left in petroleum ether (30 mL) for >30 minutes ethanol (30 mL) >30 minutes and then 30 mL water >12 hours.

7.3.2 DBS-COOH/Agarose beads

7.3.2.1 Thermal studies

The hybrid gels were prepared in glass vials. 0.3% (wt/vol) DBS-COOH was dissolved with 60 µL NaOH with the addition of water to complete a 1 mL total volume. 10 mg GDL was dissolved in the solution which was later added to 10 mg agarose. The mixture was heated and left to cool overnight. The thermal resistance of the gel system was tested by inserting the 2 mL vial gels into an oil bath. With each 1°C increase of temperature, the vial was inverted. Once the gel breaks and can no longer hold its shape the T_{gel} was recorded. The T_{gel} for this system was ca. 100°C.

7.3.2.1 Rheology

The hybrid gels were prepared in 7 mL glass vials. 0.3% (wt/vol) DBS-COOH was dissolved with 60 µL NaOH with the addition of water to complete a 1 mL total volume. 10 mg GDL was dissolved in the solution which was later added to 10 mg agarose. The mixture was heated with a heat gun and left to cool overnight. A control was also made consisting of 10 mg agarose in 1 mL water. The mixture was heated until dissolution and left overnight for complete gel formation.

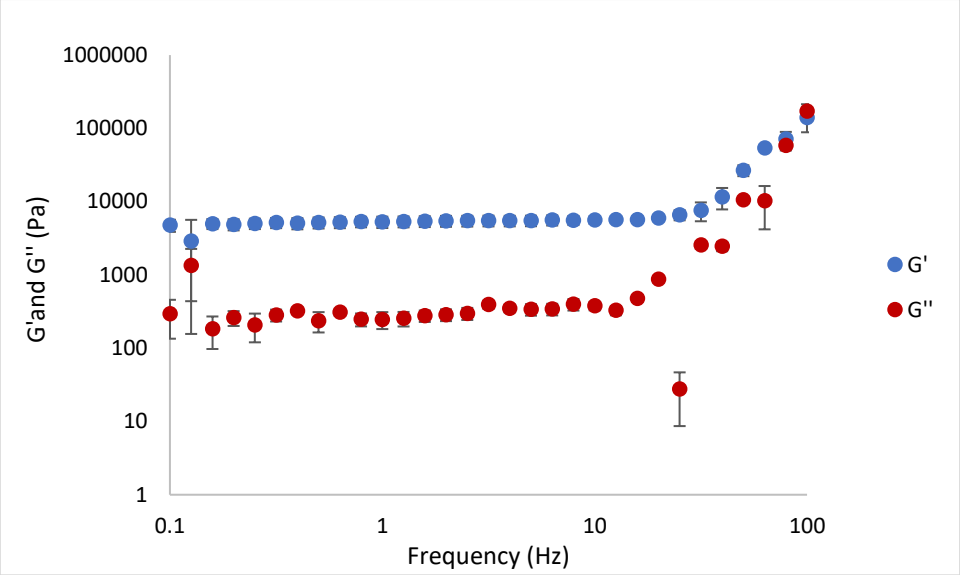

Figure 115. Elastic (Blue) and viscous (Red) moduli with increasing frequency of DBS-COOH/ Agarose (0.3% (wt/vol) DBS-COOH with 1% (wt/vol) agarose) vial gels performed using parallel plate geometry at 25°C. Error bars in the graph represent the standard error of the mean.

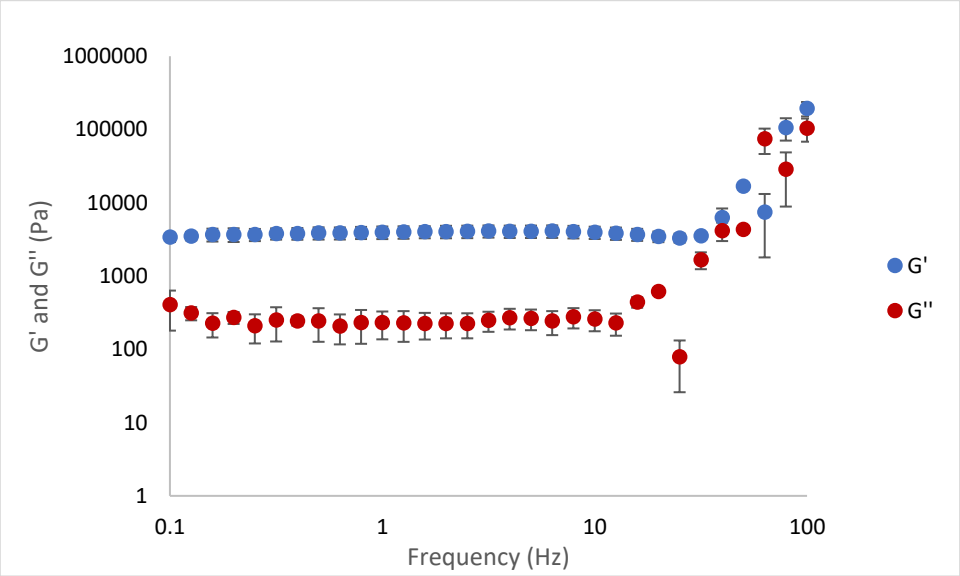

Figure 116. Elastic (Blue) and viscous (Red) moduli with increasing frequency of agarose vial gels (1% (wt/vol)) performed using parallel plate geometry at 25°C. Error bars in the graph represent the standard error of the mean.

7.3.3 Benzyl Glutamine/ Agarose Macrobeads Characterization

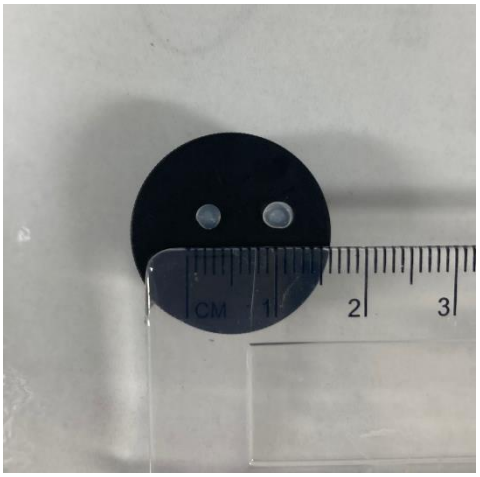

Figure 117. Benzyl glutamine/ Agarose beads (3 mm diameter).

7.3.3.1 Quantifying the Self-assembled Benzyl Glutamine in Each Bead

9 dried beads, prepared as described previously, were dried in a vacuum oven. The beads were crushed, dissolved in 0.7 mL DMSO-d_6, sonicated for >30 minutes, and were spiked with 2µL acetonitrile as an internal standard.

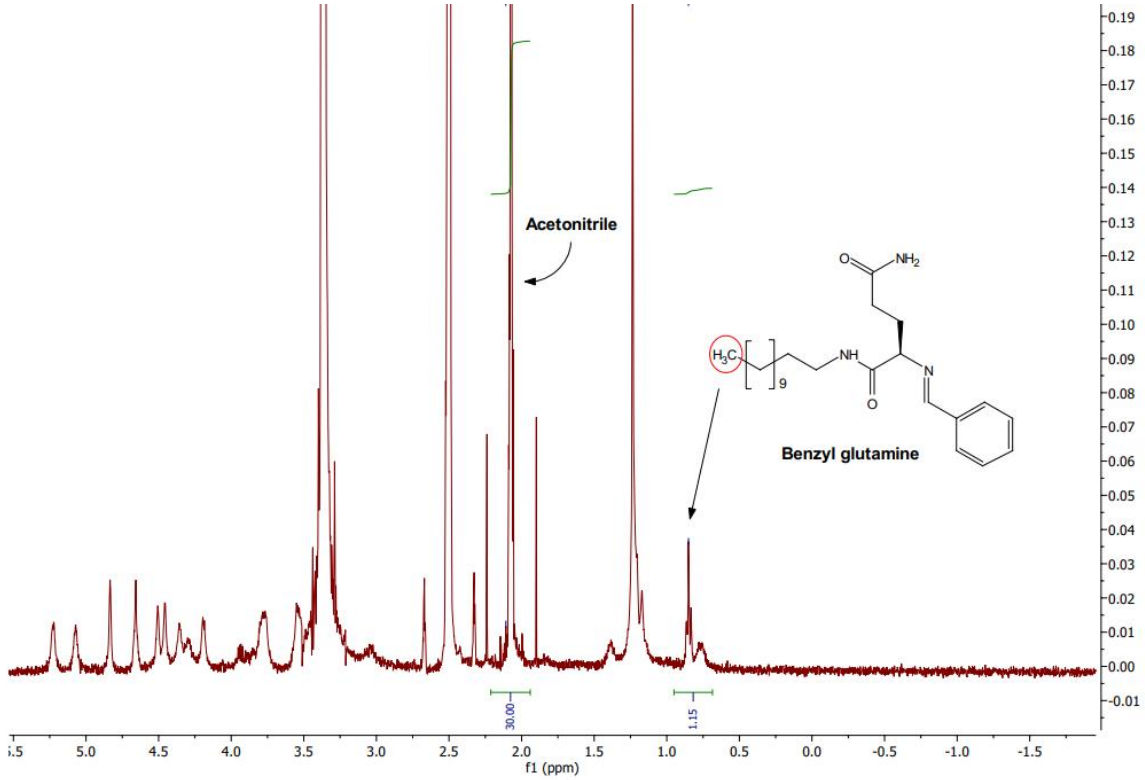

Figure 118. ^{1}H NMR of Benzyl glutamine/ Agarose beads in DMSO-d_6.

7.3.3.2 FT-IR Studies on Benzyl Glutamine/ Agarose Hybrid Gel beads

Xerogels of Benzyl glutamine/ Agarose beads and Benzyl glutamine hydrogels were prepared as previously described. The gels were dried in a vacuum oven. A small sample was placed into the infrared spectrophotometer and the spectra recorded in the range of 450-4000 cm^{-1}.

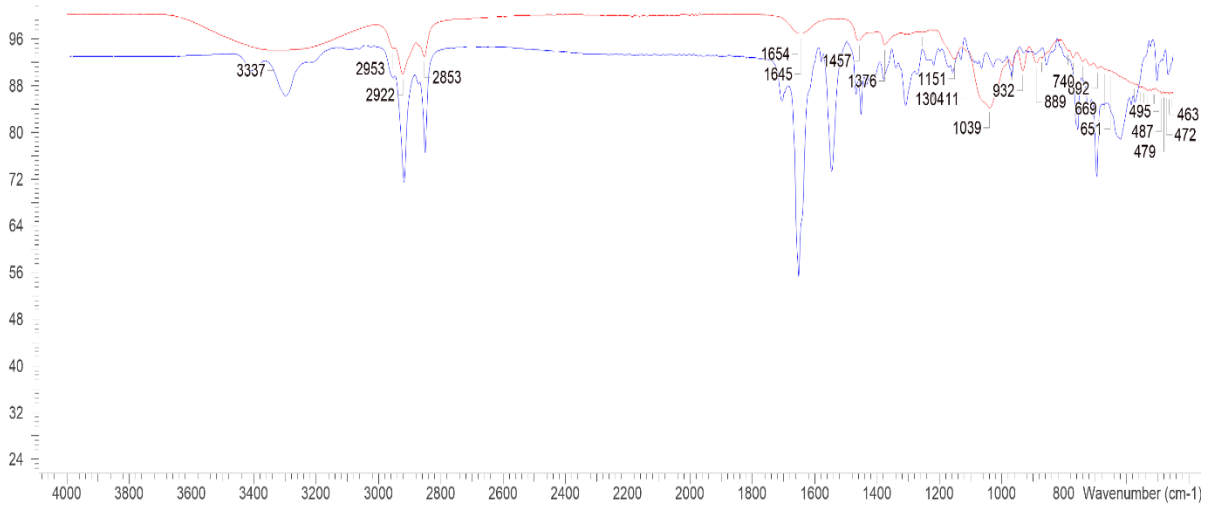

Figure 119. FT-IR spectra comparison of 0.35% (wt/vol) Benzyl glutamine vial gel (blue) and Benzyl glutamine/ Agarose beads containing 0.35% Benzyl glutamine with 1% (wt/vol) agarose (red).

7.3.3.3 Thermal Study and Rheology of Benzyl Glutamine/ Agarose Hybrid Gel System

0.35% (wt/vol) glutamine-C12 (with one molar equivalent benzaldehyde) was dissolved in 1 mL water with 10 mg agarose in glass vials. Once dispersed the solution was heated and left to cool under ambient conditions.

For the thermal study, the temperature was elevated at a rate of 1°C/30 seconds in a controlled oil bath. After each increase of 1°C the vials were removed and were inverted to test their ability to hold on to the surface of the glass. Once the gel fell, the temperature was recorded.

For the rheology study, the hybrid bulk gels were prepared as described previously, with a control made of only agarose (10 mg per 1 mL water).

7.3.4 Drug Loading and Quantification of Levodopa and Propranolol

a) Drug Loading Method

20 beads per vial or a 1 mL vial hydrogel were exposed to 1 mL of either levodopa (2.2 mg/mL) or propranolol (1 mg/mL). The vials were incubated at 37°C for >12 hours. Benzyl glutamine

was loaded with 0.5 mg/mL propranolol pre-gelation, the mixture was heated until dissolution and left to stand under ambient conditions overnight.

b) NMR and UV-Vis Quantification

Gel loading was quantified by two techniques, ^{1}H NMR and UV-Vis spectroscopy. The prepared beads were loaded as previously described. The gels were loaded with 1 mL drug solution for >12 hrs in an incubator at 37°C. The drug solution was either removed, dried and re-dissolved in D_2O with an internal standard of DMSO (for NMR analysis) or directly placed into a cuvette (for UV spectrometry).

Propranolol:

a) UV-Vis:

DBS-COOH and DBS-$CONHNH_2$ bulk gels: propranolol was quantified by using UV spectrometry by recording the absorbance (289 nm) of the drug solution after the process of loading.

b) NMR

Gel	Solvent volume (mL)	Internal Standard volume (µL)	Number of Moles	Integral	n × Integral × Mr (mg)	Drug in Gel (mg)
BG/Alginate beads	0.7	2	2.82×10^{-5}	0.72	0.34	0.66
BG/Agarose beads	0.7	2	2.82×10^{-5}	5.27	0.64	0.36
DBS-COOH/Alginate beads	1.0	4	5.63×10^{-5}	1.89	0.46	0.54
DBS-COOH/Agarose beads	1.0	4	5.63×10^{-5}	2.02	0.49	0.51
DBS-$CONHNH_2$/ Alginate beads	0.7	2	2.82×10^{-5}	4.09	0.50	0.50

DBS-CONHNH$_2$/ Agarose beads	1.0	4	2.82×10^{-5}	2.27	0.55	0.45

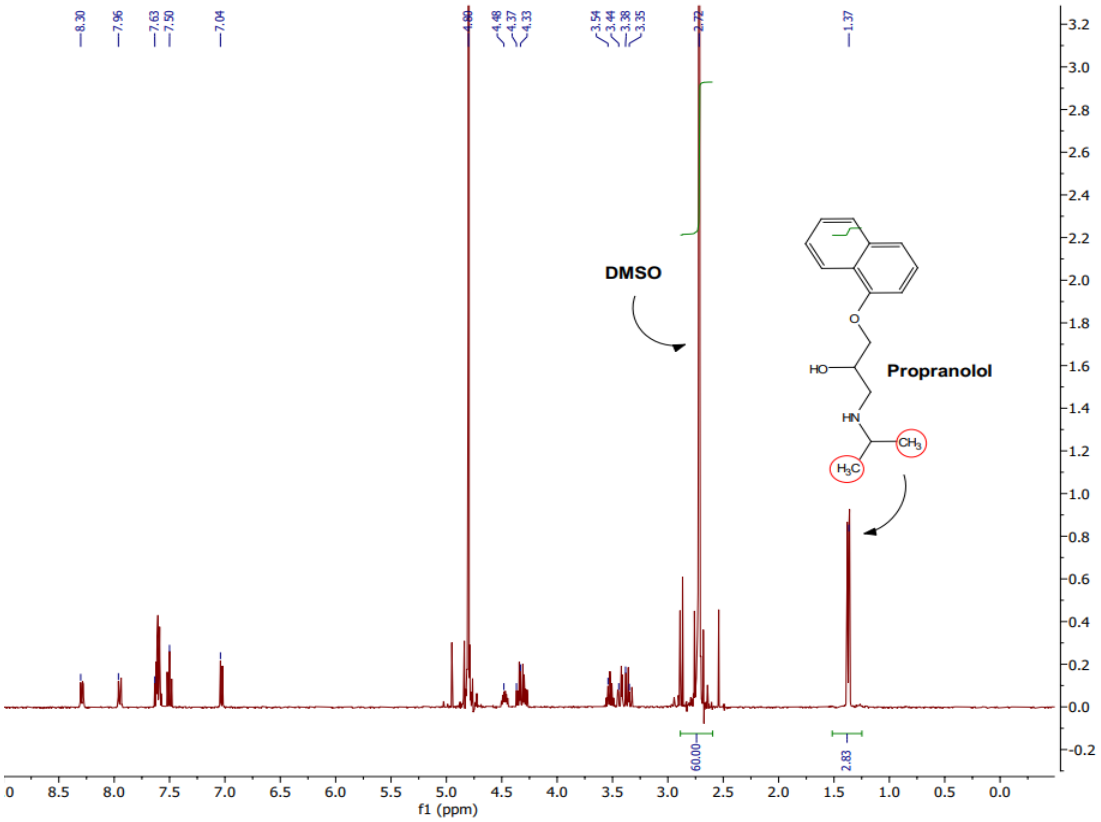

Figure 120. ^{1}H NMR spectrum of supernatant used to load Benzyl glutamine/Alginate beads with propranolol in D_2O.

Remaining graphs are found in the appendix.

Levodopa:

The same method of calculations was used to identify the quantity of drug remaining in the supernatant and hence the quantity of drug in the gel systems. The supernatant was dried and redissolved in D_2O. DMSO was added as an internal standard as described in the table below. The integral of the internal standard (δ = 2.70 ppm) is compared the hydrogen found on the benzene ring of levodopa (δ = 6.80 ppm). Remaining graphs are found in the appendix.

Gel	Solvent volume (mL)	Internal Standard volume (µL)	Number of Moles	Integral	n × integral × Mr (mg)	Drug in gel (mg)
BG/Alginate beads	1.0	2	2.82×10^{-5}	1.42	0.78	1.42
BG/ Agarose beads	0.7	2	2.82×10^{-5}	2.14	1.18	1.02
DBS-COOH vial gel	0.7	2	2.82×10^{-5}	0.92	0.52	1.68
DBS-COOH/ Alginate beads	0.7	2	2.82×10^{-5}	2.22	1.23	0.97
DBS-COOH/ Agarose beads	0.7	2	2.82×10^{-5}	2.16	1.20	1.00
DBS-$CONHNH_2$ vial gel	0.7	2	2.82×10^{-5}	1.68	0.93	1.27
DBS-$CONHNH_2$/ Alginate beads	0.7	2	2.82×10^{-5}	2.11	1.17	1.03
DBS-$CONHNH_2$/ Agarose beads	0.7	2	2.82×10^{-5}	2.31	1.28	0.92

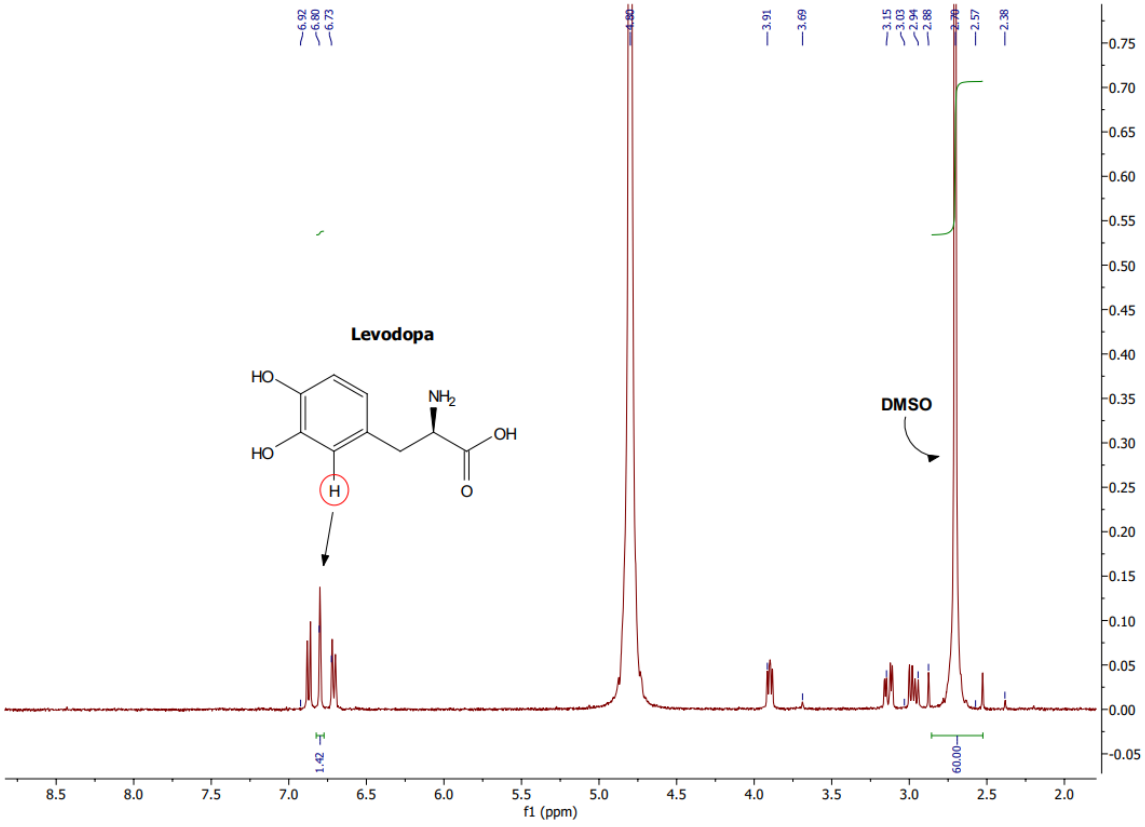

Figure 121. ^{1}H NMR spectrum of supernatant used to load Benzyl glutamine/Alginate beads with levodopa in D_2O.

7.3.5 Rheology study on Propranolol Loaded Benzyl Glutamine Hydrogel

Glutamine-C12 (3.5 mg) was added to 1.13 µL benzaldehyde and 1 mL propranolol HCl solution (0.5 mg/mL). The heated sample was pipetted into to a bottomless glass vial attached to the rheology plate. The gel was left for 3 hours for complete self-assembly. All studies were carried out using parallel plate rheology at 25 °C. For amplitude sweeps, the frequency was kept constant at 1 Hz. As for each frequency sweep, the shear strain was kept constant at a value determined by the amplitude sweep for that hydrogel.

The experiment was performed in duplicate.

7.3.6 Thermal Stability of Propranolol Loaded Benzyl Glutamine Hydrogel

Glutamine-C12 (3.5 mg) was added to 1.13 µL benzaldehyde and 1 mL propranolol HCl solution (0.5 mg/mL). The suspension was sonicated and heated until dissolution. The gel was left to cool down for >12 hours. The vial was placed in a heat regulated oil bath. With every increase in temperature of 1°C, the vial was inverted. When the gel could no longer hold its own weight, the temperature was recorded. The experiment was performed in triplicate.

7.3.6 Quantifying Mobile Propranolol in Benzyl glutamine Hydrogel

Glutamine-C12 (3.5 mg) was added to 1.13 µL benzaldehyde and 1 mL propranolol HCl solution (0.5 mg/mL) in D_2O. DMSO (2 µL) was added to the suspension to act as an internal standard. The mixture was sonicated, heated until dissolution, and quickly pipetted into a NMR tube. The tube was left undisturbed overnight, and the NMR spectrum was recorded. The integral of DMSO (δ = 2.75 ppm) was compared to the integral of the OH group on propranolol (δ = 6.98 ppm) to calculate how much mobile propranolol was within the gel network. The integrals were multiplied by a factor of 10.

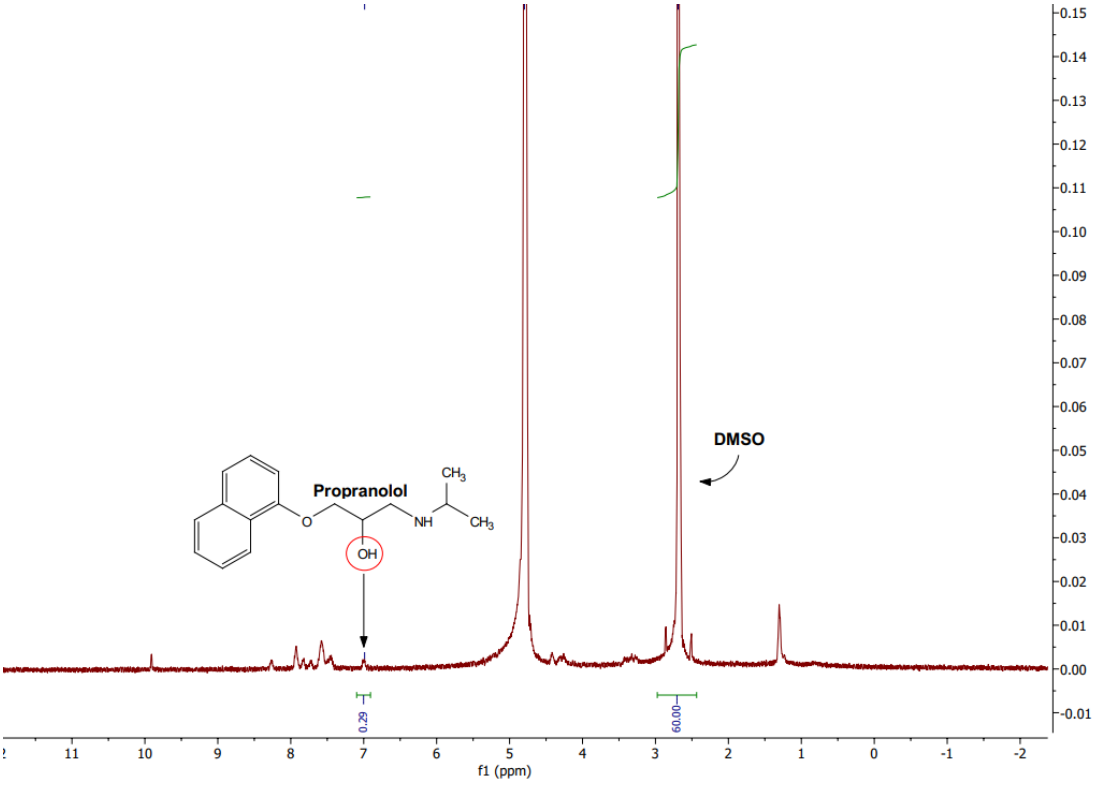

Figure 122. ^{1}H NMR spectrum of Benzyl glutamine hydrogel loaded with propranolol in D_2O (δ = 4.8 ppm) and DMSO (δ = 2.75 ppm) as an internal standard to calculate the free-flowing drug molecule in the gel network.

7.3.7 Microscopy on Propranolol Loaded Benzyl glutamine Hydrogel

Scanning electron microscopy (SEM)

The gel samples (10 µL of each gel (200 µM), in H_2O) were spread using a mounted needle on a thin piece of copper shim (to act as support); excess liquid was removed with filter paper. The gel was frozen on the copper support by submersion in nitrogen slush (ca. -210°C); after this water was removed from the gel by lyophilising on a Peltier stage, with a maximum temperature of -50°C. Once dry, the gel was knocked off the shim with a mounted needle, and the shim was mounted on an SEM stub using a carbon sticky tab. The sample was then sputter-coated with a thin layer (< 12 nm) of gold/palladium coating to prevent sample charging, before SEM imaging.

Transmission electron microscopy (TEM)

The samples were prepared with 10 µL of each gel (200 µM), in H_2O, that were placed on a copper grid (standard) with Formvar and carbon support film and allowed to set for 5 minutes. A stain (1% uranyl acetate) was applied to the grid while wet (1% in water, pH 4.5) to allow the stain to run across the grid, then most of it was wiped off with a filter paper. The grid was left to rest for 20 minutes before taking the images.

7.3.8 Drug Release study of Propranolol and Levodopa

After drug loading, the drug solutions were removed from all of the gels, and 4 mL tris buffer was added with various pH values (adjusted via the addition of NaOH or HCl solution). 2 mL aliquots were removed from the vials and were tested by UV-Vis spectroscopy each hour, with the aliquot then returned back into the vial. Absorbance was recorded at wavelengths of 289 nm (propranolol) and 288 nm (Levodopa).

7.3.9 Infrared Spectrometry

Xerogels were all prepared as previously described either in the absence or presence of the loaded drugs and were dried via a vacuum oven. A small sample was placed into the infrared spectrometer and spectra recorded in the range of 450-4000 cm^{-1}. The study compares spectra of xerogels with/without the drugs levodopa or propranolol HCl and the respective drug (used in solid form). Data is found in the appendix.

7.4 Wet spinning and 3D printing LMWG's

7.4.1 Fabrication of Benzyl Glutamine and its Derivatives into Gels Via Wet Spinning

Glutamine amide (with one molar equivalent of benzaldehyde) was dissolved in DMSO at various concentrations (0.35% up to 1.0%) and released from needle tips with sizes 20G and 23G from a syringe. The solution is released using a syringe pump at various rates (0.68, 1.7, and 3.4 µL/min) into a 7 mL water bath.

7.4.2 DMSO Quantification in Benzyl Glutamine Wet-Spun Hydrogel

60 µL 0.5% glutamine-C12(with one molar equivalent of benzaldehyde) was extruded at rate of 3.4 (µL/min) from a 26G needle into 300 µL water. The hydrogel was dried and redissolved into 0.7 ml D_2O with an internal standard, acetonitrile (2 µL) added to quantify the remaining DMSO in the gel. The ^1H NMR spectrum was used to quantify the mobile components by comparison of the integrals of relevant DMSO peak (δ = 2.50 ppm) to that of acetonitrile (δ = 2.06 ppm)

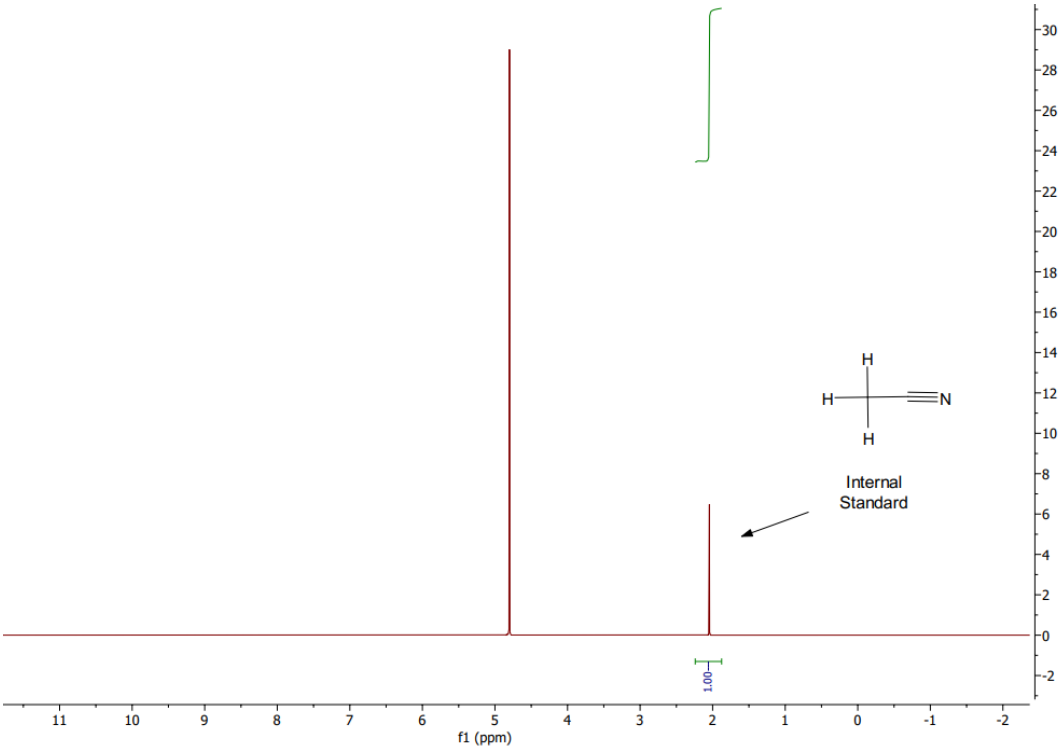

Figure 123. ^1H NMR of Benzyl glutamine gel filament prepared by wet spinning (60 µL – 0.5% wt/vol; 23G blunt tip needle, 5.1 µL/min flow rate).

7.4.3 Infrared Spectrometry for Wet-Spun Benzyl Glutamine

500 µL 0.5% glutamine-C12 (with one molar equivalent of benzaldehyde) was extruded at rate of 3.4 (µL/min) from a 26G needle into a water bath. The gel was dried in a vacuum oven.

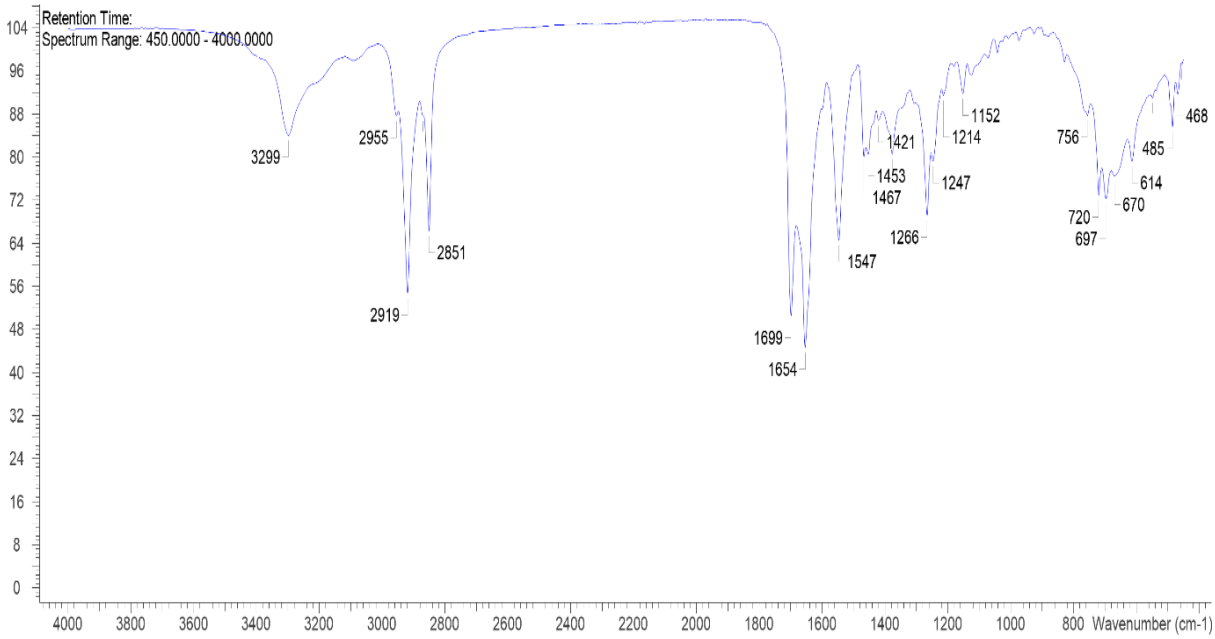

Figure 124. FT-IR of wet spun Benzyl glutamine (0.5% wt/vol).

7.4.4 Altering the Solvents for Wet-Spun Benzyl Glutamine

3% (wt/vol) glutamine-C12 (with one molar equivalent of benzaldehyde) was dissolved in methanol and is extruded with a syringe pump into several baths (water, HCl, petroleum ether, and 2-propranolol). The extrusion rate used for each bath was 1.7 µL/min, with a needle size of 23G.

7.4.5 Wet spinning of Benzyl Glutamine Derivatives (BG-C11 and BG-C14)

BG-C11 and BG-C14 were dissolved in DMSO at various concentrations (0.3 - 1.2% wt/vol) with the help of sonication. Once fully dissolved the gel solutions were extruded through a 1 mL syringe and 23G needle into a deionised water bath as well as into water baths with pH

values of 13 and 2 (with the addition of NaOH and HCl respectively). Extrusion rates were varied (0.68, 1.7, 3.4, and 10.2 µL/min) and reported.

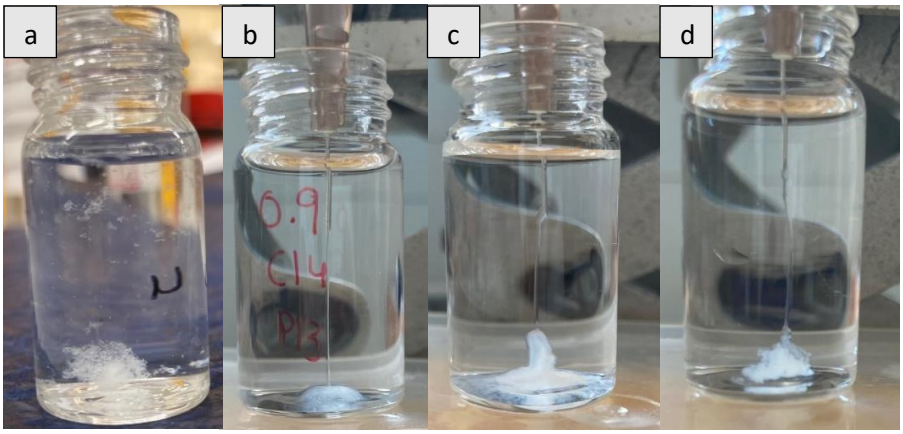

Figure 125. Representing wet-spun Benzyl glutamine derivatives- aggregates (a), Bulk gel (b), Tube-shaped structure(c), Thinner tube-shaped structure (d).

7.4.6 Infrared Spectrometry for Wet-Spun Benzyl Glutamine Derivatives

a) Preparation of BG-C11:

1.2% (wt/vol) BG-C11 dissolved in DMSO was extruded into a 2 mL water bath at a rate of 27.2 µL/min. The gel was removed and dried in a vacuum oven. The IR spectrum was then recorded directly on the dried solid.

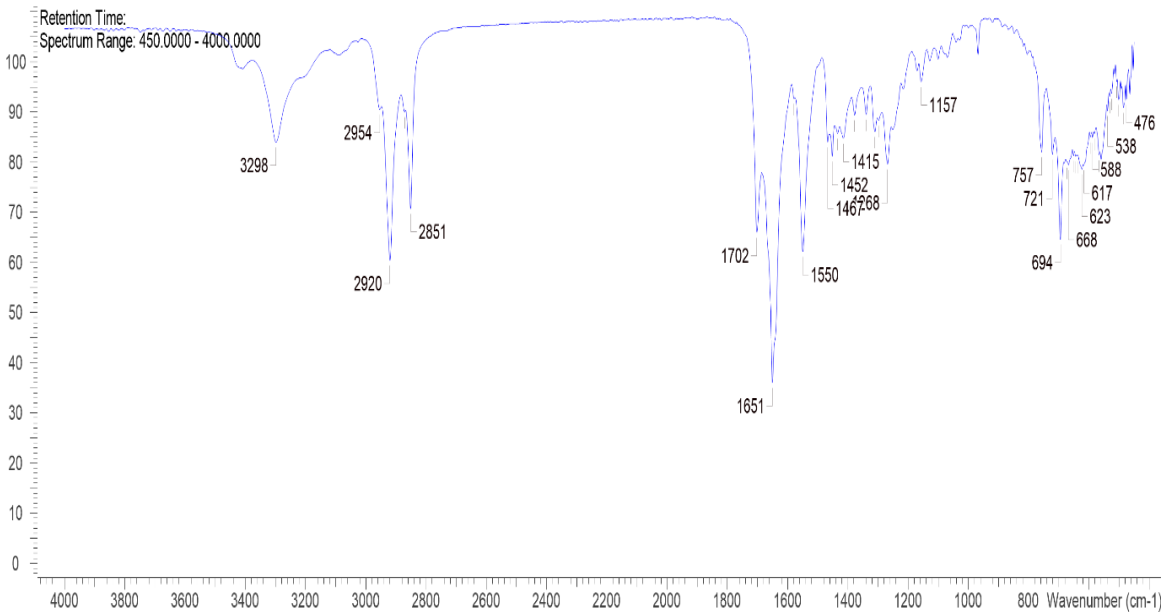

Figure 126. FT-IR of wet-spun BG-C11 (1.2% wt/vol).

b) Preparation of BG-C14:

BG-C14 0.6% (wt/vol) dissolved in DMSO was extruded into a 2 mL water bath at a rate of 27.2 µL/min. The gel was removed and dried in a vacuum oven µL/min.

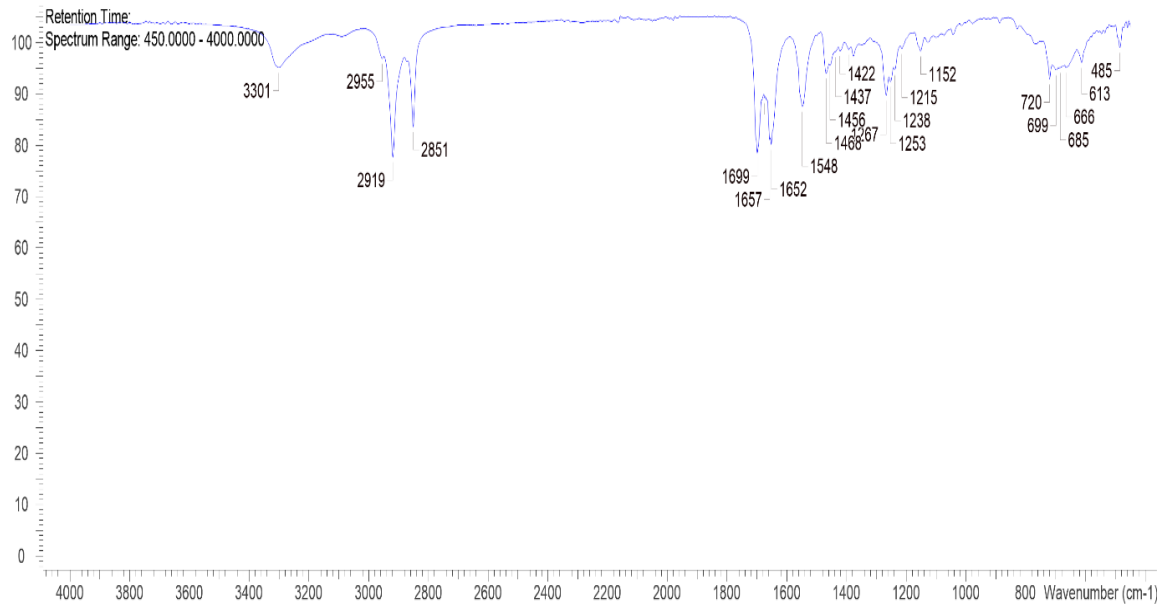

Figure 127. FT-IR of wet-spun BG-C14 (0.6% wt/vol).

7.4.7 Fabrication of Naproxen Loaded DBS-CONHNH2 Filaments

1.5% (wt/vol) DBS-$CONHNH_2$ was dissolved in 1 mL anhydrous DMSO. 0.2 mL of the solution is added to naproxen (10 mg) and was released into a water bath at the rates of 3.4, 1.7 and 0.68 µL/min with a 23G needle tip. NPX (10, 15, 20, or 30 mg) was added to 1.5% (wt/vol) DBS-$CONHNH_2$ in DMSO and tested to find the optimum drug loading for compatibility with wet-spinning.

7.4.8 ^{1}H NMR to Quantify Drug Loading Efficiency

1.5% (wt/vol) DBS-$CONHNH_2$ was dissolved in 1 mL DMSO with 10 mg NPX and extruded from a 23G needle at a rate of 0.68 µL/min. The filaments (made with 0.1 mL of the solution) were removed as soon as the entire solution had been used up from the syringe in an attempt to limit leaching/loss of NPX. The filament was dried in a vacuum oven and dissolved in 0.7 mL D_2O with the addition of 2 µL acetonitrile.

7.4.9 Microscopy Images of Wet-Spun DBS-CONHNH$_2$ Loaded with Naproxen

1.5% (wt/vol) DBS-CONHNH$_2$ was dissolved in 1 mL DMSO with 10 mg NPX and extruded from a 23G needle at a rate of 0.68 µL/min. The collected filament was placed on a copper grid and was critical-point freeze dried. The samples were mounted onto stubs and SEM images were collected.

7.4.10 Drug Release study (Wet-Spun Naproxen-Loaded DBS-CONHNH$_2$ Hydrogel)

1.5% (wt/vol) DBS-CONHNH$_2$ dissolved in DMSO was extruded with naproxen (2 mg in 0.1 mL gel solution) at a rate of 10.2 µL/min. The needle size used was 23G and the solution was released in a 2 mL water bath. Once the gel had fully formed 200 µL aliquots from the supernatant solution were removed to be tested by UV-Vis spectroscopy (329 nm). the aliquots were discarded and not replaced. The gel system was placed in an incubator at 37°C for the remaining of the 48-hour study and samples tested at regular intervals.

7.4.11 FT-IR of Naproxen Loaded DBS-CONHNH2 Wet-Spun Hydrogels

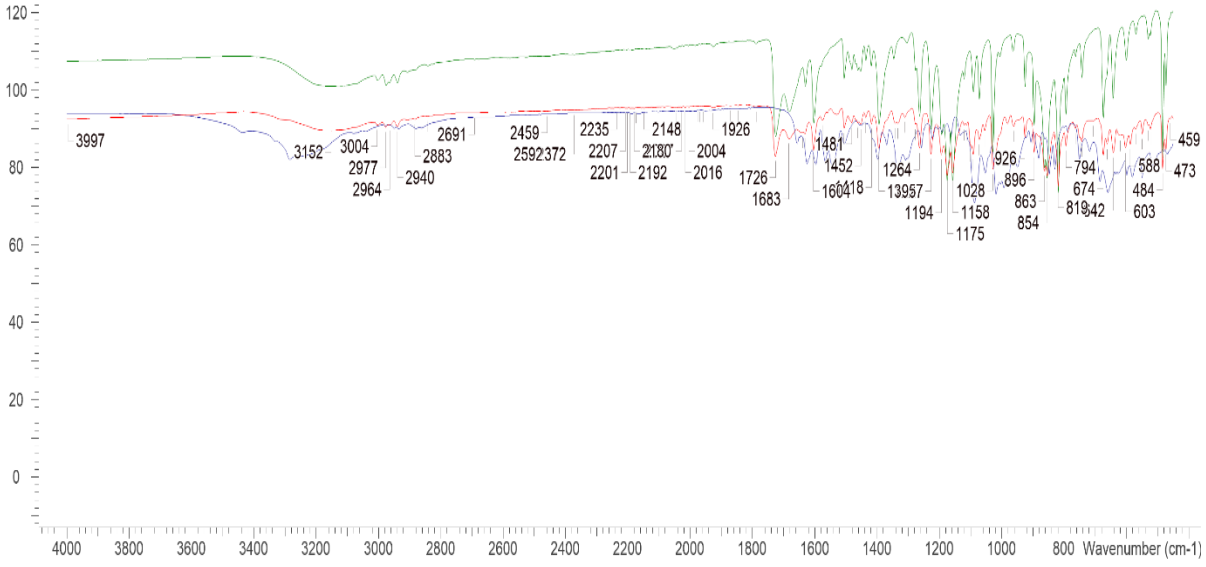

Figure 128. FTIR comparison of naproxen Loaded DBS-CONHNH$_2$ (Red spectrum) and DBS-CONHNH$_2$ Wet-Spun (Blue Spectrum) xerogels and pure naproxen (Green spectrum).

1.5% (wt/vol) DBS-$CONHNH_2$ dissolved in DMSO was extruded with and without naproxen (2 mg in 0.1 ml gel solution) at a rate of 10.2 µL/min. The needle size used was 23G and the solution was released into a 2 ml water bath. Each gel was dried in a vacuum oven and was prepared for FT-IR analysis.

7.4.12 Drug Release Study with Wet-Spun Benzyl Glutamine

0.5% (wt/vol) glutamine-C12 (with one molar equivalent of benzaldehyde) dissolved in DMSO (0.1 mL) was added to 2 mg naproxen or 1 mg propranolol HCl. The gel-drug solution was extruded from a 23G needle into a 2 mL water bath at rates of 3.4 and 10.2 µL/min for naproxen and 3.4 µL/min for propranolol HCl. For each measurement, 200 µL samples were removed with a pipette from close to the surface of the gel. The sample was diluted with 1800 µL deionised water in a cuvette. After measurement, the samples were disposed of. The drugs were detected with UV-Vis spectroscopy (NPX- 329 nm) and (Propranolol- 289 nm). Experiments were performed in duplicate.

7.4.13 FT-IR of Drug-Loaded Benzyl Glutamine Wet-Spun Hydrogels

0.5% (wt/vol) glutamine-C12(with one molar equivalent of benzaldehyde) dissolved in DMSO (0.1 mL) was added to 2 mg naproxen or 1 mg propranolol HCl respectively. The gel-drug solution was extruded from a 23G needle into a 2 mL water bath at a rate of 3.4 µL/min. The gels were removed from the water baths and dried, then directly analysed by IR spectroscopy.

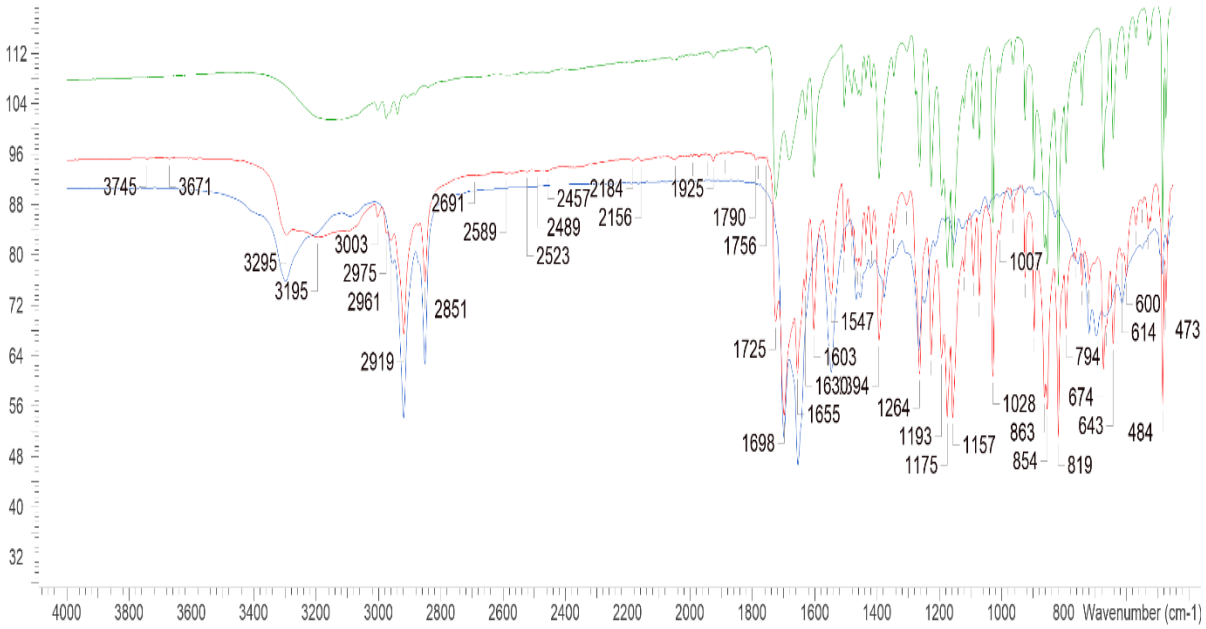

Figure 129. FT-IR spectra comparison of wet-spun Benzyl glutamine xerogel (blue spectrum), naproxen loaded wet-spun Benzyl glutamine xerogel (red spectrum), and naproxen pure drug (green spectrum).

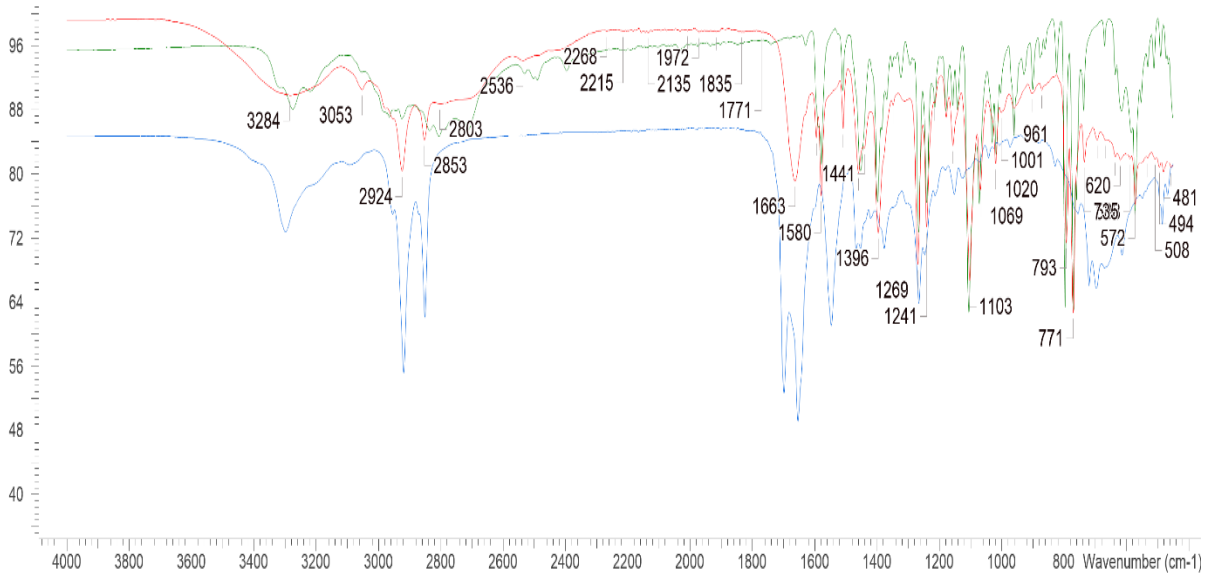

Figure 130. FT-IR spectra comparison of wet-spun Benzyl glutamine xerogel (blue spectrum), propranolol HCl loaded wet-spun Benzyl glutamine (red spectrum) xerogel and the propranolol HCl pure drug (green spectrum).

7.4.14 3D Printing Benzyl Glutamine and DBS-COOH

For both gels, a syringe pump was connected to an AxiDraw Mini printer. The drawing/writing robot moved according to the generated drawing set-up by Inkscape software. The movement speed was set up at 1% and the acceleration was set as 'very slow' which was constant throughout the printing process.

a) DBS-COOH (0.75 - 1.5% (wt/vol)) was dissolved in anhydrous DMSO. The solution was pumped with a syringe pump into a petri dish containing 40 mL water. The flow rate, needle nozzle size, concentration, and distance between the needle and dish were all altered.

Table 30. Studying the effect of altering variables in 3D printing DBS-COOH dissolved in DMSO and printed in a 40 mL water bath.

Concentration (% wt/vol)	**Needle Size (G)**	**Rate (µL/min)**	**Observation**
0.75	25	5.10	Higher concentrations (1.5% wt/vol) gave more opaque prints
1.50	25	5.10	
1.50	25	3.40	Increased rate gave thicker prints
1.50	25	12.3	
1.50	25	5.10	Moving the nozzle closer to the platform gave thicker prints
1.50	25	5.10	
1.50	25	3.40	Improved flow of stream as nozzle size increased 23G> 25G > 26G, giving smoother prints
1.50	23	3.40	
1.50	26	3.40	

b) Benzyl glutamine (0.35 - 0.5% (wt/vol) with one molar equivalent of benzaldehyde) was dissolved in anhydrous DMSO. The solution was pumped with a syringe pump into a petri dish containing 35 mL deionized water. The flow rate, needle size, concentration were all altered.

Table 31. Studying the effect of altering variables in 3D printing Benzyl glutamine dissolved in DMSO and printed in a 35 mL water bath.

Concentration (% wt/vol)	Needle Size (G)	Rate (µL/min)	Observation
0.35	26	2.38	Higher concentrations produce prints with greater stability and increased opacity
0.50	26	2.38	
0.35	26	2.38	Both displayed a lot of gel spreading. The higher flow rate increases print thickness
0.35	26	3.40	
0.50	26	5.10	Better control in spreading of ink. Increased rate thickens the prints width.
0.50	26	6.80	
0.50	26	10.2	
0.50	26	5.10	Thinner prints formed with smaller nozzle sizes – 26G > 23G
0.50	23	5.10	

7.4.15 Thixotropy of 3D printed Benzyl glutamine

0.5% (wt/vol) glutamine-C12 (with one molar equivalent of benzaldehyde) was dissolved in 1 mL DMSO. The gel was prepared with the same method described previously. The ink was used to form a square layout with 14 stacked layers in 35 mL of water inside a petri dish. The gel was gently punctured with a 26G needle in several locations and was monitored for one week to determine whether it observed any healing behaviour.

7.4.16 Biology Studies

(a) Cell line (Y201 immortalized human mesenchymal stem cells – MSCs).

Y201 MSCs were grown in a T175 flask containing Dulbecco's Modified Eagle's Medium (DMEM) with 10% of fetal bovine serum (FBS) and 1% of penicillin/streptomycin (P/S). For adherent cells, the spent medium was removed from the flask using a sterile pipette and Dulbecco's phosphate buffer saline solution (DPBS, 11 mL) was added to rinse the cells. DPBS was removed and Trypsin/EDTA (2 mL) was then added to detach the cells. The cells were

incubated at 37°C for around 5 minutes. To help cell detachment, the flask was gently tapped, and the detached cells were observed under optical microscopy. 10 mL of DMEM (10% FBS, 1% P/S) was added to neutralized trypsin and the cells were transferred into a centrifuge tube. The supernatant was removed, followed by the addition of 5 mL DMEM (10% FBS, 1% P/S) to the cell pellet. The cell count was performed using a Countess Automated Cell Counter-Thermo Fisher. Aliquots (10 µL) of cells that were prepared by the simple mixing of trypan blue (20 µL) with cell suspension (20 µL) was injected to each side of a disposable cell counting chamber slide.

(b) Viability assay

i) Benzyl glutamine preparation:

Autoclaved water (300 µL) was added into each well of a non-treated 96-well plate. Benzyl glutamine was dissolved in DMSO to give a concentration of 0.5% wt/vol (with one molar equivalent of benzaldehyde). The gel solution was extruded through a sterile syringe connected with a syringe pump (flow rate = 5.1 uL/min, 4 min/well). The gel was left to stabilise for 1.5 hours, which was then washed gently with autoclaved water (300 µL) in triplicate, and finally left in autoclaved water (300 µL) overnight. The following day, the gel was washed gently with DMEM (200 µL /well) twice with a two-hour gap between each wash.

ii) DBS-$CONHNH_2$ preparation (Prepared by Chayanan Tangsombun):

DBS-$CONHNH_2$ (0.3% wt/vol) in autoclaved water was heated until complete dissolution. 75 µL aliquots of the DBS-$CONHNH_2$ hot solution were transferred to non-treated 96-wells plate. The hydrogels were left undisturbed overnight. The following day, the gels were washed with DMEM (200 µL /well) multiple times. Once ready, the gels were soaked with 100 µL of DMEM (10% FBS, 1% P/S) and the cells (25,000 cell/well) were seeded. Finally, DMEM (10% FBS, 1% P/S) was added to reach 200 µL of solution per well. As for the control, the gel was soaked in DMEM 200 µL.

Cell viability was measured at days 0, 3 and 6. The spent medium was removed from each well and was replaced with Alamar blue solution (100 µL, 10% in DMEM). The plate was incubated at 37°C for 4 hours. After that, aliquots (20 µL) were taken from each well and then transferred to a new 96-well plate containing 180 µL of DMEM (10% FBS, 1% P/S). A control

was set up without cells for each gel. Fluorescence signals were measured by a fluorescence plate reader with the excitation wavelength at 530-560 nm and the emission wavelength 590 nm. The fluorescence of the gel alone (control) was subtracted from the fluorescence signal of gel with the cell culture.

7.4.17 Fabrication of Benzyl Glutamine/Alginate Tubes

0.35% (wt/vol) Glutamine-C12 (with one molar equivalent of benzaldehyde) were dispersed in 0.5 mL water. 0.5 mL 3% (wt/vol) alginic acid solution was added. The solution was sonicated and heated to promote gelation. The mixture was extruded from a 12 mL syringe directly into 10% (wt/vol) $CaCl_2$ solution manually or with a connecting syringe pump extruding the ink at a rate of 33.7 µL/min. The tube was left for >30 mins before it was rinsed with water to remove excess $CaCl_2$.

7.4.18 ^{1}H NMR Quantification of Self-assembled LMWG in Benzyl Glutamine/Alginate Tubes

a) Quantifying the concentration of Benzyl glutamine in the hybrid gel tube:

A sample from the BG/Alginate tube prepared as mentioned above was dried in a vacuum oven. The dried xerogel was dissolved in DMSO (0.7 mL) with an added 2 µL acetonitrile as an internal standard, and a ^{1}H NMR spectrum was recorded.

b) Determining the self-assembly of Benzyl glutamine in the hybrid tube:

Roughly 1-2 cm of the tube was placed into an NMR tube containing 0.5 mL D_2O and 2 µL DMSO as an internal standard and an ^{1}H NMR spectrum was recorded.

7.4.19 Microscopy of Benzyl Glutamine/Alginate Tubes

Tube samples were prepared as previously mentioned. The sample was critical point dried and mounted on stubs for SEM. For optical microscopy, the gel was dehydrated in a graded series of ethanol (25-100%) and embedded in LR White resin (Agar Scientific). Semi-thin

sections were cut on Leica EM UC7 ultramicrotome and stained with toluidine blue. The sections were then visualised on Zeiss Stereo Lumar V12 microscope and images collected.

7.4.20 Reduction of Benzyl Glutamine/Alginate Beads

The beads were prepared as previously described in chapter 3. 0.35% (wt/vol) glutamine-C12 (with one molar equivalent of benzaldehyde) was added to 1% (wt/vol) Alginate solution (1 mL). The mixture was sonicated and heated until dissolution. It was then dropped with a pipette into a solution of 5% (wt/vol) calcium chloride. The beads formed and were left in the solution for complete calcium cross-linking to occur (roughly 30 mins). They were then washed with distilled water to remove any residue from the calcium chloride. The beads were placed into a solution containing excess sodium borohydride for a period of 24 hours. The beads were then removed and washed with water.

7.4.21 Mass Spectrometry of Reduced Beads

10 Benzyl glutamine/Alginate beads (prepared as described previously) were submerged in a 3 mL solution of sodium borohydride (2.1 mg/mL). Left for 24 hours the beads were removed and washed with water. The beads were dried, crushed, and prepared for mass spectrometry.

7.4.22 ^{1}H NMR to Detect Amine Conversion

27 Benzyl Glutamine/ Alginate beads were submerged in a 2 mL solution of sodium borohydride (7 mg/mL). Left overnight, the beads were removed, dried, crushed, and dissolved in 0.7 mL DMSO-d_6 with 2 µL methanol as an internal standard.

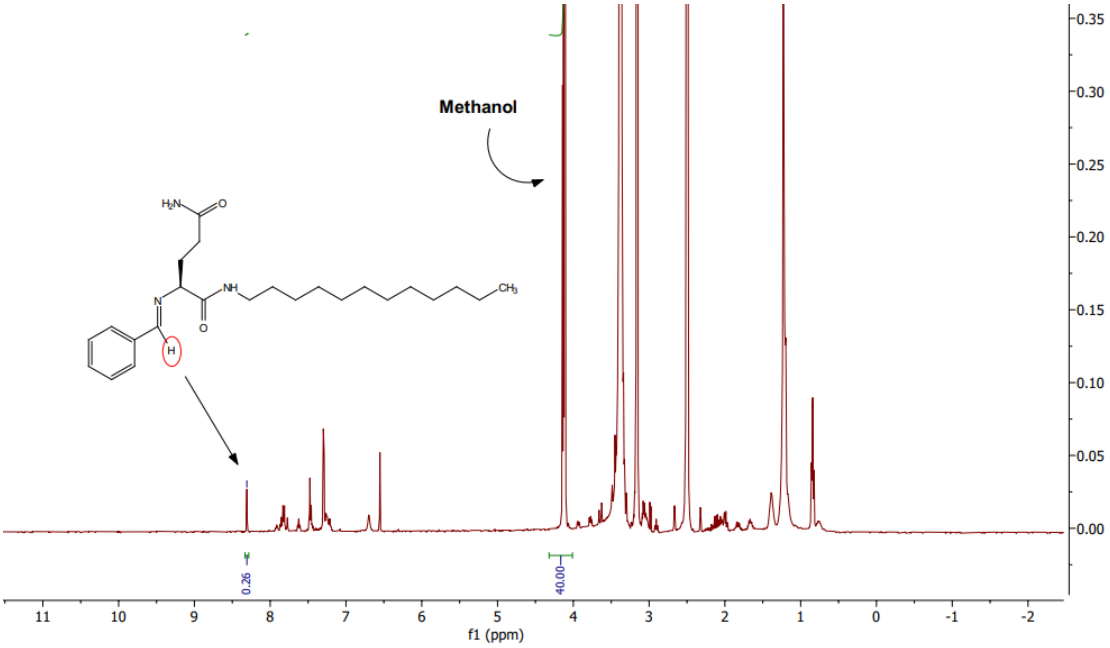

Figure 131. ^{1}H NMR of imine formation in Benzyl glutamine/Alginate beads in DMSO-d_6.

3 Benzyl glutamine/Alginate beads (prepared as described previously) were reduced with sodium borohydride (2.01 mg/mL) overnight. The beads were removed and placed into an NMR tube containing 0.7 mL D_2O. The solution was spiked with 2 µL anhydrous DMSO as an internal standard.

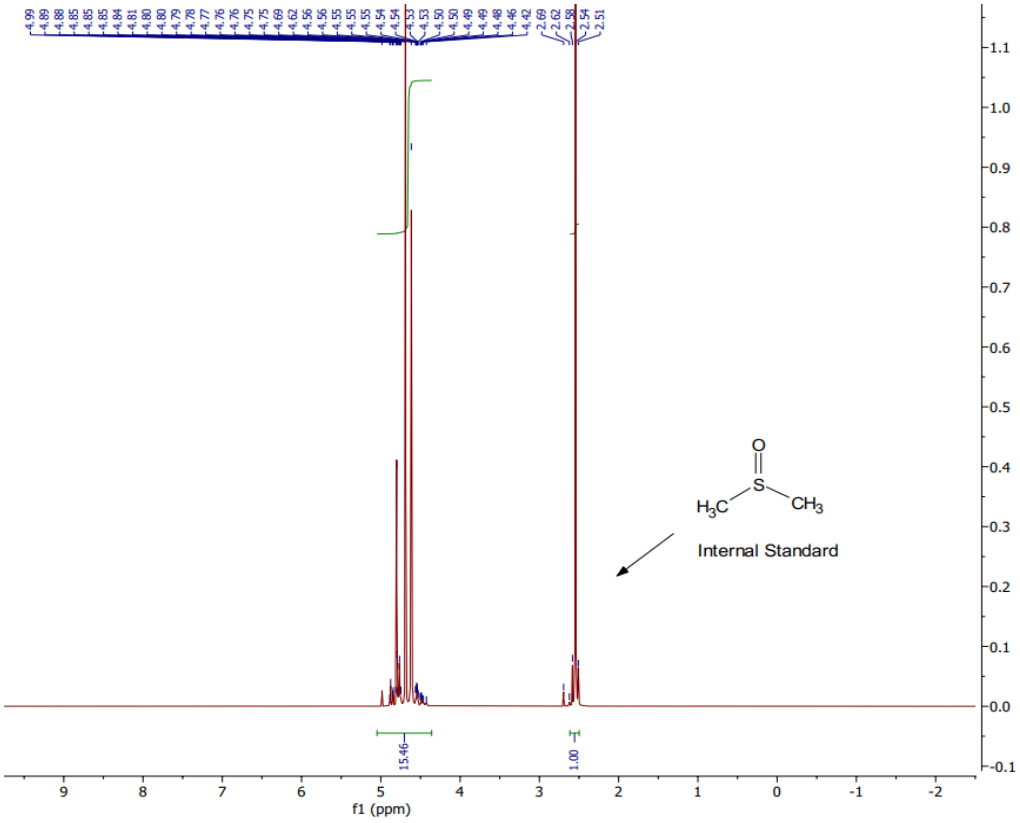

Figure 132. ^{1}H NMR of imine formation in Benzyl glutamine/Alginate beads in D_2O with DMSO as an internal standard.

References

1. K. Hawkins, A. K. Patterson, P. A. Clarke and D. K. Smith, *Journal of the American Chemical Society*, 2020, **142**, 4379-4389.
2. J. T.-W. Wang, A. C. Rodrigo, A. K. Patterson, K. Hawkins, M. M. S. Aly, J. Sun, K. T. Al Jamal and D. K. Smith, *Advanced Science*, 2021, **8**, 2101058.
3. A. Chalard, P. Joseph, S. Souleille, B. Lonetti, N. Saffon-Merceron, I. Loubinoux, L. Vaysse, L. Malaquin and J. Fitremann, *Nanoscale*, 2019, **11**, 15043-15056.
4. R. Narayanaswamy and V. P. Torchilin, *Molecules*, 2019, **24**, 603.
5. A. Song, A. A. Rane and K. L. Christman, *Acta Biomaterialia*, 2012, **8**, 41-50.
6. V. Jayawarna, M. Ali, T. A. Jowitt, A. F. Miller, A. Saiani, J. E. Gough and R. V. Ulijn, *Advanced Materials*, 2006, **18**, 611-614.
7. N. M. Sangeetha and U. Maitra, *Chemical Society Reviews*, 2005, **34**, 821-836.
8. Z. Yang, L. Wang, J. Wang, P. Gao and B. Xu, *Journal of Materials Chemistry*, 2010, **20**, 2128-2132.
9. R. Dong, Y. Pang, Y. Su and X. Zhu, *Biomaterials Science*, 2015, **3**, 937-954.
10. L. Saunders and P. X. Ma, *Macromolecular Bioscience*, 2019, **19**, 1800313.
11. Y.-Y. Xie, Y.-W. Zhang, X.-T. Qin, L.-P. Liu, F. Wahid, C. Zhong and S.-R. Jia, *Colloids and Surfaces B: Biointerfaces*, 2020, **193**, 111099.
12. X. Dou, N. Mehwish, C. Zhao, J. Liu, C. Xing and C. Feng, *Accounts of Chemical Research*, 2020, **53**, 852-862.
13. J. Omar, D. Ponsford, C. A. Dreiss, T.-C. Lee and X. J. Loh, *Chemistry – An Asian Journal*, 2022, **17**, e202200081.
14. X. Liu, X. Sun and G. Liang, *Biomaterials Science*, 2021, **9**, 315-327.
15. M. Bertasa, A. Dodero, M. Alloisio, S. Vicini, C. Riedo, A. Sansonetti, D. Scalarone and M. Castellano, *European Polymer Journal*, 2020, **123**, 109442.
16. X. Wang, S. Tang, S. Chai, P. Wang, J. Qin, W. Pei, H. Bian, Q. Jiang and C. Huang, *Carbohydrate Polymers*, 2021, **270**, 118342.
17. T. Ramdhan, S. H. Ching, S. Prakash and B. Bhandari, *Trends in Food Science & Technology*, 2020, **106**, 150-159.
18. J. F. Arokianathan, K. A. Ramya, A. P. Deshpande, A. Leemarose and G. Shanmugam, *Colloids and Surfaces A: Physicochemical and Engineering Aspects*, 2021, **618**, 126430.
19. D. M. Ryan, S. B. Anderson, F. T. Senguen, R. E. Youngman and B. L. Nilsson, *Soft Matter*, 2010, **6**, 475-479.
20. S. Wu, P. Jiang, N. Ding, Q. Hu, X. Yan, J. Liu, Y. Wang, H. Zhang, P. Yuan and Q. Yang, *Spectrochimica Acta Part A: Molecular and Biomolecular Spectroscopy*, 2021, **261**, 120078.
21. K. Subramani and W. Ahmed, in *Emerging Nanotechnologies in Dentistry*, eds. K. Subramani and W. Ahmed, William Andrew Publishing, Boston, 2012, pp. 209-224.
22. J.-P. Fan, F.-H. Tao, X.-H. Zhang, T.-T. Yuan, C.-F. Xie, H.-P. Chen and H.-L. Peng, *Colloids and Surfaces A: Physicochemical and Engineering Aspects*, 2022, **652**, 129839.
23. W. Wang, Y. Zhang and W. Liu, *Progress in Polymer Science*, 2017, **71**, 1-25.
24. W.-R. Zhuang, Y. Wang, P.-F. Cui, L. Xing, J. Lee, D. Kim, H.-L. Jiang and Y.-K. Oh, *Journal of Controlled Release*, 2019, **294**, 311-326.
25. L. E. Buerkle and S. J. Rowan, *Chemical Society Reviews*, 2012, **41**, 6089-6102.
26. J. Morris, J. Bietsch, K. Bashaw and G. Wang, *Gels*, 2021, **7**, 24.
27. J. H. Fuhrhop, S. Svenson, C. Boettcher, E. Roessler and H. M. Vieth, *Journal of the American Chemical Society*, 1990, **112**, 4307-4312.

28. H. Kobayashi, A. Friggeri, K. Koumoto, M. Amaike, S. Shinkai and D. N. Reinhoudt, *Organic Letters*, 2002, **4**, 1423-1426.
29. A. Srivastava, S. Ghorai, A. Bhattacharjya and S. Bhattacharya, *The Journal of Organic Chemistry*, 2005, **70**, 6574-6582.
30. F. Ono, K. Ichimaru, O. Hirata, S. Shinkai and H. Watanabe, *Chemistry Letters*, 2020, **49**, 156-159.
31. S. Yao, R. Brahmi, A. Bouschon, J. Chen and S. Halila, *Green Chemistry*, 2023, **25**, 330-335.
32. N. N. Adarsh, D. K. Kumar and P. Dastidar, *Tetrahedron*, 2007, **63**, 7386-7396.
33. R. Yoshisaki, S. Kimura, M. Yokoya and M. Yamanaka, *Chemistry – An Asian Journal*, 2021, **16**, 1937-1941.
34. D. Biswakarma, N. Dey and S. Bhattacharya, *Chemical Communications*, 2020, **56**, 7789-7792.
35. J.-A. Meunier, *Sur les composés que la mannite et la sorbite forment avec les aldéhydes*, Gauthier-Villars, 1891.
36. B. O. Okesola, V. M. P. Vieira, D. J. Cornwell, N. K. Whitelaw and D. K. Smith, *Soft Matter*, 2015, **11**, 4768-4787.
37. B. O. Okesola and D. K. Smith, *Chem Commun (Camb)*, 2013, **49**, 11164-11166.
38. C. C. Piras, A. G. Kay, P. G. Genever and D. K. Smith, *Chemical Science*, 2021, **12**, 3958-3965.
39. A. K. Patterson and D. K. Smith, *Chemical Communications*, 2020, **56**, 11046-11049.
40. E. J. Howe, B. O. Okesola and D. K. Smith, *Chemical Communications*, 2015, **51**, 7451-7454.
41. B. O. Okesola, S. K. Suravaram, A. Parkin and D. K. Smith, *Angewandte Chemie International Edition*, 2016, **55**, 183-187.
42. C. C. Piras, A. K. Patterson and D. K. Smith, *Chemistry – A European Journal*, 2021, **27**, 13203-13210.
43. C. C. Piras and D. K. Smith, *Chemistry – A European Journal*, 2019, **25**, 11318-11326.
44. L. Schlichter, C. C. Piras and D. K. Smith, *Chemical Science*, 2021, **12**, 4162-4172.
45. H. S. Cooke, L. Schlichter, C. C. Piras and D. K. Smith, *Chemical Science*, 2021, **12**, 12156-12164.
46. A. K. Patterson, L. H. El-Qarra and D. K. Smith, *Chemical Communications*, 2022, DOI: 10.1039/D1CC06942J.
47. G. M. Peters and J. T. Davis, *Chemical Society Reviews*, 2016, **45**, 3188-3206.
48. I. Bang, *Biochem. Z*, 1910, **26**, 293-311.
49. M. Gellert, M. N. Lipsett and D. R. Davies, *Proceedings of the National Academy of Sciences*, 1962, **48**, 2013-2018.
50. T. N. Plank and J. T. Davis, *Chemical Communications*, 2016, **52**, 5037-5040.
51. J. Dash, A. J. Patil, R. N. Das, F. L. Dowdall and S. Mann, *Soft Matter*, 2011, **7**, 8120-8126.
52. J. Hu, Q. Hu, X. He, C. Liu, Y. Kong, Y. Cheng and Y. Zhang, *Advanced Healthcare Materials*, 2020, **9**, 1901329.
53. K. J. Skilling, M. J. Stocks, B. Kellam, M. Ashford, T. D. Bradshaw, L. Burroughs and M. Marlow, *ChemMedChem*, 2018, **13**, 1098-1101.
54. T. Bhattacharyya, R. Chaudhuri, K. S. Das, R. Mondal, S. Mandal and J. Dash, *ACS Applied Bio Materials*, 2019, **2**, 3171-3177.
55. R. Vegners, I. Shestakova, I. Kalvinsh, R. M. Ezzell and P. A. Janmey, *Journal of Peptide Science*, 1995, **1**, 371-378.
56. A. M. Smith, R. J. Williams, C. Tang, P. Coppo, R. F. Collins, M. L. Turner, A. Saiani and R. V. Ulijn, *Advanced Materials*, 2008, **20**, 37-41.
57. J. Raeburn, G. Pont, L. Chen, Y. Cesbron, R. Lévy and D. J. Adams, *Soft Matter*, 2012, **8**, 1168-1174.
58. V. Prakash, Y. Christian, A. S. Redkar, A. Roy, R. Anandalakshmi and V. Ramakrishnan, *Soft Matter*, 2022, **18**, 6360-6371.
59. W. Li, X. Hu, J. Chen, Z. Wei, C. Song and R. Huang, *Journal of Materials Science: Materials in Medicine*, 2020, **31**, 73.

60. S. Debnath, A. Shome, D. Das and P. K. Das, *The Journal of Physical Chemistry B*, 2010, **114**, 4407-4415.
61. A. Croitoriu, L. E. Nita, A. G. Rusu, A. Ghilan, M. Bercea and A. P. Chiriac, *Polymers*, 2022, **14**, 3354.
62. R. Choe and S. I. Yun, *e-Polymers*, 2020, **20**, 458-468.
63. D. J. Adams, L. M. Mullen, M. Berta, L. Chen and W. J. Frith, *Soft Matter*, 2010, **6**, 1971-1980.
64. Y. Zhang, H. Gu, Z. Yang and B. Xu, *Journal of the American Chemical Society*, 2003, **125**, 13680-13681.
65. Z. Yang, G. Liang, L. Wang and B. Xu, *Journal of the American Chemical Society*, 2006, **128**, 3038-3043.
66. H. Arakawa, K. Takeda, S. L. Higashi, A. Shibata, Y. Kitamura and M. Ikeda, *Polymer Journal*, 2020, **52**, 923-930.
67. D. M. Raymond, B. L. Abraham, T. Fujita, M. J. Watrous, E. S. Toriki, T. Takano and B. L. Nilsson, *ACS Applied Bio Materials*, 2019, **2**, 2116-2124.
68. J. Raeburn, A. Zamith Cardoso and D. J. Adams, *Chemical Society Reviews*, 2013, **42**, 5143-5156.
69. C. Colquhoun, E. R. Draper, R. Schweins, M. Marcello, D. Vadukul, L. C. Serpell and D. J. Adams, *Soft Matter*, 2017, **13**, 1914-1919.
70. E. Quigley, J. Johnson, W. Liyanage and B. L. Nilsson, *Soft Matter*, 2020, **16**, 10158-10168.
71. V. Jayawarna, S. M. Richardson, A. R. Hirst, N. W. Hodson, A. Saiani, J. E. Gough and R. V. Ulijn, *Acta Biomaterialia*, 2009, **5**, 934-943.
72. A. Croitoriu, L. E. Nita, A. P. Chiriac, A. G. Rusu and M. Bercea, *Gels*, 2021, **7**, 208.
73. K. J. C. van Bommel, M. C. A. Stuart, B. L. Feringa and J. van Esch, *Organic & Biomolecular Chemistry*, 2005, **3**, 2917-2920.
74. L. Xu, M. Zhao, Y. Yang, Y. Liang, C. Sun, W. Gao, S. Li, B. He and Y. Pu, *Journal of Materials Chemistry B*, 2017, **5**, 9157-9164.
75. A. Friggeri, B. L. Feringa and J. van Esch, *Journal of Controlled Release*, 2004, **97**, 241-248.
76. W. Gao, Y. Liang, X. Peng, Y. Hu, L. Zhang, H. Wu and B. He, *Biomaterials*, 2016, **105**, 1-11.
77. B. Lorber, C. Sauter, A. Théobald-Dietrich, A. Moreno, P. Schellenberger, M. C. Robert, B. Capelle, S. Sanglier, N. Potier and R. Giegé, *Prog Biophys Mol Biol*, 2009, **101**, 13-25.
78. R. Contreras-Montoya, M. Arredondo-Amador, G. Escolano-Casado, M. C. Mañas-Torres, M. González, M. Conejero-Muriel, V. Bhatia, J. J. Díaz-Mochón, O. Martínez-Augustin, F. S. de Medina, M. T. Lopez-Lopez, F. Conejero-Lara, J. A. Gavira and L. Á. de Cienfuegos, *ACS Applied Materials & Interfaces*, 2021, **13**, 11672-11682.
79. S. Koutsopoulos, L. D. Unsworth, Y. Nagai and S. Zhang, *Proceedings of the National Academy of Sciences*, 2009, **106**, 4623-4628.
80. D. Limón, C. Jiménez-Newman, M. Rodrigues, A. González-Campo, D. B. Amabilino, A. C. Calpena and L. Pérez-García, *ChemistryOpen*, 2017, **6**, 585-598.
81. M. Ali and M. E. Byrne, *Expert Review of Clinical Pharmacology*, 2008, **1**, 145-161.
82. M. Ruponen and A. Urtti, *European Journal of Pharmaceutics and Biopharmaceutics*, 2015, **96**, 442-446.
83. X.-D. Xu, L. Liang, C.-S. Chen, B. Lu, N.-l. Wang, F.-G. Jiang, X.-Z. Zhang and R.-X. Zhuo, *ACS Applied Materials & Interfaces*, 2010, **2**, 2663-2671.
84. X. Yu, Z. Zhang, J. Yu, H. Chen and X. Li, *Nanomedicine: Nanotechnology, Biology and Medicine*, 2018, **14**, 185-193.
85. Z. Zhang, J. Yu, Y. Zhou, R. Zhang, Q. Song, L. Lei and X. Li, *Colloids and Surfaces B: Biointerfaces*, 2018, **164**, 436-443.
86. S. Senapati, A. K. Mahanta, S. Kumar and P. Maiti, *Signal Transduction and Targeted Therapy*, 2018, **3**, 7.
87. S. He, L. Mei, C. Wu, M. Tao, Z. Zhai, K. Xu and W. Zhong, *Nanoscale*, 2019, **11**, 5030-5037.
88. L. C. Costello and R. B. Franklin, *Archives of Biochemistry and Biophysics*, 2016, **611**, 100-112.

89. J. Wu, G. Li, L. Li, D. Li, Z. Dong and P. Jiang, *Nature Cell Biology*, 2021, **23**, 75-86.
90. J. Qi, T. Ding, T. Liu, X. Xia, S. Wu, J. Liu, Q. Chen, D. Zhang and H. Zhao, *Advanced Functional Materials*, 2022, **32**, 2204273.
91. H. Zhao, H. Feng, J. Liu, F. Tang, Y. Du, N. Ji, L. Xie, X. Zhao, Z. Wang and Q. Chen, *Biomaterials*, 2020, **230**, 119598.
92. F. Tang, H. Feng, Y. Du, Y. Xiao, H. Dan, H. Zhao and Q. Chen, *Chemistry – An Asian Journal*, 2018, **13**, 1962-1971.
93. B. V. Slaughter, S. S. Khurshid, O. Z. Fisher, A. Khademhosseini and N. A. Peppas, *Adv Mater*, 2009, **21**, 3307-3329.
94. S. Mantha, S. Pillai, P. Khayambashi, A. Upadhyay, Y. Zhang, O. Tao, H. M. Pham and S. D. Tran, *Materials*, 2019, **12**, 3323.
95. J. Hoque, N. Sangaj and S. Varghese, *Macromolecular Bioscience*, 2019, **19**, 1800259.
96. J. K. Mouw, G. Ou and V. M. Weaver, *Nat Rev Mol Cell Biol*, 2014, **15**, 771-785.
97. R. G. Ellis-Behnke, Y.-X. Liang, S.-W. You, D. K. C. Tay, S. Zhang, K.-F. So and G. E. Schneider, *Proceedings of the National Academy of Sciences*, 2006, **103**, 5054-5059.
98. G. A. Silva, C. Czeisler, K. L. Niece, E. Beniash, D. A. Harrington, J. A. Kessler and S. I. Stupp, *Science*, 2004, **303**, 1352-1355.
99. X. Li, S. Bian, M. Zhao, X. Han, J. Liang, K. Wang, Q. Jiang, Y. Sun, Y. Fan and X. Zhang, *Acta Biomaterialia*, 2021, **131**, 128-137.
100. H. Najafi, A. M. Tamaddon, S. Abolmaali, S. Borandeh and N. Azarpira, *Soft Matter*, 2021, **17**, 57-67.
101. Y. Hu, W. Gao, F. Wu, H. Wu, B. He and J. He, *Journal of Materials Chemistry B*, 2016, **4**, 3504-3508.
102. E. T. Pashuck, H. Cui and S. I. Stupp, *J Am Chem Soc*, 2010, **132**, 6041-6046.
103. J. M. Godbe, R. Freeman, L. F. Burbulla, J. Lewis, D. Krainc and S. I. Stupp, *ACS Biomaterials Science & Engineering*, 2020, **6**, 1196-1207.
104. C. C. Piras, P. G. Genever and D. K. Smith, *Materials Advances*, 2022, **3**, 7966-7975.
105. M. Merino-Gómez, M. Godoy-Gallardo, M. Wendner, M. A. Mateos-Timoneda, F. J. Gil and R. A. Perez, *Front Bioeng Biotechnol*, 2023, **11**, 1147943.
106. J. Y. Chia, T. Miki, H. Mihara and H. Tsutsumi, *Bioorganic & Medicinal Chemistry*, 2021, **46**, 116345.
107. C. C. Piras, P. Slavik and D. K. Smith, *Angewandte Chemie International Edition*, 2020, **59**, 853-859.
108. E. F. Banwell, E. S. Abelardo, D. J. Adams, M. A. Birchall, A. Corrigan, A. M. Donald, M. Kirkland, L. C. Serpell, M. F. Butler and D. N. Woolfson, *Nature Materials*, 2009, **8**, 596-600.
109. Y. Zhang and Y. Huang, *Frontiers in Chemistry*, 2021, **8**.
110. K. Hawkins, A. Patterson, P. Clarke and D. Smith, *Journal of the American Chemical Society*, 2020, **XXXX**.
111. J. Skopinska-Wisniewska, S. De la Flor and J. Kozlowska, *Int J Mol Sci*, 2021, **22**.
112. H. M. Willemen, T. Vermonden, A. T. M. Marcelis and E. J. R. Sudhölter, *Langmuir*, 2002, **18**, 7102-7106.
113. H. Shigemitsu and I. Hamachi, *Accounts of Chemical Research*, 2017, **50**, 740-750.
114. K. Baek, A. D. Noblett, P. Ren and L. J. Suggs, *ACS Applied Bio Materials*, 2019, **2**, 2812-2821.
115. M. de Loos, B. L. Feringa and J. H. van Esch, *European Journal of Organic Chemistry*, 2005, **2005**, 3615-3631.
116. K. Hawkins, *Catalytic Hydrogels with a Prebiotic Nature*, University of York, 2019.
117. J. H. E. Arts, H. Muijser, M. J. Appel, C. Frieke Kuper, J. G. M. Bessems and R. A. Woutersen, *Food and Chemical Toxicology*, 2004, **42**, 1389-1399.
118. I. Parseh, Y. Hajizadeh, N. Jaafarzadeh, G. Goudarzi, G. Shakerinejad, A. Badeenezhad, N. Mengelizadeh and S. Fallahizadeh, *Process Safety and Environmental Protection*, 2021, **149**, 135-143.

119. E. R. Draper and D. J. Adams, *Chem*, 2017, **3**, 390-410.
120. D. J. Adams, *Journal of the American Chemical Society*, 2022, **144**, 11047-11053.
121. R. N. Shah, N. A. Shah, M. M. Del Rosario Lim, C. Hsieh, G. Nuber and S. I. Stupp, *Proceedings of the National Academy of Sciences*, 2010, **107**, 3293.
122. M. Laurenti, A. Al Subaie, M.-N. Abdallah, A. R. G. Cortes, J. L. Ackerman, H. Vali, K. Basu, Y. L. Zhang, M. Murshed, S. Strandman, J. Zhu, N. Makhoul, J. E. Barralet and F. Tamimi, *Nano Letters*, 2016, **16**, 4779-4787.
123. H. Liu, Y. Hu, H. Wang, J. Wang, D. Kong, L. Wang, L. Chen and Z. Yang, *Soft Matter*, 2011, **7**, 5430-5436.
124. E. H. Cordes and W. P. Jencks, *Journal of the American Chemical Society*, 1962, **84**, 832-837.
125. R. G. Weiss, *Langmuir*, 2009, **25**, 8369.
126. P. Terech, I. Furman and R. G. Weiss, *The Journal of Physical Chemistry*, 1995, **99**, 9558-9566.
127. D. J. Adams, *Gels*, 2018, **4**, 32.
128. N. D. Bansode, K. R. Sindhu, C. Morel, M. Rémy, J. Verget, C. Boiziau and P. Barthélémy, *Biomaterials Science*, 2020, **8**, 3186-3192.
129. D. J. Cornwell and D. K. Smith, *Materials Horizons*, 2015, **2**, 279-293.
130. S. Liu, H. Li, B. Tang, S. Bi and L. Li, *Carbohydrate Polymers*, 2016, **135**, 101-109.
131. L. Aguero, S. Alpdagtas, E. Ilhan, D. Zaldivar-Silva and O. Gunduz, *European Polymer Journal*, 2021, **160**, 110807.
132. S. N. Pawar and K. J. Edgar, *Biomaterials*, 2012, **33**, 3279-3305.
133. N. Osafo, C. Agyare, D. D. Obiri and A. O. Antwi, InTech, 2017, DOI: 10.5772/68090.
134. I. L. Meek, M. A. F. J. Van de Laar and H. E Vonkeman, *Pharmaceuticals (Basel)*, 2010, **3**, 2146-2162.
135. P. R. A. Chivers and D. K. Smith, *Chemical Science*, 2017, **8**, 7218-7227.
136. H. Vilaça, A. C. L. Hortelão, E. M. S. Castanheira, M.-J. R. P. Queiroz, L. Hilliou, I. W. Hamley, J. A. Martins and P. M. T. Ferreira, *Biomacromolecules*, 2015, **16**, 3562-3573.
137. E. Beetge, J. du Plessis, D. G. Müller, C. Goosen and F. J. van Rensburg, *International Journal of Pharmaceutics*, 2000, **193**, 261-264.
138. C. M. White, *The Journal of Clinical Pharmacology*, 2002, **42**, 963-970.
139. P. R. Kamble, K. S. Shaikh and P. D. Chaudhari, *Adv Pharm Bull*, 2014, **4**, 197-204.
140. P. Tiwari, A. Gupta, R. R. Mehra, N. Khan, J. Harjit, C. R. Ashby, A. Basu, A. K. Tiwari, M. Singh and A. Dutt Konar, *Supramolecular Chemistry*, 2020, **32**, 495-507.
141. J. Quirk, M. Thornton and P. Kirkpatrick, *Nature Reviews Drug Discovery*, 2003, **2**, 769-770.
142. G. Das, *Int J Clin Pharmacol Ther Toxicol*, 1989, **27**, 473-477.
143. U. Mathis, M. P. Feldkaemper and F. Schaeffel, *Ophthalmic Research*, 2021, **64**, 664-674.
144. I. G. Morgan, K. Ohno-Matsui and S.-M. Saw, *The Lancet*, 2012, **379**, 1739-1748.
145. J. Cheng, Y. Yang, X. Kong, L. Zeng, Z. Chen, J. Xu and C. Zhang, *Ther Clin Risk Manag*, 2020, **16**, 735-740.
146. A. Chia, W. H. Chua, Y. B. Cheung, W. L. Wong, A. Lingham, A. Fong and D. Tan, *Ophthalmology*, 2012, **119**, 347-354.
147. M.-N. Chuang, P.-C. Fang and P.-C. Wu, *Scientific Reports*, 2021, **11**, 17344.
148. J. R. Polling, E. Tan, S. Driessen, S. E. Loudon, H.-L. Wong, A. van der Schans, J. W. L. Tideman and C. C. W. Klaver, *Eye*, 2020, **34**, 2020-2028.
149. A. Chia, W.-H. Chua, L. Wen, A. Fong, Y. Y. Goon and D. Tan, *American Journal of Ophthalmology*, 2014, **157**, 451-457.e451.
150. J. Saito, H. Imaizumi and A. Yamatani, *Journal of Pharmaceutical Health Care and Sciences*, 2019, **5**, 25.
151. Y. Jiang, Z. Zhang, Z. Wu, S. Sun, Y. Fu and B. Ke, *Current Eye Research*, 2021, **46**, 1171-1177.
152. L. T. Lim, E. Y. Ah-Kee and C. E. Collins, *Int J Ophthalmol*, 2014, **7**, 1067-1068.
153. R. Liang, Z. Luo, G. Pu, W. Wu, S. Shi, J. Yu, Z. Zhang, H. Chen and X. Li, *RSC Advances*, 2016, **6**, 76093-76098.

154. K. Thomson, C. Karouta and R. S. Ashby, *Investigative Ophthalmology & Visual Science*, 2020, **61**, 3397-3397.
155. V. M. P. Vieira, A. C. Lima, M. de Jong and D. K. Smith, *Chemistry – A European Journal*, 2018, **24**, 15112-15118.
156. C. C. Piras and D. K. Smith, *Journal of Materials Chemistry B*, 2020, **8**, 8171-8188.
157. J. Benfica, J. S. Miranda, E. S. Morais, M. G. Freire, J. A. P. Coutinho and R. de Cássia Superbi de Sousa, *ACS Sustainable Chemistry & Engineering*, 2020, **8**, 6682-6689.
158. *New England Journal of Medicine*, 2004, **351**, 2498-2508.
159. M. Kardasevic and S. M. Dinarevic, *Med Arch*, 2021, **75**, 158-161.
160. E. Baselga, B. Dembowska-Baginska, P. Przewratil, M. A. González-Enseñat, D. Wyrzykowski, A. Torrelo, J. C. López Gutiérrez, M. Rychłowska-Pruszyńska, R. de Lucas-Laguna, A. Esteve-Martinez, E. Roé, M. Zaim, Y. Menon, S. Gautier, G. Lebbé, A. Bouroubi, A. Delarue and J. J. Voisard, *Pediatrics*, 2018, **142**.
161. M. F. Raphael, J. M. P. J. Breur, F. A. E. Vlasveld, N. J. Elbert, Y. T. B. Liem, M. Kon, C. C. Breugem and S. G. M. A. Pasmans, *Expert Opinion on Drug Safety*, 2016, **15**, 199-214.
162. V. Campbell, R. Beckett, N. Abid and S. Hoey, *J Clin Res Pediatr Endocrinol*, 2018, **10**, 294-298.
163. C. Léauté-Labrèze, P. Hoeger, J. Mazereeuw-Hautier, L. Guibaud, E. Baselga, G. Posiunas, R. J. Phillips, H. Caceres, J. C. Lopez Gutierrez, R. Ballona, S. F. Friedlander, J. Powell, D. Perek, B. Metz, S. Barbarot, A. Maruani, Z. Z. Szalai, A. Krol, O. Boccara, R. Foelster-Holst, M. I. Bosch, J. Su, H. Buckova, A. Torrelo, F. Cambazard, R. Grantzow, O. Wargon, D. Wyrzykowski, J. Roessler, J. Bernabeu-Wittel, A. M. Valencia, P. Przewratil, S. Glick, E. Pope, N. Birchall, L. Benjamin, A. J. Mancini, P. Vabres, P. Souteyrand, I. J. Frieden, C. I. Berul, C. R. Mehta, S. Prey, F. Boralevi, C. C. Morgan, S. Heritier, A. Delarue and J.-J. Voisard, *New England Journal of Medicine*, 2015, **372**, 735-746.
164. C. Léauté-Labrèze, E. D. de la Roque, T. Hubiche, F. Boralevi, J.-B. Thambo and A. Taïeb, *New England Journal of Medicine*, 2008, **358**, 2649-2651.
165. X. Ma, T. Zhao, T. Ouyang, S. Xin, Y. Ma and M. Chang, *Int J Clin Exp Pathol*, 2014, **7**, 3809-3817.
166. C. H. Storch and P. H. Hoeger, *British Journal of Dermatology*, 2010, **163**, 269-274.
167. X. Ma, T. Zhao, Y. Xiao, J. Yu, H. Chen, Y. Huang, J. Liu, J. Lin and T. Ouyang, *Eur J Pediatr*, 2013, **172**, 653-659.
168. M. Kovačević, V. Lukinović Škudar, G. Maričić, G. Krnjević-Pezić and A. Stanimirović, *Acta Dermatovenerol Alp Pannonica Adriat*, 2014, **23**, 75-78.
169. Y. N. Zhai, H. T. Song, S. Q. Chen, M. X. Zhang, C. J. Li, Y. Xia and L. Wang, *Zhonghua Zheng Xing Wai Ke Za Zhi*, 2013, **29**, 25-28.
170. M. Schneider, A. Reimer, H. Cremer and P. Ruef, *World Journal of Pediatrics*, 2014, **10**, 313-317.
171. C. C. Piras, C. S. Mahon and D. K. Smith, *Chemistry – A European Journal*, 2020, **26**, 8452-8457.
172. C. C. Piras and D. K. Smith, *Chemistry – A European Journal*, 2021, **27**, 14527-14534.
173. Z. Yue, C. Li, G. A. Voth and J. M. J. Swanson, *Journal of the American Chemical Society*, 2019, **141**, 13421-13433.
174. S. Srivastava, S. Kapoor and P. S. Saraf, *Indian Journal of Pharmaceutical Education and Research*, 2008, **42**, 170-173.
175. P. J. Gupta, *Eur Rev Med Pharmacol Sci*, 2007, **11**, 165-170.
176. S. Sah and P. Kothiyal, *Indian Journal of Pharmaceutical and Biological Research*, 2016, **4**, 20-26.
177. C. C. Piras, A. G. Kay, P. G. Genever, J. Fitremann and D. K. Smith, *Chemical Science*, 2022, **13**, 1972-1981.
178. S. J. Lee, D. N. Heo, J. S. Park, S. K. Kwon, J. H. Lee, J. H. Lee, W. D. Kim, I. K. Kwon and S. A. Park, *Physical Chemistry Chemical Physics*, 2015, **17**, 2996-2999.
179. Z. Chen, J. Song, Y. Xia, Y. Jiang, L. L. Murillo, O. Tsigkou, T. Wang and Y. Li, *Materials Science and Engineering: C*, 2021, **127**, 112204.

180. E. N. Drew, C. C. Piras, J. Fitremann and D. K. Smith, *Chemical Communications*, 2022, DOI: 10.1039/D2CC04003D.
181. F. Andriamiseza, D. Bordignon, B. Payré, L. Vaysse and J. Fitremann, *Journal of Colloid and Interface Science*, 2022, **617**, 156-170.
182. G. Nicastro, L. M. Black, P. Ravarino, S. d'Agostino, D. Faccio, C. Tomasini and D. Giuri, *International Journal of Molecular Sciences*, 2022, **23**, 3105.
183. E. H. Cordes and W. P. Jencks, *Journal of the American Chemical Society*, 1963, **85**, 2843-2848.
184. P. Misra, B. Mishra and G. Behera, *International Journal of Chemical Kinetics - INT J CHEM KINET*, 1991, **23**, 639-654.
185. R. R. S. Thakur, H. L. McMillan and D. S. Jones, *Journal of Controlled Release*, 2014, **176**, 8-23.
186. F. M. DUNAGAN, P. E. McGILL, A. W. KELMAN and B. WHITING, *Rheumatology*, 1988, **27**, 48-53.
187. S. Liu, L. Tan, D. Pan and Y. Chen, *Polymer International*, 2011, **60**, 453-457.
188. L. Zhou, H. Ramezani, M. Sun, M. Xie, J. Nie, S. Lv, J. Cai, J. Fu and Y. He, *Biomaterials Science*, 2020, **8**, 5020-5028.
189. F. Puza and K. Lienkamp, *Advanced Functional Materials*, 2022, **32**, 2205345.
190. Y. Wu, Y. Zeng, Y. Chen, C. Li, R. Qiu and W. Liu, *Advanced Functional Materials*, 2021, **31**, 2107202.
191. S. Piluso, G. A. Skvortsov, M. Altunbek, F. Afghah, N. Khani, B. Koç and J. Patterson, *Biofabrication*, 2021, **13**.
192. P. Dorishetty, R. Balu, A. Gelmi, J. P. Mata, N. K. Dutta and N. R. Choudhury, *Biomacromolecules*, 2021, **22**, 3668-3678.
193. S. Hong and J. M. Song, *Biomaterials Science*, 2021, **9**, 5939-5950.
194. H. Jian, M. Wang, Q. Dong, J. Li, A. Wang, X. Li, P. Ren and S. Bai, *ACS Applied Materials & Interfaces*, 2019, **11**, 46419-46426.
195. Z. Zhou, M. Samperi, L. Santu, G. Dizon, S. Aboarkaba, D. Limón, C. Tuck, L. Pérez-García, D. J. Irvine, D. B. Amabilino and R. Wildman, *Materials & Design*, 2021, **206**, 109792.
196. M. C. Nolan, A. M. Fuentes Caparrós, B. Dietrich, M. Barrow, E. R. Cross, M. Bleuel, S. M. King and D. J. Adams, *Soft Matter*, 2017, **13**, 8426-8432.
197. M. J. S. Hill and D. J. Adams, *Soft Matter*, 2022, **18**, 5960-5965.
198. K. Firipis, D. R. Nisbet, S. J. Franks, R. M. I. Kapsa, E. Pirogova, R. J. Williams and A. Quigley, *Polymers*, 2021, **13**, 2590.
199. A. Zaszczyńska, M. Moczulska-Heljak, A. Gradys and P. Sajkiewicz, *Materials (Basel)*, 2021, **14**.
200. S. James, J. Fox, F. Afsari, J. Lee, S. Clough, C. Knight, J. Ashmore, P. Ashton, O. Preham, M. Hoogduijn, A. Ponzoni Rde, Y. Hancock, M. Coles and P. Genever, *Stem Cell Reports*, 2015, **4**, 1004-1015.
201. R. ENOMOTO, C. SUZUKI, M. OHNO, T. OHASI, R. FUTAGAMI, K. ISHIKAWA, M. KOMAE, T. NISHINO, Y. KONISHI and E. LEE, *Annals of the New York Academy of Sciences*, 2007, **1095**, 1-6.
202. Y. Chen, F. Qiao, Y. Fan, Y. Han and Y. Wang, *The Journal of Physical Chemistry B*, 2017, **121**, 7122-7132.
203. Z. Ulker, L. Alpsoy and A. Mihmanli, *Human & Experimental Toxicology*, 2013, **32**, 858-864.

Appendix

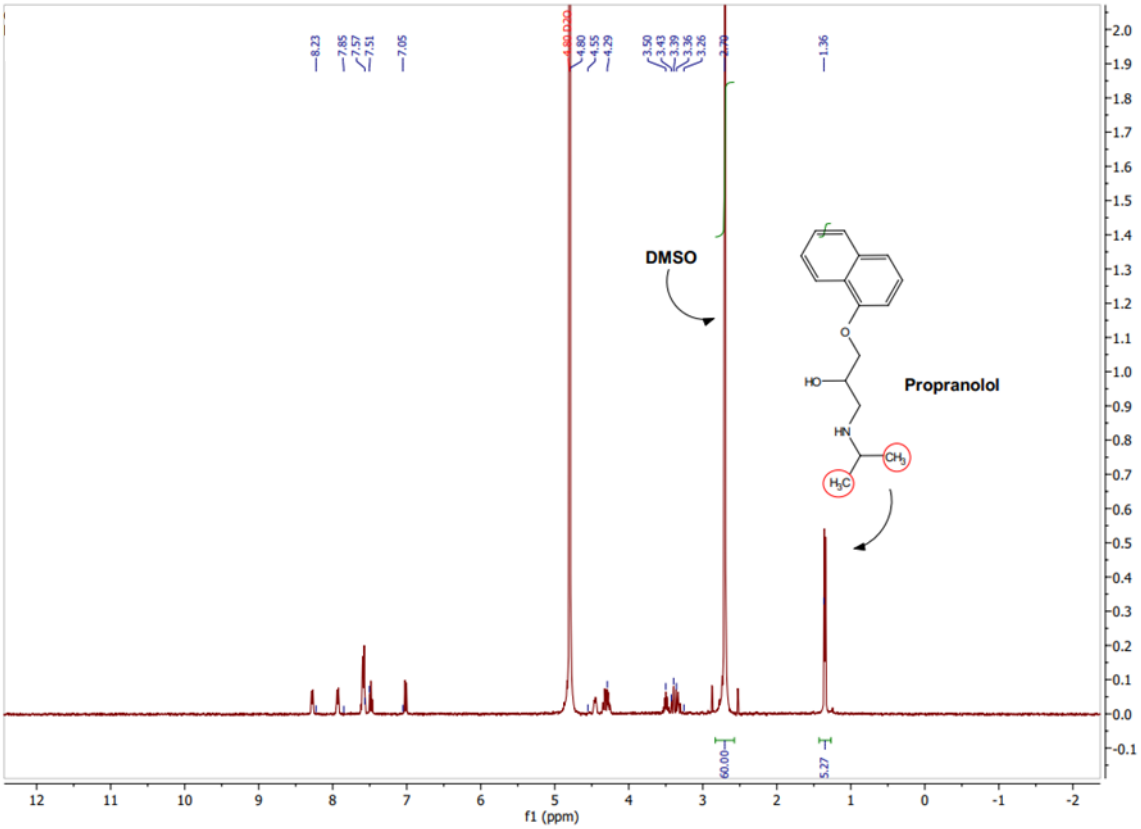

Figure 133. ^{1}H NMR spectrum of supernatant to load Benzyl glutamine/ Agarose beads with propranolol in D_2O.

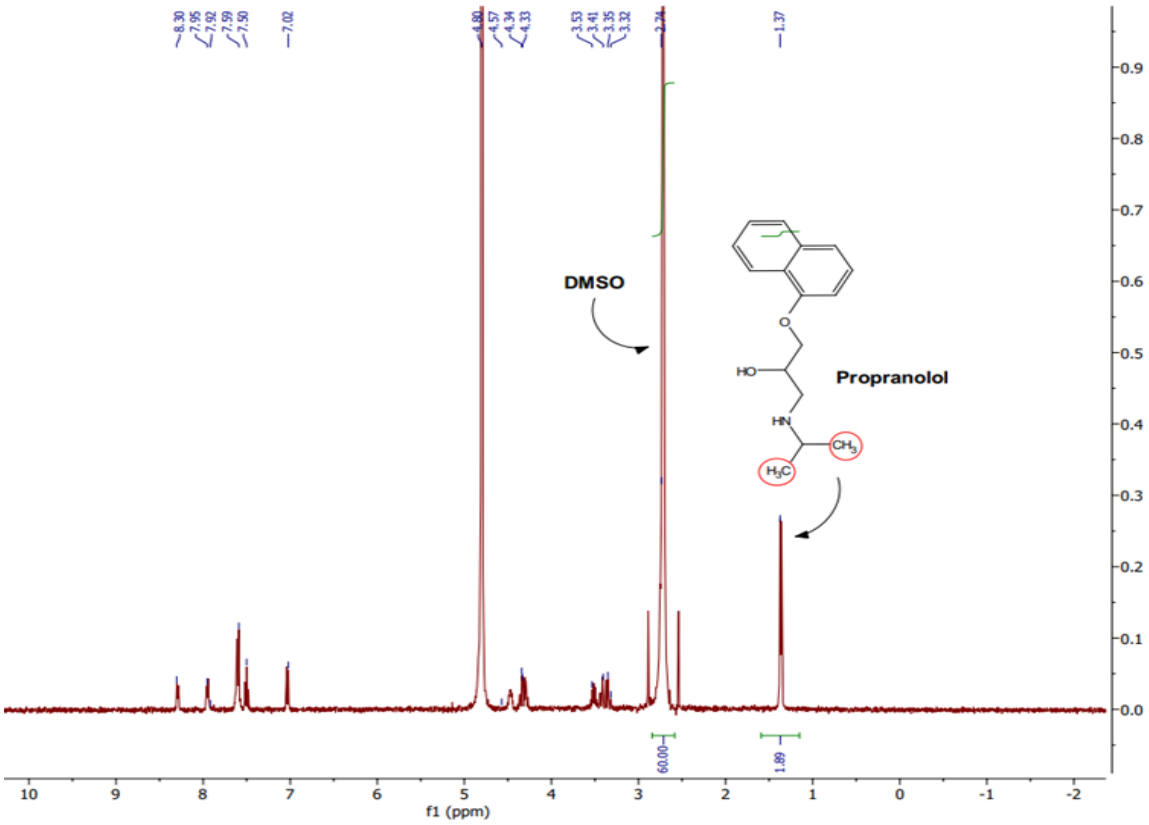

Figure 134. ^{1}H NMR spectrum of supernatant used to load DBS-COOH/Alginate beads with propranolol in D_2O.

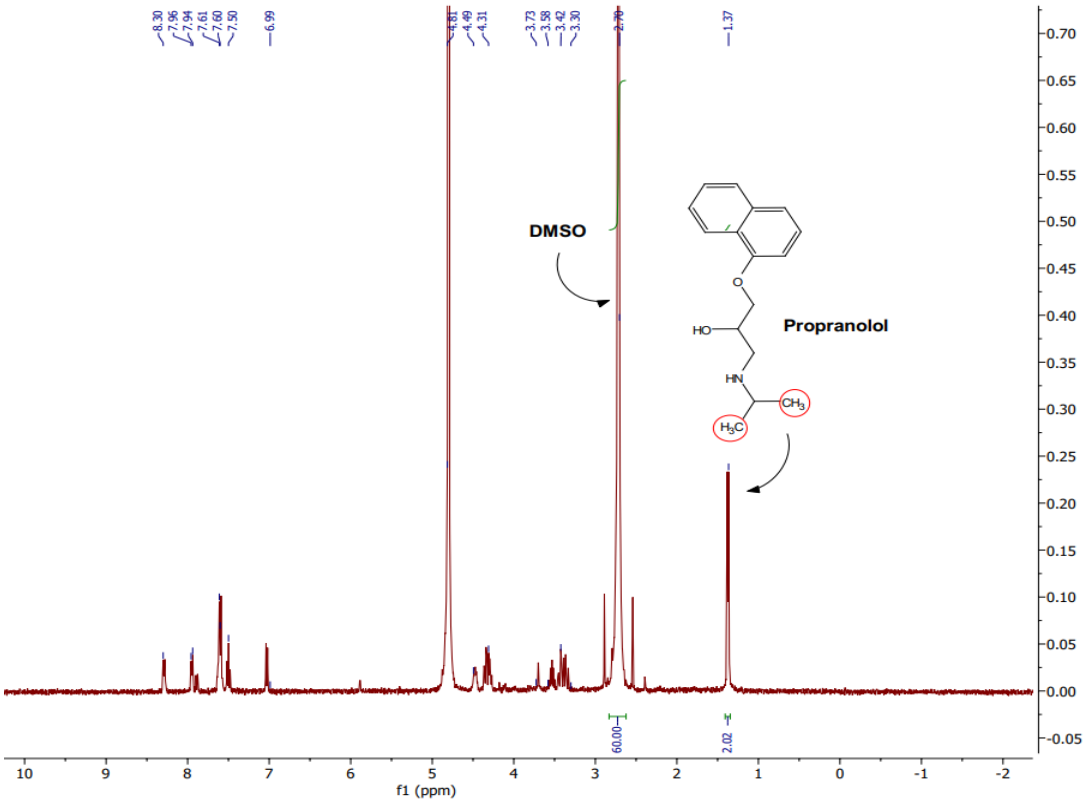

Figure 135. ^{1}H NMR spectrum of supernatant used to load DBS-COOH/ Agarose beads with propranolol in D_2O.

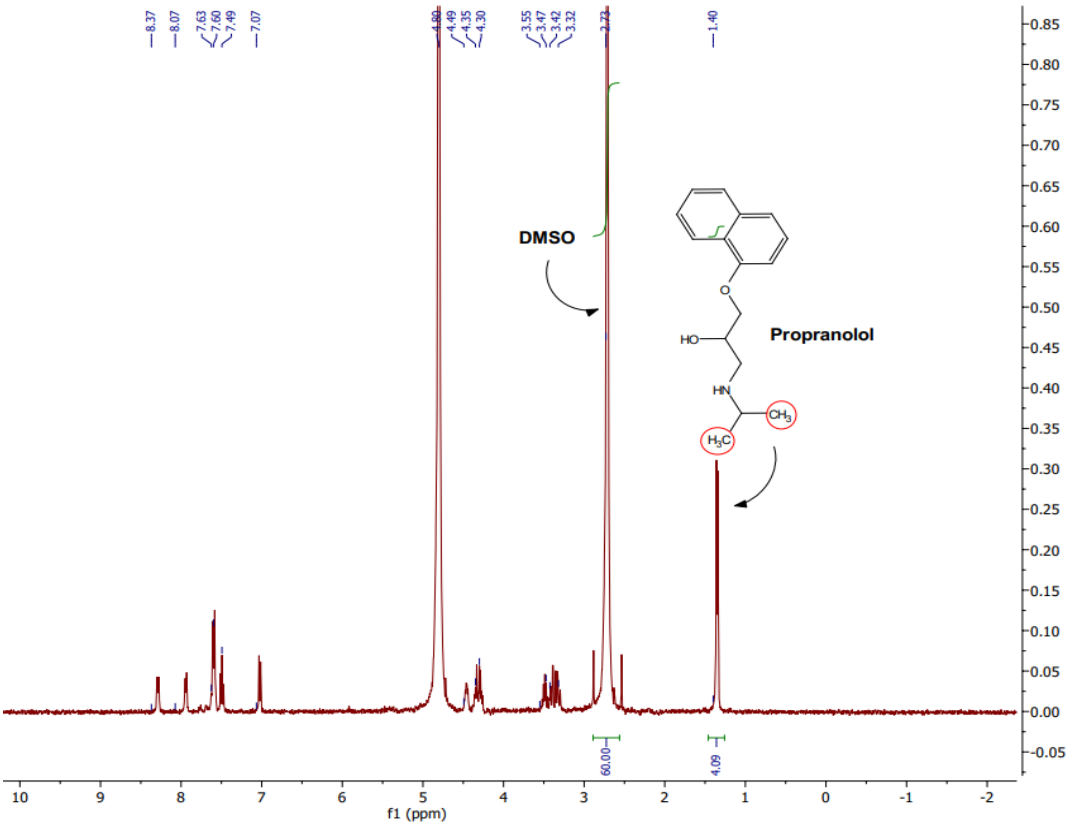

Figure 136. ^{1}H NMR spectrum of supernatant used to load DBS-CONHNH$_2$/Alginate beads with propranolol in D_2O.

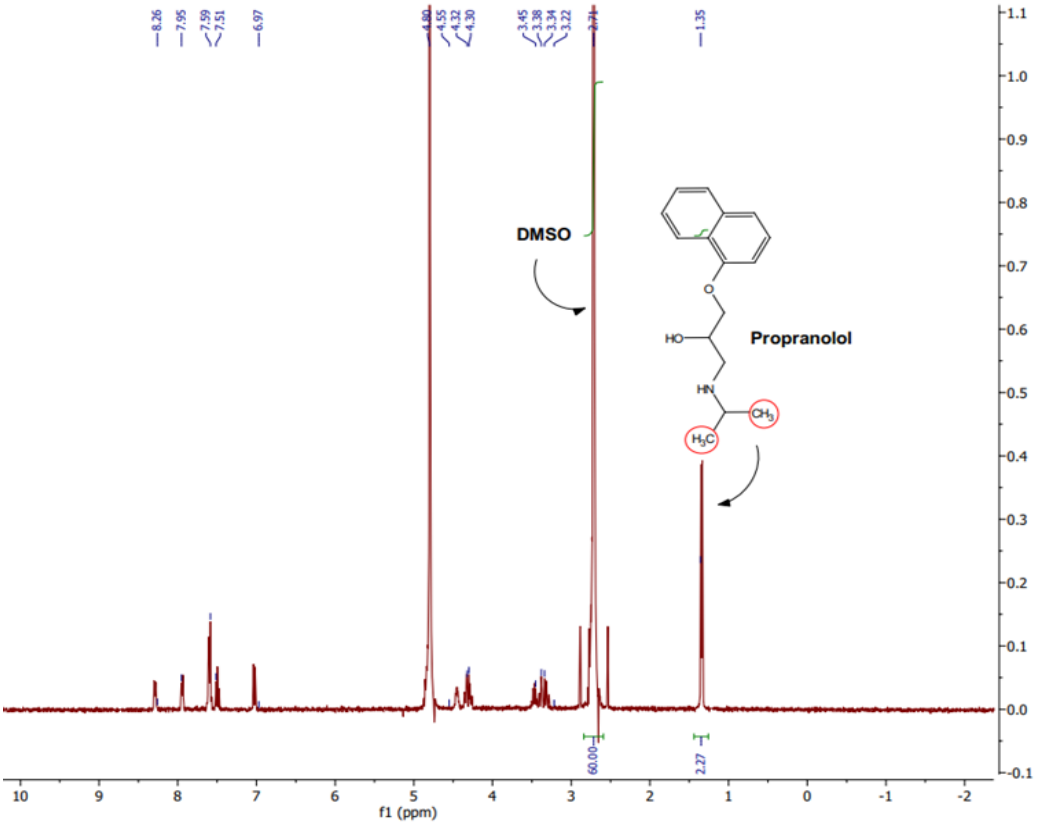

Figure 137. ^{1}H NMR spectrum of supernatant used to load DBS-CONHNH$_2$/ Agarose beads with propranolol in D_2O.

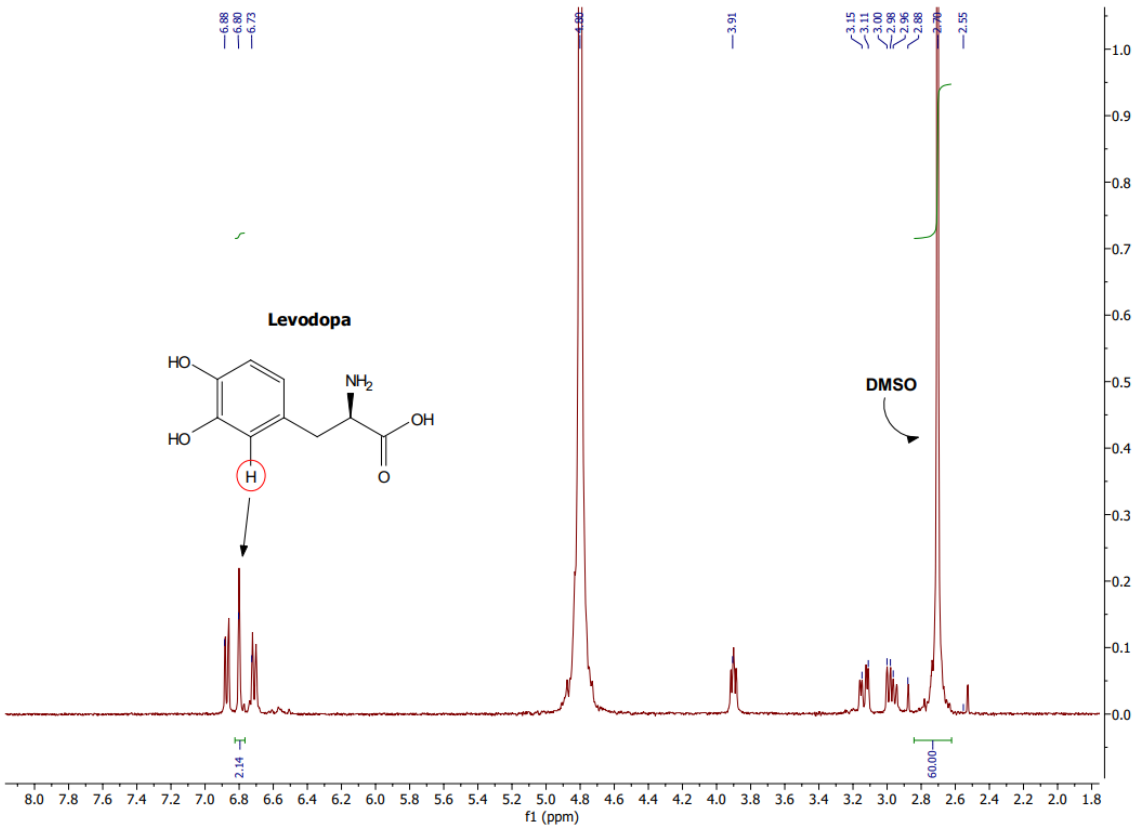

Figure 138. ^{1}H NMR spectrum of supernatant used to load Benzyl glutamine/ Agarose beads with levodopa dissolved in D_2O.

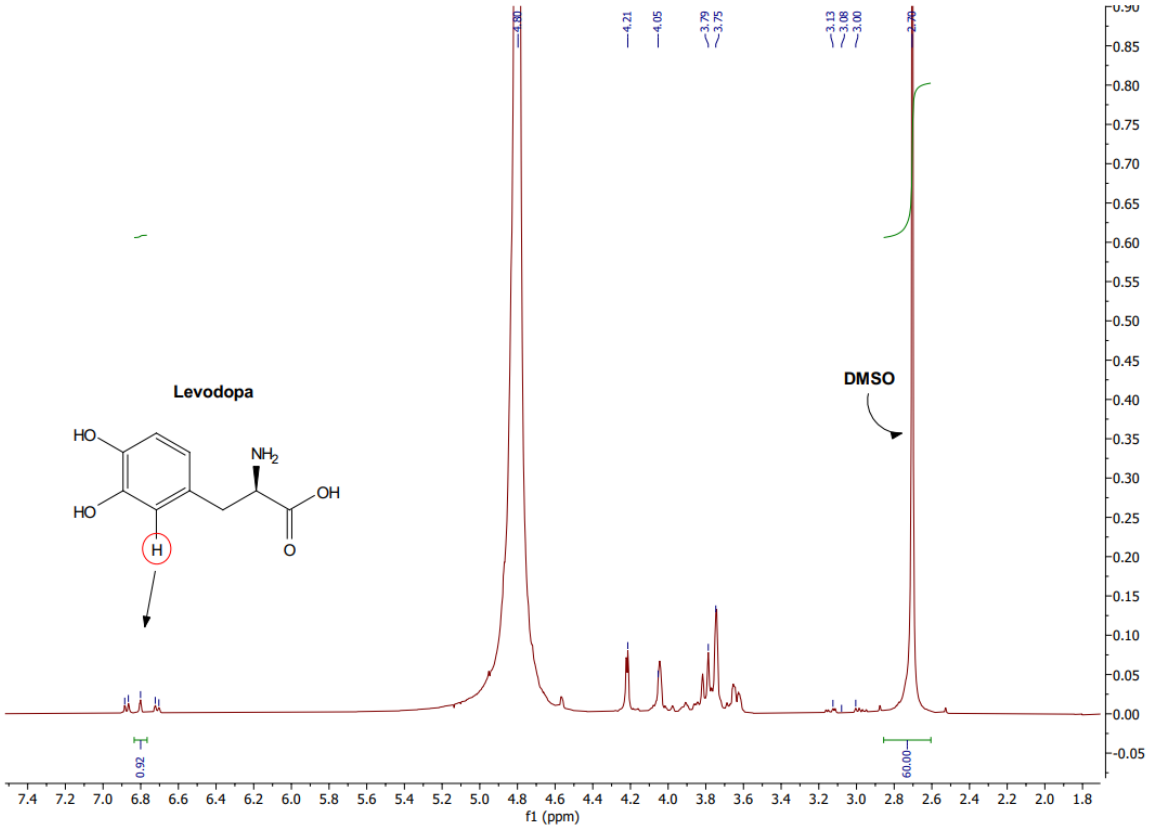

Figure 139. ^{1}H NMR spectrum of supernatant used to load DBS-COOH with levodopa dissolved in D_2O.

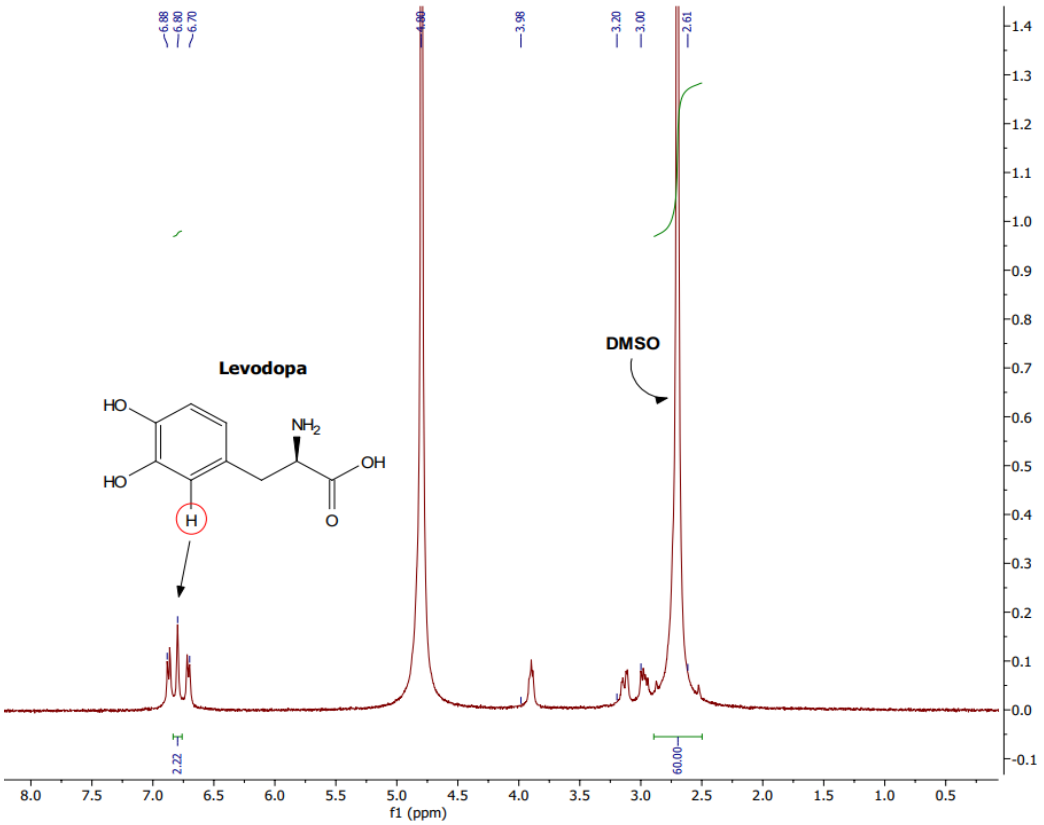

Figure 140. ^{1}H NMR spectrum of supernatant used to load DBS-COOH/Alginate beads with levodopa in D_2O.

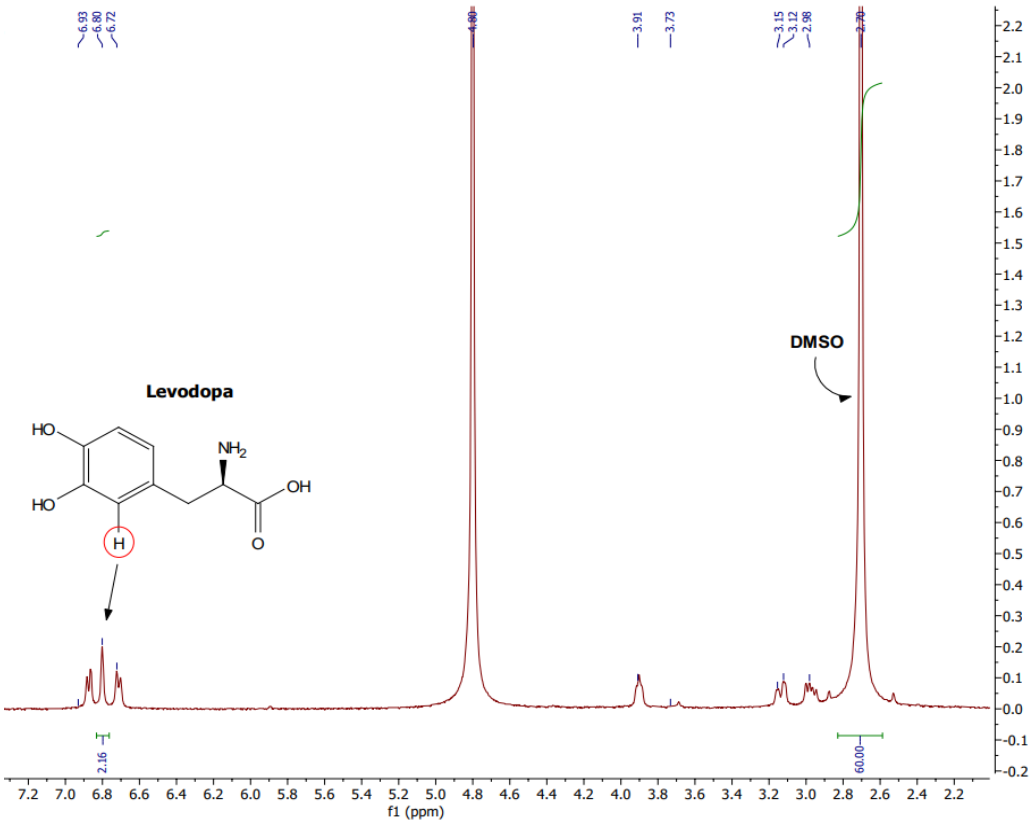

Figure 141. ^{1}H NMR spectrum of supernatant used to load DBS-COOH/agarose with levodopa dissolved in D_2O.

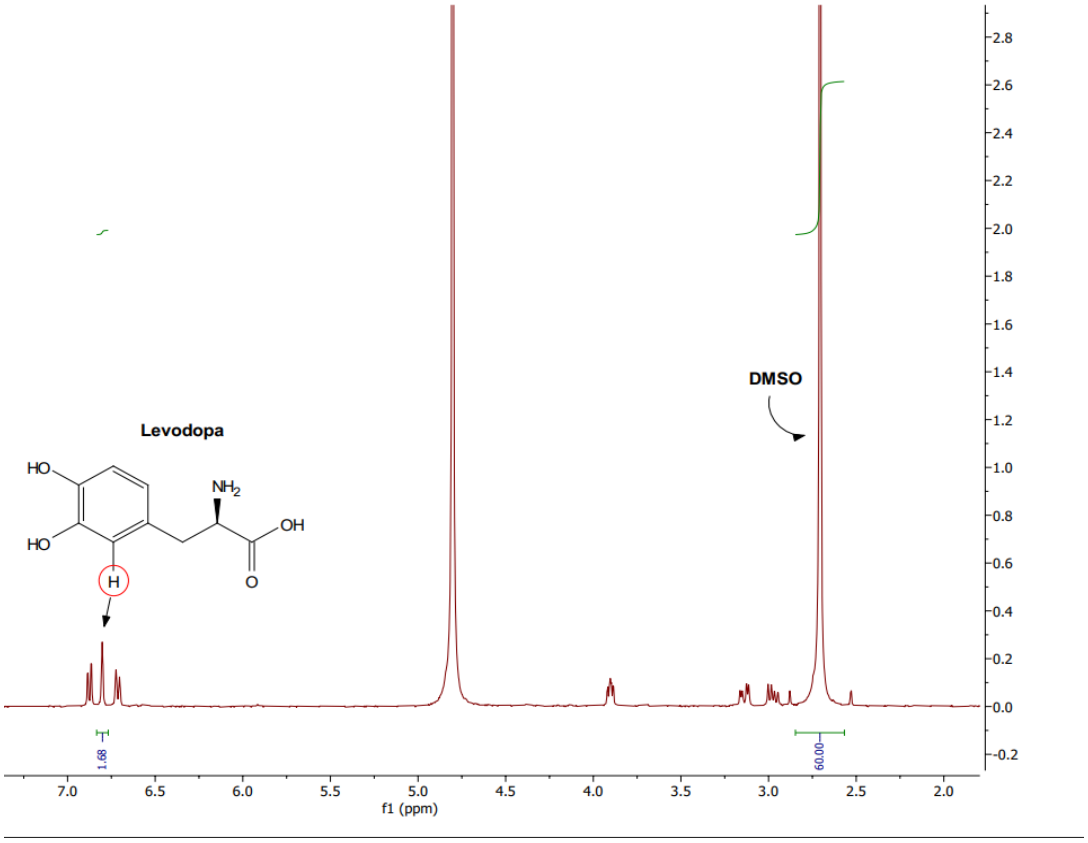

Figure 142. ^{1}H NMR spectrum of supernatant used to load DBS-$CONHNH_2$ with levodopa dissolved in D_2O.

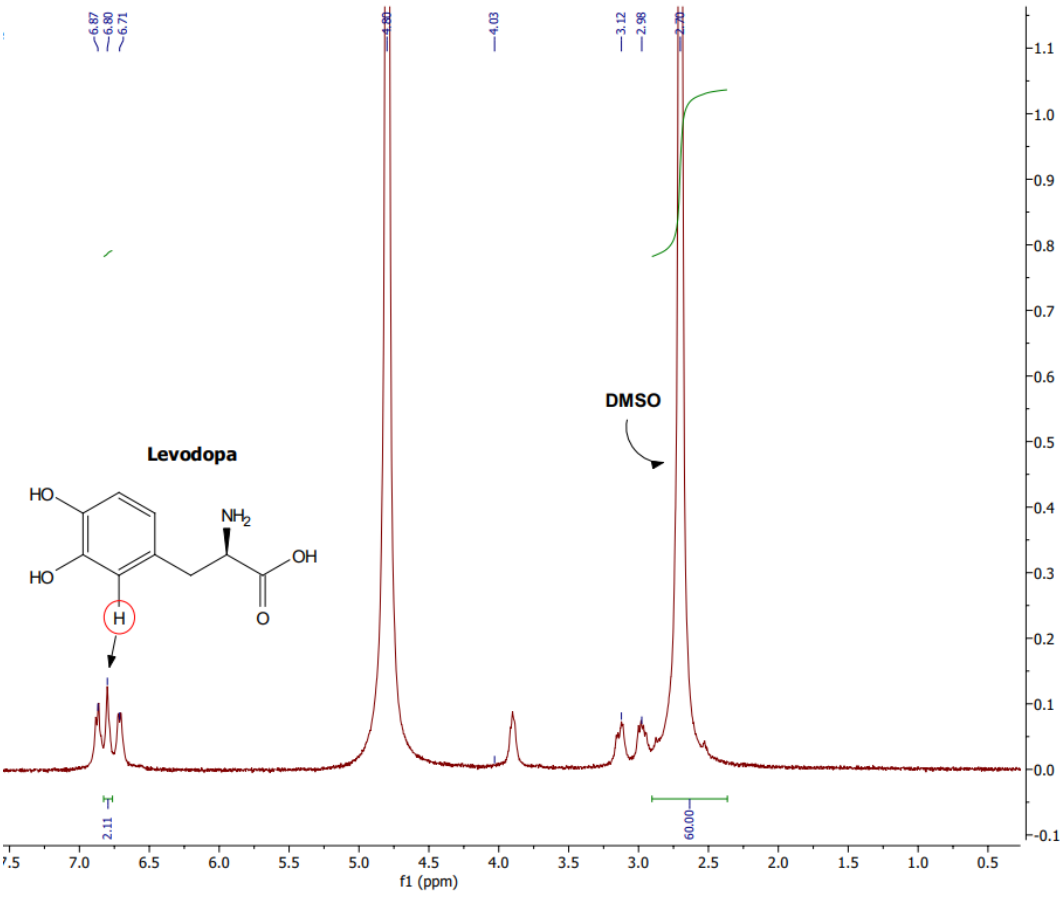

Figure 143. ^{1}H NMR spectrum of supernatant used to load DBS-CONHNH$_2$/Alginate beads with levodopa dissolved in D_2O.

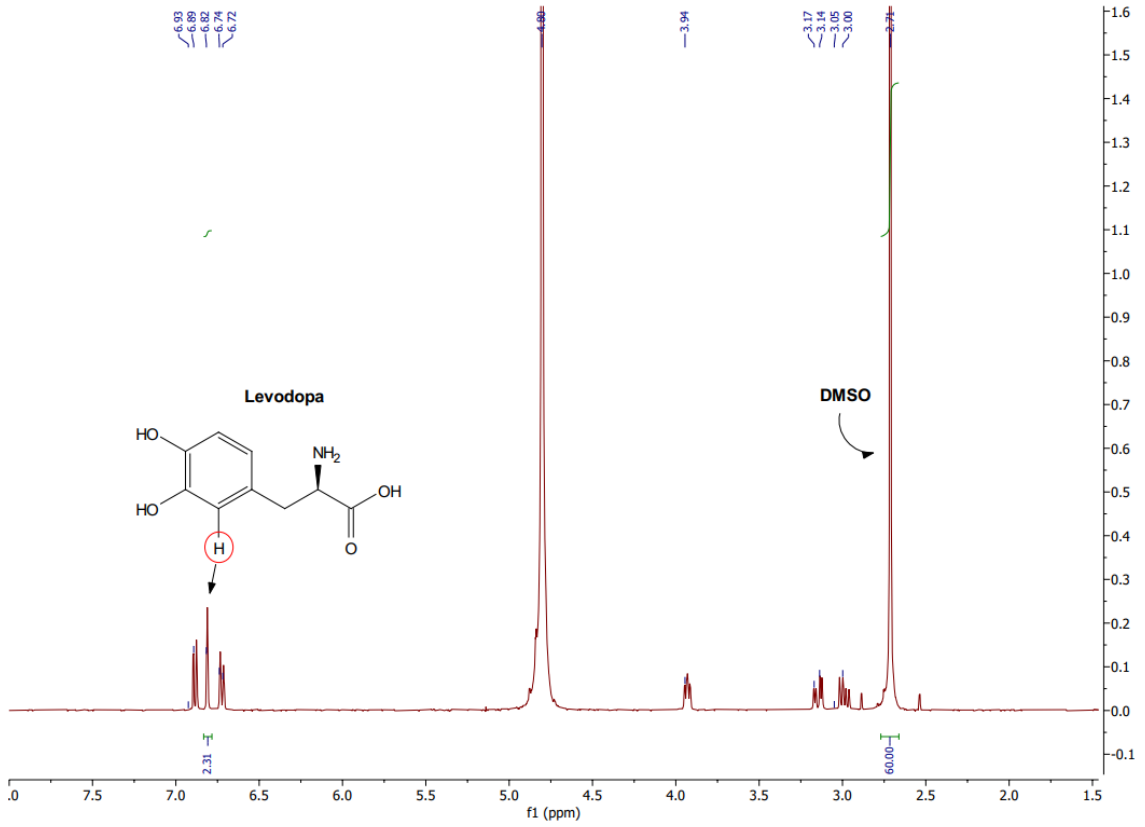

Figure 144. ^{1}H NMR spectrum of supernatant used to load DBS-CONHNH$_2$/agarose beads with levodopa dissolved in D_2O.

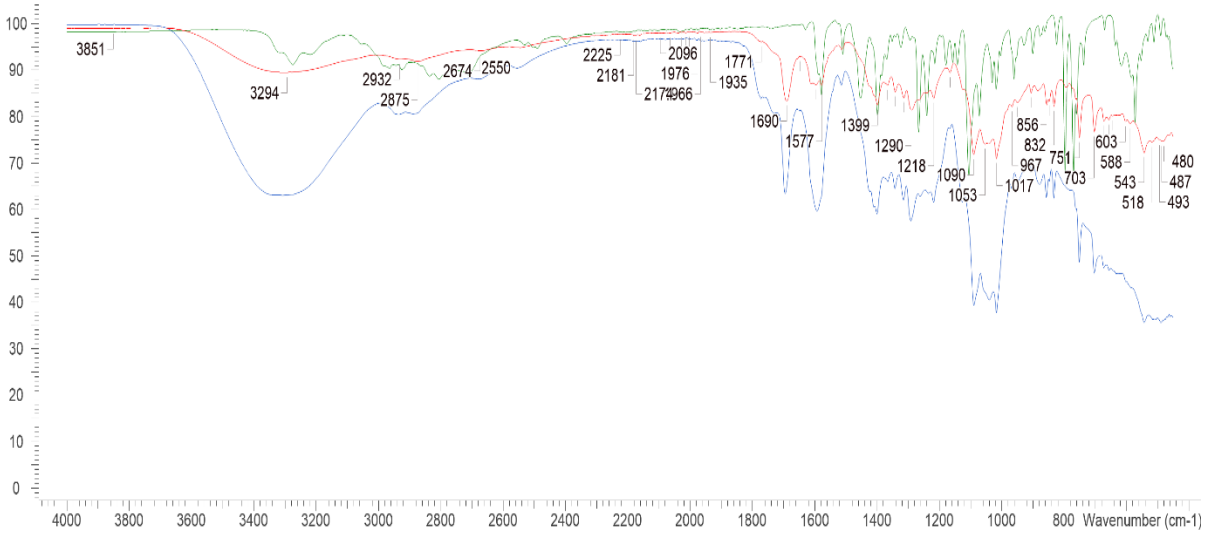

Figure 145. FT-IR spectra comparison of 0.3% (wt/vol) DBS-COOH vial xerogel (blue), propranolol dry powder (green), and propranolol loaded 0.3% (wt/vol) DBS-COOH vial xerogel (red).

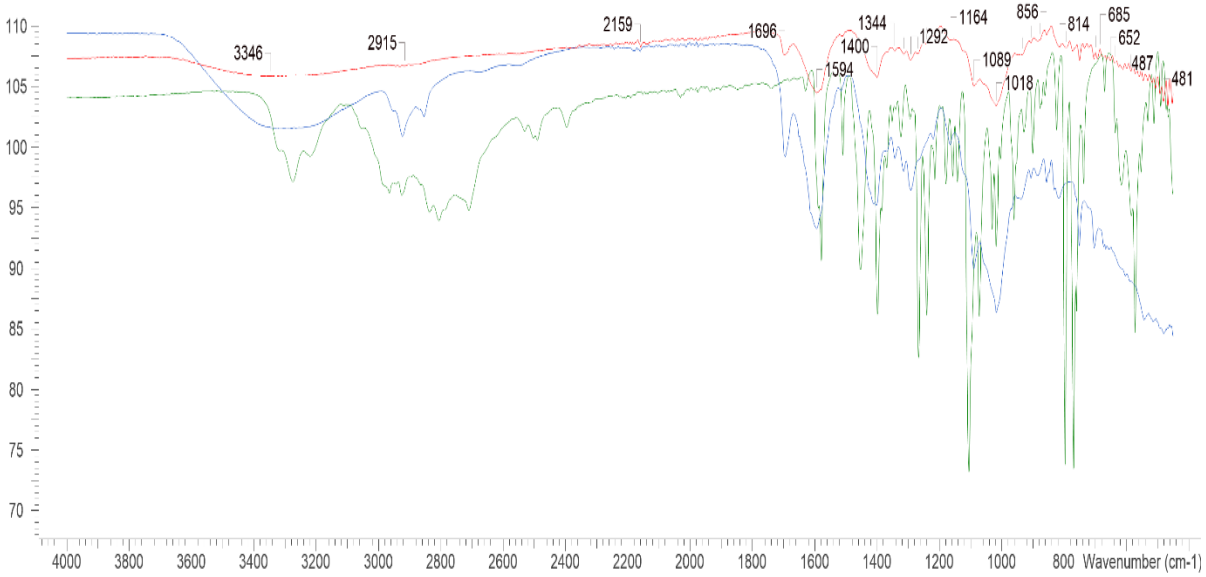

Figure 146. FT-IR spectra comparison of DBS-COOH/Alginate xerogel beads (blue) containing 0.3% (wt/vol) DBS-COOH and 1% (wt/vol) alginate, propranolol HCl dry powder (green), and propranolol loaded DBS-COOH/Alginate xerogel beads (red).

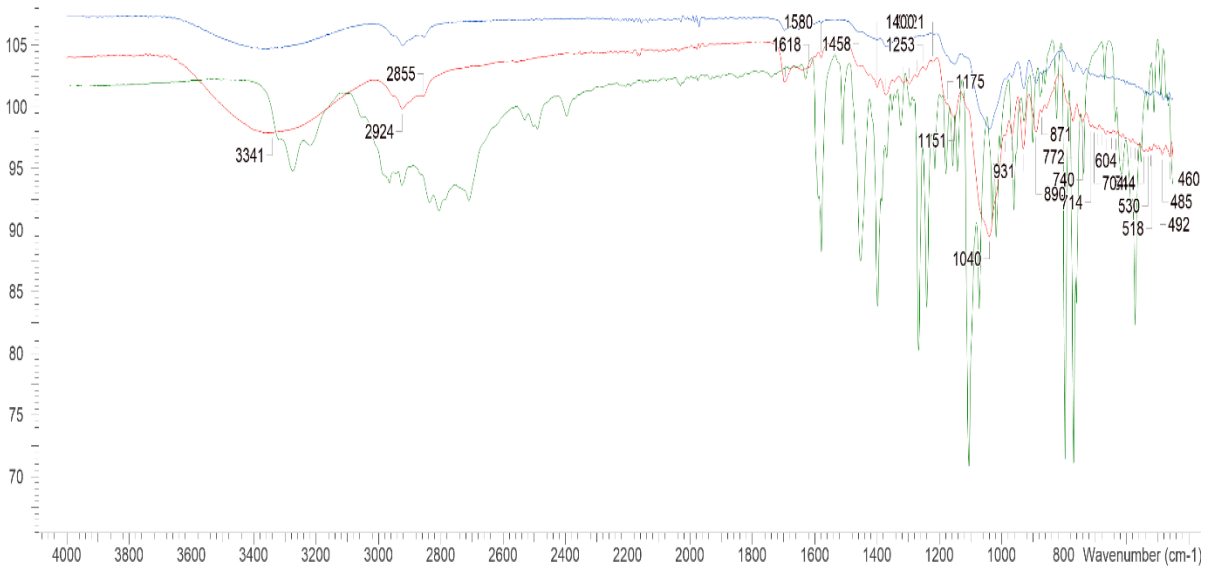

Figure 147. FT-IR spectra comparison of DBS-COOH/Agarose xerogel beads (blue) containing 0.3% (wt/vol) DBS-COOH and 1% (wt/vol) agarose, propranolol HCl dry powder (green), and propranolol loaded DBS-COOH/Agarose xerogel beads (red).

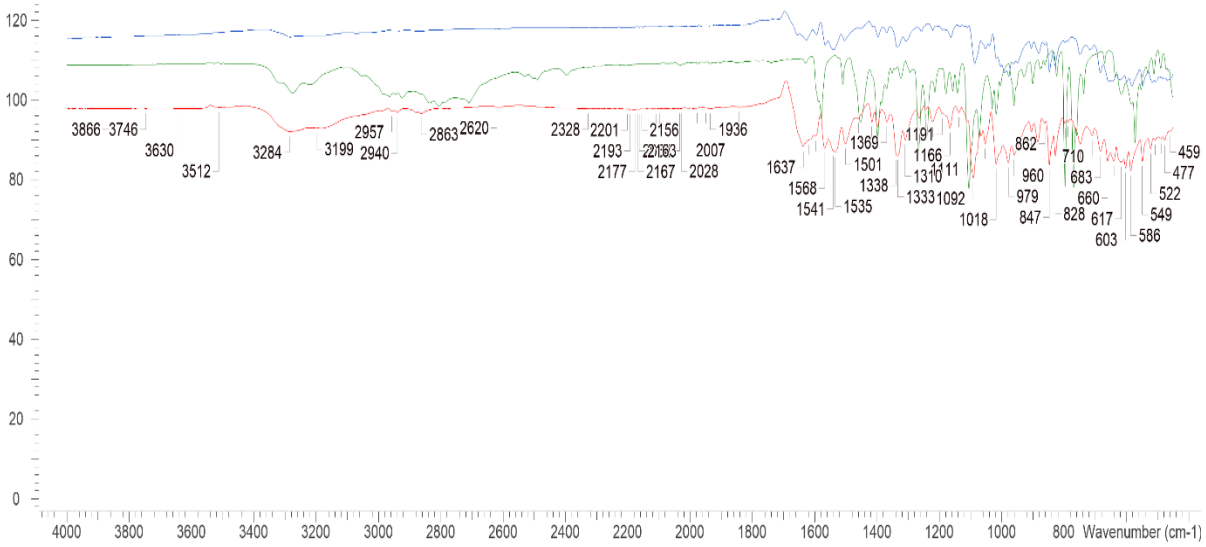

Figure 148. FT-IR spectra comparison of 0.4% (wt/vol) DBS-CONHNH$_2$ xerogel (blue), propranolol dry powder (green), and propranolol loaded DBS-CONHNH$_2$ xerogel (red).

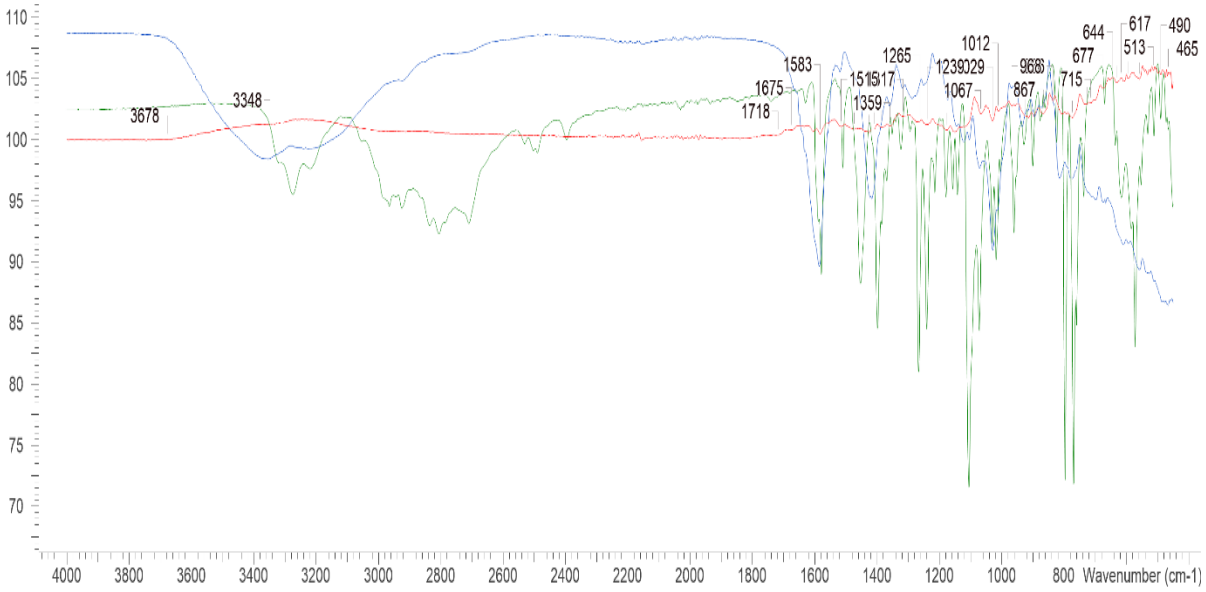

Figure 149. FT-IR spectra comparison of DBS-CONHNH$_2$/Alginate xerogel beads (blue) containing 0.4% (wt/vol) DBS-CONHNH$_2$ and 1% (wt/vol) alginate, propranolol HCl dry powder (green), and propranolol loaded DBS-CONHNH$_2$/Alginate xerogel beads (red).

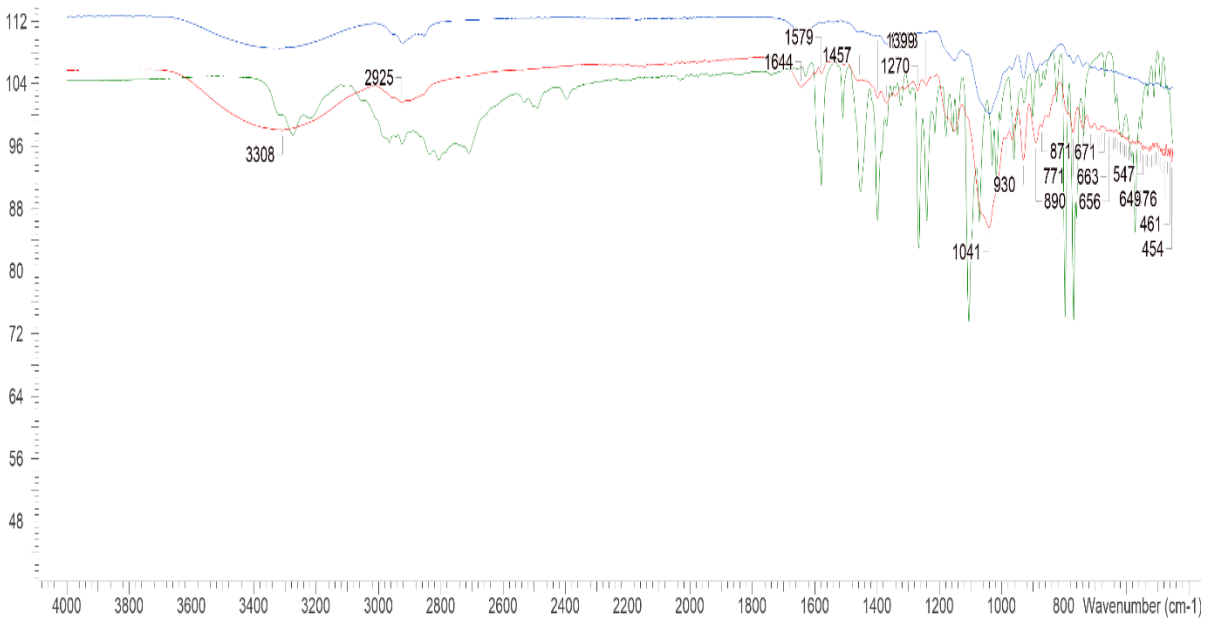

Figure 150. FT-IR spectra comparison of DBS-CONHNH2/ Agarose beads (blue) containing 0.4% (wt/vol) DBS-CONHNH2 and 1% (wt/vol) agarose xerogel, propranolol HCl dry powder (green), and propranolol loaded DBS-CONHNH2/ Agarose xerogel beads (red).

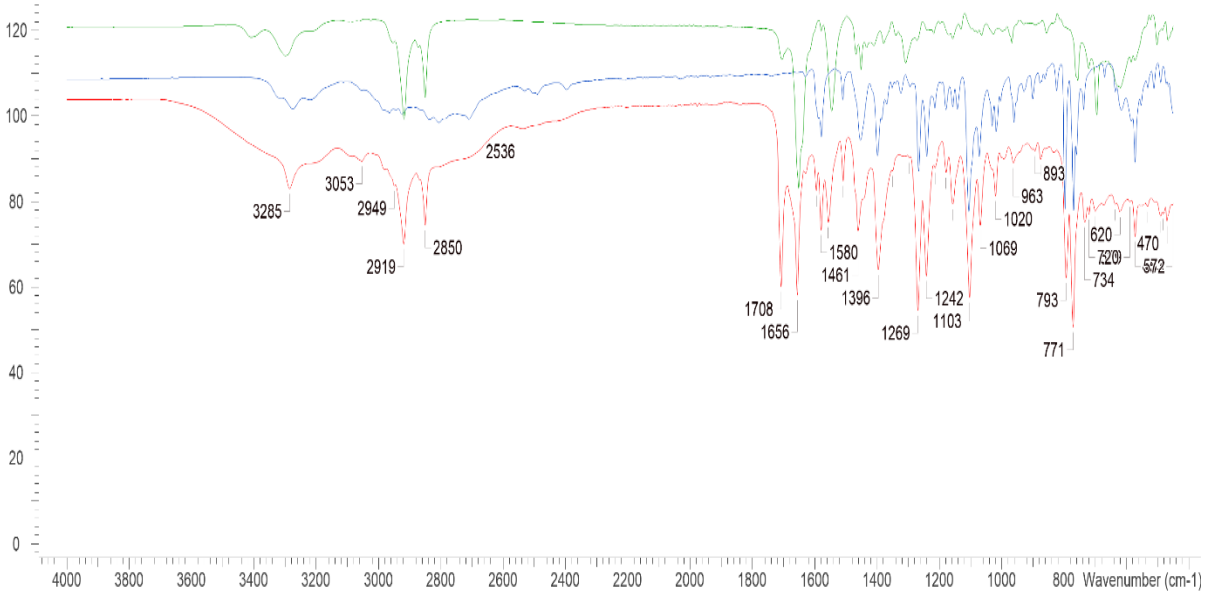

Figure 151. FT-IR spectra comparison of 0.35% (wt/vol) Benzyl glutamine vial xerogel (blue), propranolol HCl dry powder (green), and propranolol loaded Benzyl glutamine xerogel (red).

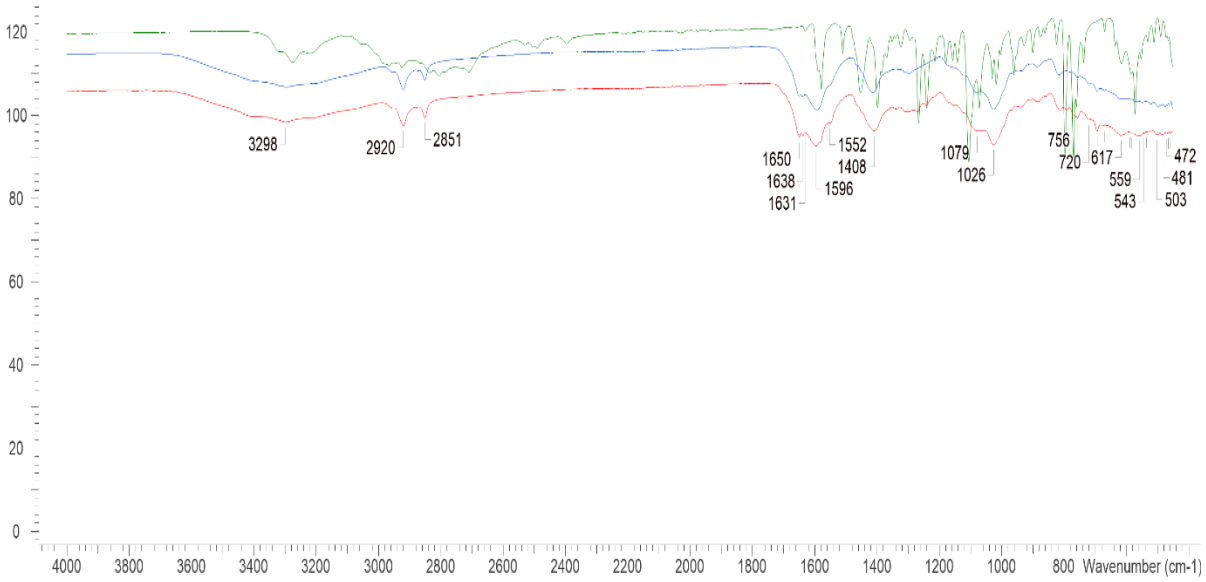

Figure 152. FT-IR spectra comparison of Benzyl glutamine/Alginate xerogel beads (blue) containing 0.35% (wt/vol) Benzyl glutamine and 1% (wt/vol) alginate, propranolol HCl dry powder (green), and Propranolol loaded Benzyl glutamine/Alginate xerogel beads (red).

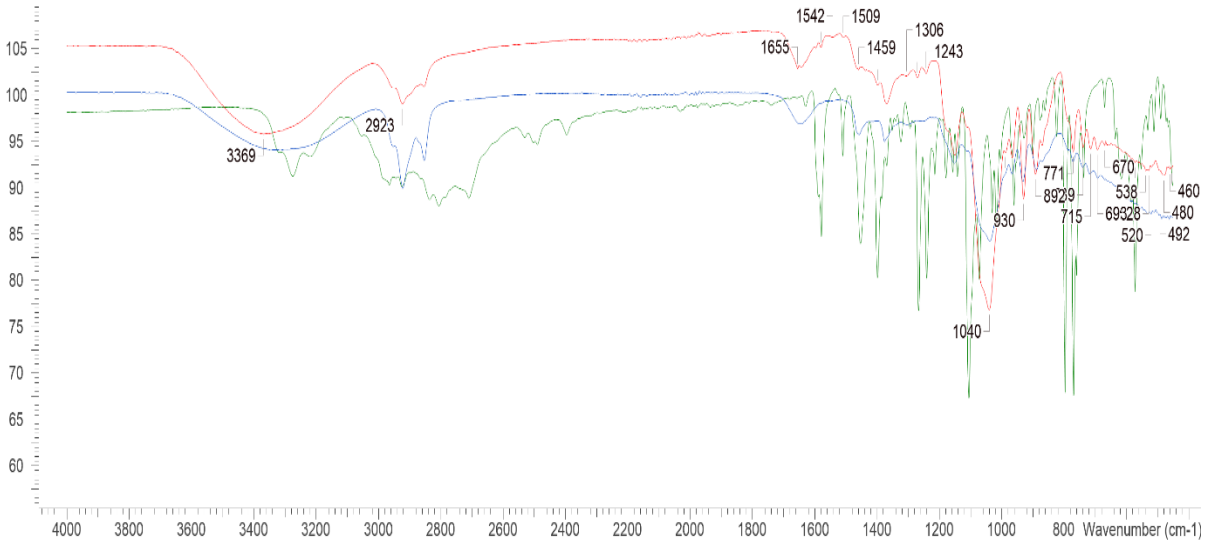

Figure 153. FT-IR spectra comparison of Benzyl glutamine/Agarose xerogel beads (blue) containing 0.35% (wt/vol) Benzyl glutamine and 1% (wt/vol) agarose, propranolol HCl dry powder (green), and propranolol loaded Benzyl glutamine/ Agarose xerogel beads (red).

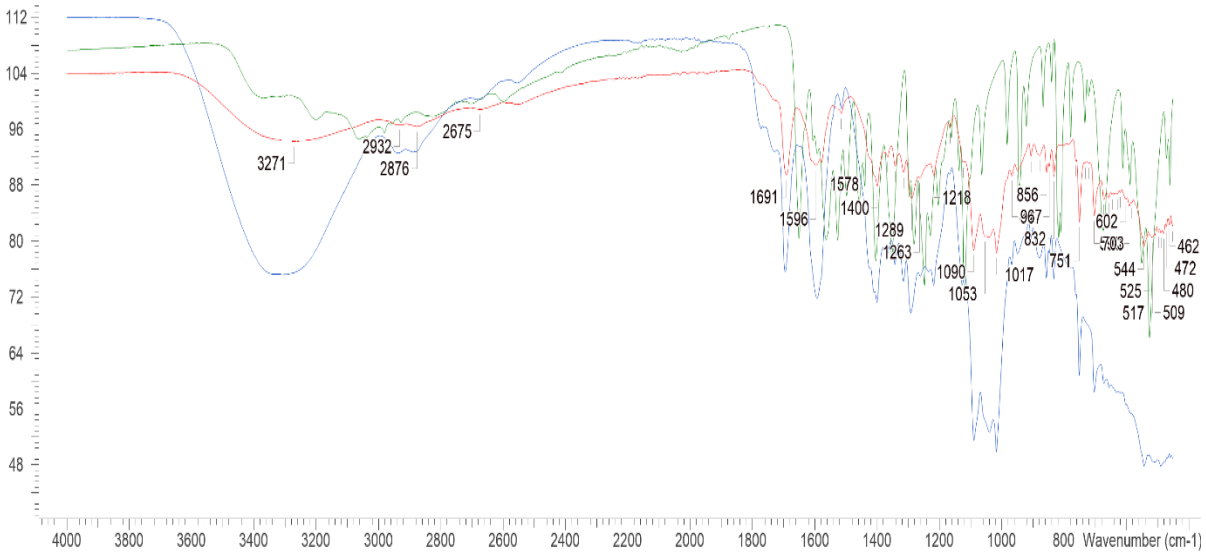

Figure 154. FT-IR spectra comparison of 0.3% (wt/vol) DBS-COOH vial xerogel (blue), levodopa dry powder (green), and levodopa loaded 0.3% (wt/vol) DBS-COOH vial xerogel (red).

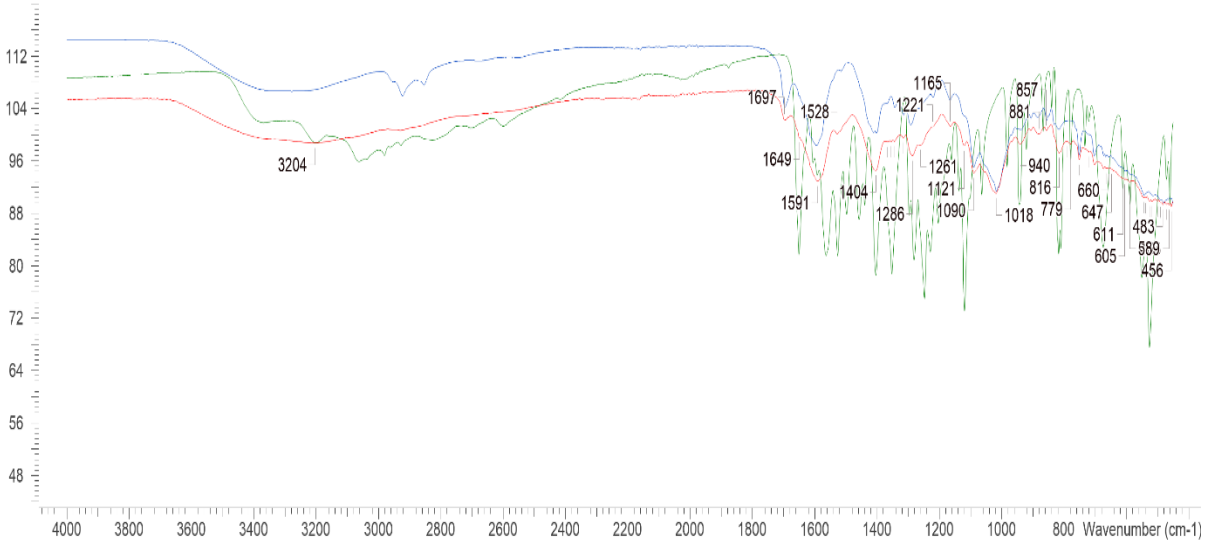

Figure 155. FT-IR spectra comparison of DBS-COOH/Alginate xerogel beads (blue) containing 0.3% (wt/vol) DBS-COOH and 1% (wt/vol) alginate, levodopa dry powder (green), and levodopa loaded DBS-COOH/Alginate xerogel beads (red).

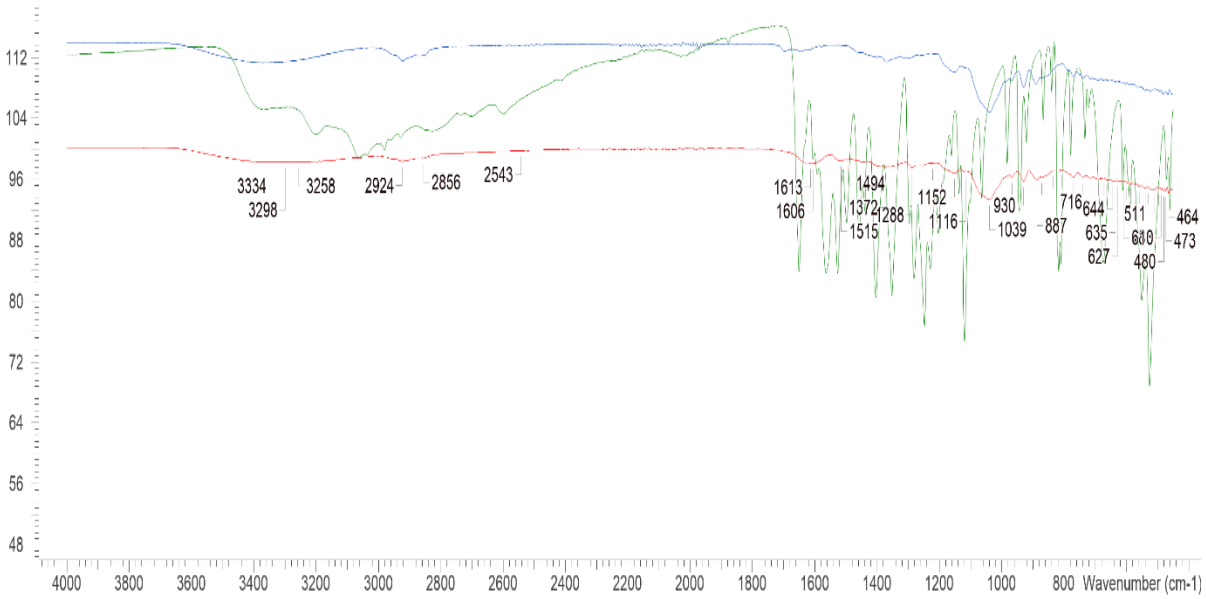

Figure 156. FT-IR spectra comparison of DBS-COOH/ Agarose xerogel beads (blue) containing 0.3% (wt/vol) DBS-COOH and 1% (wt/vol) agarose, levodopa dry powder (green), and levodopa loaded DBS-COOH/ Agarose xerogel beads (red).

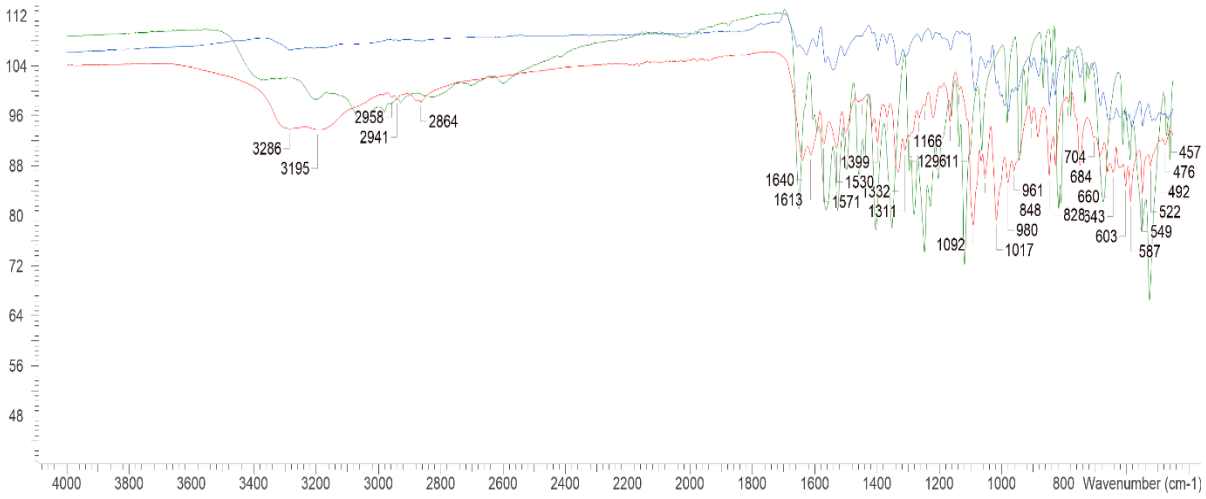

Figure 157. FT-IR spectra comparison of 0.4% (wt/vol) DBS-CONHNH2 xerogel (blue), levodopa dry powder (green), and levodopa loaded DBS-CONHNH2 xerogel (red).

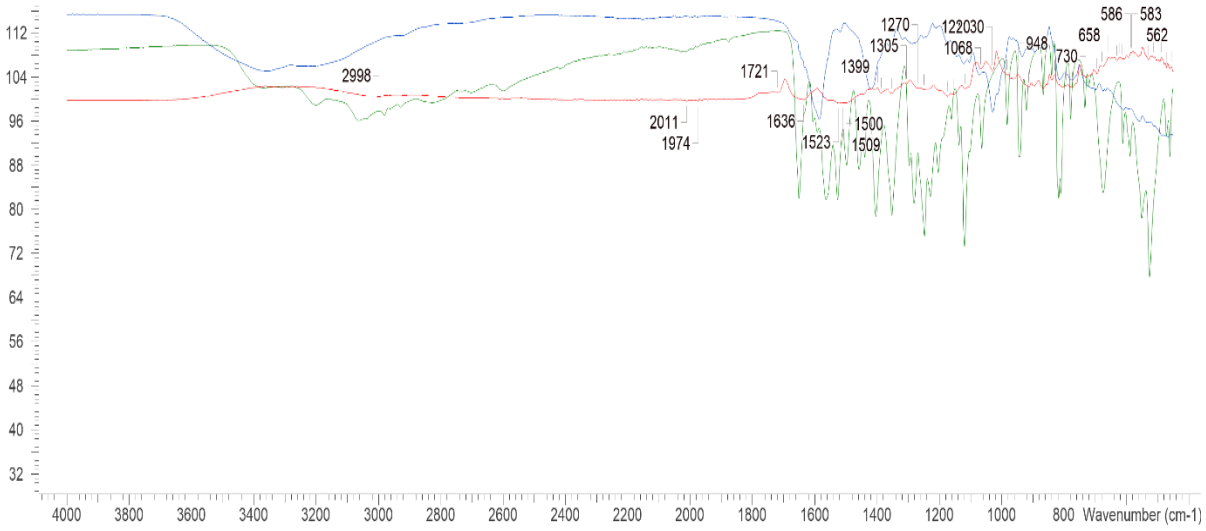

Figure 158. FT-IR spectra comparison of DBS-CONHNH$_2$/Alginate xerogel beads (blue) containing 0.4% (wt/vol) DBS-CONHNH$_2$, levodopa dry powder (green), and 1% (wt/vol) alginate and levodopa loaded DBS-CONHNH$_2$/Alginate xerogel beads (red).

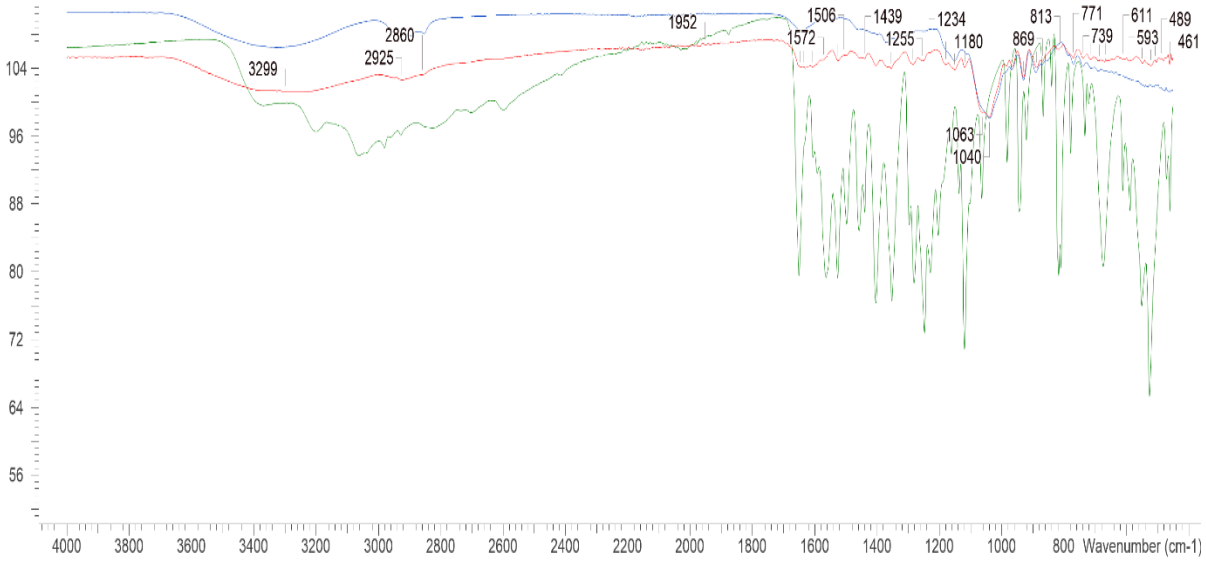

Figure 159. FT-IR spectra comparison of DBS-CONHNH$_2$/Agarose xerogel beads (blue) containing 0.4% (wt/vol) DBS-CONHNH$_2$ and 1% (wt/vol) agarose, levodopa dry powder (green), and levodopa loaded DBS-CONHNH$_2$/Agarose xerogel beads (red).

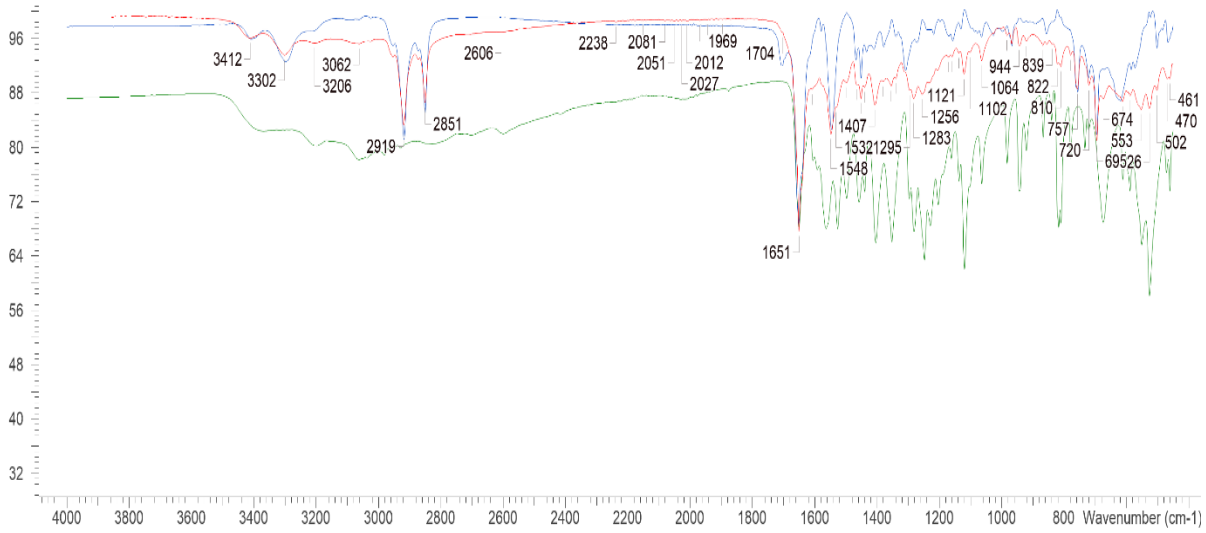

Figure 160. FT-IR spectra comparison of 0.35% (wt/vol) Benzyl glutamine vial xerogel (blue), levodopa dry powder (green), and levodopa loaded Benzyl glutamine xerogel (red).

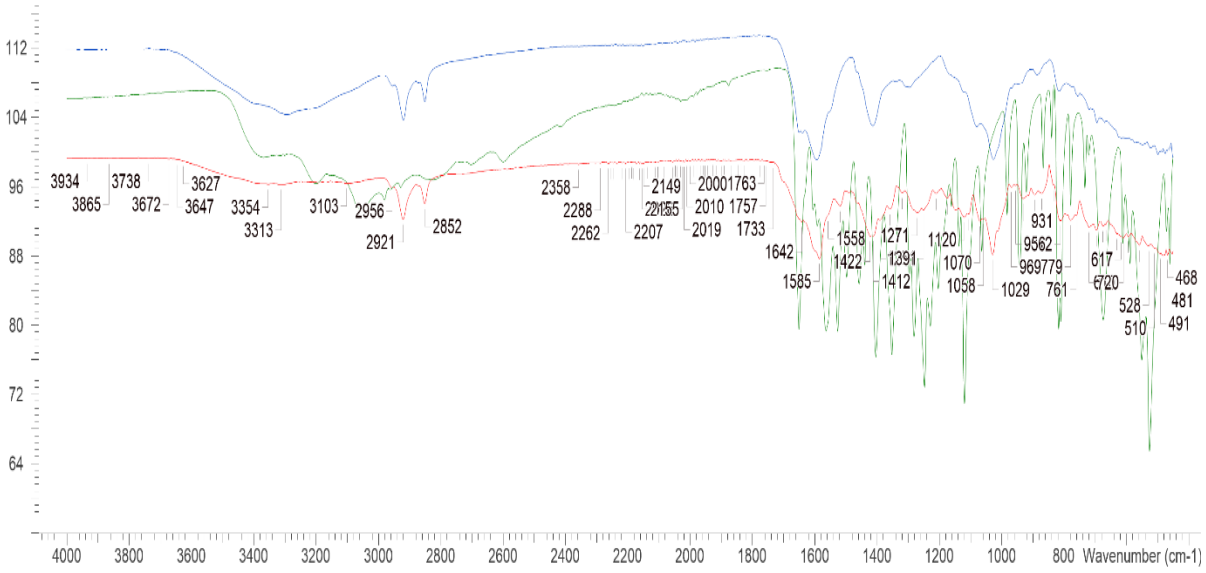

Figure 161. FT-IR spectra comparison of Benzyl glutamine/Alginate xerogel beads (blue) containing 0.35% (wt/vol) Benzyl glutamine and 1% (wt/vol) alginate, levodopa dry powder (green), and levodopa loaded Benzyl glutamine/Alginate xerogel beads (red).

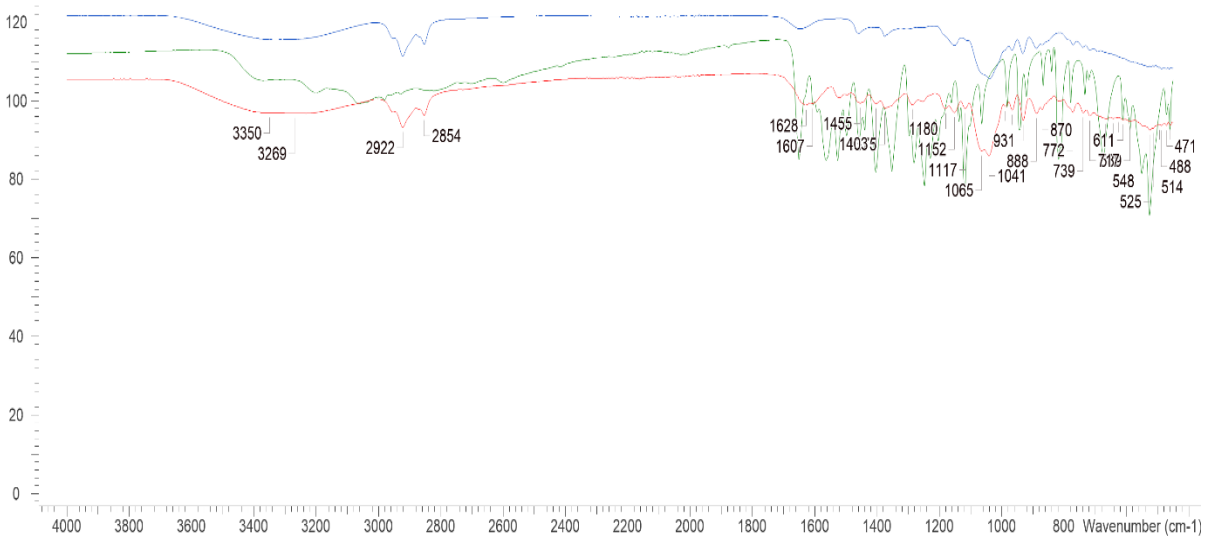

Figure 162. FT-IR spectra comparison of Benzyl glutamine/ Agarose xerogel beads (blue) containing 0.35% (wt/vol) Benzyl glutamine and 1% (wt/vol) agarose, levodopa dry powder (green), and levodopa loaded Benzyl glutamine/ Agarose xerogel beads (red).

Abbreviations

5’-GMP	5’-guanosine monophosphate
AFM	Atomic-force microscopy
Ami	Aminoglycoside
API	Active pharmaceutical ingredient
ASGP-R	Asialoglycoprotein receptor
BA	2-Formylbenzeneboronic acid
BG	Benzyl glutamine
BG-C10	Benzyl glutamine-C10
BG-C11	Benzyl glutamine-C11
BG-C12	Benzyl glutamine-C12
BG-C14	Benzyl glutamine-C14
BLT	Bicalutamide
Boc	Tert-butyloxycarbonyl
COX	Cyclooxygenase
DAP	Diaminopropane
DBS	1,3:2,4-dibenzylidene-D-sorbitol
DBS-CONHNH2	1,3:2,4-dibenzylidene-D-sorbitol-p,p'-diacylhydrazide
DBS-COOH	1,3:2,4-dibenzylidene-D-sorbitol-p,p'-dicarboxylic acid
DCM	Dichloromethane
DLS	Dynamic light scattering
DMAP	Dimethylaminopyridine
DMSO	Dimethyl sulfoxide
DMSO-d_6	Deuterated dimethyl sulfoxide
DSS	Sodium trimethylsilylpropanesulfonate
EDC	1-ethyl-3-(3-dimethylaminopropyl)carbodiimide
ESI	Electrospray ionisation
FBS	Fetal bovine serum

Fmoc	Fluorenylmethyloxycarbonyl
FT-IR	Fourier transform infrared
G	Guanosine
G'	Storage modulus
G''	Loss modulus
GdL	Glucono-δ-lactone
L-dopa	Levodopa
LMWG	Low molecular weight gelator
LVR	Linear viscoelastic region
MGC	Minimum gelation concentration
MS	Mass spectrometry
MSC	Mesenchymal stem cell
NMR	Nuclear magnetic resonance
NPX	Naproxen
NSAID	Non-steroidal anti-inflammatory drug
PD	Parkinson's disease
PG	Polymer gel
ROS	Reactive oxygen species
RSV	Rosuvastatin
SEM	Scanning electron microscopy
TEM	Transmission electron microscopy
Tgel	Gel-sol transition temperature
UV-vis	Ultraviolet-visible
β-gal	β-galactosidase